

DISSERTATION

QUANTUM DOT AND POLYMER SENSITIZATION OF
SINGLE CRYSTAL TITANIUM DIOXIDE ELECTRODES

Submitted by

Justin Sambur

Department of Chemistry

In partial fulfillment of the requirements

For the Degree of Doctor of Philosophy

Colorado State University

Fort Collins, Colorado

Summer 2011

Doctoral Committee:

Advisor: Bruce A. Parkinson

Gary E. Maciel

C. Michael Elliott

Alan K. Van Orden

Mario C. Marconi

ABSTRACT

QUANTUM DOT AND POLYMER SENSITIZATION OF SINGLE CRYSTAL TITANIUM DIOXIDE ELECTRODES

The morphology of semiconductor nanocrystals or quantum dots (QDs) and conjugated polymers at the interface of TiO₂ is expected to play an important role in the electron injection efficiency of mesoporous sensitized solar cells (SSCs). Atomic force microscopy (AFM) and photocurrent spectroscopy were employed to correlate the interfacial morphology of QDs and polymers with the sensitized photocurrent yields on planar TiO₂ single crystal electrodes. QDs prepared by the *ex situ* ligand exchange method, whereby 3-mercaptopropionic acid (MPA)-capped QDs were synthesized and directly adsorbed onto bare TiO₂ single crystals, resulted in both reproducible sensitized photocurrents and predominantly single layer surface coverages. Photoluminescence (PL) and photocurrent measurement techniques were simultaneously employed to detect electron injection from QDs to TiO₂ for a variety of long and short alkyl chain capping ligands. Quenching of the PL lifetime, often interpreted as a spectroscopic signature for electron transfer, was observed for QDs capped with long chain ligands that do not produce sensitized photocurrent. The *ex situ* ligand exchange procedure was also utilized to adsorb single layers of MPA-capped

CdSe/ZnS core/shell (CS) and PbS QDs onto single crystal TiO₂ electrodes. Despite a potential energy barrier for photo-excited carriers in the CdSe core imposed by the wide band gap ZnS shell, type-I CS QDs effectively sensitized single crystal TiO₂ electrodes and continued to operate in a regenerative mode in an aerated, corrosive iodide electrolyte for more than 20 h. PbS quantum dots adsorbed on TiO₂ single crystals exhibited for the first time hot electron injection from higher QD excited states and absorbed photon-to-current efficiencies greater than 100% due to multiple exciton collection.

The nanoscale morphology and photoactivity of conjugated polyelectrolytes (CPEs) deposited from different solvents onto single crystal TiO₂ was investigated with atomic force microscopy (AFM) and photocurrent spectroscopy. Absorbed photon-to-current efficiencies approaching 50% were measured for CPE layers as thick as 4 nm on TiO₂. The research herein suggests that controlling surface morphology of QD and polymer sensitizers may lead to the development of inexpensive, high-efficiency sensitized solar cells.

TO MY FAMILY:

MOM, DAD, KEITH, COURTNEY AND SYDNEY
WILLIE AND SMOKEY

AND MY SPARK, DELI

ACKNOWLEDGEMENTS

I express my deepest gratitude to my advisor and mentor Professor Bruce A. Parkinson. He not only trained me to think like a scientist, but also to think outside the box. Bruce encouraged me early on to pursue an academic career and allowed me to present research at scientific meetings. I am forever indebted to him for imparting his knowledge upon me and for the most enjoyable and rewarding graduate school experience I could have imagined.

I am grateful for the collaborators who contributed to the work in this thesis: Dave Schut and Thomas Novet at Voxel Inc., Profs. Kirk Schanze and John Reynolds at the University of Florida and the Van Orden group at CSU.

The Chemistry Department at Colorado State University provided an excellent environment to conduct research. I would like to thank Profs. C. Michael Elliott, Amy Prieto, Matt Shores, Alan Kennan for their expertise, guidance and support. I would like to thank Prof. Alan Van Orden for assistance with my independent research proposal and for his help in our fruitful collaboration. I would like to thank my colleagues, Shannon Riha, Joe Mondloch, Doug Shepherd, Derrick Johnson, Tim Arthur, and James Mosby, a group of extremely smart, talented and motivated scientists who pushed me to work harder throughout graduate school. I would also like to thank all of the Parkinson Group members who guided me over the years, especially Bengt Jackel, Jennifer Schuttlefield, Manashi Nath, Mike Woodhouse, Dave Seley, Dae Jin Choi and

Yunfeng Lui. Special thanks to The Chain: Matt, Dave, Dave, Chris and John for providing much needed humor and emotional support.

I am so lucky to have my parents Robin and Michael. Thanks for instilling good values in me and for always providing ALL the tools I need to succeed (without hesitation). You guys make it all too easy.

Thanks to my brother Keith for being the best example of a role model. Thanks for your support and guidance, especially when it comes to real-world issues that I am not qualified to tackle. Thanks to his wife Courtney for being my favorite sister and for bringing us Sydney, the most beautiful Sambur in the clan.

I would like to thank the Sambur and Plourde families for putting up with Deli and I living 2000 miles away. We moved away from home at 22 to start an experiment, and of course, we got great results. Thanks for visiting us over the years.

Finally, to Deli, thanks for being my best friend. You were the only person who had to deal with me when things weren't going well- thanks for putting up with those late nights. You continue to adjust your life and career so that I can pursue my goals- I am forever grateful for your sacrifices. I am so lucky to have you, I love you.

Justin B. Sambur

May 2011

TABLE OF CONTENTS

	ABSTRACT.....	ii
	ACKNOWLEDGEMENTS.....	iv
I.	INTRODUCTION.....	1
	Dissertation format.....	1
	Dye sensitization of single crystal electrodes.....	2
	Semiconductor nanocrystal sensitizers.....	6
	Conjugated polyelectrolyte sensitizers.....	7
	References.....	7
II.	THE INFLUENCE OF SURFACE CHEMISTRY ON THE BINDING AND ELECTRONIC COUPLING OF CADMIUM SELENIDE QUANTUM DOTS TO SINGLE CRYSTAL TITANIUM DIOXIDE SURFACES.....	12
	Abstract.....	13
	Introduction.....	14
	Experimental Methods.....	16
	Results and Discussion.....	20
	Conclusions.....	43
	Acknowledgements.....	44
	References.....	44
	Future Work.....	53
III.	IN-SITU STUDIES OF PHOTOLUMINESCENCE QUENCHING IN SINGLE CRYSTAL QUANTUM DOT SENSITIZED SOLAR CELLS..	55
	Abstract.....	56
	Introduction.....	57
	Experimental Methods.....	58
	Results and Discussion.....	63
	Conclusions.....	72
	Supporting Information.....	73
	Acknowledgements.....	76
	References.....	76

	Future Work.....	82
IV.	CADMIUM SELENIDE/ZINC SULFIDE CORE/SHELL QUANTUM DOT SENSITIZATION OF LOW INDEX TITANIUM DIOXIDE SINGLE CRYSTAL SURFACES.....	85
	Abstract.....	87
	Introduction.....	88
	Experimental Methods.....	91
	Results and Discussion.....	94
	Conclusions.....	107
	Acknowledgements.....	107
	References.....	108
	Future Work.....	112
V.	MULTIPLE EXCITON COLLECTION IN A SENSITIZED PHOTOVOLTAIC SYSTEM.....	115
	Abstract.....	116
	Introduction.....	117
	Experimental Methods.....	121
	Results and Discussion.....	126
	Acknowledgements.....	140
	References.....	140
	Future Work.....	145
VI.	INTERFACIAL MORPHOLOGY AND PHOTOELECTROCHEMISTRY OF CONJUGATED POLYELECTROLYTES ADSORBED ON SINGLE CRYSTAL TITANIUM DIOXIDE.....	148
	Abstract.....	149
	Introduction.....	150
	Experimental Methods.....	154
	Results and Discussion.....	158
	Conclusions.....	180
	Supporting Information.....	181
	Acknowledgements.....	187
	References.....	187
	Future Work.....	191
VII.	Appendix.....	193

CHAPTER I

INTRODUCTION

I.1 Dissertation format

This dissertation is written according to the journals-format style as described in the Colorado State Graduate School Thesis and Dissertation Manual whereby "...the student may include manuscripts published in, accepted by, submitted to, and/or prepared for submission to scholarly journals and proceedings (or modified from those versions)." Following these guidelines, this dissertation consists of three published and two submitted manuscripts formatted according to standards set by the American Chemical Society. Justin B. Sambur contributed significantly to all research described herein. Each chapter is bridged by a short overview of the work and specific contributions from Justin B. Sambur.

Chapter I provides a short historical introduction of single crystal dye sensitization and motivation for employing quantum dots (QDs) and conjugated polymer electrolyte (CPEs) as sensitizers. Chapter II evaluates several surface chemistry procedures used to adsorb QDs onto nanocrystalline TiO₂ surfaces. Chapter III compares photoluminescence quenching to photocurrent measurements in order to characterize electron injection from QDs to single crystal oxide substrates. Chapter IV addresses stability issues of QD sensitized

solar cells by demonstrating electron injection from type-I CdSe/ZnS core/shell nanocrystals. Chapter V demonstrates for the first time hot electron injection and multiple exciton collection from PbS QDs to TiO₂ single crystal electrodes. Chapter VI correlates interfacial morphology and sensitized photocurrent yields for variable band gap CPE sensitizers.

1.2.1 Dye sensitization of single crystal electrodes

Spitler and Parkinson recently reviewed historical scientific advances in the field of single crystal dye sensitization.[1] In the late 1960s, Gerischer and Tributsch demonstrated sustainable photocurrents from organic dyes adsorbed onto single crystal ZnO electrodes in the presence of reducing agents.[2,3] This photoelectrochemical experiment not only introduced the use of visible light absorbing molecules for spectral sensitization of stable, large band gap semiconductors but also provided evidence for an electron injection mechanism from dye excited states to explain spectral sensitization of silver halide crystals by organic dyes.[4] Shortly thereafter, Tributsch and Calvin identified the possibility of exploiting dye-sensitized metal oxide photoelectrodes in solar energy conversion applications.[5,6] Figure 1 (taken from reference [1]) shows the primary thermodynamic and kinetic processes, first proposed by Gerischer and Willig, that describe dye sensitization of a semiconductor electrode.[7,8]

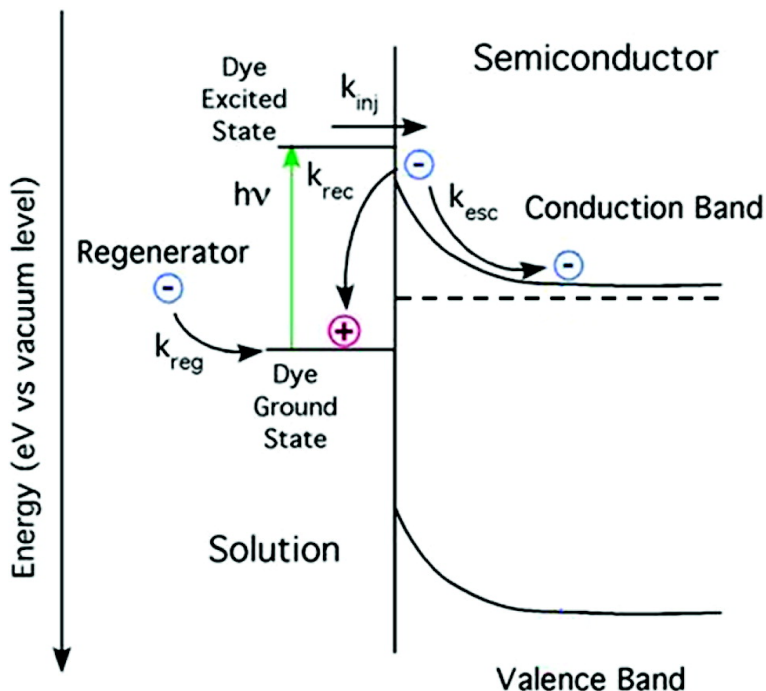


Figure 1. Energy level diagram and rate processes depicting electron injection from a photo-excited dye molecule adsorbed on a bulk n-type semiconductor electrode.

The energy level diagram in Figure 1 illustrates the fundamental energetic constraint for efficient electron injection whereby the excited state of the sensitizer must lie above (on the vacuum scale) the conduction band level of the semiconductor. Photo-excitation of the dye molecule results in electron transfer from the dye excited state to the conduction band of the semiconductor with a rate k_{inj} . The ground state of the photo-oxidized dye is reduced (also referred to as regenerated) by a redox species (regenerator) in solution at a rate k_{reg} . Injected electrons are rapidly swept away from the semiconductor/electrolyte interface at a rate k_{esc} due to the electric field gradient in the depletion region of the semiconductor. The depletion width and magnitude of the electric field at the interface is determined in part by the doping density of the semiconductor, the

electrochemical potential of the electrolyte and the applied bias.[9] However, injected electrons can recombine with the photo-oxidized dye at a rate (k_{rec}) or with oxidized redox species at the electrode surface. In order to realize unity quantum yields for electron injection, the rates for the forward processes (k_{inj} , k_{esc} and k_{reg}) must be faster than recombination (k_{rec}) pathways.

Early work by Spitler and Calvin quantified internal (absorbed photon-to-current efficiency, APCE) and external (incident photon-to-current efficiency, IPCE) quantum efficiencies of single crystal TiO_2 and ZnO electrodes immersed in aqueous xanthene and rhodamine dye solutions.[10,11] The photocurrent spectra resembled the solution absorption spectra of the dyes but relatively low APCEs on the order of 1-2% were measured. At the same time, near unity injection yields were reported for tris(bipyridine)Ru(II) sensitizers in an acetonitrile electrolyte at a rutile TiO_2 electrode.[12] Although it was not clear what caused the disparity between the two experiments, surface contamination may have inhibited dye adsorption or interfered with electronic coupling between the dye and the semiconductor conduction band.[1] It was not until Spitler and Parkinson employed an easily cleavable 1.1-1.2 eV band gap layered semiconductor n-WSe₂ as a clean, atomically flat electrode sensitized with an infrared cyanine dye that reproducible unity injection yields were routinely reported.[13] Thus eliminating surface contamination via the use of clean, reproducible electrode surfaces was established as a crucial experimental factor to study single crystal dye sensitization.

Despite near unity electron injection yields, utilizing n-type single crystals as anodes in photoelectrochemical photovoltaic devices is impractical due to low light absorption by the monolayer of dye. O'Regan and Grätzel circumvented this issue by exploiting high surface mesoporous nanocrystalline TiO₂ films to increase the optical density of dye sensitized photoanodes.[14] Since its inception in 1991, the mesoporous dye sensitized solar cell (DSSC) has only seen modest gains in power conversion efficiency from 7 to 11.5% despite thousands of literature reports on the subject.[15] The highest efficiency devices consist of Ru polypyridal coordination complex sensitizers chemically linked to a mesoporous TiO₂ support immersed in an iodide-based (I⁻/I₃⁻) electrolyte. Given the roughly 1000-fold enhancement of the electron injection and regeneration rate processes compared to various recombination processes, these device components have not been independently improved because the kinetic relationship is unique to the TiO₂/Ru dye/iodide electrolyte system.[15-17]

Parkinson and co-workers modeled the Ru dye system on various crystallographic orientations of rutile and naturally occurring anatase single crystals.[18] Despite reports of approximately 80% APCE values for dye sensitized mesoporous TiO₂ films,[19] internal quantum efficiency of dye sensitized single crystal electrodes were extremely low.[18] It was not until a UV cleaning treatment of the electrode surface was introduced, whereby extremely oxidizing valence band holes could oxidize unwanted surface contaminants prior to dye adsorption, that reproducible near-unity APCE values were observed.[20,21] From the work with the layered semiconductors and single

crystal TiO₂, it was clear that surface preparation and cleanliness was an extremely important experimental parameter that lead to high internal quantum efficiency of single crystal photoanodes. Appendix I of this dissertation discusses recent progress in TiO₂ surface preparation procedures.

I.2.2. Semiconductor nanocrystal sensitizers

In the early 1980s, Ekimov *et al.* and Brus reported the quantum size effect in the optical spectra of small semiconductor crystallites embedded in glasses and in solution, respectively.[22-24] Brus' laboratory accelerated the field by precisely controlling the diameter of nanometer-sized semiconductor crystallites using colloidal chemistry and derived physical models to explain the size-dependent optical spectra.[25] The term 'quantum dot' was coined by Mark Reed and refers to the zero-dimensional size of the semiconductor nanocrystallites.[26]

Since Serpone *et al.* demonstrated electron transfer from CdS to TiO₂ colloids[27], semiconductor sensitized metal oxide solar cells have been actively explored.[28,29] It is generally thought that semiconductor nanocrystals or quantum dots (QDs) may be superior sensitizers to molecular dyes (either organic or inorganic complexes) because they potentially offer increased light absorption over the entire visible spectrum, enhanced stability due to their inorganic nature and straightforward low-temperature solution processing.[28-30] However, the power conversion efficiency and stability of QD sensitized solar cells (QDSSCs) is not currently competitive with DSSCs.[30] The research in this dissertation addresses several issues related to surface chemistry of QDs,

morphology of QDs at the oxide surface and long term stability of QDSSCs using model single crystal TiO₂ photoanodes.

I.2.3. Conjugated polyelectrolyte sensitizers

Conjugated polyelectrolytes (CPEs) contain electrolyte groups on the repeat unit structure of the conjugated polymer backbone and may be dissolved as cationic, anionic or zwitterionic species in various solvents.[31] Chemical modification of the polymer backbone, pendant electron withdrawing or donating side groups, conjugation and number of repeat units can be employed to control the physical, optical and electronic properties of the CPE.[32] CPEs sensitizers potentially offer similar advantages as QDs, namely panchromatic light absorption and bulk solution processing.

Visible light absorbing CPEs with variable highest occupied and lowest unoccupied molecular orbital gaps (HOMO-LUMO gap) were recently synthesized[33] and electron transfer to TiO₂ nanoparticles were demonstrated.[34] To date, power conversion efficiency of polymer sensitized solar cells remain on the order of 1-3%.[35-43] Since morphology is expected to play an extremely important role in charge separation at the polymer/TiO₂ interface, the research in this dissertation correlated CPE morphology and sensitized photocurrent yields at single crystal TiO₂ electrodes.

I.3. References

- (1) Spitler, M. T.; Parkinson, B. A. Dye Sensitization of Single Crystal Semiconductor Electrodes *Acc. Chem. Res.* **2009**, *42*, 2017.
- (2) Gerischer, H.; Tributsch, H. Electrochemistry of ZnO monocrystal spectral sensitivity *Berichte Der Bunsen-Gesellschaft Fur Physikalische Chemie* **1968**, *72*, 437.

- (3) Tributsch, H.; Gerischer, H. Electrochemical investigations on mechanism of sensitization and supersensitization of ZnO monocrystals *Berichte Der Bunsen-Gesellschaft Fur Physikalische Chemie* **1969**, 73, 251.
- (4) Mees, C.; James, T. *Theory of the Photographic Process*; Macmillan: New York, 1966.
- (5) Tributsch, H. Reaction of excited chlorophyll molecules at electrodes and in photosynthesis *Photochem. Photobiol.* **1972**, 16, 261.
- (6) Tributsch, H.; Calvin, M. Electrochemistry of excited molecules - photoelectrochemical reactions of chlorophylls *Photochem. Photobiol.* **1971**, 14, 95.
- (7) Gerischer, H. In *Physical Chemistry*; Eyring, M., Jost, W., Henderson, D., Eds.; Academic Press: New York, 1970; Vol. 4A, p 463.
- (8) Gerischer, H.; Willig, F. In *Topics in Current Chemistry*; Boshke, F., Ed.; Springer-Verlag: Berlin, 1976; Vol. 61, p 31.
- (9) Bard, A.; Faulkner, L. *Electrochemical Methods- Fundamentals and Applications*; 2nd ed.; John Wiley & Sons: New York, 2000.
- (10) Spitler, M. T.; Calvin, M. Electron transfer at sensitized TiO₂ electrodes *J. Chem. Phys.* **1977**, 66, 4294.
- (11) Spitler, M.; Calvin, M. Adsorption and oxidation of rhoadmine-B at ZnO electrodes *J. Chem. Phys.* **1977**, 67, 5193.
- (12) Clark, W. D. K.; Sutin, N. Spectral sensitization of n-type titanium dioxide electrodes by polypyridineruthenium(II) complexes *J. Amer. Chem. Soc.* **1977**, 99, 4676.
- (13) Spitler, M.; Parkinson, B. A. Efficient infrared dye sensitization of van der Waals surfaces of semiconductor electrodes *Langmuir* **1986**, 2, 549.
- (14) O'Regan, B.; Grätzel, M. A low-cost high-efficiency solar cell based on dye sensitized colloidal TiO₂ films *Nature* **1991**, 353, 737.
- (15) Elliott, C. M. Dye sensitized solar cells: Out with both baby and bathwater *Nat. Chem.* **2011**, 3, 188.
- (16) Hagfeldt, A.; Gratzel, M. Molecular Photovoltaics *Acc. Chem. Res.* **2000**, 33, 269.
- (17) Hagfeldt, A.; Gratzel, M. Light-Induced Redox Reactions in Nanocrystalline Systems *Chem. Rev.* **1995**, 95, 49.

- (18) Fillinger, A.; Soltz, D.; Parkinson, B. A. Dye Sensitization of Natural Anatase Crystals with a Ruthenium-Based Dye *J. Electrochem. Soc.* **2002**, *149*, A1146.
- (19) Enea, O.; Moser, J.; Gratzel, M. Achievement of incident photon to electric current conversion yields exceeding 80% in the spectral sensitization of titanium dioxide by coumarin *J. Electroanalytical. Chem.* **1989**, *259*, 59.
- (20) Lu, Y.; Jaeckel, B.; Parkinson, B. A. Preparation and Characterization of Terraced Surfaces of Low-Index Faces of Anatase, Rutile, and Brookite *Langmuir* **2006**, *22*, 4472.
- (21) Lu, Y.; Choi, D.-j.; Nelson, J.; Yang, O. B.; Parkinson, B. A. Adsorption, Desorption, and Sensitization of Low-Index Anatase and Rutile Surfaces by the Ruthenium Complex Dye N3 *J. Electrochem. Soc.* **2006**, *153*, E131.
- (22) Ekimov, A. I.; Onushchenko, A. A. Quantum size effect in the optical-spectra of semiconductor micro-crystals *Sov. Phys. Semicond.* **1982**, *16*, 775.
- (23) Ekimov, A. I.; Onushchenko, A. A. Quantum size effect in 3-dimensional microscopic semiconductor crystals *JETP Lett.* **1981**, *34*, 345.
- (24) Brus, L. E. A simple model for the ionization potential, electron affinity, and aqueous redox potentials of small semiconductor crystallites *J. Chem. Phys.* **1983**, *79*, 5566.
- (25) Bawendi, M. G.; Steigerwald, M. L.; Brus, L. E. The Quantum Mechanics of Larger Semiconductor Clusters ("Quantum Dots") *Annu. Rev. Phys. Chem.* **1990**, *41*, 477.
- (26) Reed, M. A.; Randall, J. N.; Aggarwal, R. J.; Matyi, R. J.; Moore, T. M.; Wetsel, A. E. Observation of discrete electronic states in a zero-dimensional semiconductor nanostructure *Phys. Rev. Lett.* **1988**, *60*, 535.
- (27) Serpone, N.; Borgarello, E.; Gratzel, M. Visible light induced generation of hydrogen from H₂S in mixed semiconductor dispersions; improved efficiency through inter-particle electron transfer *Chem. Comm.* **1984**, 342.
- (28) Kamat, P. V. Quantum Dot Solar Cells. Semiconductor Nanocrystals as Light Harvesters *J. Phys. Chem. C* **2008**, *112*, 18737.
- (29) Hodes, G. Comparison of Dye-and Semiconductor-Sensitized Porous Nanocrystalline Liquid Junction Solar Cells *J. Phys. Chem. C* **2008**, *112*, 17778.

- (30) Kamat, P. V.; Tvrdy, K.; Baker, D. R.; Radich, J. G. Beyond Photovoltaics: Semiconductor Nanoarchitectures for Liquid-Junction Solar Cells *Chem. Rev.* **2010**, *110*, 6664.
- (31) Schanze, K. S.; Shelton, A. H. Functional Polyelectrolytes *Langmuir* **2009**, *25*, 13698.
- (32) Jiang, H.; Taranekar, P.; Reynolds, J. R.; Schanze, K. S. Conjugated Polyelectrolytes: Synthesis, Photophysics, and Applications *Angew. Chem., Int. Ed.* **2009**, *48*, 4300.
- (33) Zhao, X.; Pinto, M. R.; Hardison, L. M.; Mwaura, J.; Muller, J.; Jiang, H.; Witker, D.; Kleiman, V. D.; Reynolds, J. R.; Schanze, K. S. Variable Band Gap Poly(arylene ethynylene) Conjugated Polyelectrolytes *Macromolecules* **2006**, *39*, 6355.
- (34) Jiang, H.; Zhao, X.; Shelton, A. H.; Lee, S. H.; Reynolds, J. R.; Schanze, K. S. Variable-Band-Gap Poly(arylene ethynylene) Conjugated Polyelectrolytes Adsorbed on Nanocrystalline TiO₂: Photocurrent Efficiency as a Function of the Band Gap *ACS Appl. Mater. Interfaces* **2009**, *1*, 381.
- (35) Kim, Y.-G.; Walker, J.; Samuelson, L. A.; Kumar, J. Efficient Light Harvesting Polymers for Nanocrystalline TiO₂ Photovoltaic Cells *Nano Letters* **2003**, *3*, 523.
- (36) Bhongale, C. J.; Thelakkat, M. Efficient hybrid polymer/titania solar cells sensitized with carboxylated polymer dye *Sol. Energy Mater. Sol. Cells* **2010**, *94*, 817.
- (37) Arango, A. C.; Carter, S. A.; Brock, P. J. Charge transfer in photovoltaics consisting of interpenetrating networks of conjugated polymer and TiO₂ nanoparticles *Appl. Phys. Lett.* **1999**, *74*, 1698.
- (38) Liu, J.; Kadnikova, E. N.; Liu, Y.; McGehee, M. D.; Fréchet, J. M. J. Polythiophene Containing Thermally Removable Solubilizing Groups Enhances the Interface and the Performance of Polymer/Titania Hybrid Solar Cells *J. Amer. Chem. Soc.* **2004**, *126*, 9486.
- (39) Liu, X.; Zhu, R.; Zhang, Y.; Liu, B.; Ramakrishna, S. Anionic benzothiadiazole containing polyfluorene and oligofluorene as organic sensitizers for dye-sensitized solar cells *Chem. Commun.* **2008**, 3789.
- (40) Mwaura, J. K.; Zhao, X.; Jiang, H.; Schanze, K. S.; Reynolds, J. R. Spectral Broadening in Nanocrystalline TiO₂ Solar Cells Based on Poly(p-phenylene ethynylene) and Polythiophene Sensitizers *Chem. Mater.* **2006**, *18*, 6109.

- (41) Oey, C. C.; et al. Polymer-TiO₂ solar cells: TiO₂ interconnected network for improved cell performance *Nanotechnology* **2006**, *17*, 706.
- (42) Saji, V. S.; Zong, K.; Pyo, M. NIR-absorbing poly(thieno[3,4-b]thiophene-2-carboxylic acid) as a polymer dye for dye-sensitized solar cells *J. Photochem. Photobiol., A* **2010**, *212*, 81.
- (43) van Hal, P. A.; Christiaans, M. P. T.; Wienk, M. M.; Kroon, J. M.; Janssen, R. A. J. Photoinduced Electron Transfer from Conjugated Polymers to TiO₂ *J. Phys. Chem. B* **1999**, *103*, 4352.

CHAPTER II

THE INFLUENCE OF SURFACE CHEMISTRY ON THE BINDING AND ELECTRONIC COUPLING OF CADMIUM SELENIDE QUANTUM DOTS TO SINGLE CRYSTAL TITANIUM DIOXIDE SURFACES

This dissertation chapter contains the manuscript of a research article published in *Langmuir* **2010**, 26 (7), 4839-4847. Atomic force microscopy and photocurrent spectroscopy were employed to correlate the morphology of CdSe quantum dots deposited on TiO₂ single crystals by various surface chemical procedures with the photo-excited electron transfer yields.

The following are contributions to this article from Justin B. Sambur: (i) prepared nanocrystal samples and single crystal electrodes, (ii) performed all AFM and photocurrent measurements; (iii) co-wrote the manuscript with Prof. Parkinson and responded to reviewer comments in order to publish the manuscript in *Langmuir* in it's current form.

The Influence of Surface Chemistry on the Binding and Electronic Coupling of CdSe Quantum Dots to Single Crystal TiO₂ Electrodes

Justin B. Sambur, Shannon C. Riha, DaeJin Choi and Bruce A. Parkinson

II.1 Abstract

Sensitization of mesoporous nanocrystalline TiO₂ solar cells with quantum confined semiconductor nanocrystals (QDs) has some advantages over organic dyes or inorganic complex sensitizers, yet the reported efficiencies of laboratory devices are not currently competitive with dye sensitized cells. Several methods previously utilized to bind CdSe QDs to mesoporous TiO₂ films were investigated using low index faces of both anatase and rutile TiO₂ polytypes as model systems. The *in situ* ligand exchange method, where 3-mercaptopropionic acid (MPA) covered TiO₂ crystal surfaces are treated with trioctylphosphine (TOP)/trioctylphosphine oxide (TOPO) TOP/TOPO-capped CdSe QDs, resulted in very irreproducible and usually low sensitized photocurrents. The *ex situ* ligand exchange method, whereby MPA-capped QDs are synthesized and directly adsorbed onto bare TiO₂ single crystals, resulted in both reproducible sensitized photocurrents and surface coverages that are verified with atomic force microscopy (AFM). Purification of the nanocrystals and adjustment of the pH of the sensitization solution to >10.2 was found to prevent QD agglomeration and takes advantage of the dual chemical functionality of MPA to directly link the QDs to the TiO₂ surface. The spectral response of the incident photon-to-current

efficiencies of CdSe QDs were directly compared to the commonly used sensitizer *cis*-di(thiocyanato)-bis(4,4'-di-carboxy-2,2'-bipyridine)ruthenium(II) (N3) on the same single crystals.

II.2 Introduction

Dye sensitized solar cells (DSSCs) represent a cheap and potentially scalable low cost photovoltaic technology.[1] Colloidal semiconductor quantum dots (QDs; e.g. CdS[2-10], CdSe[11-37], InAs[38], InP[39], PbS[40], etc.) are attractive alternatives to molecular dyes as sensitizers for wide band gap oxide materials such as SnO₂, ZnO, and TiO₂. Potential advantages of quantum dot sensitized solar cells (QDSSCs) include: 1) increased light absorption due to very high molar extinction coefficients of $\sim 1 \times 10^5 \text{ cm}^{-1}\text{M}^{-1}$ at the first excitonic peak in comparison with $\sim 1.3 \times 10^4 \text{ cm}^{-1}\text{M}^{-1}$ for typical Ru-based dyes, 2) increased stability due to the inorganic nature, 3) due to quantum confinement effects the manipulation of particle size and composition allows for optimization of spectral matching to the solar spectrum, and lastly 4) potentially increased efficiency from high energy photons (more than twice the QD band gap) that could generate multiple excitons per incident photon, although the efficiency of this phenomena in QD materials versus bulk semiconductors is still being debated.[41-49] Despite such potential advantages, a major breakthrough in the power conversion efficiency of QDSSCs that equals or exceeds typical Ru-based DSSCs has not been reported.

As previously discussed in a comprehensive review by Hodes, several fundamental issues differentiate QDSSCs from DSSCs.[50] These issues

include: 1) multiple layers of QDs adsorbing on the oxide surface, 2) new electrolyte compositions and 3) new charge recombination pathways due to the plethora of QD surface states.[50] Despite the need for research on such important issues, recent papers on QDSSCs report problems with low QD adsorption and irreproducibility between multiple devices with identical surface modification procedures.[36,51] Given the poor initial performance and indications of irreproducibility it appears that fundamental studies are needed to shed light on the underlying chemistry and mechanisms governing the poor initial performance of QDSSCs when compared to DSSCs.

In order to circumvent QD adsorption problems in mesoporous TiO_2 films, several research groups avoided the use of separately synthesized colloidal quantum dots and instead utilized chemical bath deposition or successive ionic layer adsorption and reaction (SILAR) to grow semiconductor QDs directly on the oxide architecture.[52-60] Although these techniques ensure high optical densities in the visible region, the precise control of particle size and crystallinity, afforded by typical bulk solution-based syntheses, are sacrificed. In addition, many pioneering studies of multiple exciton generation and two-photon absorption processes have been performed on nearly monodispersed colloidal QDs prepared via bulk solution-based methods due to the high quality of these nanomaterials.[61,62]

Our research group has extensively used dye sensitization on single crystal surfaces as a simplified model system for investigating the basic processes associated with charge injection into a semiconductor electrode.[63-

66] The well-characterized surfaces of single crystals are ideal for correlating the amounts and structure of QD and dye molecules on the semiconductor surface via scanning probe microscopies and other optical and electrochemical techniques. Photoelectrochemical measurements provide information concerning the yields of electron transfer and regeneration rates. Using these complementary techniques we evaluate the efficacy of the predominant surface chemistries used to covalently bind *colloidal* CdSe QDs to TiO₂. In addition, competitive adsorption experiments, with ligands commonly used in excess to kinetically stabilize QDs, revealed that they can strongly influence QD adsorption and thus sensitized charge injection.

II.3 Experimental Methods

Materials. Cadmium acetate dihydrate, cadmium oxide, 3-mercaptopropionic acid (MPA), sodium hydroxide, sodium sulfide, sodium sulfite, selenium powder, tetraethylammonium hydroxide, tetrabutylammonium perchlorate, tetradecylphosphonic acid (TDPA), tri-n-octylphosphine (TOP, tech grade 90%), tri-n-octylphosphine oxide (TOPO, 99%) were all of the highest purity unless otherwise stated and purchased from Sigma Aldrich. Acetonitrile, ethanol, and isopropyl alcohol were all of ACS grade and purchased from Sigma Aldrich.

Co(dtb)₃²⁺ (where dtb = 4,4'-di-*tert*-butyl-2,2'-bipyridine) was synthesized according to literature procedures and *cis*-di(thiocyanato)-bis(4,4;-di-carboxy-2,2'-bipyridine)ruthenium(II) (N3) was provided by Dr. C. Michael Elliott at Colorado State University. MPA-capped CdSe QDs were purchased from Ocean

Nanotech (Springdale, Arkansas). In the text these QDs will be referred to as ON-MPA/CdSe QDs.

Preparation of TOPO/TOP-capped CdSe QDs. TOPO/TOP-capped CdSe QDs were prepared by a method previously published by Peng and co-workers.[67] Briefly, 51.4 mg of CdO, 223.2 mg of TDPA and 3.7768 g of TOPO were placed in a 3-neck flask and heated to approximately 300 °C under argon flow to form a homogenous colorless solution. The temperature was then lowered to 270 °C and the selenium precursor consisting of 51.4 mg Se powder dissolved in 2.0 g TOP was swiftly injected. The reaction was allowed to proceed until the desired particle size was achieved, at which point the heating mantle was removed. The unpurified nanocrystals were stored in the dark under ambient conditions. In order to remove excess TOPO/TOP from the stock reaction mixture, 100 µL aliquots of stock were precipitated with methanol and centrifuged at 3000 rpm. The supernatant was discarded and the nanocrystals were dried under a nitrogen stream. The nanocrystals were then re-dissolved in toluene and the washing procedure was repeated three times. These QDs will be referred to as TOP/TOPO-capped CdSe QDs.

Preparation of MPA-capped CdSe QDs. MPA-capped CdSe QDs were prepared by a method adapted from previously published work by Chen *et al.*[68] In a 3-neck round bottom flask, a solution of 64.0 mg (0.24 mmol) of cadmium acetate dihydrate and 50.2 µL (0.58 mmol) of MPA in 100 mL of 18 MΩ Millipore water was adjusted to pH 10.5 with NaOH. After degassing for 30 minutes with N₂ a 5 mL aqueous solution of sodium selenosulfate (prepared by sonicating 1.3 mg Se

powder and 5.0 mg sodium sulfate for several hours until the selenium completely dissolved) was swiftly injected via syringe while continuously purging with nitrogen for an additional 30 minutes. The reaction was monitored for several days with until a desired particle size, derived from the spectral position of the first excitonic feature in the UV-Visible absorption spectrum, was obtained. The heating mantle was removed and the nanocrystal stock solution was stored in the dark under ambient conditions. In order to purify the stock reaction mixture, 500 μ L aliquots were precipitated with isopropyl alcohol and centrifuged at 3000 rpm. The supernatant was discarded and the nanocrystals were dried under a nitrogen stream. The nanocrystals were then re-suspended in Millipore water and the pH was adjusted to 10.5 with tetraethylammonium hydroxide. These QDs will be referred to as Aq-MPA/CdSe QDs.

Preparation of TiO₂ single crystal surfaces. Mechanically polished crystals of rutile (110), (100) and (101) were obtained from Commercial Crystal Laboratories. The anatase samples were naturally occurring mineral crystals that were mined in Hargvidda, Tyssedal in Norway. These bipyramidal crystals exhibited low-energy growth surfaces with large wedge-shaped (101) faces and (001) end caps. The crystals were polished and annealed according to our previously published procedures.[69] The crystals were mounted on copper disks with Ga/In eutectic to ensure an ohmic contact. A copper wire was soldered to the back of the disk and fed through a glass rod, at which point the entire electrode was sealed with epoxy (Epotek 377) and silicone rubber (RTV) and allowed to dry for a few hours. Prior to dye or QD sensitization, the crystals were

gently polished for 30 seconds with a soft polishing cloth using 20 nm colloidal silica (Buehler, Inc.), followed by a 5-10 second immersion in 10% aqueous HF solution and rinsing with copious amounts of 18 M Ω Millipore water. The electrodes were then illuminated at 1.0 V versus a stainless steel wire in 1 M HCl for 20 min using 370 nm UV light emitting diodes in a quartz photoelectrochemical cell. The strongly oxidizing holes generated during the UV treatment process greatly enhanced the sensitization yields by removing unwanted contaminants from the TiO₂ surface.[64] Following UV treatment, the electrodes were immediately rinsed with Millipore water, dried with a nitrogen stream for 5 seconds, and immersed in either toluene/aqueous 0.4 mg/ml QD dispersions or 1.0 mM ethanolic dye solutions in the dark for 5 min. Prolonged exposure to either sensitizer did not result in higher photocurrent yields. The electrodes were *immediately* rinsed with the same solvent and dried with N₂ prior to photoelectrochemical or atomic force microscopy measurements. To determine if contamination of any dissolved epoxy in the organic solvent affected the TOP/TOPO-capped QD surface coverage, 10 ml of QDs were pipetted directly on the electrode surface for 5 min and subsequently rinsed and dried with nitrogen. The results did not differ from electrodes completely immersed in the toluene TOP/TOPO-capped dispersion.

Photoelectrochemical measurements. Photoelectrochemical measurements were performed at short circuit in a two-electrode configuration with a platinum wire counter electrode. Two electrolytes were employed: 1) 10 mM Co(dtb)₃²⁺ mediator with 0.10 M tetrabutylammonium perchlorate supporting electrolyte in

acetonitrile and 2) 10 mM Na₂S, 10 mM S in 0.1 M NaOH. The electrolyte was not deoxygenated unless specifically stated. Incident photon to current efficiency spectra were measured using a Stanford Research Systems (SRS) model SR570 low noise current preamplifier connected between the working and counter electrodes. The signal from the pre-amplifier was then fed into a SRS model SR830 DSP lock-in amplifier. Illumination from a 100 W Oriel lamp (385 nm cut-off filter) was passed through a computer controlled grating monochromator (2 nm step interval) and chopped at 10 Hz to provide a modulated photocurrent signal. The raw photocurrent signal was corrected for photon flux using a lamp power spectrum recorded at 2 nm intervals using a thermopile detector.

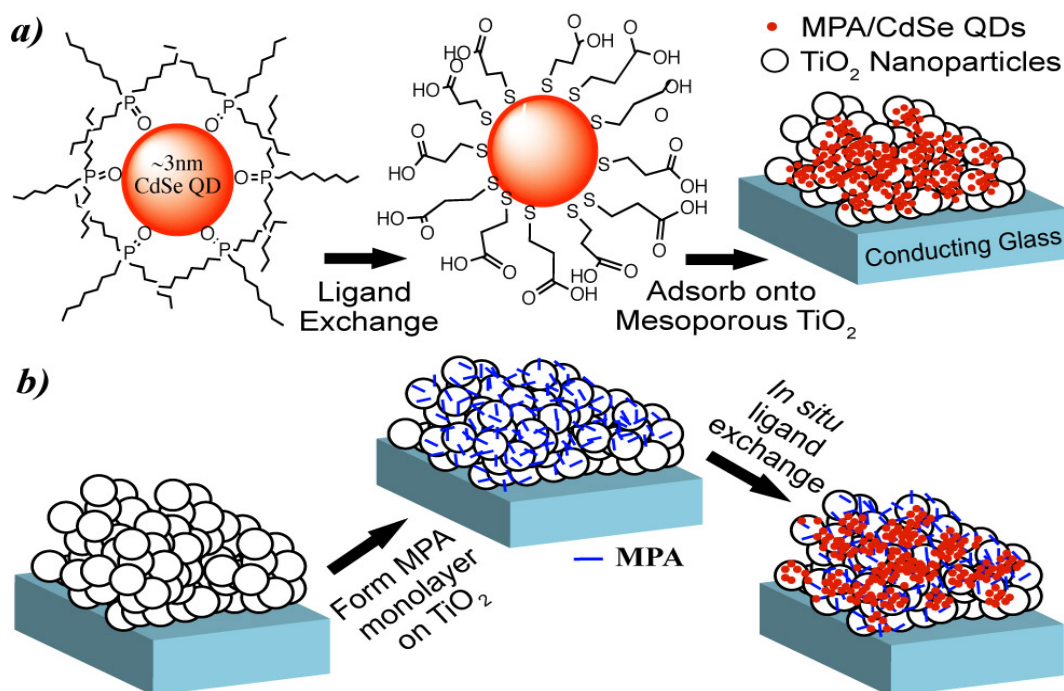
Atomic force microscopy (AFM) measurements. Tapping mode AFM (Digital Instruments Nanoscope IIIA controller and a multimode SPM) was used to characterize the polished surface. TETRA-18 boron doped silicon tips from K-Tek Nanotechnology with a 3.5 N/m force constant and resonant frequency of ~90 kHz were used. Images were processed using WSxM (Nanotec Electronica) software.[70]

II.4 Results and Discussion

We will first evaluate the primary strategies employed in the QDSSC literature to deposit *colloidal* CdSe QDs onto TiO₂ nanoparticle films. We used photocurrent spectroscopy to compare the various CdSe QD deposition techniques and their sensitization yields with those of N3 dye on the same single crystal surfaces. The morphology of the QDs on the surface resulting from each

deposition technique was determined via AFM measurements and related to the photocurrent yields. The results presented herein are similar on rutile (110), (100) and (101) and anatase (101) and (001) surfaces.

High quality monodisperse semiconductor quantum dots are generally prepared via the hot injection method in an excess of bulky organic surfactants.[67,71] Interest in applications of quantum dots has led to elegant techniques to exchange the bulky organic surfactants for polymers, peptides, amino acids or other small molecules of varying chemical functionality that are useful in particular applications.[72-74] The ligand exchange strategies, and the general surface modification methods used to bind colloidal QDs to TiO₂, are illustrated in Schemes 1a and 1b. Scheme 1a involves the *ex-situ* ligand exchange of reversibly bound, bulky organic ligands (typically TOPO/TOP) for a bi-functional linker molecule (typically MPA). Scheme 1b illustrates the *in-situ* ligand exchange process, whereby a freshly prepared TiO₂ nanoparticle film is first exposed to a concentrated solution of MPA, rinsed with excess solvent, and then exposed to a solution of unmodified QDs (e.g. capped with TOP/TOPO, oleic acid, pyridine etc.). The literature on the surface chemistry of titanium dioxide and metal chalcogenides suggest that the thiol and carboxylic acid moieties of MPA would bind to the QD and oxide surfaces, respectively.[75] We also evaluated direct adsorption of TOPO/TOP capped QDs from an organic solvent which has been reported by Guijarro *et al.*[36]



Scheme 1. Cartoon illustrating the (a) *ex situ* ligand exchange method whereby bulky organic TOP/TOPO ligands are replaced with a bifunctional linker molecule (e.g. MPA) prior to QD adsorption on TiO₂ and the (b) *in situ* ligand exchange method where MPA is adsorbed on TiO₂ first and subsequently exposed to TOP/TOPO capped QDs.

We initially studied TOP/TOPO-capped CdSe QD sensitization on TiO₂ single crystals using both direct adsorption and the *in-situ* ligand exchange technique due to their synthetic simplicity and wide use in the literature. Figure 1 shows typical IPCE spectra of various ~2.8 nm CdSe QDs exposed to a MPA modified rutile (101) TiO₂ surface (MPA-TiO₂). The photocurrent response for N3 dye on the same rutile (101) single crystal is shown for comparison. For thoroughly washed TOP/TOPO-capped CdSe samples, the IPCE values at the first excitonic peak, as well as wavelengths to the blue, were comparable to the peak IPCE value for N3 and mimicked the solution absorption spectrum of the QDs in toluene. Exposure of the crystal to an unwashed aliquot from the same

stock solution of QDs produced no measurable photocurrent. An intermediate regime using a ~50,000x dilution of the original stock solution of QDs in toluene exhibited an ~80% decrease in the IPCE value at the first excitonic peak compared to the thoroughly washed sample.

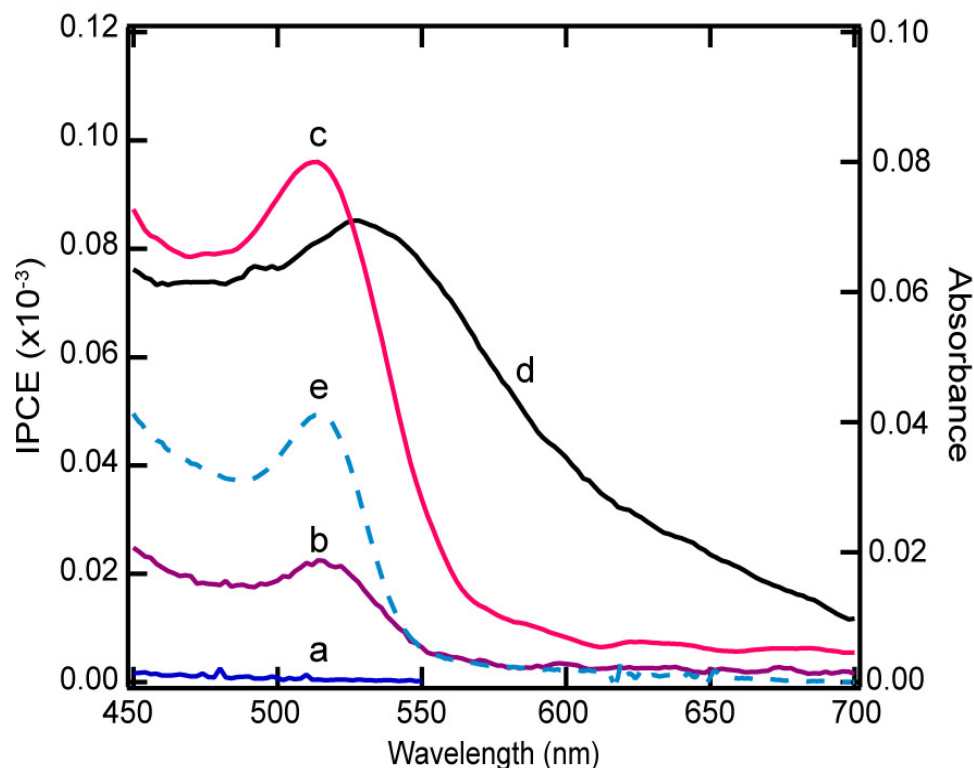


Figure 1. IPCE spectra of (a) unwashed, (b) dilute, and (c) thoroughly washed TOP/TOPO-capped CdSe QDs adsorbed on an MPA-modified rutile (101) TiO₂ single crystal measured at short circuit in an acetonitrile electrolyte with Co(dtb)₃²⁺ as a mediator. The IPCE of spectra of N3 dye (d) on the same unmodified TiO₂ crystal is shown for comparison. The solution absorbance spectra of the TOP/TOPO-capped CdSe QDs in toluene (e) is also shown.

Although the trend in Figure 1 suggests excess TOP/TOPO in the sensitization solution inhibits QD binding or somehow prevents photocurrent

generation at the QD/TiO₂ interface, the reproducibility of photocurrent generation employing either the *in-situ* ligand exchange or direct adsorption technique was less than 10%. However, the poor results with these surface chemistry techniques to produce sensitized photocurrent on TiO₂ single crystals is in stark contrast to the implementation of both strategies on nanocrystalline TiO₂ films. Despite the irreproducibility using either strategy, the trend in Figure 1 indicated that the presence of excess organic surfactant decreased the photocurrent yield either due to inefficient QD adsorption or poor electron (hole) injection from the QDs to the TiO₂ conduction band (electrolyte). Figure 2a shows an AFM image of an atomically smooth rutile (110) TiO₂ crystal with remnants of the colloidal silica polish embedded into the surface; these particles can be removed by a 20 minute sonication in water. After modification with MPA, the rutile (110) crystal was exposed to unwashed TOP/TOPO-capped QDs (Figure 2b). In some regions of the surface the adsorbed unwashed TOP/TOPO-capped QDs showed a single layer of individual QDs whereas large agglomerated QD structures (some exceeding 125 nm in height) dominated the surface (Figure 2c). The small photocurrent signals perhaps originate only from the QDs in the first layer (Figure 2b), where there exists sufficient electronic coupling between the QDs and TiO₂. Thus the source of the inconsistency in the photocurrent measurements is likely due to QD agglomeration (Figure 2c). Agglomeration is a dynamic process governed by several factors (e.g. ligand concentration, temperature, solvent, light exposure) that dictate the adsorption/desorption of ligands that kinetically stabilize the QDs. We attribute

the streaking in the regions between the QDs in Figure 2b to residual soft organic TOP/TOPO ligands, which dampens the interaction of the tip with the hard TiO₂ substrate under the low applied tapping force. The physisorbed ligands may be manipulated, moved or picked up by the tapping AFM tip during scanning. Phase imaging of the surface showed differences in the relative hardness between bare TiO₂ and TOP/TOPO-covered regions. The excess organic ligands may also prohibit many TOP/TOPO-capped QDs from binding to the surface. Whereas Guijarro *et al* reported less agglomeration using MPA-modified TiO₂ surfaces under slightly different experimental conditions, we did not observe differences in surface coverages with bare (direct adsorption) or MPA-modified surfaces.[36,76] However photocurrent measurements were not correlated with QD coverages determined via AFM on their single crystal substrates.

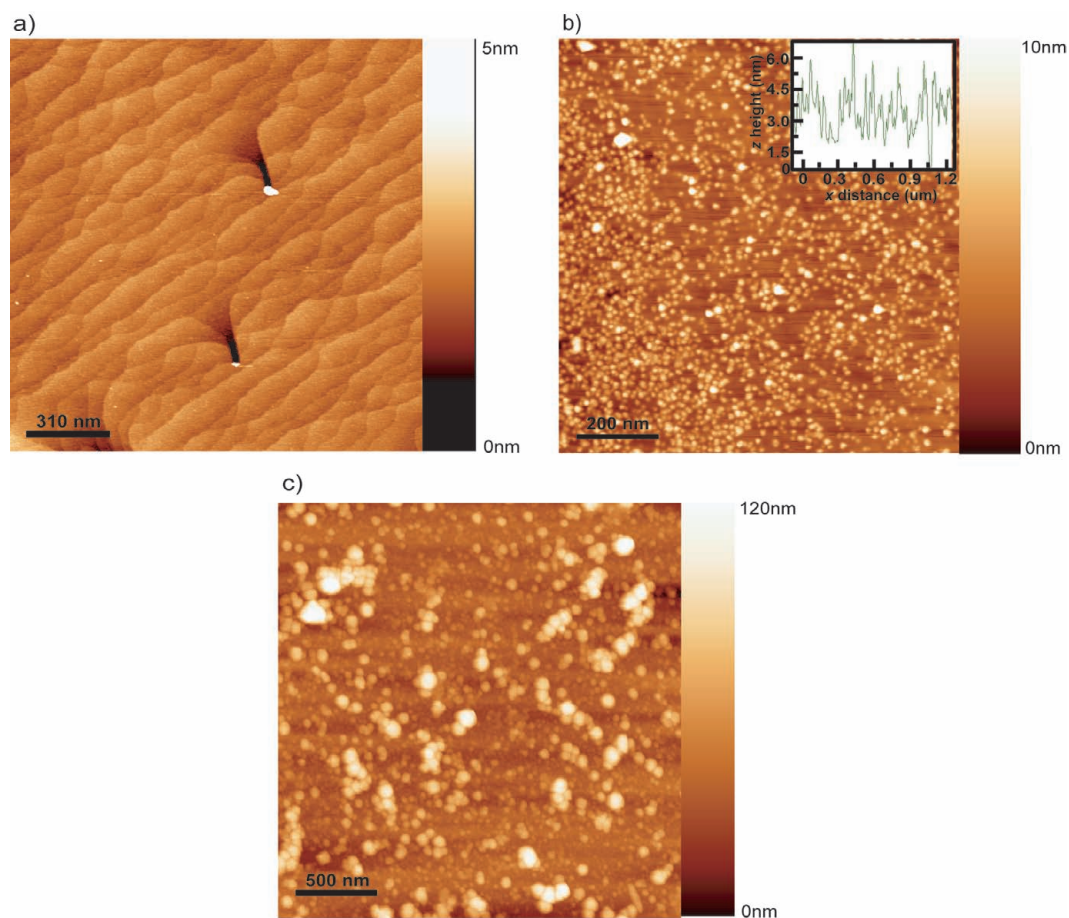


Figure 2. AFM images of (a) bare rutile (110) TiO_2 , (b) after modification with MPA and exposure to unwashed TOP/TOPO capped QDs from toluene and (c) more common regions showing QD agglomeration.

The deleterious effect of excess organic surfactant (in this case TOPO/TOP) on the observed photocurrent yields for unwashed and dilute TOP/TOPO capped CdSe QDs is best understood from the previous work on ligand dynamics of colloidal QDs.[76] In the presence of excess organic ligand, the equilibrium expression for bound versus vacant surface sites favors bound sites, thus stabilizing the nanocrystals. Therefore sensitization by unwashed QDs on MPA- TiO_2 surfaces is not favored due to the high concentration of bulky organic surfactants in the sensitization solution preventing MPA penetration into

the TOPO/TOP ligand shell that would be required for good electronic coupling to the surface via *in situ* ligand exchange. In the case of diluted QD samples, TOPO/TOP desorbing from the nanocrystal surface is not immediately replaced by excess ligand, exposing reactive nanocrystal surface binding sites. These reactive surface sites also lead to agglomeration of the partially TOP/TOPO-capped nanocrystals (Figure 2c). The inefficiency of the *in situ* ligand exchange process for thoroughly washed QD samples is readily explained by the pH dependence of the dissociation of thiolate ligands from CdSe nanocrystals reported by Peng and co-workers.[77,78] Through a pseudo steady-state titration method it was demonstrated that 2.8 nm CdSe QDs precipitated at approximately pH 5 could be subsequently re-dissolved in basic solution (pH 9.5). The precipitation of CdSe nanocrystals was attributed to the protonation of the thiol group of MPA ($pK_a^{SH} = 10.2$). The sensitization solutions in this study were adjusted to pH 10.5 because to deprotonate the SH group allowing it to bind to Cd sites on the QD surface without the need for excess MPA. However the *in situ* ligand exchange is performed in organic solvents that stabilize the organic-capped QDs, and thus deprotonation of the surface-bound thiol is not favored. As a result, the thiolate-Cd bond is not formed and nanocrystals are not covalently linked by MPA to the TiO₂ surface via MPA. Therefore we propose that the *in situ* ligand exchange process on single crystal TiO₂ substrates does not result in covalently bound QDs, and rather the bare, reactive surfaces of some CdSe QDs are physisorbed to MPA or unmodified TiO₂ surfaces in an uncontrolled fashion.

It is interesting to note that we do not observe a shift in the QD IPCE spectrum when compared to the solution absorption spectrum, as is the case for monomeric molecular dyes adsorbed on single crystals.[79] The spectral shift for adsorbed dyes is attributed to the change in the dielectric environment of the surface bound dye when compared to the bulk solution. Qualitatively, the much larger, nearly spherical QD has only a portion of its surface influenced by the different dielectric constant of the semiconductor surface in comparison to a molecular dye. Recent papers have attributed the red shift in the IPCE spectra for QDs adsorbed on mesoporous TiO₂ films to agglomerated QD structures.[36,80,81] If QD agglomeration does indeed lead to a red shift in the IPCE spectra, then our results suggest that the agglomerated QD structures do not effectively inject electrons into TiO₂ crystals.

Another important issue regarding the chemistry of the *in-situ* ligand exchange is the fate of the bulky organic surfactants that initially cap the CdSe QDs. In a recent report by Kamat and co-workers, a residual phosphorous peak was found in the energy dispersive X-ray spectroscopy (EDS) spectra after the ligand exchange process.[34] The presence of phosphorus may be unavoidable considering the previous discussion and the following complications. It is known from ultra-high vacuum (UHV) studies that acetic acid monolayers can protect the atomic cleanliness of a freshly prepared TiO₂ crystal surfaces removed from the vacuum and exposed to air for subsequent re-introduction into the UHV chamber.[82] Moreover, exposure to a solution of longer-chain carboxylic acids under ambient conditions was found to displace the acetic acid monolayers. If

one also considers the careful studies by Buhro and co-workers, who identified the important effects of various impurities in commercially obtained organic chemicals on a conventional synthesis of QDs, there may be several phosphonic acid impurities present in any given QD stock solution if careful purification of starting materials was not undertaken.[83] Depending on a specific washing procedure and sample purity, hydrophobic interactions between the long chain hydrocarbon tails of QD ligands may allow for phosphonate head groups to protrude from the organic ligand shell. In addition, it is well known that phosphonates bind more strongly to TiO_2 than carboxylates, and thus it appears to be essential to avoid the presence of excess organic ligands and capping agents during the CdSe QD adsorption process.[84]

To further illustrate the subtle competitive adsorption effects of certain organic impurities resulting from *in-situ* ligand exchange, and shed light on the issues of irreproducibility of QD binding on MPA-modified TiO_2 single crystals, we exposed a variety of modified TiO_2 surfaces to N3 dye solutions. N3 was chosen for its wide spread use and similar carboxylate- TiO_2 binding motif. Figure 3 shows the IPCE spectra of N3 adsorbed on TOPO, MPA and TOP modified anatase (001) TiO_2 crystals. The results were similar when MPA, TOP and TOPO were simultaneously dissolved with N3 in methanol (TOP experiment performed in a drybox). TOPO and MPA did not inhibit N3 binding, whereas TOP significantly inhibited N3 binding. N3 photocurrent spectra on bare anatase (001) surfaces were similar to the MPA and TOPO modified TiO_2 surfaces. The IPCE values for the N3 spectra on the rutile (101) surface in Figure 1 were lower

than IPCE values shown for the anatase (001) surface in Figure 3. We previously studied the kinetics of N3 dye adsorption and its photocurrent spectra on anatase (101), anatase (001), rutile (100) and rutile (001) surfaces.[64] The IPCE differences between the different TiO₂ polymorphs and surface orientations were attributed to different N3 binding geometries and reactivity of the surface binding sites. In addition, variability between crystals of the same surface orientation may be due to differences in doping density and lattice defects, which are especially important for naturally occurring anatase crystals with natural dopants and impurities. In contrast to dyes adsorbed on different TiO₂ crystal surfaces, distinct differences in the QD sensitized photocurrent yields due to a specific TiO₂ polymorph or surface orientation are not observed. This can be rationalized when considering the “lattice matching” criteria that we proposed to explain the variation of N3 and dicarboxylated thiocyanine dyes on the various low index TiO₂ surfaces. The rigidity of the bonding on a molecule such as N3, and the need to attach it to the surface by more than one binding site, requires a match between the distances between the carboxylate groups on the dye and the unsaturated Ti sites on the crystal surface. The large size of the QDs and the large numbers of carboxylate groups on their surface may obviate the lattice matching criteria and may result in many more linkages than from a small molecule. Due to the slight variability between crystals (especially the natural anatase) of the same surface orientation, IPCE spectra of all CdSe QD samples were compared to N3 dye on the same single crystal.

Although the competitive adsorption measurements involving N3 do not explain the irreproducibility of QD binding due to the tremendous size difference of the two sensitizers, their similar carboxylate linkages to TiO_2 indicates that the washing procedure is essential to remove trace amounts of TOP or phosphonic acid impurities in TOPO prior to sensitization. This effect may be even more important for reversibly bound oleic acid-capped QDs, whereby the long chain carboxylate desorbs from the QD surface and could displace TiO_2 -bound MPA molecules.[35] More detailed investigations are underway regarding the various TOPO impurities, as well as other organic ligands commonly used to cap the CdSe QDs, and the effects of competitive adsorption on QD binding to TiO_2 .

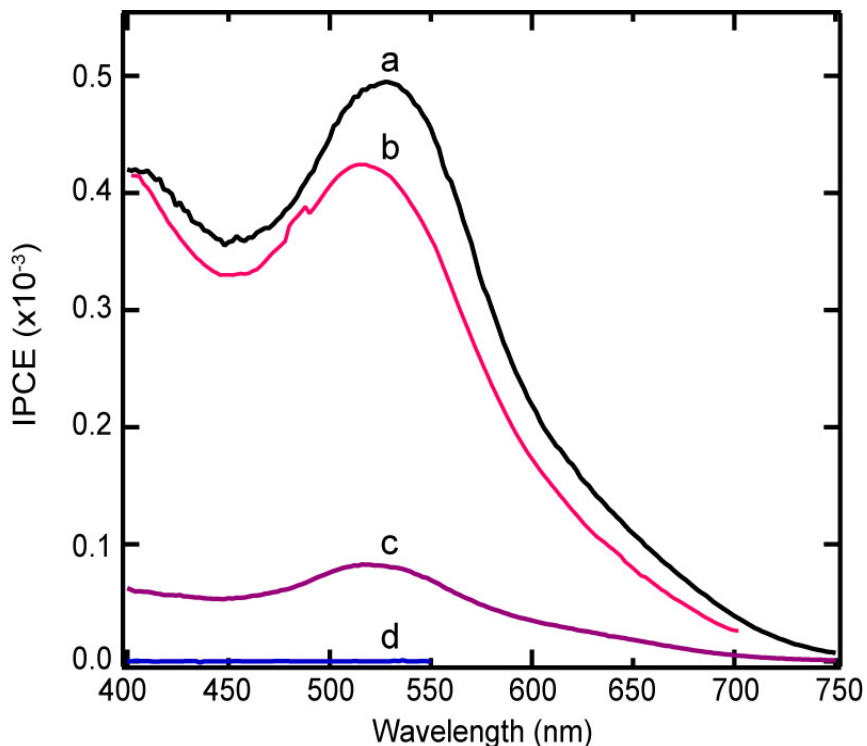


Figure 3. IPCE spectra of (a) N3 on TOPO-modified, (b) MPA-modified and (c) TOP-modified TiO_2 surfaces on an anatase (001) TiO_2 single crystal measured at short circuit in an acetonitrile electrolyte with $\text{Co}(\text{dtb})_3^{2+}$ mediator. N3 photocurrent spectra on bare anatase (001) (d) surfaces were similar to the MPA and TOPO modified TiO_2 surfaces.

Despite such observations regarding the *in situ* ligand exchange process on single crystal TiO₂ substrates, the reported power conversion efficiencies of QDSSCs prepared by the *in-situ* ligand exchange technique are in the range of 1-2%.^[51] Moreover, use of surface chemistry strategies to adsorb CdSe QDs on TiO₂ was not essential to achieve moderate power conversion efficiencies. Studies by Nozik and co-workers with TOP/TOPO capped InAs QDs demonstrated a power conversion efficiency of 0.3% and 1.7% at one and ~0.05 sun, respectively.^[38] Likewise, Gimenez *et al.* avoided the use of ligand exchange altogether and rather identified sensitization time and solvent to be critical for direct CdSe QD adsorption on TiO₂.^[85] Gratzel and co-workers reported in some experiments with the reversibly bound ligand pyridine capping the CdSe QDs that substantial adsorption onto TiO₂ nanoparticle films could be achieved without the use of linker molecules (although their best results did use MPA).^[51] Although their pyridine-capped CdSe QDs allowed for the use of polar solvents, the pH of their sensitization solutions was not sufficiently basic to allow thiolate binding to the bare CdSe surface. Thus, it is not clear whether the MPA linker was absolutely essential or even useful during the *in situ* ligand exchange process or if the QDs were simply physisorbed in the pores of TiO₂ nanoparticle films.

Due to the poor IPCE values and irreproducibility with the *in-situ* ligand exchange technique, that we believe is primarily due to the inability to effectively form the MPA-nanocrystal bond and competitive adsorption of organic ligands

with the sensitizers, we sought to avoid the use of organic capping ligands altogether. In theory the *ex-situ* ligand exchange removes organic capping groups prior to exposure to the oxide and produces MPA-capped CdSe QDs capable of being suspended in polar solvents whose carboxylic acid functional groups can bind directly to TiO₂ surfaces. In practice however, we found the ligand exchange technique to be non trivial and time-consuming (often 12-24 hr). In some cases, residual organic ligand is still present on the QD surface.[86] Although the technique is reliable and effective for producing MPA-capped QDs, our efforts to reproducibly rely on the *ex-situ* ligand exchange technique to yield stable water or methanol stock solutions of suspended QDs were unsuccessful (often the QDs precipitated in <12 hr under ambient conditions). Instead we employed a synthesis developed by Chen *et al*, whereby MPA-capped CdSe QDs were prepared directly in water and the use of organic surfactant ligands is completely avoided.[68] Among the advantages of the aqueous synthesis is the flexibility in choice of the short-chain organic acid capping ligand (e.g. cysteine, thioglycolic acid, etc.), mild synthetic conditions, as well as the stability of the QD suspensions under ambient conditions. A broad size-distribution is often obtained and we have been unable to synthesize larger QDs with a first excitonic peak maxima at wavelengths >550 nm despite 10 days of continuous refluxing during growth.

The results with CdSe QDs prepared via the aqueous approach (Aq-MPA/CdSe) will now be compared to commercially prepared MPA-capped QDs (ON-MPA/CdSe) that used organic ligand exchange. Figure 4 shows the optical

absorption and corresponding photoluminescence spectra of our as-prepared Aq-MPA/CdSe QDs in water. Indeed the nanoparticles demonstrate quantum confinement effects, as their first excitonic peaks shift to longer wavelengths with increasing reaction time. The ~ 40 nm full-width half-maximum value of the photoluminescence spectra indicates a broad size distribution, to be expected for the long incubation period adopted to grow the larger particles. Although adjustments to the synthesis can be made to prepare larger particles in a shorter reaction time, we were mainly interested in avoiding the use of organic ligands in the reaction to directly synthesize MPA-capped QDs.

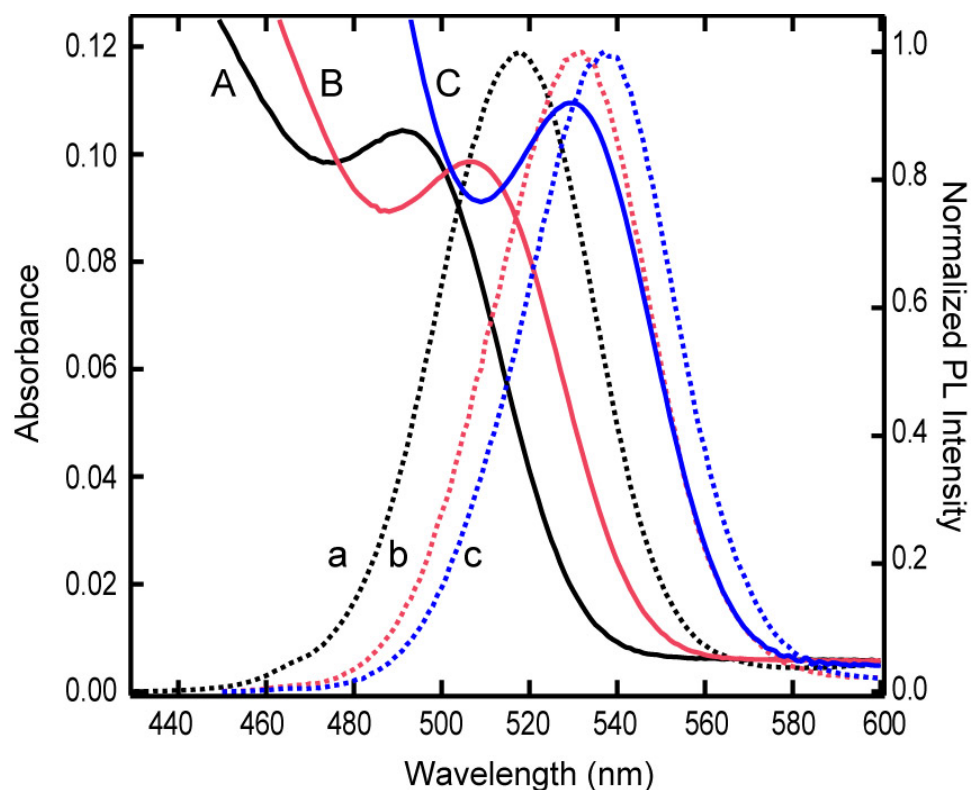


Figure 4. Solution absorbance (solid lines) and photoluminescence spectra (dashed lines) of MPA-capped CdSe QDs synthesized in water after 2 days (A,a), 4 days (B,b) and 7 days (C,c) reaction time.

When the as-prepared QDs were exposed to bare rutile and anatase TiO₂ crystal surfaces, no significant sensitized photocurrents were detected. The pH of the stock Aq-MPA/CdSe sample was 9.3 after 10 days of continuous refluxing. However, when stock Aq-MPA/CdSe aliquots were precipitated with isopropyl alcohol and re-suspended in water and adjusted to pH 10.5 with tetraethylammonium hydroxide, a significant, reproducible sensitization photocurrent signal was detected on a rutile (001) single crystal (Figure 5). Sensitized photocurrents with comparable yields were also obtained using purified Aq-MPA/CdSe QD dispersions (as well as ON-MPA/CdSe QDs) in the presence of excess MPA to adjust the sensitization solution to as low as pH 6.[77,78] The purification of the stock Aq-MPA/CdSe QDs was critical to achieve reproducible results, presumably due to removing unreacted precursor species from the stock mixture. Similar results were observed on other rutile crystal faces as well as anatase (001) and (101). The IPCE value of the MPA-capped QDs at the first excitonic peak exceeded that of N3 on the same rutile (001) crystal. If one considers the electron injection efficiency of photoexcited N3 into TiO₂ to be near unity, then comparing the photocurrents of both sensitizers on the same crystal implies the light absorption by the Aq-MPA/CdSe QDs at the first excitonic peak (and towards the high energy region), exceeds that of N3. This result was consistent with the measurement of the extinction coefficient ϵ for >3nm ligand exchanged CdSe QDs with hydrophilic thiols at the first excitonic peak (~530nm) of approximately $2 \times 10^{-5} \text{ cm}^{-1}\text{M}^{-1}$, whereas ϵ_{N3} at 532 nm is $1 \times 10^{-4} \text{ cm}^{-1}\text{M}^{-1}$. [87,88] However, due to the large size of the CdSe QDs it is likely

that dye molecules occupying the same volume as a 3-4 nm spherical QD will exhibit a greater light harvesting efficiency than the QDs. The benefit of employing an inorganic semiconductor sensitizer, with a high density of states in the high-energy region of the solar spectrum, is evident in the steep rise in photocurrent in the blue region of the spectrum. Previous studies by Gratzel and co-workers of CdSe QD sensitized nanocrystalline TiO₂ films did not exhibit the steep increase in photocurrent in the high energy region of the visible spectrum ($\lambda < 500\text{nm}$) where the light harvesting efficiency of the QDs is extremely high.[51] The poor response in the high energy region of the spectrum using TiO₂ single crystal substrates may be caused by absorption of incident light by the electrolyte, as we also observed similar poor IPCE values in the high energy region of the spectrum when either high concentrations of blue-light absorbing Co(dtb)₃²⁺ or sulfide/polysulfide mediators or long path lengths through the solution were used.

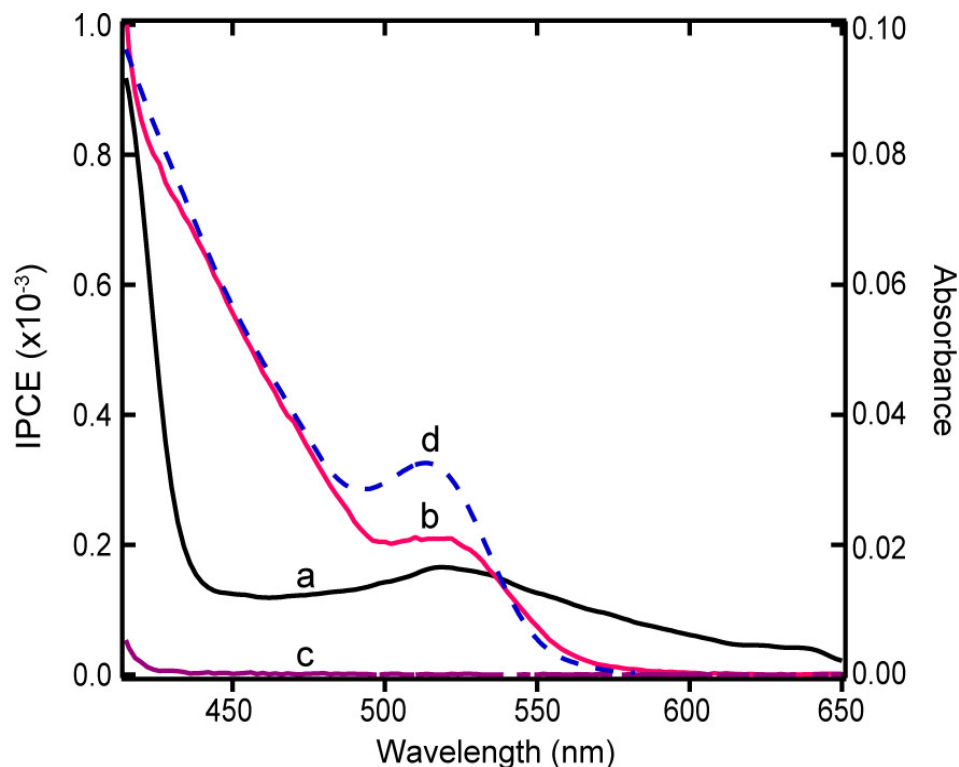


Figure 5. IPCE spectra of (a) N3 and (b) MPA-capped QDs synthesized in water on a rutile (001) TiO₂ single crystal measured at short circuit in an acetonitrile electrolyte with Co(dtb)₃²⁺ mediator. The IPCE spectrum of the bare crystal (c) and the absorbance spectrum of the MPA-capped QDs (d) in water is shown for reference.

Most importantly, the sensitized photocurrents obtained using MPA-capped QDs synthesized directly in water were extremely reproducible and very stable under extended illumination. These QD-sensitized electrodes showed no loss of photocurrent even after exposure to room lights in air for one week whereas N3-sensitized crystals showed some loss of photocurrent. Interestingly, the Aq-MPA/CdSe QDs were equally stable in both aqueous sulfide/polysulfide electrolyte and with the Co(dtb)₃ mediator in acetonitrile.

We also compared the adsorption of MPA-capped CdSe QDs prepared with both aqueous and organic synthetic approaches on TiO₂ single crystals.

Figure 6a shows the photocurrent spectra of commercially obtained ON-MPA/CdSe compared to N3 on the same anatase (001) crystal. The N3 IPCE spectrum was measured in an acetonitrile electrolyte with the $\text{Co}(\text{dtb})_3^{2+}$ mediator, whereas the ON-MPA/CdSe IPCE spectra were measured in a sulfide/polysulfide electrolyte initially and after 15 hr of continuous $40 \mu\text{W}/\text{cm}^2$ illumination at 580 nm. The choice of electrolyte was dictated by the stability of the ON-MPA/CdSe QDs, as shown in Figure 6b. In an air saturated electrochemical cell with a cobalt mediator, the ON-MPA/CdSe QD sensitized photocurrent immediately and irreversibly decayed. If the electrolyte was first purged with N_2 a steady photocurrent was measured for 2 h but decayed immediately if exposed to air. An $\sim 80\%$ decrease in the IPCE value at the first excitonic peak was measured when the sample was left in solution in the dark for several hours, suggesting that the cobalt mediator is not responsible for photocurrent decay but instead air oxidation of the QD sample is occurring. This sensitivity to air saturated electrolytes was not observed for Aq-MPA/CdSe QDs. In the case of the sulfide/polysulfide electrolyte, the photocurrent is extremely stable over the course of 15 hours.

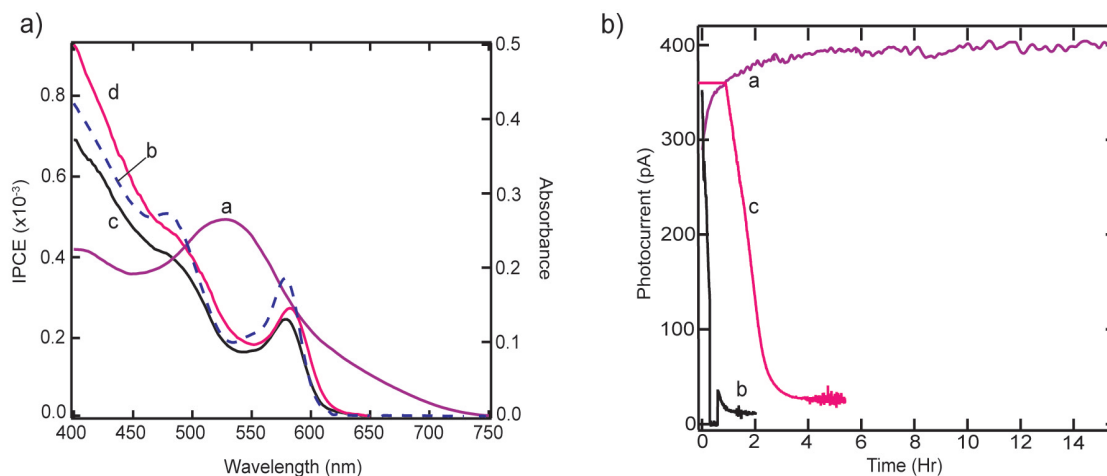


Figure 6. a) IPCE spectra of (a) N3 on an unmodified anatase (001) TiO_2 single crystal measured at short circuit in an acetonitrile electrolyte with a $\text{Co}(\text{dtb})_3^{2+}$ mediator. The solution absorbance spectrum in water (b) is compared with the IPCE spectra of (c) ligand exchanged MPA-capped QDs (purchased from Ocean Nanotech) initially and (d) after 15 hr illumination measured at short circuit in a sulfide/polysulfide electrolyte. Figure 6b shows the photocurrent versus time for the MPA-capped QDs adsorbed on the same crystal in (a) sulfide/polysulfide electrolyte, and (b) un-purged and (c) purged $\text{Co}(\text{dtb})_3^{2+}$ mediator in acetonitrile.

The contrasting behavior in sensitivity to oxidation between the ligand exchanged ON-MPA/CdSe QDs and Aq-MPA/CdSe QDs is intriguing. The ON-MPA/CdSe QDs and Aq-MPA/CdSe QDs are equally stable in basic pH solutions when stored in the dark. However, upon deposition onto TiO_2 single crystals, the ligand exchanged QDs developed an acute sensitivity to oxygen whereas the Aq-MPA/CdSe QDs were stable. Only when the sulfide/polysulfide electrolyte was employed, which acts as a scavenger for dissolved oxygen in the electrolyte as well as an efficient inner sphere hole scavenger for the QDs, did the photocurrents for the ligand exchanged QDs stabilize. Perhaps the surface chemistry of MPA on the ON-MPA/CdSe QDs differs from that of the Aq-MPA/CdSe QDs making them prone to oxidation. Further studies to elucidate the

reason for the stability difference between the two samples are currently underway.

Lastly, the morphology of ON-MPA/CdSe QDs and Aq-MPA/CdSe QDs adsorbed on the same rutile (110) crystal was investigated using AFM. In one preparation (Figure 7a), the rutile crystal was immersed in the QD sensitization solution followed by purposefully precipitating the QDs by adjusting the sensitization solution to $\text{pH} < 6$ with perchloric acid. A thin film of agglomerated Aq-MPA/CdSe QDs about 40 nm in height was observed in the AFM images. If the aqueous sample was adjusted to $\text{pH} 10.5$ a sub-monolayer surface coverage of QDs was observed (Figure 7b). The 6-7 nm z height of the Aq-MPA/CdSe QD 'monolayer' revealed that the QDs were stacked, because TEM showed a particle diameter of approximately 2.8 to 3.2 nm that was consistent with a diameter deduced from the optical absorption data.[87] Perhaps the bilayer structure of the Aq-MPA/CdSe helps to protect or stabilize the QDs directly linked to the TiO_2 surface by preventing surface oxidation and resulted in the increased stability compared to the monolayer structure of the ON-MPA/CdSe QDs. The monolayer of ON-MPA/CdSe QDs (Figure 7c) was very densely packed with fewer agglomerated or 'double-stacked' QD features than the Aq-MPA/CdSe QDs. The monolayer exhibited an average z height of approximately 3.0-3.5 nm, in excellent agreement with a single layer of QDs.

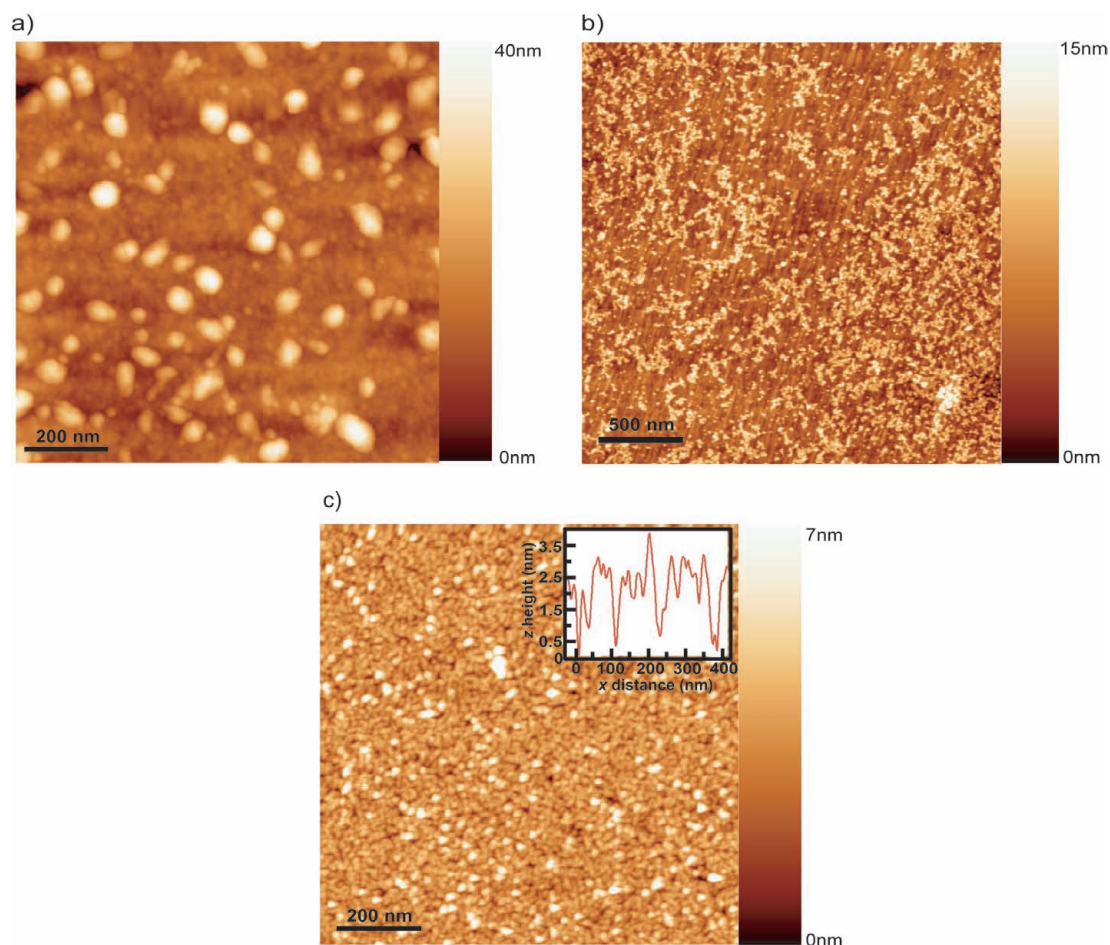


Figure 7. AFM images of (a) MPA-capped QDs synthesized in water and exposed to rutile (110) TiO_2 at pH 6 and (b) pH 10.5, Figure 7c shows MPA-capped CdSe QDs (Ocean Nanotech) adsorbed from pH 10.5 solution.

Several important concerns arise from the AFM results. First, when comparing our results with the images obtained by Guijarro *et al*, where agglomeration of QDs was also observed, it appears that the assumption of spontaneous QD monolayer formation on TiO_2 is not analogous to binding monolayers of molecular dyes through single or chelating chemical bonds.[36] In our experience the washing process was crucial to avoid QD agglomeration on the TiO_2 single crystal surfaces. However different QD batches may require similar subtle adjustments (e.g. pH, temperature, time, solvent) to achieve

uniform monolayer coverage. The situation becomes more complicated for nanocrystalline TiO₂ films, where all interfaces are not easily accessible both for adsorption, due to clogging pores on the outside of the film especially if QDs agglomerate, and to ensure efficient washing to remove physisorbed QDs that may not be electronically coupled to the substrate. Such QDs will contribute to the optical absorption but not to the photocurrent generation resulting in low absorbed photon-to-current efficiencies (APCE).

Secondly, the TOP/TOPO-capped QDs directly adsorbed from toluene onto bare TiO₂ crystals formed layers of relatively high coverage. However, our inability to consistently measure photocurrents from adsorbed TOP/TOPO-capped QDs with and without ligand exchange suggests that agglomerated TOP/TOPO-capped QDs do not inject electrons into the TiO₂ conduction band. Only when TOP/TOPO is desorbed, as proposed by Guijarro *et al*, do the QDs form a direct contact with the surface, as is the case for chemically deposited QD layers.[36] However desorption of TOP/TOPO produces unpassivated QDs that may be extremely prone to oxidation and/or agglomeration hindering both device stability and performance.

Our results indicate that on a given TiO₂ substrate the IPCE values of both MPA-capped QD samples for the high energy region (<500 nm or 2.5 eV) exceeds the maximum IPCE for N3 dye. Using larger CdSe QDs will increase spectral coverage, as well as shift the sharp photocurrent onset to longer wavelengths. However, there seems to be some disparity between our results with aqueous synthesized MPA-CdSe QDs on single crystal TiO₂ substrates and

those reported by Lee *et al.* and Mora-Seró *et al.* using aqueous synthesized QDs adsorbed on mesoporous TiO₂ films.[21,23] Lee *et al.* partly attributed their poor power conversion efficiencies (0.009% in a corrosive iodide electrolyte) to the negatively charged QDs inability to properly diffuse through the TiO₂ architecture. Mora-Seró *et al.* utilized surface photovoltage spectroscopy to demonstrate the efficiency of charge injection from various QD sizes, however a power conversion efficiency or IPCE values were not reported. We believe that if the pH of the sensitizing solution is not properly controlled to deprotonate the thiol group of MPA, covalent bonding of the QDs to the TiO₂ will not occur and instead physisorbed QDs will result, with much poorer electronic coupling to the surface and correspondingly low device efficiencies.

II.5 Conclusions

A variety of surface treatments were investigated in order to evaluate the efficiency of QD adsorption and subsequent sensitized photocurrent generation on single crystals of a variety of low index anatase and rutile surfaces. The *in-situ* ligand exchange of MPA-modified TiO₂ for TOP/TOPO-capped CdSe QDs yielded irreproducible sensitized photocurrents despite the direct observation of the presence of TOP/TOPO-capped QDs on the surface with AFM. The *ex situ* ligand exchange resulted in MPA-capped QDs that directly bind to TiO₂ after purification and adjustment of the sensitization solution to sufficiently basic pH (>10.2) so as to promote QD stability through thiolate-QD binding. AFM imaging of MPA-capped CdSe QDs on TiO₂ surfaces also showed near monolayer QD coverages. The sensitized photocurrent yields of these surfaces were

reproducible and on all crystal faces studied and the IPCE values of MPA-capped CdSe QDs exceeded the maximum IPCE value for N3 dye in the high-energy region (<500 nm or 2.5 eV) of the spectrum. Excess organic ligands (specifically TOP), if present during the *in situ* ligand exchange, may prevent QD binding or inhibit charge injection by agglomerating around the QDs. We believe that these results for TiO₂ single crystals will help guide the future development of high efficiency QDSSCs.

II.6 Acknowledgements

We would like to thank Dr. C. Michael Elliott for the cobalt mediator and N3 dye and Dr. Amy Prieto for assistance with the synthesis of CdSe QDs. This work was funded by the Division of Chemical Sciences, Geosciences, and Biosciences, Office of Basic Energy Sciences of the U.S. Department of Energy through Grant #DE-FG03-96ER14625.

II.7 References

- (1) Grätzel, M. Solar energy conversion by dye-sensitized photovoltaic cells *Inorg. Chem.* **2005**, *44*, 6841.
- (2) Gerischer, H.; Luebke, M. A particle size effect in the sensitization of titanium dioxide electrodes by a cadmium sulfide deposit *J. Electroanal. Chem.* **1986**, *204*, 225.
- (3) Spanhel, L.; Weller, H.; Henglein, A. Photochemistry of semiconductor colloids. 22. Electron ejection from illuminated cadmium sulfide into attached titanium and zinc oxide particles *J. Am. Chem. Soc.* **1987**, *109*, 6632.
- (4) Gopidas, K. R.; Bohorquez, M.; Kamat, P. V. Photophysical and photochemical aspects of coupled semiconductors: charge-transfer processes in colloidal cadmium sulfide-titania and cadmium sulfide-silver(I) iodide systems *J. Phys. Chem.* **1990**, *94*, 6435.

- (5) Vogel, R.; Pohl, K.; Weller, H. Sensitization of highly porous, polycrystalline titanium dioxide electrodes by quantum sized cadmium sulfide *Chem. Phys. Lett.* **1990**, *174*, 241.
- (6) Vogel, R.; Hoyer, P.; Weller, H. Quantum-Sized PbS, CdS, Ag₂S, Sb₂S₃, and Bi₂S₃ Particles as Sensitizers for Various Nanoporous Wide-Bandgap Semiconductors *J. Phys. Chem.* **1994**, *98*, 3183.
- (7) Sant, P. A.; Kamat, P. V. Interparticle electron transfer between size-quantized CdS and TiO₂ semiconductor nanoclusters *Phys. Chem. Chem. Phys.* **2002**, *4*, 198.
- (8) Lee, W.; Lee, J.; Lee, S.; Yi, W.; Han, S.; Cho, B. W. Enhanced charge collection and reduced recombination of CdS/TiO₂ quantum-dots sensitized solar cells in the presence of single-walled carbon nanotubes *Appl. Phys. Lett.* **2008**, *92*, 153510/1.
- (9) Sun, W.-T.; Yu, Y.; Pan, H.-Y.; Gao, X.-F.; Chen, Q.; Peng, L.-M. CdS Quantum Dots Sensitized TiO₂ Nanotube-Array Photoelectrodes *J. Am. Chem. Soc.* **2008**, *130*, 1124.
- (10) Baker, D.; Kamat, P. Photosensitization of TiO₂ Nanostructures with CdS Quantum Dots: Particulate versus Tubular Support Architectures *Adv. Funct. Mater.* **2009**, *19*, 805.
- (11) Liu, D.; Kamat, P. V. Electrochemical rectification in cadmium selenide + titanium dioxide coupled semiconductor films *J. Electroanal. Chem.* **1993**, *347*, 451.
- (12) Nasr, C.; Kamat, P. V.; Hotchandani, S. Photoelectrochemical behavior of coupled SnO₂/CdSe nanocrystalline semiconductor films *J. Electroanal. Chem.* **1997**, *420*, 201.
- (13) Shen, Q.; Arae, D.; Toyoda, T. Photosensitization of nanostructured TiO₂ with CdSe quantum dots: effects of microstructure and electron transport in TiO₂ substrates *J. Photochem. Photobiol., A* **2004**, *164*, 75.
- (14) Shen, Q.; Katayama, K.; Yamaguchi, M.; Sawada, T.; Toyoda, T. Study of ultrafast carrier dynamics of nanostructured TiO₂ films with and without CdSe quantum dot deposition using lens-free heterodyne detection transient grating technique *Thin Solid Films* **2005**, *486*, 15.
- (15) Diguna, L. J.; Murakami, M.; Sato, A.; Kumagai, Y.; Ishihara, T.; Kobayashi, N.; Shen, Q.; Toyoda, T. Photoacoustic and photoelectrochemical characterization of inverse opal TiO₂ sensitized with CdSe quantum dots *Jpn. J. Appl. Phys.* **2006**, *45*, 5563.

- (16) Robel, I.; Subramanian, V.; Kuno, M.; Kamat, P. V. Quantum dot solar cells. Harvesting light energy with CdSe nanocrystals molecularly linked to mesoscopic TiO₂ films *J. Am. Chem. Soc.* **2006**, *128*, 2385.
- (17) Shen, Q.; Katayama, K.; Sawada, T.; Yamaguchi, M.; Toyoda, T. Optical absorption, photoelectrochemical, and ultrafast carrier dynamic investigations of TiO₂ electrodes composed of nanotubes and nanowires sensitized with CdSe quantum dots *Jpn. J. Appl. Phys.* **2006**, *45*, 5569.
- (18) Ahn, J.; Mane, R. S.; Todkar, V. V.; Han, S. Invasion of CdSe nanoparticles for photosensitization of porous TiO₂ *Int. J. Electrochem. Sci.* **2007**, *2*, 517.
- (19) Diguna, L. J.; Shen, Q.; Sato, A.; Katayama, K.; Sawada, T.; Toyoda, T. Optical absorption and ultrafast carrier dynamics characterization of CdSe quantum dots deposited on different morphologies of nanostructured TiO₂ films *Mater. Sci. Eng., C* **2007**, *27*, 1514.
- (20) Diguna, L. J.; Shen, Q.; Kobayashi, J.; Toyoda, T. High efficiency of CdSe quantum-dot-sensitized TiO₂ inverse opal solar cells *Appl. Phys. Lett.* **2007**, *91*, 3.
- (21) Lee, H. J.; Kim, D.; Yoo, J.; Bang, J.; Kim, S.; Park, S. Anchoring cadmium chalcogenide quantum dots (QDs) onto stable oxide semiconductors for QD sensitized solar cells *Bull. Korean Chem. Soc.* **2007**, *28*, 953.
- (22) Leschkies, K. S.; Divakar, R.; Basu, J.; Enache-Pommer, E.; Boercker, J. E.; Carter, C. B.; Kortshagen, U. R.; Norris, D. J.; Aydil, E. S. Photosensitization of ZnO Nanowires with CdSe Quantum Dots for Photovoltaic Devices *Nano Lett.* **2007**, *7*, 1793.
- (23) Mora-Seró, I.; Bisquert, J.; Dittrich, T.; Belaidi, A.; Susa, A. S.; Rogach, A. L. Photosensitization of TiO₂ Layers with CdSe Quantum Dots: Correlation between Light Absorption and Photoinjection *J. Phys. Chem. C* **2007**, *111*, 14889.
- (24) Shen, Q.; Yanai, M.; Katayama, K.; Sawada, T.; Toyoda, T. Optical absorption, photosensitization, and ultrafast carrier dynamic investigations of CdSe quantum dots grafted onto nanostructured SnO₂ electrode and fluorine-doped tin oxide (FTO) glass *Chem. Phys. Lett.* **2007**, *442*, 89.
- (25) Tena-Zaera, R.; Katty, A.; Bastide, S.; Levy-Clement, C. Annealing Effects on the Physical Properties of Electrodeposited ZnO/CdSe Core-Shell Nanowire Arrays *Chem. Mater.* **2007**, *19*, 1626.

- (26) Kongkanand, A.; Tvrdy, K.; Takechi, K.; Kuno, M.; Kamat, P. Quantum Dot Solar Cells. Tuning Photoresponse through Size and Shape Control of CdSe–TiO₂ Architecture *J. Am. Chem. Soc.* **2008**, *130*, 4007.
- (27) Lee, W.; Kwak, W.; Min, S. K.; Lee, J.; Chae, W.; Sung, Y.; Han, S. Spectral broadening in quantum dots-sensitized photoelectrochemical solar cells based on CdSe and Mg-doped CdSe nanocrystals *Electrochem. Commun.* **2008**, *10*, 1699.
- (28) Lee, W.; Kang, S. H.; Min, S. K.; Sung, Y.; Han, S. Co-sensitization of vertically aligned TiO₂ nanotubes with two different sizes of CdSe quantum dots for broad spectrum *Electrochem. Commun.* **2008**, *10*, 1579.
- (29) Lee, Y.; Huang, B. M.; Chien, H. T. Highly Efficient CdSe-Sensitized TiO₂ Photoelectrode for Quantum-Dot-Sensitized Solar Cell *Chem. Mater.* **2008**, *20*, 6903.
- (30) Lopez-Luke, T.; Wolcott, A.; Xu, L.; Chen, S.; Wen, Z.; Li, J.; De La Rosa, E.; Zhang, J. Z. Nitrogen-Doped and CdSe Quantum-Dot-Sensitized Nanocrystalline TiO₂ Films for Solar Energy Conversion Applications *J. Phys. Chem. C.* **2008**, *112*, 1282.
- (31) Mora-Sero, I.; Dittrich, T.; Susa, A. S.; Rogach, A. L.; Bisquert, J. Large improvement of electron extraction from CdSe quantum dots into a TiO₂ thin layer by N3 dye coabsorption *Thin Solid Films* **2008**, *516*, 6994.
- (32) Shen, Q.; Kobayashi, J.; Diguna, L. J.; Toyoda, T. Effect of ZnS coating on the photovoltaic properties of CdSe quantum dot-sensitized solar cells *J. Appl. Phys.* **2008**, *103*, 084304/1.
- (33) Si, H. Y.; Sun, Z. H.; Zhang, H. L. Photoelectrochemical response from CdSe-sensitized anodic oxidation TiO₂ nanotubes *Colloids Surf., A* **2008**, *313*, 604.
- (34) Bang, J.; Kamat, P. Quantum Dot Sensitized Solar Cells. A Tale of Two Semiconductor Nanocrystals: CdSe and CdTe *ACS Nano* **2009**, *3*, 1467.
- (35) Chen, J.; Song, J.; Sun, X.; Deng, W.; Jiang, C.; Lei, W.; Huang, J.; Liu, R. An oleic acid-capped CdSe quantum-dot sensitized solar cell *Appl. Phys. Lett.* **2009**, *94*, 153115.
- (36) Guijarro, N.; Lana-Villarreal, T.; Mora-Seró, I.; Bisquert, J.; Gómez, R. CdSe Quantum Dot-Sensitized TiO₂ Electrodes: Effect of Quantum Dot Coverage and Mode of Attachment *J. Phys. Chem. C.* **2009**, *113*, 4208.
- (37) Tvrdy, K.; Kamat, P. Substrate Driven Photochemistry of CdSe Quantum Dot Films: Charge Injection and Irreversible Transformations on Oxide Surfaces *J. Phys. Chem. A.* **2009**, *113*, 3765.

- (38) Yu, P.; Zhu, K.; Norman, A. G.; Ferrere, S.; Frank, A. J.; Nozik, A. J. Nanocrystalline TiO₂ solar cells sensitized with InAs quantum dots *J. Phys. Chem. B.* **2006**, *110*, 25451.
- (39) Zaban, A.; Micic, O. I.; Gregg, B. A.; Nozik, A. J. Photosensitization of Nanoporous TiO₂ Electrodes with InP Quantum Dots *Langmuir* **1998**, *14*, 3153.
- (40) Hyun, B.-R.; Zhong, Y.-W.; Bartnik, A. C.; Sun, L.; AbrunãÉa, H. D.; Wise, F. W.; Goodreau, J. D.; Matthews, J. R.; Leslie, T. M.; Borrelli, N. F. Electron Injection from Colloidal PbS Quantum Dots into Titanium Dioxide Nanoparticles *ACS Nano* **2008**, *2*, 2206.
- (41) Kamat, P. V. Quantum Dot Solar Cells. Semiconductor Nanocrystals as Light Harvesters *J. Phys. Chem. C.* **2008**, *112*, 18737.
- (42) Ellingson, R. J.; Beard, M. C.; Johnson, J. C.; Yu, P. R.; Micic, O. I.; Nozik, A. J.; Shabaev, A.; Efros, A. L. Highly efficient multiple exciton generation in colloidal PbSe and PbS quantum dots *Nano Lett.* **2005**, *5*, 865.
- (43) Shabaev, A.; Efros, A. L.; Nozik, A. J. Multiexciton generation by a single photon in nanocrystals *Nano Lett.* **2006**, *6*, 2856.
- (44) Beard, M. C.; Knutsen, K. P.; Yu, P. R.; Luther, J. M.; Song, Q.; Metzger, W. K.; Ellingson, R. J.; Nozik, A. J. Multiple exciton generation in colloidal silicon nanocrystals *Nano Lett.* **2007**, *7*, 2506.
- (45) Luque, A.; Marti, A.; Nozik, A. J. Solar cells based on quantum dots: multiple exciton generation and intermediate bands *MRS Bull.* **2007**, *32*, 236.
- (46) Nozik, A. J. Multiple exciton generation in semiconductor quantum dots *Chem. Phys. Lett.* **2008**, *457*, 3.
- (47) Trinh, M. T.; Houtepen, A. J.; Schins, J. M.; Hanrath, T.; Piris, J.; Knulst, W.; Goossens, A. P. L. M.; Siebbeles, L. D. A. In spite of recent doubts carrier multiplication does occur in PbSe nanocrystals *Nano Lett.* **2008**, *8*, 1713.
- (48) Nair, G.; Bawendi, M. G. Carrier multiplication yields of CdSe and CdTe nanocrystals by transient photoluminescence spectroscopy *Phys. Rev. B.* **2007**, *76*, 081304.
- (49) Nair, G.; Geyer, S.; Chang, L.; Bawendi, M. Carrier multiplication yields in PbS and PbSe nanocrystals measured by transient photoluminescence *Phys. Rev. B.* **2008**, *78*, 125325.

- (50) Hodes, G. Comparison of Dye- and Semiconductor-Sensitized Porous Nanocrystalline Liquid Junction Solar Cells *J. Phys. Chem. C* **2008**, *112*, 17778.
- (51) Lee, H. J.; Yum, J.-H.; Leventis, H. C.; Zakeeruddin, S. M.; Haque, S. A.; Chen, P.; Seok, S. I.; Grätzel, M.; Nazeeruddin, M. K. CdSe Quantum Dot-Sensitized Solar Cells Exceeding Efficiency 1% at Full-Sun Intensity *J. Phys. Chem. C* **2008**, *112*, 11600.
- (52) Gorer, S.; Hodes, G. Quantum-size effects in the study of chemical solution deposition mechanism of semiconductor films *J. Phys. Chem.* **1994**, *98*, 5338.
- (53) Niitsoo, O.; Sarkar, S. K.; Pejoux, C.; Ruhle, S.; Cahen, D.; Hodes, G. Chemical bath deposited CdS/CdSe-sensitized porous TiO₂ solar cells *J. Photochem. Photobiol., A* **2006**, *181*, 306.
- (54) Mane, R. S.; Lokhande, C. D. Chemical deposition method for metal chalcogenide thin films *Mater. Chem. Phys.* **2000**, *65*, 1.
- (55) Chang, C.; Lee, Y. Chemical bath deposition of CdS quantum dots onto mesoscopic TiO₂ films for application in quantum-dot-sensitized solar cells *Appl. Phys. Lett.* **2007**, *91*, 053503/1.
- (56) Lin, S.; Lee, Y.; Chang, C.; Shen, Y.; Yang, Y. Quantum dot-sensitized solar cells: Assembly of CdS-quantum dot coupling techniques of self-assembled monolayer and chemical bath deposition *Appl. Phys. Lett.* **2007**, *90*, 143517/1.
- (57) Metin, H.; Erat, S.; Ari, M.; Bozoklu, M. Characterization of CdSe films prepared by chemical bath deposition method *Optoelectron. Adv. Mat.* **2008**, *2*, 92.
- (58) Lee, H.; Leventis, H. C.; Moon, S.-J.; Chen, P.; Ito, S.; Haque, S. A.; Torres, T.; Nüesch, F.; Geiger, T.; Zakeeruddin, S. M.; Grätzel, M.; Nazeeruddin, M. K. PbS and CdS Quantum Dot-Sensitized Solid-State Solar Cells: "Old Concepts, New Results" *Adv. Funct. Mater.* **2009**, *19*, 2735.
- (59) Lee, H.; Chen, P.; Moon, S.; Sauvage, F.; Sivula, K.; Bessho, T.; Gamelin, D.; Comte, P.; Zakeeruddin, S.; Seok, S.; Grätzel, M.; Nazeeruddin, M. Regenerative PbS and CdS Quantum Dot Sensitized Solar Cells with a Cobalt Complex as Hole Mediator *Langmuir* **2009**, *25*, 7602.
- (60) Li, J. J.; Wang, Y. A.; Guo, W.; Keay, J. C.; Mishima, T. D.; Johnson, M. B.; Peng, X. Large-Scale Synthesis of Nearly Monodisperse CdSe/CdS Core/Shell Nanocrystals Using Air-Stable Reagents via Successive Ion Layer Adsorption and Reaction *J. Am. Chem. Soc.* **2003**, *125*, 12567.

- (61) He, G.; Tan, L.; Zheng, Q.; Prasad, P. Multiphoton absorbing materials: molecular designs, characterizations, and applications *Chem. Rev.* **2008**, *108*, 1245.
- (62) Xing, G.; Ji, W.; Zheng, Y.; Ying, J. Two- and three-photon absorption of semiconductor quantum dots in the vicinity of half of lowest exciton energy *Appl. Phys. Lett.* **2008**, *93*, 241114.
- (63) Takeda, N.; Parkinson, B. A. Adsorption morphology, light absorption, and Sensitization yields for squaraine dyes on SnS₂ surfaces *J. Am. Chem. Soc.* **2003**, *125*, 5559.
- (64) Lu, Y. F.; Choi, D. J.; Nelson, J.; Yang, O.; Parkinson, B. Adsorption, Desorption, and Sensitization of Low-Index Anatase and Rutile Surfaces by the Ruthenium Complex Dye N3 *J. Electrochem. Soc.* **2006**, *153*, E131.
- (65) Lu, Y. F.; Spitler, M. T.; Parkinson, B. A. Dependent Photoinduced Desorption of a Dicarboxylated Cyanine Dye from the Surface of Single-Crystal *Langmuir* **2007**, *23*, 11637.
- (66) Ushiroda, S.; Ruzycski, N.; Lu, Y.; Spitler, M. T.; Parkinson, B. A. Dye sensitization of the anatase (101) crystal surface by a series of dicarboxylated thiocyanine dyes *J. Am. Chem. Soc.* **2005**, *127*, 5158.
- (67) Peng, Z. A.; Peng, X. Formation of High-Quality CdTe, CdSe, and CdS Nanocrystals Using CdO as Precursor *J. Am. Chem. Soc.* **2000**, *123*, 183.
- (68) Chen, X.; Hutchison, J. L.; Dobson, P. J.; Wakefield, G. Highly luminescent monodisperse CdSe nanoparticles synthesized in aqueous solution *J. Mater. Sci.* **2009**, *44*, 285.
- (69) Lu, Y.; Jaekel, B.; Parkinson, B. A. Preparation and characterization of terraced surfaces of low-index faces of anatase, rutile, and brookite *Langmuir* **2006**, *22*, 4472.
- (70) Horcas, I.; Fernandez, R.; Gomez-Rodriguez, J. M.; Colchero, J.; Gomez-Herrero, J.; Baro, A. M. WSXM: A software for scanning probe microscopy and a tool for nanotechnology *Rev. Sci. Instrum.* **2007**, *78*, 013705.
- (71) Murray, C. B.; Norris, D. J.; Bawendi, M. G. Synthesis and characterization of nearly monodisperse CdE (E = S, Se, Te) semiconductor nanocrystallites *J. Am. Chem. Soc.* **1993**, *115*, 8706.
- (72) Wang, X.-S.; Dykstra, T. E.; Salvador, M. R.; Manners, I.; Scholes, G. D.; Winnik, M. A. Surface Passivation of Luminescent Colloidal Quantum Dots with Poly(Dimethylaminoethyl methacrylate) through a Ligand Exchange Process *J. Am. Chem. Soc.* **2004**, *126*, 7784.

- (73) Owen, J. S.; Park, J.; Trudeau, P. E.; Alivisatos, A. P. Reaction chemistry and ligand exchange at cadmium-selenide nanocrystal surfaces *J. Am. Chem. Soc.* **2008**, *130*, 12279.
- (74) Wang, X.; et al. Synthesis of water-soluble CdSe quantum dots by ligand exchange with p-sulfonatocalix(n)arene (n = 4, 6) as fluorescent probes for amino acids *Nanotechnology* **2008**, *19*, 205501.
- (75) Lawless, D.; Kapoor, S.; Meisel, D. Bifunctional Capping of CdS Nanoparticles and Bridging to TiO₂ *J. Phys. Chem.* **1995**, *99*, 10329.
- (76) Kalyuzhny, G.; Murray, R. Ligand effects on optical properties of CdSe nanocrystals *J. Phys. Chem. B.* **2005**, *109*, 7012.
- (77) Aldana, J.; Wang, Y. A.; Peng, X. G. Photochemical instability of CdSe nanocrystals coated by hydrophilic thiols *J. Am. Chem. Soc.* **2001**, *123*, 8844.
- (78) Aldana, J.; Lavelle, N.; Wang, Y. A.; Peng, X. G. Size-dependent dissociation pH of thiolate ligands from cadmium chalcogenide nanocrystals *J. Am. Chem. Soc.* **2005**, *127*, 2496.
- (79) Parkinson, B. A. Dye sensitization of van der Waals surfaces of tin disulfide photoanodes *Langmuir* **1988**, *4*, 967.
- (80) Sarkar, S. K.; Hodes, G. Charge Overlap Interaction in Quantum Dot Films: A Time Dependence and Suppression by Cyanide Adsorption *J. Phys. Chem. B.* **2005**, *109*, 7214.
- (81) Leatherdale, C. A.; Bawendi, M. G. Observation of solvatochromism in CdSe colloidal quantum dots *Phys. Rev. B.* **2001**, *63*, 165315.
- (82) Ishibashi, T.; Uetsuka, H.; Onishis, H. An Ordered Retinoate Monolayer Prepared on Rutile TiO₂ (110) *J. Phys. Chem. B.* **2004**, *108*, 17166.
- (83) Wang, F.; Tang, R.; Buhro, W. E. The Trouble with TOPO; Identification of Adventitious Impurities Beneficial to the Growth of Cadmium *Nano Lett.* **2008**, *8*, 3521.
- (84) Bae, E.; Choi, W. Effect of the Anchoring Group (Carboxylate vs Phosphonate) in Ru-Complex-Sensitized TiO₂ on Hydrogen Production under Visible Light *J. Phys. Chem. B.* **2006**, *110*, 14792.
- (85) Gimenez, S.; Mora-Sero, I.; Macor, L.; Guijarro, N.; Lana-Villareal, T.; Gomez, R.; Diguna, L. J.; Shen, Q.; Toyoda, T.; Bisquert, J. Improving the performance of colloidal quantum-dot-sensitized solar cells *Nanotechnology* **2009**, *20*, 295204.

- (86) von Holt, B.; Kudera, S.; Weiss, A.; Schrader, T. E.; Manna, L.; Parak, W. J.; Braun, M. Ligand exchange of CdSe nanocrystals probed by optical spectroscopy in the visible and mid-IR *J. Mater. Chem.* **2008**, *18*, 2728.
- (87) Yu, W. W.; Qu, L. H.; Guo, W. Z.; Peng, X. G. Experimental determination of the extinction coefficient of CdTe, CdSe, and CdS nanocrystals *Chem. Mater.* **2003**, *15*, 2854.
- (88) Hagfeldt, A.; Gratzel, M. Molecular Photovoltaics *Acc. Chem. Res.* **2000**, *33*, 269.
- (89) Mora-Sero, I.; Gimenez, S.; Moehl, T.; Fabregat-Santiago, F.; Lana-Villareal, T.; Gomez, R.; Bisquert, J. Factors determining the photovoltaic performance of a CdSe quantum dot sensitized solar cell: the role of the linker molecule and of the counter electrode *Nanotechnology* **2008**, *19*.
- (90) Liu, P.; Wang, Q.; Li, X. Studies on CdSe/l-cysteine Quantum Dots Synthesized in Aqueous Solution for Biological Labeling *J. Phys. Chem. C.* **2009**, *113*, 7670.
- (91) Mora-Sero, I.; Likodimos, V.; Gimenez, S.; Martinez-Ferrero, E.; Albero, J.; Palomares, E.; Kontos, A. G.; Falaras, P.; Bisquert, J. Fast Regeneration of CdSe Quantum Dots by Ru Dye in Sensitized TiO₂ Electrodes *J. Phys. Chem. C.* **2010**, *114*, 6755.
- (92) Xu, X.; Gimenez, S.; Mora-Sero, I.; Abate, A.; Bisquert, J.; Xu, G. Influence of cysteine adsorption on the performance of CdSe quantum dots sensitized solar cells *Mater. Chem. Phys.* **2010**, *124*, 709.
- (93) Kovalenko, M. V.; Scheele, M.; Talapin, D. V. Colloidal Nanocrystals with Molecular Metal Chalcogenide Surface Ligands *Science* **2009**, *324*, 1417.
- (94) Kovalenko, M. V.; Bodnarchuk, M. I.; Zaumseil, J.; Lee, J.-S.; Talapin, D. V. Expanding the Chemical Versatility of Colloidal Nanocrystals Capped with Molecular Metal Chalcogenide Ligands *J. Am. Chem. Soc.* **2010**, *132*, 10085.
- (95) Min, Y. J.; Akbulut, M.; Kristiansen, K.; Golan, Y.; Israelachvili, J. The role of interparticle and external forces in nanoparticle assembly *Nat. Mater.* **2008**, *7*, 527.
- (96) Talapin, D. V.; Lee, J.-S.; Kovalenko, M. V.; Shevchenko, E. V. Prospects of Colloidal Nanocrystals for Electronic and Optoelectronic Applications *Chem. Rev.* **2009**, *110*, 389.
- (97) Luther, J. M.; Beard, M. C.; Song, Q.; Law, M.; Ellingson, R. J.; Nozik, A. J. Multiple Exciton Generation in Films of Electronically Coupled PbSe Quantum Dots *Nano Lett.* **2007**, *7*, 1779.

- (98) Luther, J. M.; Law, M.; Song, Q.; Perkins, C. L.; Beard, M. C.; Nozik, A. J. Structural, Optical, and Electrical Properties of Self-Assembled Films of PbSe Nanocrystals Treated with 1,2-Ethanedithiol *ACS Nano* **2008**, *2*, 271.
- (99) Fokkink, L. G. J.; de Keizer, A.; Lyklema, J. Specific ion adsorption on oxides: Surface charge adjustment and proton stoichiometry *J. Colloid Interface Sci.* **1987**, *118*, 454.

II.8 Future Work

This study did not systematically investigate alternative QD surface ligands or various adsorption conditions (e.g. temperature, salt concentration etc.) to optimize electron transfer quantum yields. Other promising capping ligands that may increase the electronic coupling between CdSe and TiO₂ include thioglycolic acid[89], cysteine[90-92], bifunctional π -conjugated systems (e.g. mercaptobenzoic acids, aminothiophenols or mercaptophenols) or molecular metal chalcogenides.[93,94] Aside from capping ligands, it is important to consider Coulombic, van der Waals, charge-dipole, dipole-dipole, entropic, capillary, convective, shear, and other forces[95,96] that govern CdSe QD-QD and CdSe QD-TiO₂ interactions. Indeed subtle differences in surface coverages and morphologies were observed for colloidal MPA-capped CdSe QDs synthesized by different procedures (aqueous solution synthesis yielded low coverage QD bilayers whereas densely packed single layers were observed for *ex situ* ligand exchanged QDs). Specific physical and chemical differences between the two samples could include free ligand concentration, unreacted precursors or QD concentration. QD solution concentration is particularly

significant considering ~0.4 mg CdSe QDs/ml were employed for single crystal TiO₂ sensitization and it has been shown that close packed monolayers can be physisorbed onto a variety of substrates from 5-400 mg/ml QD solutions.[97,98]

One approach is to evaluate effects of free ligand *and* MPA-capped QD concentration on the TiO₂ surface coverage and morphology is to maintain the pH of the sensitization solution $>pK_a^{SH}$ using buffered solutions (sensitization solutions in this study were not buffered). In addition, it may be useful to vary the size of the cations or anions in the buffer solution to evaluate effects of specific ion adsorption on the TiO₂ surface.[99]

CHAPTER III

IN-SITU STUDIES OF PHOTOLUMINESCENCE QUENCHING IN SINGLE CRYSTAL QUANTUM DOT SENSITIZED SOLAR CELLS

This dissertation chapter contains a manuscript that was submitted to *Nano Letters*. This study addresses the use of photoluminescence quenching data to indicate electron injection in QD sensitized solar cells. The work was a collaborative effort between the Parkinson and Van Orden groups.

The following are contributions to this article from Justin B. Sambur: (i) co-designed experiments with Douglas Shepherd, Prof. Van Orden and Prof. Parkinson; (ii) prepared QD samples, performed AFM and photocurrent measurements for QD-sensitized TiO₂ single crystals; (iii) edited the original manuscript written by Douglas Shepherd.

In-Situ Studies of Photoluminescence Quenching in Single Crystal Quantum Dot Sensitized Solar Cells

Douglas Shepherd, Justin B. Sambur, Yong-Qi Liang,
Bruce A. Parkinson, and Alan Van Orden

III.1 Abstract

Utilizing time-correlated single photon counting and internal photon conversion efficiency we studied both the fluorescence intensity, fluorescence decay time, and sensitized photocurrents from CdSe quantum dots coupled to single crystal TiO₂ and ZnO substrates through a variety of capping ligands. We find that for all configurations of capping ligands and substrate the photoluminescence decay rate is quenched compared to the free quantum dots in solution; whereas, only the short chain capping ligands that promote electron coupling to the substrate produce photocurrents. The longer chain capping groups both inhibit the electron injection and promote QD clustering on the surface where interactions between the individual quantum dots or the quantum dots and substrate alter the radiative rate.

III.2 Introduction

Semiconductor quantum dots (QDs) have shown great potential in a variety of applications, ranging from fluorescent bio-imaging[1-3] to solar energy conversion[4-7] Due to the size and material dependent band gaps[8-10], relative ease of ligand exchange[11,12] and possibility of multiple exciton generation.[13,14] QDs are actively explored as the light-harvesting layer in thin films[15-20] hybrid QD-polymer solar cells[21-25] and QD-sensitized solar cells (QDSSCs).[26-36] Regardless of the device architecture, overall efficiency partly depends on separation of photo-excited electron-hole pairs and collection of carriers at their respective contacts on a time scale faster than radiative or non-radiative recombination pathways.[37-48]

Optical measurements that probe the lifetime and bleach of the QD excited state, such as time resolved photoluminescence (trPL) and transient absorption (TA), have been extensively used to determine electron transfer rates in QDSSCs by comparing optical signatures of QDs in solution or QDs adsorbed on an insulating surface to QDs adsorbed on mesoporous metal oxide supports.[44] Studies have shown that there is a quenching of the PL intensity and radiative lifetime of the QDs once coupled to the electron acceptor, but very few of these experiments have attempted to measure the photo-response on the same system. Bonn and co-workers recently utilized trPL, TA, terahertz spectroscopy (THz-S), and photocurrent-voltage behavior to study electron injection from the lowest excited states of PbSe QDs to mesoporous TiO₂ or SnO₂ nanoparticle films.[45] By varying the energetics of the electron acceptor

(TiO₂ or SnO₂ nanoparticles), Bonn and co-workers were able to confirm electron injection only occurs when energetically possible (the SnO₂ system) via THz-S and photocurrent measurements but that solely characterizing the system via optical methods indicates electron injection in both systems (SnO₂ and TiO₂).

Although ultrafast optical experiments may provide useful information regarding the time scale of electron injection, these methods do not measure current in an external circuit. Since the absorption and photoluminescence characteristics of QDs are critically dependent on surface chemical treatments,[49] interpretation of changes in optical properties may be complicated by the surrounding medium (e.g. colloidal QDs, QDs adsorbed on insulators or QDs adsorbed on metal oxides). Here we have utilized a model system consisting of dispersed CdSe QDs on single crystal semiconducting substrates, TiO₂ and ZnO, at submonolayer coverages.[50] By varying the capping ligands, we focus exclusively on the effect of ligand chemistry on both sensitized photocurrent yields and quenching of the PL lifetime of the QDs, whose lowest excited states have sufficient energy to inject electrons into the conduction bands of TiO₂ and ZnO.

III.3 Experimental Methods

The QDs examined in this study consisted of CdSe core QDs capped with one of four ligands: trioctylphosphine oxide (TOPO), oleic acid (OA), 11-mercaptoundecanoic acid (MUA), and 3-mercaptopropionic acid (MPA). OA-capped QDs were synthesized via a hot-injection method. TOPO-capped QDs were purchased as a solid powder from Ocean Nanotech (QCO-600-0050,

Springdale, Arkansas). The excitonic peak absorption maxima occurred at 526 nm and 578 nm for the synthesized and Ocean Nanotech QDs (ON-QDs) respectively, corresponding to average core diameters of 2.8 nm and 3.8 nm.[51]

Synthesis of OA-capped QDs. CdSe QDs were synthesized via the hot-injection method.[52] Typically, 0.256 g CdO (2.0 mmol, 99.998 %, Alfa-Aesar) was dissolved in 1.6 ml oleic acid (OA, 5.0 mmol, 90%, Alfa-Aesar) and 8.0 ml 1-octadecene (90%, Acros) and heated to 165°C under a N₂ atmosphere to form a clear solution. A solution of 0.156 g Se (2.0 mmol, 99.999%, Alfa-Aesar) dissolved in 0.922 g Tri-n-octylphosphine (2.5 mmol, TOP, 90%, Alfa-Aesar) and 4.0 ml 1-octadecene was injected at 195°C. Growth at 180°C for various time intervals (1 min to 8 min) generates the QDs of desired size. Then the reaction was quenched via the injection of 10 ml toluene.

Ligand exchange of OA-capped QDs. Short (MPA) and long (MUA) bifunctional linker molecules were used to replace the OA ligands on the CdSe QDs. Typically, the CdSe QDs in 0.8 ml toluene (OD ~70) were precipitated with ethanol (absolute purity, Pharmco-Aaper). Then the precipitated solid was transferred to 60 ml methanol (99.9%, Fisher scientific) in a 3-neck flask, followed by the addition of 0.080 g MUA (0.4 mmol), or 80 ul MPA (0.9 mmol) and 1.0 g tetramethyl ammonium hydroxide pentahydrate (TMAH, 5.5 mmol, 98%, Alfa-Aesar). The solution of CdSe QDs was refluxed for >6h under an N₂ atmosphere. The final clear solution was precipitated with excess ethyl acetate (99.98%, EMD), and the precipitate was separated by centrifugation. MPA or MUA capped QDs were dissolved in ethanol and diluted to suitable concentration

(whereby the optical density at the 1s transition was 0.2) for sensitization of TiO₂ or ZnO.

Ligand exchange of TOPO-QDs. We followed an adapted procedure developed by Peng and co-workers for CdSe core QDs.[11,12] Briefly, 40 ml of MPA was added to 15 ml of methanol and adjusted to pH 11 with tetraethylammonium hydroxide. After degassing the solution for 30 min with high purity nitrogen, approximately 50 mg of CdSe QD powder was added and refluxed for 12 hr at 80°C. Following the ligand exchange procedure, the solution was centrifuged at 3000 rpm, and the supernatant was decanted. The methanol solution of MPA-capped CdSe QDs was stored in the dark under ambient conditions and was stable to aggregation for more than one year.

Preparation of TiO₂ single crystals. One-side mechanically polished crystals (10 mm x 10 mm x 1 mm) of rutile (110) were obtained from MTI Crystal Corporation (Richmond, CA). The as-received crystals were polished using 20 nm colloidal silica solution on Buehler polishing pads and annealed in air at 750°C for 6 hours.[53] The crystals were reductively doped by annealing for 30 min at 650°C in a 30:10 sccm stream of N₂:H₂. Following the reduction step, the crystals were re-polished with colloidal silica and annealed in N₂ for 3 hr in an N₂ atmosphere. The crystals were polished and annealed in N₂ up to five times until the AFM images of the TiO₂ crystals exhibited a terraced surface structure. The crystals were mounted on copper disks with Ga/In eutectic to ensure an ohmic contact. A copper wire was soldered to the back of the disk and fed through a glass rod, at

which point the entire electrode was sealed with epoxy (Epotek 377) and silicone rubber (RTV) and allowed to dry for a few hours.

Preparation of ZnO crystals. ZnO single crystals (0001, 10 mm x 10 mm x 1 mm) were purchased from MTI Inc. The samples were cleaned by ultrasonication in ethanol followed by immersion in 3.0 M NaOH solution for 5 minutes.

Sensitization of the single crystal electrodes. Bare crystals for AFM and photocurrent measurements were pre-characterized via AFM prior to QD adsorption. Epoxy-mounted and unmounted TiO₂ crystals were immersed for 1 hr in methanol solutions of MPA ON-QDs and ethanol solutions of MUA-QDs. 5 μ L aliquots of TOPO-QDs dissolved in toluene were pipetted on the crystal surface continuously for 20 min to avoid epoxy degradation from the organic solvent. The electrodes were rinsed with the same solvent used for QD adsorption and dried immediately with a 15 psi stream of N₂.

Photoelectrochemical measurements. Photoelectrochemical measurements were performed at short circuit in an aqueous sulfide electrolyte using a two-electrode configuration with a platinum wire counter electrode. Incident photon to current efficiency (IPCE) spectra were measured using a Stanford Research Systems (SRS) model SR570 low noise current preamplifier connected between the working and counter electrodes. The signal from the pre-amplifier was then fed into a SRS model SR830 DSP lock-in amplifier. Illumination from a 100 W Oriel lamp (385 nm cut-off filter) was passed through a computer controlled grating monochromator (2 nm step interval) and chopped at 13 Hz to provide a modulated photocurrent signal. The raw photocurrent signal was corrected for

photon flux using a lamp power spectrum recorded at 2 nm intervals using as themopile detector.

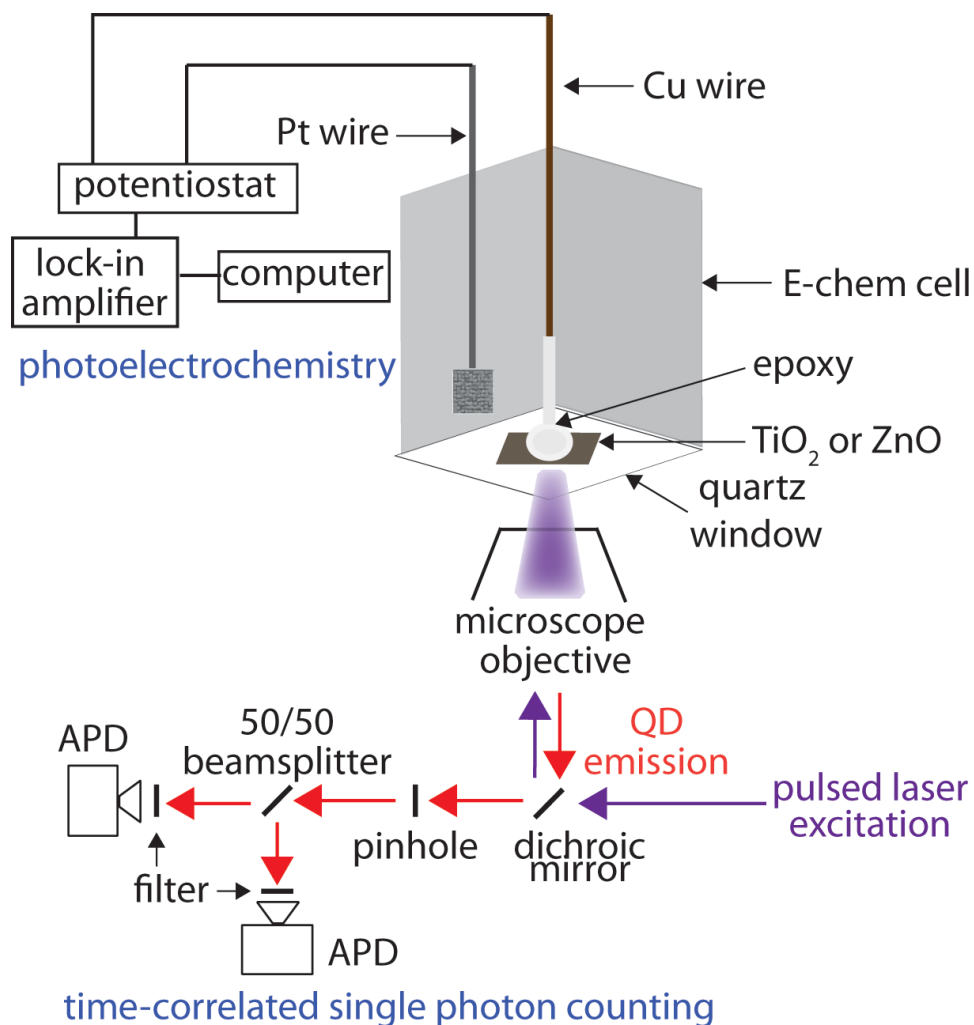
AFM Measurements. Tapping mode AFM (Digital Instruments Nanoscope IIIA controller and a multimode SPM) was used to characterize the CdSe QDs using an Olympus AC160TS probe with a 42 N/m force constant and resonant frequency of ~300 kHz. AFM images were processed using Digital Instruments software.

Photoluminescence Decay Measurements. A sample chamber consisting of a 75 mm optical glass coverslip on the bottom with plastic sides and top was constructed. The top of the chamber was drilled with two holes to allow for the electrode and counter-electrode wires to protrude. The sample chamber was mounted on the stage of an inverted optical microscope (Zeiss Axiovert S100) equipped with a piezoelectric scanner (Nanonics NIS-30 SC-100/28) for positioning in the optical probe region of the microscope. Excitation was provided by a 440-nm pulsed diode laser (PicoQuant LDH-P-C 440) operating at a pulse repetition rate of 10 MHz and pulse width of ~100 picoseconds. The laser light was focused onto the stage using a .85 NA/60x microscope objective to form an approximately 1.0- μm -diameter optical probe region at the bottom surface of the semiconductor. An average power of approximately 350 nW was used to give a time-averaged excitation intensity of approximately 20 W/cm^2 . Emitted fluorescence was collected by the same microscope objective and directed onto a single-photon counting avalanche photodiode detector (APD) (Perkin Elmer SPCM-14AQR). The emission was spatially filtered using a 50- μm

diameter pinhole located in the image plane of the microscope and spectrally filtered using a 510 nm longpass filter before reaching the detector. The output of the APD was directed to a time-correlated single-photon counting module (PicoQuant TimeHarp 200) to record the photon data. The photon data was post-processed using vendor-supplied software (Picoquant SymPhoTime) to obtain fluorescence intensity trajectories, fluorescence decay histograms, and autocorrelation functions for each area.

III.4 Results and Discussion

To address the above issues, we constructed a functional liquid junction cell on top of a confocal microscope (Scheme 1). This allows for direct measurements of the PL decay of QDs within a confocal region at the exact conditions under which incident photon to current efficiency measurements are completed. The major difference is that the small confocal spot size (approx. 1 micron in diameter) does not illuminate enough QDs to obtain a stable photocurrent measurement, so we are unable to simultaneously correlate spatially variations in QD surface coverage to PL decay and photocurrent response.



Scheme 1. Experimental setup for time correlated single photon counting and photoelectrochemical measurements. Although photocurrents could not be measured simultaneously due to the small laser spot size ($\sim 1 \mu\text{m}$), the same crystals were used to measure photocurrent spectra using monochromatic excitation that illuminated the entire crystal surface.

In order to directly compare the sensitized photocurrent yields it is important to determine the QD surface coverage. Figure 1 shows atomic force microscopy (AFM) images of TiO_2 and ZnO before and after adsorption of MPA, MUA, OA or TOPO-capped CdSe QDs. Bare rutile (110) TiO_2 (Figure 1A) exhibited flat terraces with an average width of 70 nm (residual silica particles

from polishing can be removed with HF immersion) whereas the clean ZnO (0001) surface (Figure 1E) exhibited a root mean square roughness of 0.1 nm without well-defined terraces. We detail the synthesis and ligand exchange procedures for the QDs as well as surface preparation of the semiconducting oxides in the supporting information. Due to the bifunctional chemical moieties used to chemically bind MPA (Figure 1B and 1F) and MUA-capped (Figure 1C and 1G) QDs to the oxide surface, these QDs predominantly adsorb in a single layer on TiO₂ and ZnO. However some regions of the TiO₂ crystal exhibited MPA-QD clusters consisting of 3 or more nanocrystals (see supporting information Figure S1). In contrast, QDs capped with bulky OA or TOPO ligands (Figure 1D and 1H) form large clusters with varying surface coverage at least partly because surface chemical bonds are not formed between OA or TOPO-capped QDs and the metal oxide surfaces. The surface morphology of the QDs studied herein agree well with previous studies using thoroughly washed aqueous MPA-QD samples.[50,54]

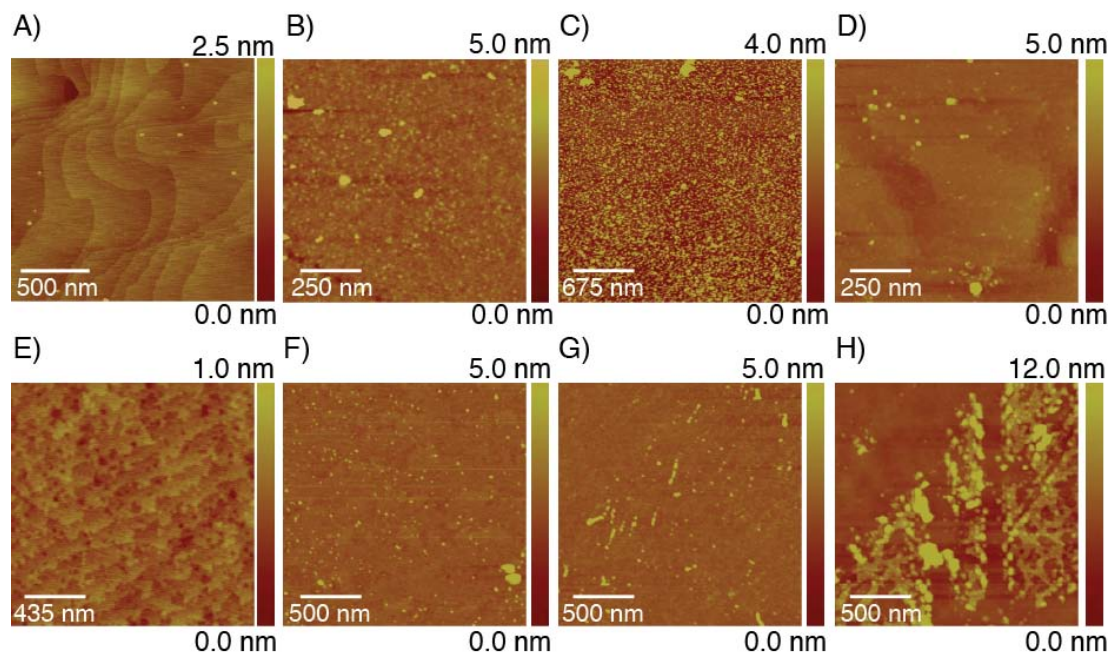


Figure 1. AFM images of A) bare rutile TiO₂ (110) and after 1 hr immersion in B) ON-MPA QDs, C), synthesized MUA-QDs and D) ON-TOPO-QDs. E) bare ZnO (0001) and after 1 hr immersion in F) synthesized MPA-capped, G) synthesized MUA-capped and H) synthesized OA-capped QDs.

Figures 2A and B show the incident photon-to-current efficiency (IPCE) spectra of single crystal TiO₂ or ZnO electrodes sensitized with the same QD samples used for AFM measurements. The IPCE value at the first excitonic peak for MPA-capped QDs is 12.5 and 5.7 times larger than MUA-capped QDs on TiO₂ and ZnO, respectively. OA and TOPO-capped QDs showed negligible photocurrent generation on both substrates. It is evident that short alkyl chain bifunctional linker molecules (MPA) increase the electronic coupling between QD and substrate compared to long chain ligands. PL measurements previously demonstrated faster electron transfer rate constants for QDs capped with short chain ligands to TiO₂.^[40,43,55]

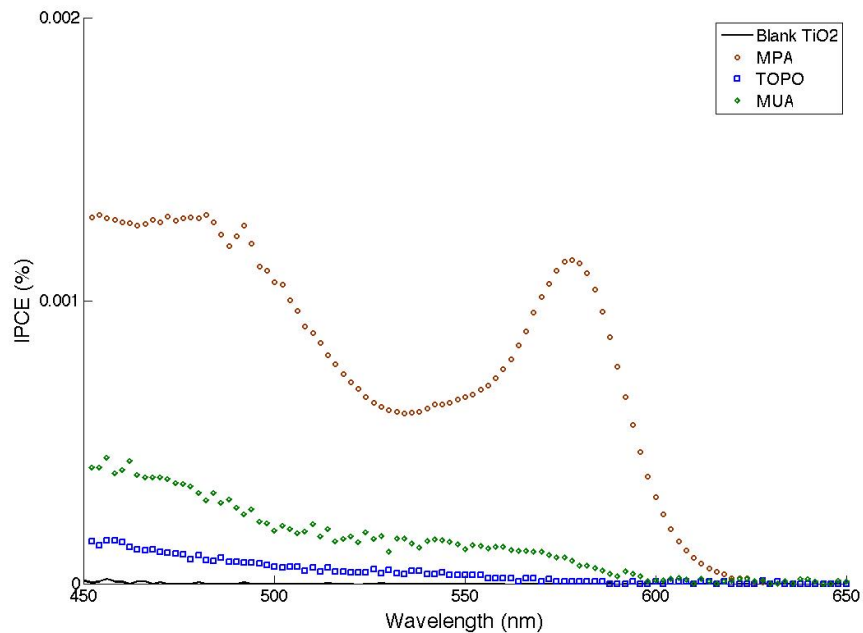
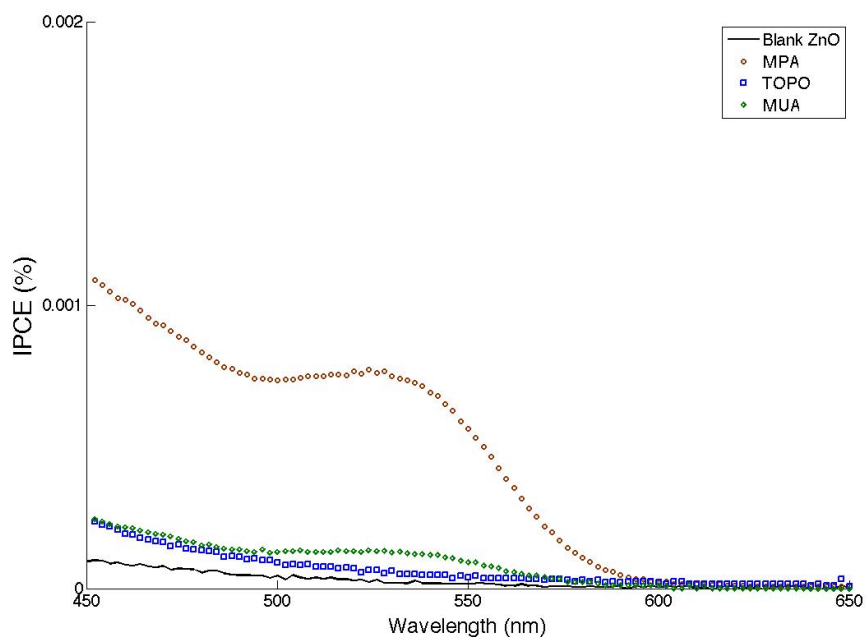
A**B**

Figure 2. a) IPCE spectra of a rutile (110) TiO₂ single crystal electrode sensitized with MPA ON-QDs, TOPO ON-QDs and synthesized MUA-QDs (acquired in 0.5 M Na₂S in 0.1 M NaOH) at short circuit in a two-electrode configuration versus a platinum wire) and b) a ZnO (0001) single crystal electrode sensitized with synthesized MPA, MUA and TOPO QDs.

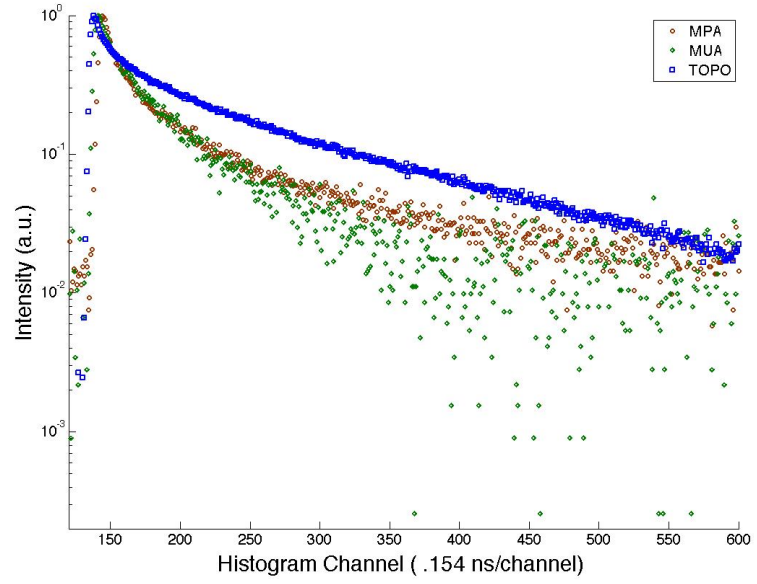
Time-correlated single photon counting (TCSPC) was used to measure the photoluminescence (PL) decay of QDs in solution, adsorbed on glass or adsorbed on single crystal oxides. Figure 3A shows that the PL decay of solubilized MPA and MUA-capped CdSe QDs are quenched compared to the TOPO or OA-capped CdSe QDs, a well-known effect of capping CdSe QD with thiols.[12] An aliquot of each solution was then dried on a glass cover slip and the PL decay traces were measured (Figure 3B). All of the PL decays are fit to

$$I(t) = Ae^{-t/\tau_1} + Be^{-t/\tau_2} \quad \text{Eq. (1)}$$

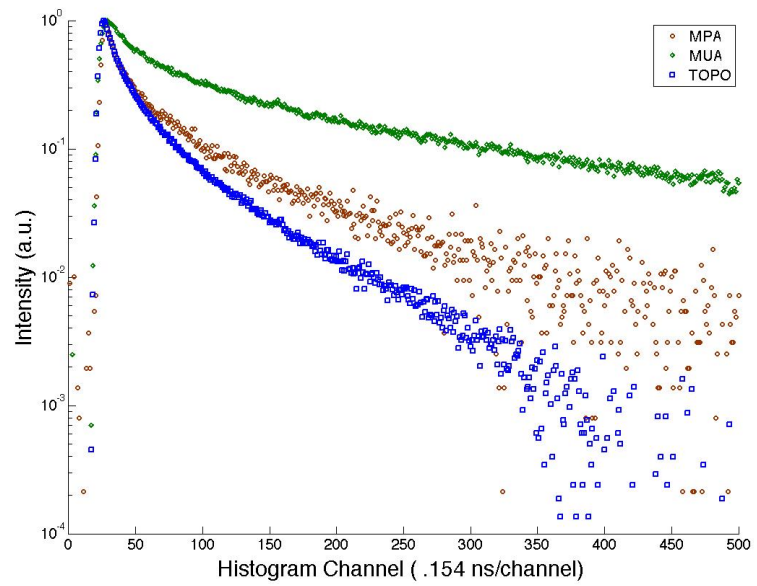
and summarized for each type of ligand in Table 1. The lifetimes are quenched on the glass substrate compared to solution, particularly for the OA and TOPO-capped QDs. The multi-exponential photoluminescence decay is due to the lack of a shell and chemical modifications to the CdSe QDs. For comparison, the photoluminescence decay from high quantum yield TOPO-capped CdSe/ZnS is shown in the supporting information.

Figure 3C and 3D show the PL decay of the MPA, MUA, OA and TOPO-capped QDs on TiO₂ and ZnO, respectively. All the PL decays in Figure 3C and 3D were obtained in the same electrolyte and short-circuit configuration as the IPCE measurements, so that we are measuring the photoresponse of the QDs in the same surrounding environment as the IPCE measurements. Notably, all samples show quenched PL decays relative to those in Figure 3A, which is quantified by fitting the PL decays to Eq. 1, summarized in Table 2. Of particular note is that for the TiO₂ sensitized with TOPO-capped QDs, the PL decay is quenched to a higher degree than any other sample.

A



B



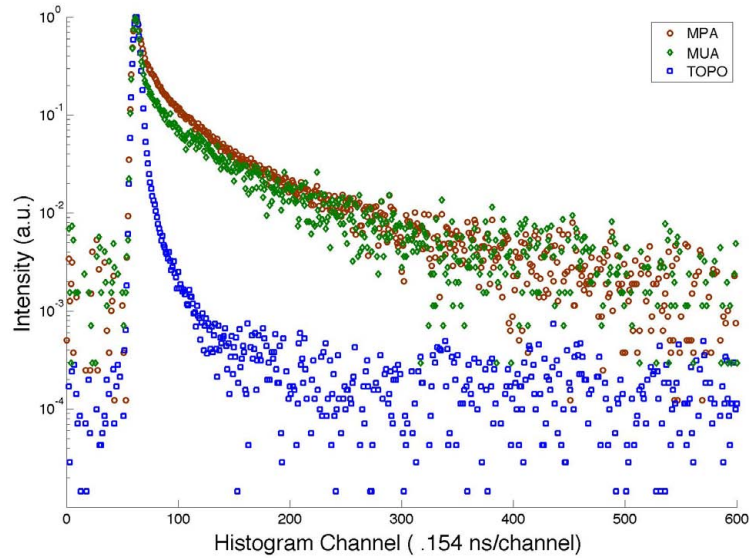
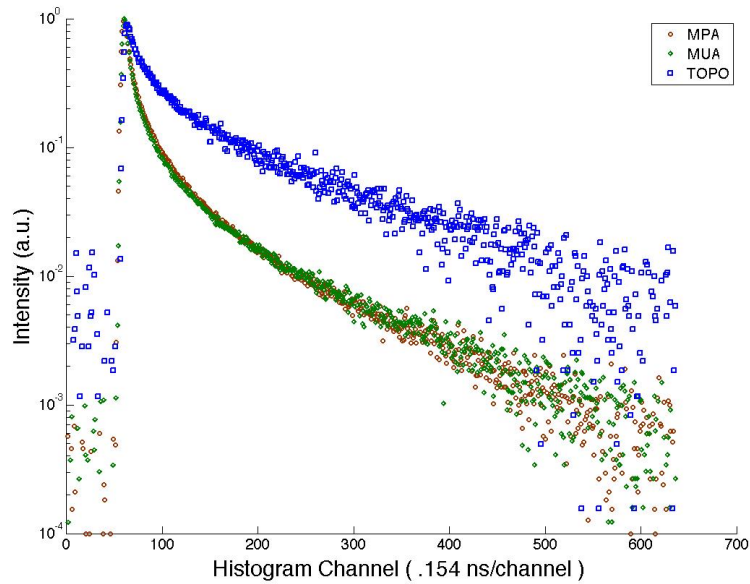
C**D**

Figure 3. PL Decay for MPA, MUA, and TOPO-capped CdSe QDs in (A) solution, (B) glass (deposited with the same procedure as the TiO₂ and ZnO substrates), (C) TiO₂ (no MUA PL decay), and (D) ZnO. All decays are fit to equation 1, taking into account the instrument response function.

Quenching of the QD PL lifetime is generally interpreted as electron injection from the QD excited state to the oxide conduction band.[40,43,56,57]

Comparison of the photocurrent spectra and PL decay data indicates that this

interpretation can be misleading. Although the PL lifetime is quenched for all samples, the photocurrent spectra are highly ligand-dependent. Most notably, the TOPO-capped sample shows the highest percentage of quenching in the lifetime(s) despite essentially no sensitized photocurrent.

What factors account for the disparity between photoelectrochemical and time-resolved PL measurements in QD-sensitized metal oxide systems? Photocurrent measurements accurately quantify injected electrons by measuring current flow in an external circuit. Time-resolved PL measurements rely on radiative recombination events to indicate the rate of electron transfer and thus are an indirect measurement. Several possible explanations to account for the quenched PL data are discussed below.

Given the similar initial lifetimes in solution, with small differences due to quenching from the thiol ligands,[12] we must assume that QD-substrate coupling is not the only process that can quench the fluorescence lifetime. Possible sources of this quenching are QD-QD interactions,[45,58] QD charging[59] and QD-electrolyte interactions.[12,49,60] While QD-electrolyte interactions are mediated by different surface ligands,[12,49,60] we see no difference between fluorescence decays of all three types of QDs in dilute solution of electrolyte (see supporting information Figure S2). However, QD-QD interactions have been shown to greatly influence the flow of energy in coupled systems. On insulating substrates, the Van Orden group has shown that small clusters of core-shell QDs interact, causing a reduction in lifetime and variations in the blinking pattern.[58,61] The Bonn group proposed that similar clusters of

PbSe QDs found in PbSe QD – TiO₂ nanoparticle slurries may be detrimental to the overall performance of the device, postulating a similar mechanism to the Van Orden group.[45] As shown in Figure 2G, the TOPO-capped QDs tend to form clusters on the surface of both substrates, which suggests that QD-QD interactions are responsible for the lifetime quenching rather than charge transfer to the semiconducting substrate. Additionally, it is likely that charge transfer can also occur from the QD or QD trap states to a surface trap state on the semiconducting substrate.[59,62] It is easy to extend both of these interactions to see how one QD in a cluster may become charged, and therefore become a non-radiative recombination center,[59] and then other QDs in close proximity are quenched by energy transfer to this non-radiative recombination center. This process is also possible with the mercaptoalkyl acid-capped QDs, but the rate of charge transfer to the semiconducting substrates is much faster than for the TOPO-capped QDs and the MAA-capped QDs tend to form well-dispersed monolayers, limiting the amount of QD-QD interactions.

III.5 Conclusions

We have observed changes in the photoluminescence decay of TOPO-capped CdSe QDs deposited on single crystal ZnO and TiO₂ that match the signatures of efficient charge transfer, yet these samples show no sensitization in IPCE measurements. MPA and MUA-capped CdSe QDs show similar changes in photoluminescence decay once deposited onto ZnO or TiO₂, but contrary to the TOPO-capped QDs the IPCE measurements confirm charge transfer from the QDs producing a sensitized current in the semiconductor. The exact

mechanism responsible for quenching of the photoluminescence in the TOPO-capped QDs remains unknown however electronic coupling between adjacent and similar-sized QDs (with bulky organic ligands) has been reported in the literature and it is possible that interaction with static traps in the semiconductor may alter the radiative rate.[58,61] Going forward, we suggest that future experiments investigating the time dynamics of charge separation in QDSSCs independently confirm charge transfer through IPCE and J-V measurements.

III.6 Supporting Information

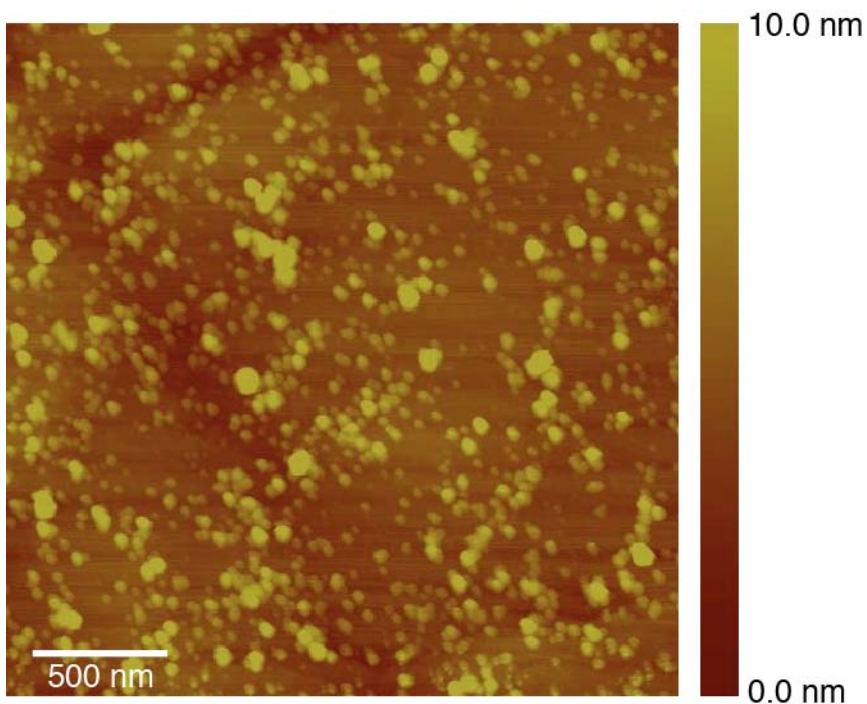


Figure S1. AFM image showing a region of clustered MPA-capped QDs adsorbed on rutile (110) TiO₂, although single layers of MPA-capped QDs were predominantly observed.

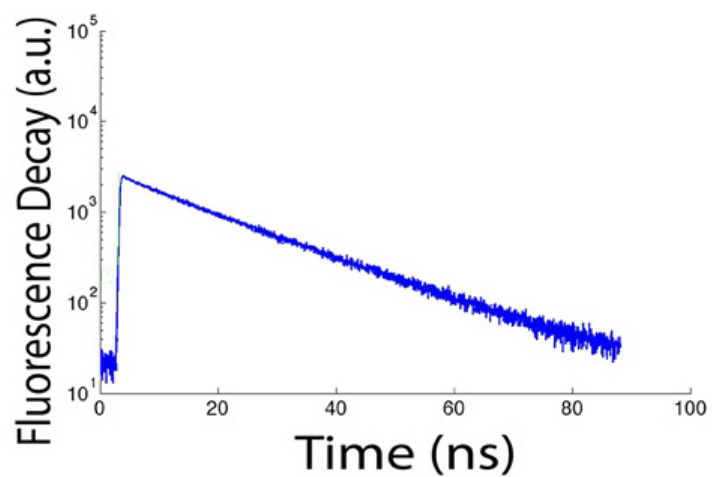


Figure S2. Photoluminescence decay trace from high quantum yield TOPO-capped CdSe/ZnS in hexanes.

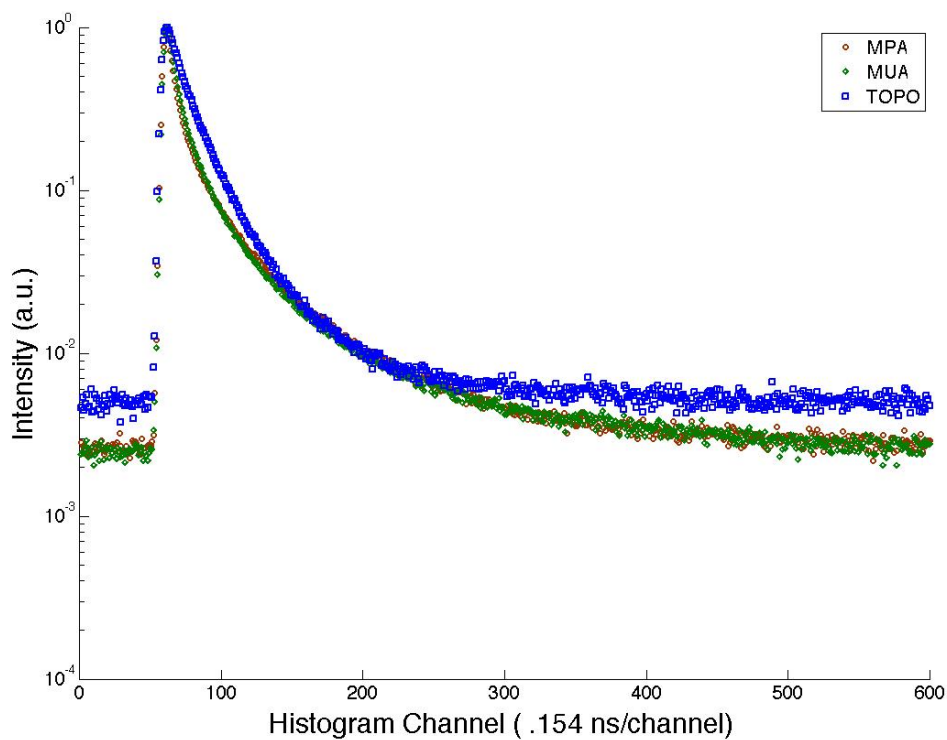


Figure S3. PL Decay traces of QD samples in solution.

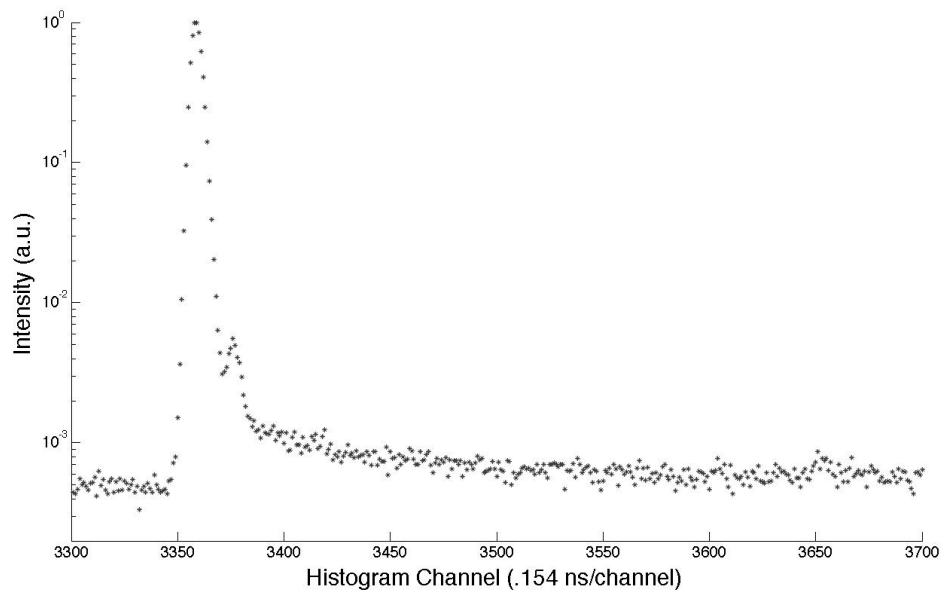


Figure S4. Measurement of the instrument response function used to fit the PL decay traces.

Tabulated PL data

Ligand		Solution	Glass
MPA	t ₁ (% quenching)	4.7 ns (0%)	0.9 ns (80%)
	t ₂ (% quenching)	17.2 ns (0%)	6.9 (61%)
MUA	t ₁ (% quenching)	3.5 ns (0%)	2.8 ns (20%)
	t ₂ (% quenching)	16.7 ns (0%)	11.6 ns (31%)
TOPO/OA	t ₁ (% quenching)	4.0 ns (0%)	0.7 ns (82%)
	t ₂ (% quenching)	16.4 (0%)	5.5 ns (77%)

Table 1. Summary of fitting the PL decays shown in Figure 3A and 3B to equation (1).

Ligand		TiO ₂	ZnO
MPA	t ₁ (% quenching)	0.4 ns (90%)	0.7 ns (83%)
	t ₂ (% quenching)	1.7 ns (90%)	5.2 (68%)
MUA	t ₁ (% quenching)	0.4 ns (89%)	0.6 ns (83%)
	t ₂ (% quenching)	1.9 ns (90%)	5.0 ns (70%)
TOPO/OA	t ₁ (% quenching)	0.3 ns (93%)	0.8 ns (83%)
	t ₂ (% quenching)	2.0 (88%)	7.5 ns (57%)

Table 2. Summary of fitting the PL decays shown in Figure 3C and 3D to equation (1).

III.7 Acknowledgements.

This work was supported by the Center for Revolution Solar Photovoltaics, Colorado Renewal Energy Collobatory and DOE – Basic Energy Sciences. The authors thank Dr. Martin Gelfand and Kevin Whitcomb for useful conversations on both the photoluminescence measurements and data analysis.

III.8 References

- (1) Reiss, P.; Protière, M.; Li, L. Core/Shell Semiconductor Nanocrystals *Small* **2009**, *5*, 154.
- (2) Michalet, X.; Pinaud, F. F.; Bentolila, L. A.; Tsay, J. M.; Doose, S.; Li, J. J.; Sundaresan, G.; Wu, A. M.; Gambhir, S. S.; Weiss, S. Quantum Dots for Live Cells, in Vivo Imaging, and Diagnostics *Science* **2005**, *307*, 538.
- (3) Medintz, I. L.; Uyeda, H. T.; Goldman, E. R.; Mattoussi, H. Quantum dot bioconjugates for imaging, labelling and sensing *Nat. Mater.* **2005**, *4*, 435.
- (4) Kamat, P. V. Quantum Dot Solar Cells. Semiconductor Nanocrystals as Light Harvesters *J. Phys. Chem. C.* **2008**, *112*, 18737.

- (5) Hodes, G. Comparison of Dye-and Semiconductor-Sensitized Porous Nanocrystalline Liquid Junction Solar Cells *J. Phys. Chem. C*. **2008**, *112*, 17778.
- (6) Nozik, A. J.; Beard, M. C.; Luther, J. M.; Law, M.; Ellingson, R. J.; Johnson, J. C. Semiconductor Quantum Dots and Quantum Dot Arrays and Applications of Multiple Exciton Generation to Third-Generation Photovoltaic Solar Cells *Chem. Rev.* **2010**, *110*, 6873.
- (7) Johnston, K. W.; Pattantyus-Abraham, A. G.; Clifford, J. P.; Myrskog, S. H.; Hoogland, S.; Shukla, H.; Klem, E. J. D.; Levina, L.; Sargent, E. H. Efficient Schottky-quantum-dot photovoltaics: The roles of depletion, drift, and diffusion *Appl. Phys. Lett.* **2008**, *92*, 122111.
- (8) Ekimov, A. I.; Efros, A. L.; Onushchenko, A. A. Quantum size effect in semiconductor microcrystals *Solid State Commun.* **1993**, *88*, 947.
- (9) Alivisatos, A. P. Semiconductor Clusters, Nanocrystals, and Quantum Dots *Science* **1996**, *271*, 933.
- (10) Burda, C.; Chen, X.; Narayanan, R.; El-Sayed, M. A. Chemistry and Properties of Nanocrystals of Different Shapes *Chem. Rev.* **2005**, *105*, 1025.
- (11) Aldana, J.; Lavelle, N.; Wang, Y. A.; Peng, X. G. Size-dependent dissociation pH of thiolate ligands from cadmium chalcogenide nanocrystals *J. Am. Chem. Soc.* **2005**, *127*, 2496.
- (12) Aldana, J.; Wang, Y. A.; Peng, X. G. Photochemical instability of CdSe nanocrystals coated by hydrophilic thiols *J. Am. Chem. Soc.* **2001**, *123*, 8844.
- (13) Nozik, A. J. Multiple exciton generation in semiconductor quantum dots *Chem. Phys. Lett.* **2008**, *457*, 3.
- (14) Sambur, J. B.; Novet, T.; Parkinson, B. A. Multiple Exciton Collection in a Sensitized Photovoltaic System *Science* **2010**, *330*, 63.
- (15) Luther, J.; Law, M.; Beard, M.; Song, Q.; Reese, M.; Ellingson, R.; Nozik, A. Schottky Solar Cells Based on Colloidal Nanocrystal Films *Nano Lett* **2008**, *8*, 3488.
- (16) Luther, J. M.; Gao, J. B.; Lloyd, M. T.; Semonin, O. E.; Beard, M. C.; Nozik, A. J. Stability Assessment on a 3% Bilayer PbS/ZnO Quantum Dot Heterojunction Solar Cell *Adv. Mater.* **2010**, *22*, 3704.
- (17) Pattantyus-Abraham, A. G.; Kramer, I. J.; Barkhouse, A. R.; Wang, X.; Konstantatos, G.; Debnath, R.; Levina, L.; Raabe, I.; Nazeeruddin, M. K.;

- Gratzel, M.; Sargent, E. H. Depleted-Heterojunction Colloidal Quantum Dot Solar Cells *ACS Nano* **2010**, *4*, 3374.
- (18) Gao, J. B.; Luther, J. M.; Semonin, O. E.; Ellingson, R. J.; Nozik, A. J.; Beard, M. C. Quantum Dot Size Dependent J-V Characteristics in Heterojunction ZnO/PbS Quantum Dot Solar Cells *Nano Lett.* **2011**, *11*, 1002.
- (19) Leschkies, K. S.; Beatty, T. J.; Kang, M. S.; Norris, D. J.; Aydil, E. S. Solar Cells Based on Junctions between Colloidal PbSe Nanocrystals and Thin ZnO Films *ACS Nano* **2009**, *3*, 3638.
- (20) Gur, I.; Fromer, N. A.; Geier, M. L.; Alivisatos, A. P. Air-stable all-inorganic nanocrystal solar cells processed from solution *Science* **2005**, *310*, 462.
- (21) Plass, R.; Pelet, S.; Krueger, J.; Gratzel, M.; Bach, U. Quantum Dot Sensitization of Organic/Inorganic Hybrid Solar Cells *J. Phys. Chem. B.* **2002**, *106*, 7578.
- (22) Zhou, Y.; Riehle, F. S.; Yuan, Y.; Schleiermacher, H.-F.; Niggemann, M.; Urban, G. A.; Kruger, M. Improved efficiency of hybrid solar cells based on non-ligand-exchanged CdSe quantum dots and poly(3-hexylthiophene) *Appl. Phys. Lett.* **2010**, *96*, 013304.
- (23) Lokteva, I.; Radychev, N.; Witt, F.; Borchert, H.; Parisi, J.; Kolny-Olesiak, J. Surface Treatment of CdSe Nanoparticles for Application in Hybrid Solar Cells: The Effect of Multiple Ligand Exchange with Pyridine *J. Phys. Chem. C.* **2010**, *114*, 12784.
- (24) Martinez-Ferrero, E.; Albero, J.; Palomares, E. Materials, Nanomorphology, and Interfacial Charge Transfer Reactions in Quantum Dot/Polymer Solar Cell Devices *J. Phys. Chem. Lett.* **2010**, *1*, 3039.
- (25) Gur, I.; Fromer, N. A.; Chen, C.-P.; Kanaras, A. G.; Alivisatos, A. P. Hybrid Solar Cells with Prescribed Nanoscale Morphologies Based on Hyperbranched Semiconductor Nanocrystals *Nano Lett.* **2006**, *7*, 409.
- (26) Fuke, N.; Hoch, L. B.; Kuposov, A. Y.; Manner, V. W.; Werder, D. J.; Fukui, A.; Koide, N.; Katayama, H.; Sykora, M. CdSe Quantum-Dot-Sensitized Solar Cell with 100% Internal Quantum Efficiency *ACS Nano* **2010**, *4*, 6377.
- (27) Yu, P.; Zhu, K.; Norman, A. G.; Ferrere, S.; Frank, A. J.; Nozik, A. J. Nanocrystalline TiO₂ solar cells sensitized with InAs quantum dots *J. Phys. Chem. B.* **2006**, *110*, 25451.

- (28) Zaban, A.; Micic, O. I.; Gregg, B. A.; Nozik, A. J. Photosensitization of Nanoporous TiO₂ Electrodes with InP Quantum Dots *Langmuir* **1998**, *14*, 3153.
- (29) Sun, W.-T.; Yu, Y.; Pan, H.-Y.; Gao, X.-F.; Chen, Q.; Peng, L.-M. CdS Quantum Dots Sensitized TiO₂ Nanotube-Array Photoelectrodes *J. Am. Chem. Soc.* **2008**, *130*, 1124.
- (30) Shen, Q.; Arae, D.; Toyoda, T. Photosensitization of nanostructured TiO₂ with CdSe quantum dots: effects of microstructure and electron transport in TiO₂ substrates *J. Photochem. Photobiol., A* **2004**, *164*, 75.
- (31) Niitsoo, O.; Sarkar, S. K.; Pejoux, C.; Ruhle, S.; Cahen, D.; Hodes, G. Chemical bath deposited CdS/CdSe-sensitized porous TiO₂ solar cells *J. Photochem. Photobiol., A* **2006**, *181*, 306.
- (32) Mora-Seró, I.; Bisquert, J.; Dittrich, T.; Belaidi, A.; Susa, A. S.; Rogach, A. L. Photosensitization of TiO₂ Layers with CdSe Quantum Dots: Correlation between Light Absorption and Photoinjection *J. Phys. Chem. C* **2007**, *111*, 14889.
- (33) Lee, H.; Chen, P.; Moon, S.; Sauvage, F.; Sivula, K.; Bessho, T.; Gamelin, D.; Comte, P.; Zakeeruddin, S.; Seok, S.; Grätzel, M.; Nazeeruddin, M. Regenerative PbS and CdS Quantum Dot Sensitized Solar Cells with a Cobalt Complex as Hole Mediator *Langmuir* **2009**, *25*, 7602.
- (34) Lee, H. J.; Yum, J.-H.; Leventis, H. C.; Zakeeruddin, S. M.; Haque, S. A.; Chen, P.; Seok, S. I.; Grätzel, M.; Nazeeruddin, M. K. CdSe Quantum Dot-Sensitized Solar Cells Exceeding Efficiency 1% at Full-Sun Intensity *J. Phys. Chem. C* **2008**, *112*, 11600.
- (35) Lee, H.; Leventis, H. C.; Moon, S.-J.; Chen, P.; Ito, S.; Haque, S. A.; Torres, T.; Nüesch, F.; Geiger, T.; Zakeeruddin, S. M.; Grätzel, M.; Nazeeruddin, M. K. PbS and CdS Quantum Dot-Sensitized Solid-State Solar Cells: "Old Concepts, New Results" *Adv. Funct. Mater.* **2009**, *19*, 2735.
- (36) Lee, Y.; Huang, B. M.; Chien, H. T. Highly Efficient CdSe-Sensitized TiO₂ Photoelectrode for Quantum-Dot-Sensitized Solar Cell *Chem. Mater.* **2008**, *20*, 6903.
- (37) Boulesbaa, A.; Huang, Z.; Wu, D.; Lian, T. Competition between Energy and Electron Transfer from CdSe QDs to Adsorbed Rhodamine B *J. Phys. Chem. C* **2010**, *114*, 962.
- (38) Boulesbaa, A.; Issac, A.; Stockwell, D.; Huang, Z.; Huang, J.; Guo, J.; Lian, T. Ultrafast Charge Separation at CdS Quantum Dot/Rhodamine B Molecule Interface *J. Am. Chem. Soc.* **2007**, *129*, 15132.

- (39) Cho, B.; Peters, W. K.; Hill, R. J.; Courtney, T. L.; Jonas, D. M. Bulklike Hot Carrier Dynamics in Lead Sulfide Quantum Dots *Nano Lett.* **2010**, *10*, 2498.
- (40) Dibbell, R. S.; Watson, D. F. Distance-Dependent Electron Transfer in Tethered Assemblies of CdS Quantum Dots and TiO₂ Nanoparticles *J. Phys. Chem. C.* **2009**, *113*, 3139.
- (41) Guijarro, N. s.; Shen, Q.; Gimenez, S.; Mora-Sero, I. n.; Bisquert, J.; Lana-Villarreal, T.; Toyoda, T.; Gomez, R. Direct Correlation between Ultrafast Injection and Photoanode Performance in Quantum Dot Sensitized Solar Cells *J. Phys. Chem. C.* **2010**, *114*, 22352.
- (42) Hyun, B.-R.; Bartnik, A. C.; Lee, J.-K.; Imoto, H.; Sun, L.; Choi, J. J.; Chujo, Y.; Hanrath, T.; Ober, C. K.; Wise, F. W. Role of Solvent Dielectric Properties on Charge Transfer from PbS Nanocrystals to Molecules *Nano Lett.* **2010**, *10*, 318.
- (43) Jin, S.; Lian, T. Electron Transfer Dynamics from Single CdSe/ZnS Quantum Dots to TiO₂ Nanoparticles *Nano Lett.* **2009**, *9*, 2448.
- (44) Leventis, H. C.; O'Mahony, F.; Akhtar, J.; Afzaal, M.; O'Brien, P.; Haque, S. A. Transient Optical Studies of Interfacial Charge Transfer at Nanostructured Metal Oxide/PbS Quantum Dot/Organic Hole Conductor Heterojunctions *J. Am. Chem. Soc.* **2010**, *132*, 2743.
- (45) Pijpers, J. J. H.; Koole, R.; Evers, W. H.; Houtepen, A. J.; Boehme, S.; de Mello Donega, C.; Vanmaekelbergh, D.; Bonn, M. Spectroscopic Studies of Electron Injection in Quantum Dot Sensitized Mesoporous Oxide Films *J. Phys. Chem. C.* **2010**, *114*, 18866.
- (46) Rawalekar, S.; Kaniyankandy, S.; Verma, S.; Ghosh, H. N. Ultrafast Charge Carrier Relaxation and Charge Transfer Dynamics of CdTe/CdS Core-Shell Quantum Dots as Studied by Femtosecond Transient Absorption Spectroscopy *J. Phys. Chem. C.* **2010**, *114*, 1460.
- (47) Stockwell, D.; Yang, Y.; Huang, J.; Anfuso, C.; Huang, Z.; Lian, T. Comparison of Electron-Transfer Dynamics from Coumarin 343 to TiO₂, SnO₂, and ZnO Nanocrystalline Thin Films: Role of Interface-Bound Charge-Separated Pairs *J. Phys. Chem. C.* **2010**, *114*, 6560.
- (48) Tachibana, Y.; Moser, J. E.; Gratzel, M.; Klug, D. R.; Durrant, J. R. Subpicosecond interfacial charge separation in dye-sensitized nanocrystalline titanium dioxide films *J. Phys. Chem.* **1996**, *100*, 20056.
- (49) Kalyuzhny, G.; Murray, R. Ligand effects on optical properties of CdSe nanocrystals *J. Phys. Chem. B.* **2005**, *109*, 7012.

- (50) Sambur, J. B.; Riha, S. C.; Choi, D.; Parkinson, B. A. Influence of Surface Chemistry on the Binding and Electronic Coupling of CdSe Quantum Dots to Single Crystal TiO₂ Surfaces *Langmuir* **2010**, *26*, 4839.
- (51) Yu, W. W.; Qu, L. H.; Guo, W. Z.; Peng, X. G. Experimental determination of the extinction coefficient of CdTe, CdSe, and CdS nanocrystals *Chem. Mater.* **2003**, *15*, 2854.
- (52) Peng, Z. A.; Peng, X. Formation of High-Quality CdTe, CdSe, and CdS Nanocrystals Using CdO as Precursor *J. Am. Chem. Soc.* **2000**, *123*, 183.
- (53) Lu, Y.; Jaeckel, B.; Parkinson, B. A. Preparation and characterization of terraced surfaces of low-index faces of anatase, rutile, and brookite *Langmuir* **2006**, *22*, 4472.
- (54) Sambur, J. B.; Parkinson, B. A. CdSe/ZnS Core/Shell Quantum Dot Sensitization of Low Index TiO₂ Single Crystal Surfaces *J. Am. Chem. Soc.* **2010**, *132*, 2130.
- (55) Kongkanand, A.; Tvrđy, K.; Takechi, K.; Kuno, M.; Kamat, P. V. Quantum Dot Solar Cells. Tuning Photoresponse through Size and Shape Control of CdSe-TiO₂ Architecture *J. Am. Chem. Soc.* **2008**, *130*, 4007.
- (56) Robel, I.; Subramanian, V.; Kuno, M.; Kamat, P. V. Quantum dot solar cells. Harvesting light energy with CdSe nanocrystals molecularly linked to mesoscopic TiO₂ films *J. Am. Chem. Soc.* **2006**, *128*, 2385.
- (57) Acharya, K. P.; Hewa-Kasakarage, N. N.; Alabi, T. R.; Nemitz, I.; Khon, E.; Ullrich, B.; Anzenbacher, P.; Zamkov, M. Synthesis of PbS/TiO₂ Colloidal Heterostructures for Photovoltaic Applications *J. Phys. Chem. C.* **2010**, *114*, 12496.
- (58) Shepherd, D. P.; Whitcomb, K. J.; Milligan, K. K.; Goodwin, P. M.; Gelfand, M. P.; Orden, A. V. Fluorescence Intermittency and Energy Transfer in Small Clusters of Semiconductor Quantum Dots *J. Phys. Chem. C.* **2010**, *114*, 14831.
- (59) Li, S.; Steigerwald, M. L.; Brus, L. E. Surface States in the Photoionization of High-Quality CdSe Core/Shell Nanocrystals *ACS Nano* **2009**, *3*, 1267.
- (60) Algar, W. R.; Krull, U. J. Luminescence and Stability of Aqueous Thioalkyl Acid Capped CdSe/ZnS Quantum Dots Correlated to Ligand Ionization *Chem. Phys. Chem.* **2007**, *8*, 561.
- (61) Yu, M.; Orden, A. V. Enhanced Fluorescence Intermittency of CdSe-ZnS Quantum-Dot Clusters *Phys. Rev. Lett.* **2006**, *97*, 237402.

- (62) Smith, A. M.; Duan, H.; Rhyner, M. N.; Ruan, G.; Nie, S. A systematic examination of surface coatings on the optical and chemical properties of semiconductor quantum dots *Phys. Chem. Chem. Phys.* **2006**, *8*, 3895.

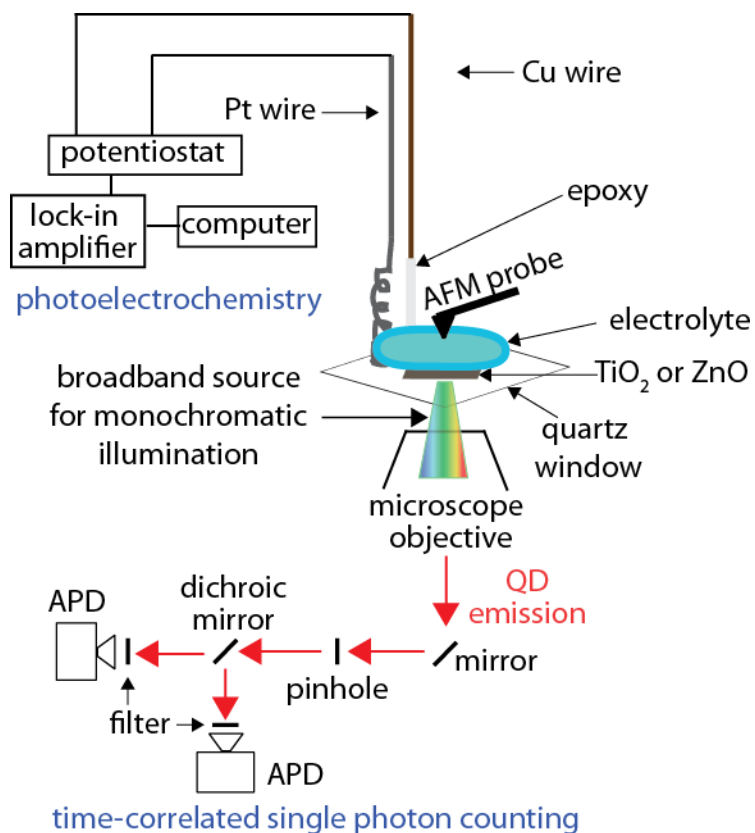
III.9 Future Work

Ideally the pathway for photogenerated electron-hole pairs in QD sensitizers would be strictly limited to electron injection into the metal oxide (TiO₂, ZnO or SnO) conduction band and hole injection into a liquid electrolyte or solid-state hole conductor. Thus the photoluminescence intensity of QD sensitizers would be entirely quenched. Given that QD emission was non-zero on the TiO₂ or ZnO surface, it is clear that the quantum yield for electron injection is not unity.

Rather than analyzing the quenching of a normalized PL signal, future experiments should quantify the QD PL quantum yield (QY) on the TiO₂ surface as a function of the QD size, capping ligand, electrolyte composition and metal oxide substrate (whose conduction band positions dictate the driving force for electron injection). Elucidating the QD PL QY on the surface may provide useful information regarding the mechanism for radiative recombination pathways at QD-metal oxide interfaces. For example, if the timescale for hole injection into cobalt-based electrolytes is an order of magnitude faster than polysulfide electrolytes, then the observed PL QY of the QD on the oxide surface may decrease. Although a decrease in the QY indicates a decrease in radiative recombination, non-radiative recombination processes may still play an important role in electron-hole pair separation within the QD. In order to take non-radiative recombination processes into account, it is important to perform

photoelectrochemical measurements as well as time-resolved optical measurements in QD-sensitized solar cells.

An interesting observation from these experiments is that QD clustering may play an important role in QD-sensitized solar cells. One way to elucidate clustering effects is to compare individual QD behavior with QD clusters.[58] The experimental setup shown in Scheme 2 has the potential to perform simultaneous AFM, photoelectrochemical and time-correlated single photon counting measurements on individual QDs adsorbed on single crystal TiO₂. However several hurdles remain to achieve single-QD resolution: 1) the signal to noise ratio for single-QD optical measurements strictly depends on the ability of incident monochromatic illumination and QD emission to pass through the metal oxide electrode and 2) photocurrent measurements of individual QDs may require insulation of the macroscopic electrode with epoxy in order to limit the dark current and 3) QDs must be adsorbed in low coverage so that the spacing between QDs is less than the ~1 μm laser spot size. Circumventing such experimental hurdles may provide unprecedented insight into QD-QD and QD-metal oxide electronic interactions and thus lead to the development of highly efficient QDSSCs.



Scheme 2. Experimental setup to perform simultaneous AFM, electrochemical and photocurrent measurements.

CHAPTER IV

CADMIUM SELENIUM/ZINC SULFIDE CORE/SHELL QUANTUM DOT SENSITIZATION OF LOW INDEX TITANIUM DIOXIDE SINGLE CRYSTAL SURFACES

This dissertation chapter contains the adapted manuscript of a research article published in the *Journal of the American Chemical Society* **2010**, *132*, 2130-2131. The work demonstrated for the first time photo-induced electron transfer from CdSe/ZnS quantum dots (deposited from a colloidal solution) to the conduction band of TiO₂ single crystal electrodes. Due to the strict page limit of communications published in the *Journal of the American Chemical Society*, the original manuscript was expanded in this dissertation to include additional introduction, motivation for the work and a comprehensive discussion of material contained in the supporting information section. The supporting information figures provide evidence for a photoelectrochemical size-selective etching mechanism of core CdSe QDs in iodide electrolytes. Figure SX denotes additional figures that did not appear in the published manuscript.

The following are contributions to this article from Justin B. Sambur: (i) prepared nanocrystal samples and single crystal electrodes, (ii) performed all AFM and photocurrent measurements; (iii) co-wrote the manuscript with Prof. Parkinson and responded to reviewer comments in order to publish the manuscript in the *Journal of the American Chemical Society* in its current form.

CdSe/ZnS Core/Shell Quantum Dot Sensitization of Low Index TiO₂ Single Crystal Surfaces

Justin B. Sambur and Bruce A. Parkinson

IV.1 Abstract

Quantum dots (QDs) are actively explored as alternative sensitizers to inorganic complexes in sensitized solar cells (SSC) due their interesting physical, optical and electronic properties. It is thought that the inorganic nature of QDs should provide enhanced stability over the entirely organic or inorganic complex dyes, yet the long-term stability of laboratory QD-SSC devices has not been investigated in detail. A general approach to synthesize high stability QDs involves coating the core material with a wide band gap inorganic shell material (type-I CS QD). However, the electronic structure of the resulting core/shell (CS) structure has potential barriers for both electron and hole transfer, suggesting inefficient charge carrier separation for type-I CS QDs. Herein we demonstrate that type-I CdSe/ZnS CS QDs can effectively sensitize single crystal TiO₂ electrodes and continue to operate in a regenerative mode in an aerated iodide electrolyte for more than 20 hours. Core CdSe QDs degrade rapidly in the same electrolyte presumably due to Cd²⁺ dissolution and Se deposition on the QD surface. The possibility of exploring new core/shell nanomaterials in a variety of electrolyte/mediator combinations may result in more efficient and stable QD-SSCs.

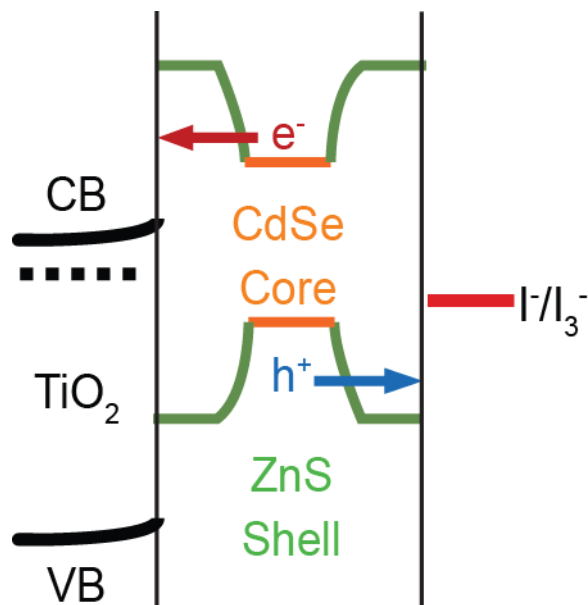
IV.2 Introduction

Quantum dots (QDs) or semiconductor nanocrystals are actively being explored as sensitizers in sensitized solar cells. QDs may offer the advantages of enhanced stability compared to conventional dyes, as well as high light absorption that can be tuned to cover a large fraction of the solar spectrum simply by changing their size.[1,2] Despite such beneficial attributes quantum dot sensitized solar cells (QDSSCs) have not achieved efficiencies or stabilities competitive with conventional dye sensitized solar cells. This is at least partially due to a lack of fundamental understanding of the surface chemistry of QD adsorption in nanocrystalline TiO₂ films that leads to low QD coverages (<50%) on the nanoporous materials.[3] Furthermore the structure and distribution of QDs on nanocrystalline TiO₂ surfaces is difficult to determine since the surface is not flat and mostly inaccessible to scanning probes and electron beams.

We previously addressed the effect of nanocrystal sensitizer morphology on a planar TiO₂ electrode (e.g. single layer of nanocrystals or thick films adsorbed on TiO₂ etc.) on the incident photon-to-current efficiency (IPCE) yields and concluded that QDs modified with bifunctional linker molecules adsorbed uniformly in a single layer over the electrode surface reproducibly resulted in IPCE yields comparable to inorganic Ru-complex sensitizers.[4] The surface chemistry strategy increased the electronic coupling between QD sensitizers and the TiO₂ electron acceptor. Aside from increasing electronic coupling between QD and the oxide acceptor via ligand control, other approaches include manipulating the QD size [5,6] or chemical composition[7-11] to optimize the

driving force for electron injection and the electron transfer rate. Decreasing the size of the nanocrystal increases the band gap and therefore increases the driving force for electron injection between QD and TiO₂ conduction band levels.[5,6] Chemical modification such as doping[12-19], alloying[20,21] or growing epitaxial inorganic shell layers around the nanocrystal core[22-26] can affect the stability and electronic properties[27-29] of the material.

This work focuses on sensitization of TiO₂ with core/shell nanocrystals deposited from colloidal solutions. Core/shell nanomaterials give rise to interesting electronic properties due to so-called band engineering[13,28,30], whereby the wavefunctions of photo-excited electrons and holes can be spatially confined to different regions of the core/shell nanocrystal (shown in Scheme 1). The electronic structure of type-I core/shell nanocrystals confines the photo-excited electron and hole to the core, thus promoting radiative recombination with measured PL quantum yields as high as 80%.[25,26] In addition to the high PL quantum yield, type-I core/shell nanocrystals exhibit far superior resistance to photo-degradation. Due to their excellent photochemical stability, high PL quantum yield and ability to modify the particle surface with different chemical moieties, type-I core/shell nanocrystals are being actively explored as fluorescent tags in the field of bio-imaging.[31]



Scheme 1. Cartoon illustrating energy positions of CdSe/ZnS QDs relative to bulk TiO_2 and the I^-/I_3^- redox couple. Epitaxial growth of the larger band gap ZnS shell imposes a potential energy barrier (green lines) for electrons and holes to separate from the lowest excited states of the CdSe core (orange lines).

The effects of VB and CB offsets on charge carrier dynamics on a variety of core/shell nanocrystals has primarily been investigated by ultrafast optical methods, such as time-resolve photoluminescence (PL) spectroscopy, to demonstrate accelerated or decelerated charge carrier lifetimes.[30,32,33] Band engineering of semiconductor nanocrystals may allow for improved current rectification in sensitized photovoltaic devices by promoting a slow electron (or hole) transfer process relative to a deleterious recombination pathway.[32,34] However, photocurrent measurements of core/shell nanocrystal sensitizers on mesoporous oxides have yet to demonstrate improved long-term stability or photovoltaic characteristics due to band engineering.

It is generally accepted that the propensity for photo-excited electron-hole pairs to recombine in type-I core/shell nanocrystals (giving rise to high PL quantum yields) inhibits their use as sensitizers in a QDSSC where the electron-hole pairs must be effectively separated. However, their resistance to photo-degradation is highly attractive for the realization of QDSSCs exhibiting long-term stability. Herein we address structure and stability issues associated with QD sensitization by using single crystal semiconducting oxide surfaces as model interfaces to study the sensitization yields and surface structures for both 3-mercaptopropionic acid (MPA) capped core CdSe QDs (core-QDs) and MPA capped CdSe/ZnS core shell (CS-QDs).

IV.3 Experimental Methods

Materials. 3-mercaptopropionic acid (MPA) and tetraethylammonium hydroxide were all of the highest purity unless otherwise stated and purchased from Sigma Aldrich. Ethyl acetate, ether and methanol was of ACS grade and purchased from Sigma Aldrich.

MPA-capped CdSe QDs in water and octadecylamine-capped CdSe/ZnS QD powder were purchased from Ocean Nanotech (Springdale, Arkansas).

Ligand exchange of octadecylamine-capped CdSe/ZnS QDs. We followed an adapted procedure developed by Peng and co-workers for CdSe core QDs.[35] Briefly, 40 ml of MPA was added to 15 ml of methanol and adjusted to pH 11 with tetraethylammonium hydroxide. After degassing the solution for 30 min with high purity nitrogen, 5.0 mg of octadecylamine-capped CdSe/ZnS QD powder was added and refluxed for 12 hr at 80°C. Following the ligand exchange procedure,

the QDs were precipitated with ethyl acetate and ether, centrifuged at 3000 rpm, and the supernatant was decanted. The CdSe/ZnS QDs were re-dissolved in 18 M Ω Millipore water. This procedure was repeated two more times and the final MPA-capped CdSe/ZnS QDs dispersed in water were used as sensitization solutions.

Preparation of TiO₂ single crystal surfaces. Mechanically polished crystals of rutile (110), and (001) were obtained from Commercial Crystal Laboratories. The anatase samples were naturally occurring mineral crystals that were mined in Hargvidda, Tyssedal in Norway. These bipyramidal crystals exhibited low-energy growth surfaces with large wedge-shaped (101) faces and (001) end caps. The crystals were polished and annealed according to our previously published procedures.[36] The crystals were mounted on copper disks with Ga/In eutectic to ensure an ohmic contact. A copper wire was soldered to the back of the disk and fed through a glass rod, at which point the entire electrode was sealed with epoxy (Epotek 377) and silicone rubber (RTV) and allowed to dry for a few hours. Prior to dye or QD sensitization, the crystals were gently polished for 30 seconds with a soft polishing cloth using 20 nm colloidal silica (Buehler, Inc.), followed by a 5-10 second immersion in 10% aqueous HF solution and rinsing with copious amounts of 18 M Ω Millipore water. The electrodes were then illuminated at 1.0 V versus a stainless steel wire in 1 M HCl for 20 min using 370 nm UV light emitting diodes in a quartz photoelectrochemical cell. The strongly oxidizing holes generated during the UV treatment process greatly enhanced the sensitization yields by removing unwanted contaminants from the TiO₂ surface.[37] Following

UV treatment, the electrodes were quickly rinsed with Millipore water, dried with a nitrogen stream for 5 seconds, and immersed in 0.4 mg/ml aqueous QD dispersions in the dark for 5 min. Prolonged exposure to either sensitizer did not result in higher photocurrent yields.

Photoelectrochemical measurements. Photoelectrochemical measurements were performed at short circuit in an aqueous 0.25 M KI electrolyte using a two-electrode configuration with a platinum wire counter electrode. Incident photon to current efficiency (IPCE) spectra were measured using a Stanford Research Systems (SRS) model SR570 low noise current preamplifier connected between the working and counter electrodes. The signal from the pre-amplifier was then fed into a SRS model SR830 DSP lock-in amplifier. Illumination from a 100 W Oriel lamp (385 nm cut-off filter) was passed through a computer controlled grating monochromator (2 nm step interval) and chopped at 10 Hz to provide a modulated photocurrent signal. The raw photocurrent signal was corrected for photon flux using a lamp power spectrum recorded at 2 nm intervals using a thermopile detector.

Atomic force microscopy (AFM) measurements. Tapping mode AFM (Digital Instruments Nanoscope IIIA controller and a multimode SPM) was used to characterize the core CdSe QDs on rutile (110) using TETRA-18 boron doped silicon tips from K-Tek Nanotechnology with a 3.5 N/m force constant and resonant frequency of ~90 kHz. The bare and MPA-CdSe/ZnS QD-modified rutile (001) AC mode images were obtained with an Asylum Research AFM using Olympus AC160TS with a 42 N/m force constant and resonant frequency of ~300

kHz. AFM images were processed using WSxM (Nanotec Electronica) software.[38]

IV.4 Results and Discussion

Figure S1 shows the absorbance spectra of CS-QDs capped with native octadecylamine ligands and MPA. The absorbance spectra of the CS-QDs are essentially unaffected by the ligand environment, suggesting that the particle diameter (and band gap) is unaffected.[39] The PL spectra of the same samples (nearly identical optical density) indicate that the ligand environment significantly affects the PL peak intensity, but does not shift the peak position. Photoluminescence quenching of thiol-passivated CdSe nanocrystals has previously been attributed to hole trapping by surface states.[40] Most importantly, the core/shell structure and nanocrystal diameter remained intact after the ligand exchange.

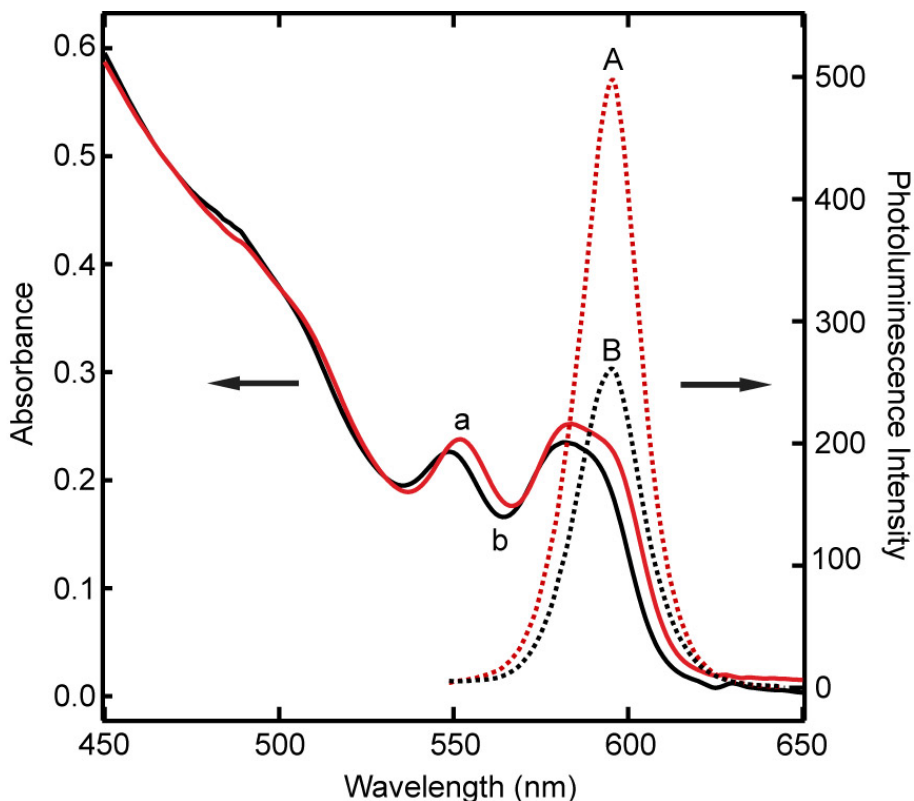


Figure S1. The solid lines represent the solution absorbance spectra of (a) octadecylamine-capped CS-QDs dissolved in toluene and (b) MPA-capped CS-QDs dissolved in water after the ligand exchange procedure was performed. The dashed lines represent the photoluminescence intensity (corresponding to samples used for absorbance measurements excited at 400 nm) of (A) octadecylamine-capped CS-QDs dissolved in toluene and (B) MPA-capped CS-QDs dissolved in water.

The atomically flat rutile (001) TiO_2 surface shown in the tapping mode atomic force microscopy (AFM) image (Figure 1a) allows us to evaluate if the QD coverage is uniform or dominated by 2D or 3D clusters as we and others have previously observed.[4] We recently determined that reproducible monolayer coverages of CdSe QDs covalently bound to single crystal TiO_2 surfaces was governed by both QD purity and the pH of treatment solutions.[4] QDs purified to remove surfactants and dispersed in basic (pH 10.2) aqueous solutions enable MPA ligands to form stable thiolate-Cd chemical bonds (pK_a^{SH} of MPA = 10.2)

without excess MPA in solution and reproducibly results in QD-TiO₂ attachment.[41] The AFM image in Figure 1b shows a rutile (001) surface covered with core-QDs. Figures 1c and 1d show a large area and high-resolution scan of a rutile (110) surface after CS-QD adsorption, respectively. The height profiles measured in Figures 1b and 1c indicate respective 3.5 and 5.0 nm z-heights of the QDs above the bare TiO₂ surface. Due to tip effects it is difficult to accurately determine the particle diameter directly from x-y measurements but it is clear from the high resolution AFM image in Figure 1d that large structures arise from clusters of individual QDs rather than large nanocrystals.

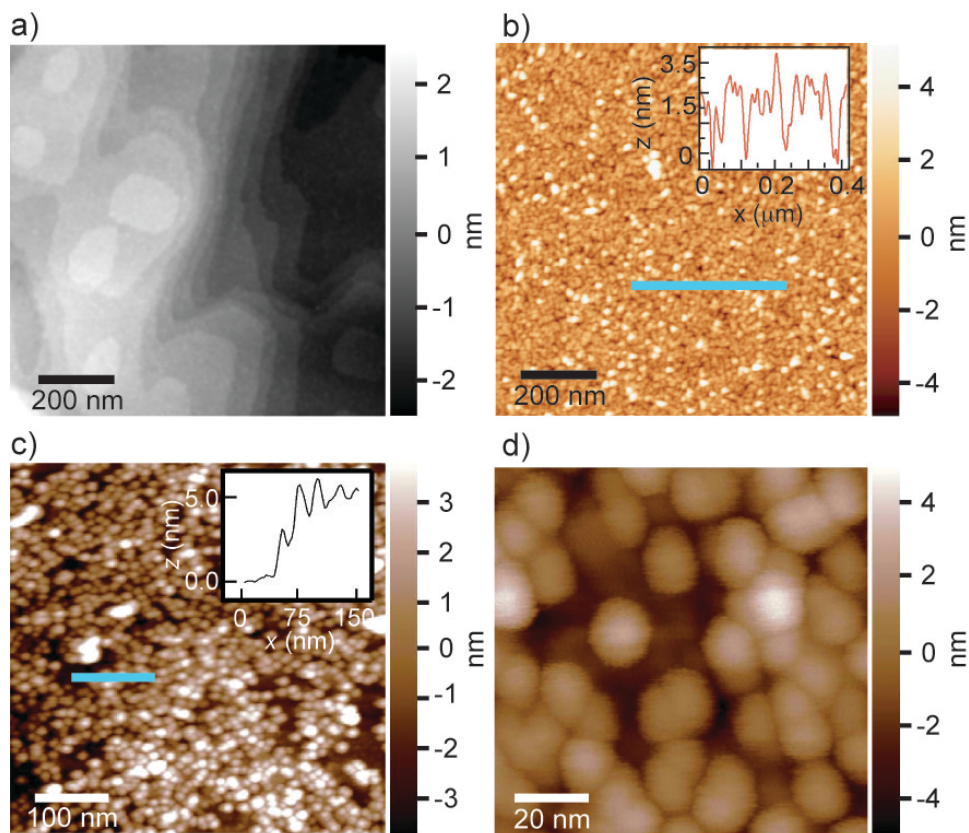


Figure 1. AFM images of a) bare rutile (001), b) core CdSe QDs on rutile (110), c and d) CS-QDs adsorbed on the same rutile (001) surface. The teal bars indicate regions representing the height profiles.

The optical absorption spectra of core CdSe and CS-QDs in water are shown in Figure 2a. The $1S_{3/2}-1S_e$ absorption maxima at 577 nm for the core-QDs corresponds to a diameter of about 3.8 nm, in good agreement with primarily a core-QD monolayer determined via AFM.[39] To determine the CS-QD particle diameter, the monolayer thickness of the ZnS shell was calculated according to the 3.1 Å distance between consecutive planes along the [002] axis in bulk wurtzite ZnS.[42] According to the manufacturer, a 2 to 3 ML ZnS shell was epitaxially grown in solution on a 4.0 nm CdSe core. Therefore the average CS-QD diameter ranges from 5.2 nm to 5.9 nm, which is also in good agreement with the AFM results for CS-QDs. Therefore the sensitization conditions primarily result in a single layer of core and CS-QDs with some agglomerated structures consisting of 2 particles stacked in the z direction.

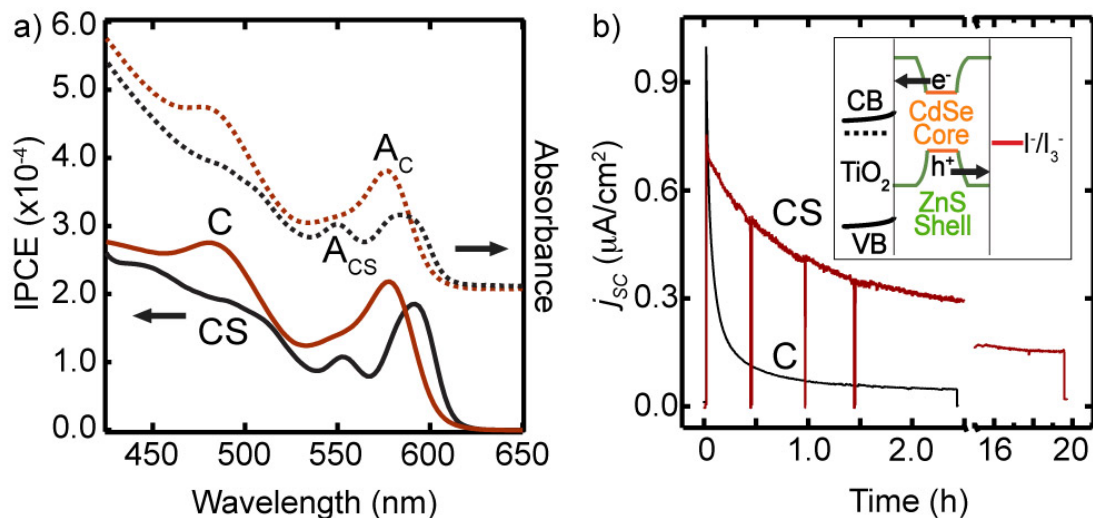


Figure 2. a) The solid lines represent IPCE spectra of core (C) and core/shell (CS) MPA-capped CdSe QDs adsorbed on an anatase (001) electrode surface measured in an aqueous iodide (0.25 M KI) electrolyte at short circuit versus a Pt wire. The corresponding solution absorbance spectrum (dashed lines) of the core (A_C) and CS (A_{CS}) QD samples in water are also shown. b) Photocurrent versus time of C and CS QDs adsorbed on an anatase (001) electrode surface with 47.7 mW/cm^2 illumination at 532 nm. The spikes on trace CS result from momentary blocking of the light. The inset shows an illustration of the pathway for electrons and holes for photo-excited CS-QDs.

The incident photon to current efficiency (IPCE) spectra (Figure 2a) of core CdSe and CS-QDs on an anatase (001) electrode surface in an aqueous iodide electrolyte mimics the corresponding solution absorbance spectra and exhibited similar IPCE values. Sensitization of TiO_2 with CS-QDs is distinguished by an additional peak at 550 nm as well as a distinct red shift and broadening in the first exciton peak due to partial overlap of the exciton wave function with the ZnS shell.[42] To the best of our knowledge, this is the first demonstration of sensitizing TiO_2 with colloidal solutions of core shell QDs. Similar results were obtained on other low index anatase and rutile crystals as shown in Figure S2.

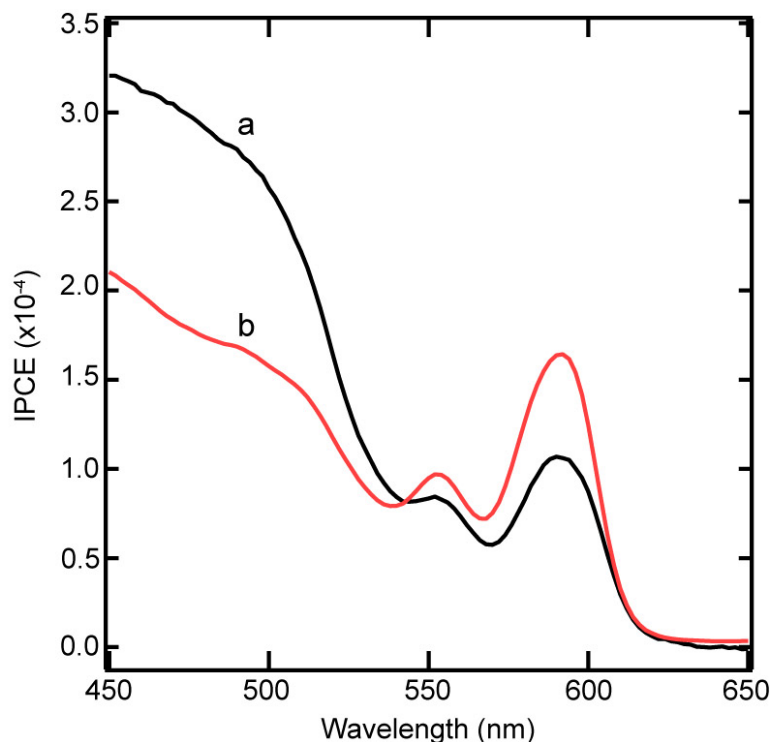


Figure S2. IPCE spectra of CS-CdSe QDs on (a) anatase (101) and (b) rutile (110) measured in an aerated aqueous iodide electrolyte at short circuit versus a Pt wire.

The energy level diagram in the inset of Figure 2b shows type-I band alignment whereby the conduction and valence band (CB and VB) positions of ZnS result in a potential energy barrier for electrons to inject into the CB of TiO₂ and for holes to inject into the electrolyte. Type-I CS-QDs energy alignments produce a quantum well usually favoring exciton recombination and luminescence rather than dissociation.[30] Thus the potential barriers for charge carrier separation from the band alignment in Figure 2b suggests that type-I CS-QDs would not be effective at injecting electrons into TiO₂. However, recent experiments by Lian and co-workers reported an average electron transfer rate from single 4.0 nm CdSe/ZnS QDs coated with a ~4 nm amphiphilic polymer to

TiO₂ nanoparticles of $3.2 \times 10^7 \text{ s}^{-1}$, slower than the $6.3 \times 10^8 \text{ s}^{-1}$ electron transfer rate reported for 3.7 nm CdSe core QDs.[6,43] Likewise, Makhal et al. recently reported electron transfer rates of $3.3 \times 10^9 \text{ s}^{-1}$ and $2.9 \times 10^8 \text{ s}^{-1}$ for 2.4 nm and 4.2 nm diameter CdSe/ZnS CS-QDs respectively, which are comparable to core CdSe QDs.[44] Additionally, hole injection into a sulfide electrolyte was not inhibited from ZnS-coated CdSe QDs deposited on TiO₂ inverse opals (chemical bath deposited ZnS only on the outer exposed surface of CdSe QDs).[45] Despite the type-I CS structure, experimental results suggest the overlap between electron and hole wave functions of CdSe/ZnS QDs and the TiO₂ CB and regenerator orbitals is sufficient for charge separation.

Although the interfacial electronic structure of TiO₂/type-I CS-QDs/electrolyte seems unfavorable for sensitized solar cells, the stable, wide band gap shell material should result in improved device stability. Cadmium chalcogenide photoanodes are generally unstable in aqueous and organic iodide-based electrolytes due to rapid metal iodide formation leading to degradation.[1] Figure 2b shows a short circuit photocurrent stability test (47.7 mW/cm² of 532 nm laser light or ~0.5 sun) of core and CS-QDs adsorbed on an anatase (001) surface in an aerated iodide electrolyte. The photocurrent of the core-QDs decayed by half ($\tau_{1/2}$) in 2.4 min and after 2.4 hours had decayed by over 90%, whereas $\tau_{1/2}$ of the CS-QDs was 84.1 min but retained 21.2% of the initial photocurrent signal even after 20 hr of continuous illumination. Both the core and CS-QDs are stable for extended periods (>30 hrs) in sulfide/polysulfide electrolytes routinely used to stabilize cadmium chalcogenide photoanodes. The

normalized IPCE spectra of the CS-QDs taken before and after the stability test were similar (Figure S3), whereas the IPCE spectrum of the cores was entirely different (Figures S4).

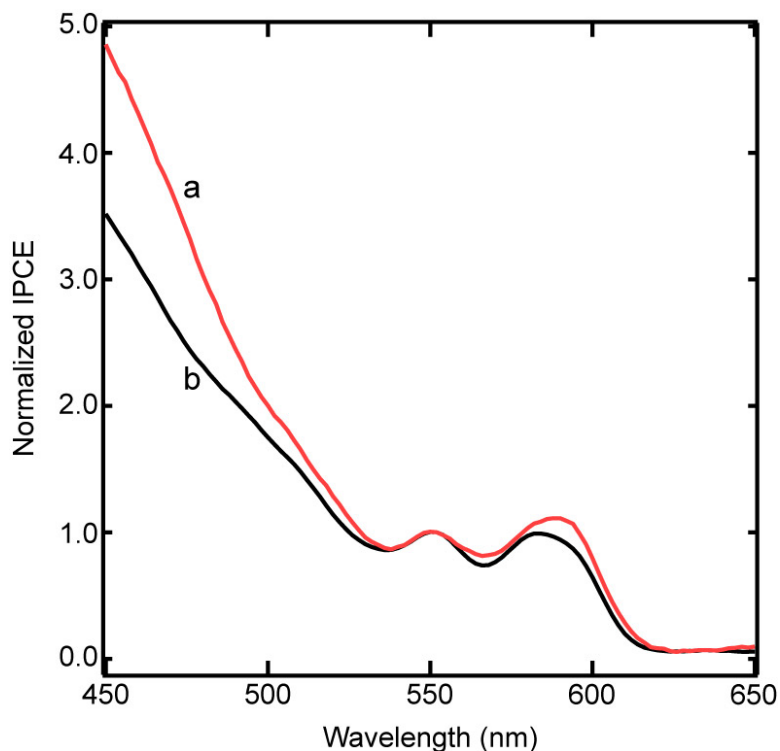


Figure S3. IPCE spectra of CS-QDs (normalized to IPCE values at $\lambda = 550$ nm) measured on an anatase (001) electrode (a) before and (b) after 20 hrs of continuous 47.7 mW/cm^2 illumination with a green 532 nm laser in an aerated aqueous iodide electrolyte. This figure corresponds to measurements performed before and after Figure 2b, trace a.

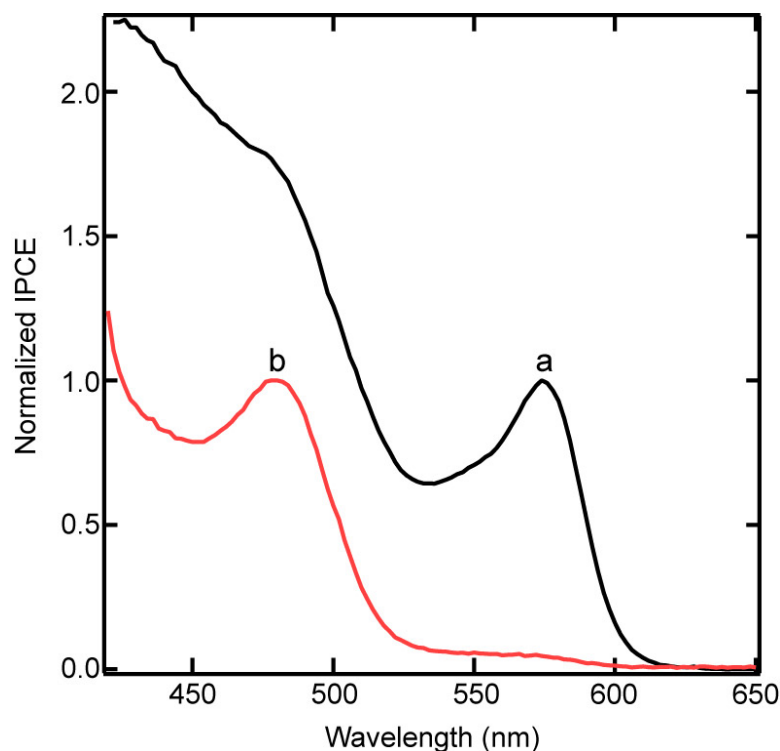


Figure S4. IPCE spectra of core QDs normalized to the values at the maxima of the excitonic features measured on an anatase (001) electrode (a) before and (b) after 20 hrs of continuous 47.7 mW/cm² illumination with a green 532 nm laser in an aerated aqueous iodide electrolyte. This figure corresponds to measurements performed before and after Figure 2b, trace b.

An alternative explanation for the sensitization currents measured for the CS QDs is that electron injection occurs only when defects in the ZnS shell from the synthesis or ligand exchange allows the CdSe core to directly contact the TiO₂ surface. Despite a decrease in the quantum yield upon transfer to the aqueous phase, the solution absorbance and luminescence spectra of the CS QDs before and after ligand exchange did not exhibit significant spectral shifts, suggesting the ZnS shell remained intact (Figure S1). The AFM images indicated monolayer coverage for both core and CS QDs and the comparable IPCE spectra (Figure 1a) on the same anatase (001) surface suggests that the majority

of intact CS QDs are injecting. In addition the CS QDs are stable and retain the same IPCE spectral features (Figure S3) in an aqueous iodide electrolyte long after the photocurrent from the core QDs has completely decayed. These observations clearly demonstrate that intact type-I CS CdSe/ZnS QDs produced the sensitized photocurrents.

Photoelectrochemical etching of core CdSe QDs

The onset of photocurrent in the normalized IPCE spectrum (Figure S4) after long-term monochromatic illumination occurred at approximately 530 nm, coinciding with the incident photon energy. In addition, the distinct blue shift in the first excitonic peak position indicated an increase in the QD band gap and a 1.8 nm decrease in particle diameter.[39]

We used photocurrent spectroscopy to further elucidate the photoelectrochemical decomposition of core CdSe QDs sensitizers on TiO₂ in aqueous iodide electrolytes. Figure S5 shows the normalized IPCE spectra of core CdSe QDs before and after pro-longed monochromatic illumination at different photon energies. The exciton peak at 580 nm, corresponding to the initial core CdSe QD photocurrent spectrum, was not altered after prolonged exposure to the aqueous iodide electrolyte in the dark. After 12 hour illumination with 2.07 eV photons (600 nm) illumination however, the exciton peak is blue-shifted to 560 nm. After illumination of the same electrode with 2.14 eV photons, the exciton peak is further shifted to shorter wavelengths (540 nm). Thus photocurrent spectroscopy revealed a decrease in the core CdSe QD particle size upon illumination with photon energies larger than the nanocrystal band gap.

The photoelectrochemical corrosion process ceased when the incident photon energy was less than the nanocrystal band gap, thus defining the size of the nanocrystal.

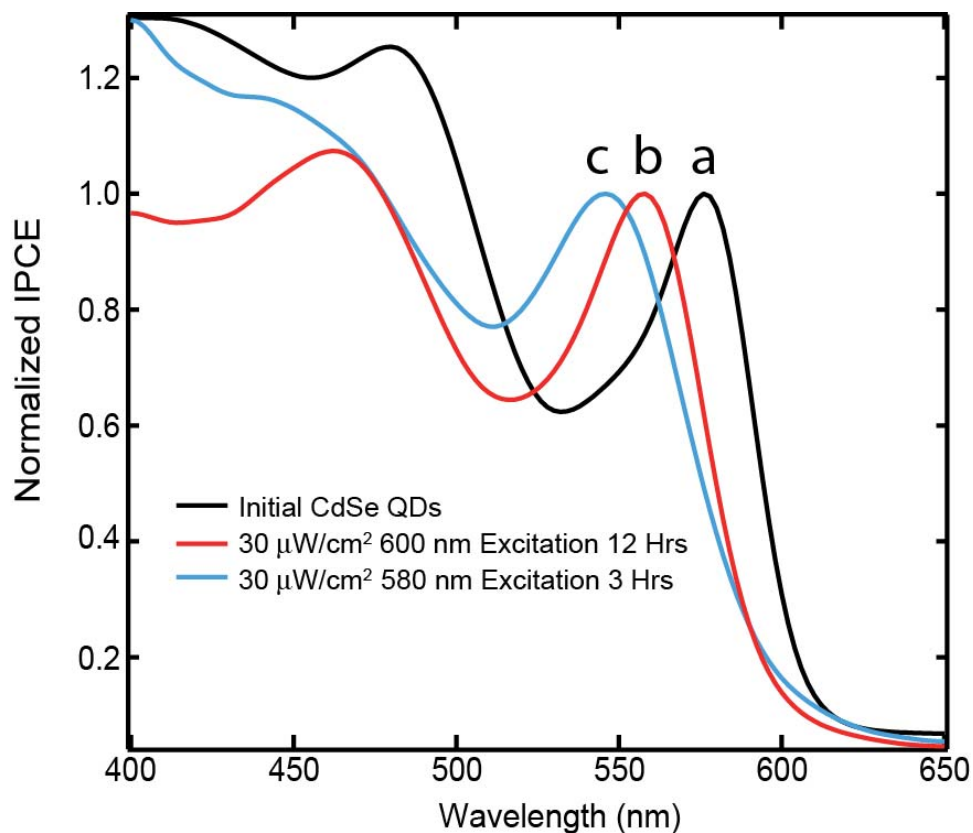
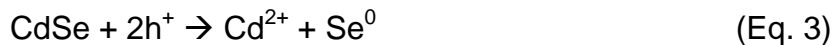
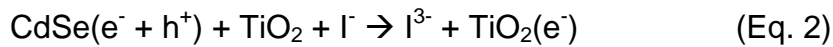


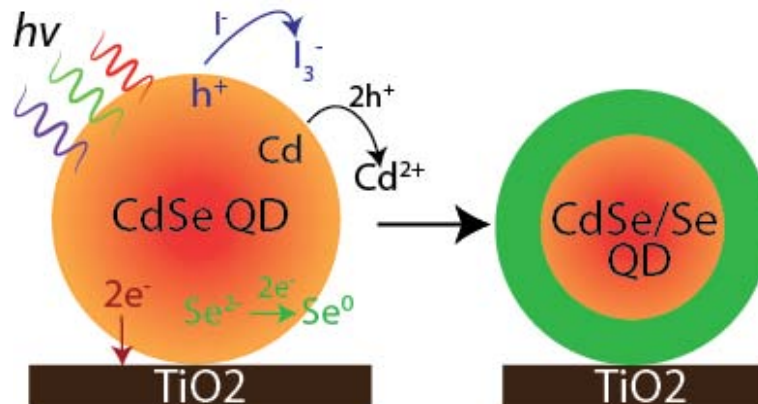
Figure S5. IPCE spectra of core QDs normalized to the values at the maxima of the excitonic features measured on an anatase (001) electrode (a) before and (b) after 12 hrs of continuous $30 \mu\text{W}/\text{cm}^2$ monochromatic illumination 600 nm and (c) after an additional 3 hrs of continuous $30 \mu\text{W}/\text{cm}^2$ monochromatic illumination at 580 nm in an aerated aqueous iodide electrolyte.

Although we did not identify the decomposition products of thiol-passivated CdSe nanocrystals adsorbed on TiO_2 , experimental results of previous studies in the literature support the proposed photocorrosion mechanism shown in Scheme S2. Previous studies demonstrated size-selective photo-etching of CdS, PbS, ZnS, ZnTe, ZnO and CdTe colloidal nanocrystal

solutions using monochromatic illumination.[46-50] The photochemical etching process could decrease the average particle size as much as 30 Å and narrowed the nanocrystal size distribution by 30%.[47] The reaction mechanisms of metal chalcogenide nanocrystal photoetching were primarily based on earlier work using bulk polycrystalline or single crystal electrodes. For example, Memming and co-workers investigated photoelectrochemical etching of bulk CdS single crystal electrodes in aerated aqueous 0.1 M KCl electrolyte and identified Cd^{2+} and SO_4^{2-} as the decomposition products.[51] The proposed reaction schemes for bulk CdS were shown by Matsumoto et al. to accurately describe the photocorrosion of CdS nanocrystals in aerated aqueous solution.[50] Early work by Gerisher identified the photocorrosion reaction products at bulk CdSe electrodes to be soluble Cd^{2+} ions and a surface layer of Se.[52] Although additional studies using bulk single crystal and polycrystalline CdSe electrodes confirm the photocorrosion products identified by Gerisher[53-55], photocorrosion products of CdSe nanocrystals have not been identified. Instead, Peng and co-workers qualitatively described a decomposition mechanism of colloidal CdSe nanocrystals passivated by MPA (based on results in colloidal solutions with and without excess ligand) where diffusion of O_2 into the nanocrystal ligand shell caused oxidation of MPA into soluble disulfides and therefore un-passivated nanocrystals agglomerated and precipitated from solution.[56] However, quantitative mechanistic studies during photocorrosion of thiol capped CdTe nanocrystals identified a similar mechanism to bulk CdSe photocorrosion, where a Te-rich surface layer formed on the nanocrystals.[48,49]

Given the historical literature of photocorrosion of metal chalcogenides, we propose a photoelectrochemical etching mechanism (cartoon illustration in Scheme 2) similar to bulk CdSe electrodes to explain the degradation of CdSe QDs in sensitized solar cells operating in iodide electrolytes. Equation 1 describes the formation of electron-hole pairs in CdSe QDs from monochromatic illumination. The exciton is separated at the TiO₂/QD/electrolyte interface via electron injection into the TiO₂ conduction band and hole transfer to the I⁻ acceptor (Equation 2). However, the sensitized system is not chemically stable to reduction by I⁻ and thus anodic oxidation of CdSe from photoexcited holes causes dissolution of Cd and deposition of elemental Se on the nanocrystal surface. This hypothesis is supported by the high solubility of Cd²⁺ in aqueous solution[53] and the observation of Se rich layers observed on bulk CdSe electrodes under similar experimental conditions.[54]





Scheme 2. Cartoon illustrating the photoelectrochemical decomposition of CdSe QDs adsorbed on single crystal TiO₂. Photogenerated electrons are injected into the TiO₂ conduction band while holes may oxidize I⁻ to I³⁻ or lead to CdSe dissolution by oxidizing Se²⁻ to Se⁰. The resulting nanocrystal consists of a surface layer of Se⁰ and is schematically shown as a CdSe/Se core/shell nanocrystal.

IV.5 Conclusions

The results presented herein may have important implications for a variety of QD or nanoparticle materials previously found to be unstable in sensitized solar cells. For instance type-II CS QD materials may improve charge separation and limit recombination by promoting the forward electron transfer reactions while limiting the reverse processes due to the spatial separation of the electron and hole in different regions of the type-II CS-QD.[30] The possibility of exploring new core/shell nanomaterials in a variety of electrolyte/mediator combinations may result in more efficient and stable QDSSCs.

IV.6 Acknowledgements

We thank Jason Li and Mario Viani of Asylum Research for assistance with AFM images. This work was funded by the DOE-BES Grant #DE-FG03-96ER14625.

IV.7 References

- (1) Hodes, G. Comparison of Dye- and Semiconductor-Sensitized Porous Nanocrystalline Liquid Junction Solar Cells *J. Phys. Chem. C* **2008**, *112*, 17778.
- (2) Kamat, P. V. Quantum Dot Solar Cells. Semiconductor Nanocrystals as Light Harvesters *J. Phys. Chem. C* **2008**, *112*, 18737.
- (3) Mora-Sero, I.; Gimenez, S.; Fabregat-Santiago, F.; Gomez, R.; Shen, Q.; Toyoda, T.; Bisquert, J. Recombination in Quantum Dot Sensitized Solar Cells *Acc. Chem. Res* **2009**, *42*, 1848.
- (4) Sambur, J. B.; Riha, S. C.; Choi, D.; Parkinson, B. A. Influence of Surface Chemistry on the Binding and Electronic Coupling of CdSe Quantum Dots to Single Crystal TiO₂ Surfaces *Langmuir* **2010**, *26*, 4839.
- (5) Robel, I.; Kuno, M.; Kamat, P. V. Size-Dependent Electron Injection from Excited CdSe Quantum Dots into TiO₂ Nanoparticles *J. Am. Chem. Soc.* **2007**, *129*, 4136.
- (6) Kongkanand, A.; Tvrdy, K.; Takechi, K.; Kuno, M.; Kamat, P. Quantum Dot Solar Cells. Tuning Photoresponse through Size and Shape Control of CdSe – TiO₂ Architecture *J. Am. Chem. Soc.* **2008**, *130*, 4007.
- (7) Bang, J.; Park, J.; Lee, J. H.; Won, N.; Nam, J.; Lim, J.; Chang, B. Y.; Lee, H. J.; Chon, B.; Shin, J.; Park, J. B.; Choi, J. H.; Cho, K.; Park, S. M.; Joo, T.; Kim, S. ZnTe/ZnSe (Core/Shell) Type-II Quantum Dots: Their Optical and Photovoltaic Properties *Chem. Mater.* **2009**, *22*, 233.
- (8) Chuang, C.-H.; Lo, S. S.; Scholes, G. D.; Burda, C. Charge Separation and Recombination in CdTe/CdSe Core/Shell Nanocrystals as a Function of Shell Coverage: Probing the Onset of the Quasi Type-II Regime *J. Phys. Chem. Lett.* **2010**, *1*, 2530.
- (9) Sitt, A.; Sala, F. D.; Menagen, G.; Banin, U. Multiexciton Engineering in Seeded Core/Shell Nanorods: Transfer from Type-I to Quasi-type-II Regimes *Nano Lett.* **2009**, *9*, 3470.
- (10) He, J.; Reyner, C. J.; Liang, B. L.; Nunna, K.; Huffaker, D. L.; Pavarelli, N.; Gradkowski, K.; Ochalski, T. J.; Huyet, G.; Dorogan, V. G.; Mazur, Y. I.; Salamo, G. J. Band Alignment Tailoring of InAs_{1-x}Sb_x/GaAs Quantum Dots: Control of Type I to Type II Transition *Nano Lett.* **2010**, *10*, 3052.
- (11) Lo, S. S.; Mirkovic, T.; Chuang, C.-H.; Burda, C.; Scholes, G. D. Emergent Properties Resulting from Type-II Band Alignment in Semiconductor Nanoheterostructures *Adv. Mater.* **2010**, *23*, 180.

- (12) Smith, D. K.; Luther, J. M.; Semonin, O. E.; Nozik, A. J.; Beard, M. C. Tuning the Synthesis of Ternary Lead Chalcogenide Quantum Dots by Balancing Precursor Reactivity *ACS Nano* **2010**, *5*, 183.
- (13) Pan, D.; Wang, X.; Zhou, Z. H.; Chen, W.; Xu, C.; Lu, Y. Synthesis of Quaternary Semiconductor Nanocrystals with Tunable Band Gaps *Chem. Mater.* **2009**, *21*, 2489.
- (14) Li, G.; Jiang, Y.; Wang, Y.; Wang, C.; Sheng, Y.; Jie, J.; Zapien, J. A.; Zhang, W.; Lee, S.-T. Synthesis of CdSXSe_{1-X} Nanoribbons with Uniform and Controllable Compositions via Sulfurization: Optical and Electronic Properties Studies *J. Phys. Chem. C.* **2009**, *113*, 17183.
- (15) Nag, A.; Sapra, S.; Gupta, S.; Prakash, A.; Ghangrekar, A.; Periasamy, N.; Sarma, D. Luminescence in Mn-doped CdS nanocrystals *Bull. Mater. Sci.* **2008**, *31*, 561.
- (16) Chen, H.-Y.; Chen, T.-Y.; Son, D. H. Measurement of Energy Transfer Time in Colloidal Mn-Doped Semiconductor Nanocrystals *J. Phys. Chem. C.* **2010**, *114*, 4418.
- (17) Norris, D. J.; Efros, A. L.; Erwin, S. C. Doped Nanocrystals *Science* **2008**, *319*, 1776.
- (18) Norris, D. J.; Yao, N.; Charnock, F. T.; Kennedy, T. A. High-Quality Manganese-Doped ZnSe Nanocrystals *Nano Lett.* **2000**, *1*, 3.
- (19) Lu, W.; Gao, P.; Jian, W. B.; Wang, Z. L.; Fang, J. Perfect Orientation Ordered in-Situ One-Dimensional Self-Assembly of Mn-Doped PbSe Nanocrystals *J. Am. Chem. Soc.* **2004**, *126*, 14816.
- (20) Zhu, Y. F.; Lang, X. Y.; Jiang, Q. The Effect of Alloying on the Bandgap Energy of Nanoscaled Semiconductor Alloys *Adv. Funct. Mater.* **2008**, *18*, 1422.
- (21) Maikov, G. I.; Vaxenburg, R.; Sashchiuk, A.; Lifshitz, E. Composition-Tunable Optical Properties of Colloidal IV-VI Quantum Dots, Composed of Core/Shell Heterostructures with Alloy Components *ACS Nano* **2010**, *4*, 6547.
- (22) Zhang, W.; Chen, G.; Wang, J.; Ye, B.-C.; Zhong, X. Design and Synthesis of Highly Luminescent Near-Infrared-Emitting Water-Soluble CdTe/CdSe/ZnS Core/Shell/Shell Quantum Dots *Inorg. Chem.* **2009**, *48*, 9723.
- (23) Wang, X.; Ren, X.; Kahen, K.; Hahn, M. A.; Rajeswaran, M.; Maccagnano-Zacher, S.; Silcox, J.; Cragg, G. E.; Efros, A. L.; Krauss, T. D. Non-blinking semiconductor nanocrystals *Nature* **2009**, *459*, 686.

- (24) Pietryga, J. M.; Werder, D. J.; Williams, D. J.; Casson, J. L.; Schaller, R. D.; Klimov, V. I.; Hollingsworth, J. A. Utilizing the Lability of Lead Selenide to Produce Heterostructured Nanocrystals with Bright, Stable Infrared Emission *J. Am. Chem. Soc.* **2008**, *130*, 4879.
- (25) Peng, X.; Schlamp, M. C.; Kadavanich, A. V.; Alivisatos, A. P. Epitaxial Growth of Highly Luminescent CdSe/CdS Core/Shell Nanocrystals with Photostability and Electronic Accessibility *J. Am. Chem. Soc.* **1997**, *119*, 7019.
- (26) Fernée, M. J.; et al. Inorganic surface passivation of PbS nanocrystals resulting in strong photoluminescent emission *Nanotechnology* **2003**, *14*, 991.
- (27) Talapin, D. V.; Lee, J.-S.; Kovalenko, M. V.; Shevchenko, E. V. Prospects of Colloidal Nanocrystals for Electronic and Optoelectronic Applications *Chem. Rev.* **2009**, *110*, 389.
- (28) Peng, X. Band Gap and Composition Engineering on a Nanocrystal (BCEN) in Solution *Acc. Chem. Res* **2010**, *43*, 1387.
- (29) Murphy, C. J. Spatial Control of Chemistry on the Inside and Outside of Inorganic Nanocrystals *ACS Nano* **2009**, *3*, 770.
- (30) Reiss, P.; Protière, M.; Li, L. Core/Shell Semiconductor Nanocrystals *Small* **2009**, *5*, 154.
- (31) Arya, H.; Kaul, Z.; Wadhwa, R.; Taira, K.; Hirano, T.; Kaul, S. C. Quantum dots in bio-imaging: Revolution by the small *Biochem. Biophys. Res. Commun.* **2005**, *329*, 1173.
- (32) Kim, S.; Fisher, B.; Eisler, H.-J.; Bawendi, M. Type-II Quantum Dots: CdTe/CdSe(Core/Shell) and CdSe/ZnTe(Core/Shell) Heterostructures *J. Am. Chem. Soc.* **2003**, *125*, 11466.
- (33) Aldeek, F.; Balan, L.; Medjahdi, G.; Roques-Carmes, T.; Malval, J.-P.; Mustin, C.; Ghanbaja, J.; Schneider, R. Enhanced Optical Properties of Core/Shell/Shell CdTe/CdS/ZnO Quantum Dots Prepared in Aqueous Solution *J. Phys. Chem. C.* **2009**, *113*, 19458.
- (34) Zhu, H.; Song, N.; Lian, T. Controlling Charge Separation and Recombination Rates in CdSe/ZnS Type I Core,àíShell Quantum Dots by Shell Thicknesses *J. Am. Chem. Soc.* **2010**, *132*, 15038.
- (35) Aldana, J.; Wang, Y. A.; Peng, X. G. Photochemical instability of CdSe nanocrystals coated by hydrophilic thiols *J. Am. Chem. Soc.* **2001**, *123*, 8844.

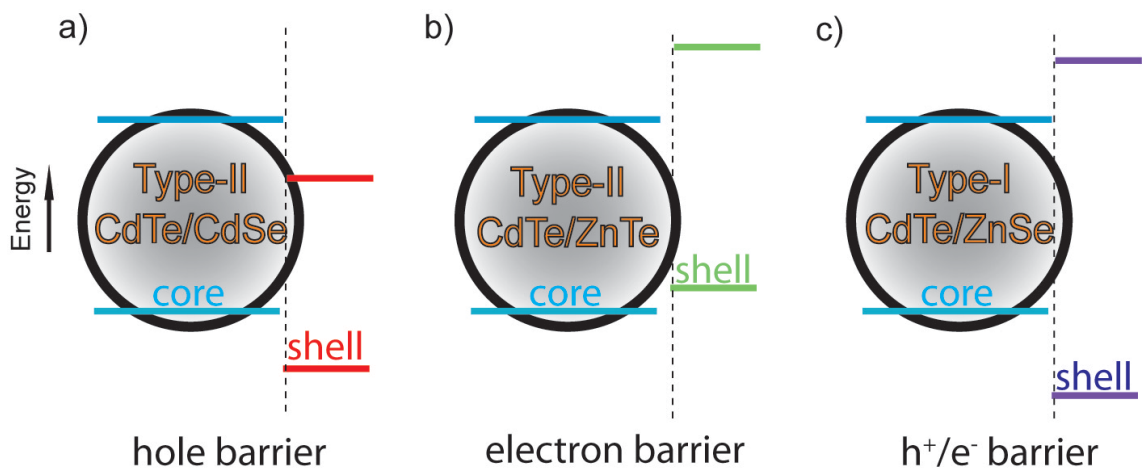
- (36) Lu, Y.; Jaeckel, B.; Parkinson, B. A. Preparation and characterization of terraced surfaces of low-index faces of anatase, rutile, and brookite *Langmuir* **2006**, *22*, 4472.
- (37) Ushiroda, S.; Ruzycski, N.; Lu, Y.; Spitler, M. T.; Parkinson, B. A. Dye sensitization of the anatase (101) crystal surface by a series of dicarboxylated thiocyanine dyes *J. Am. Chem. Soc.* **2005**, *127*, 5158.
- (38) Horcas, I.; Fernandez, R.; Gomez-Rodriguez, J. M.; Colchero, J.; Gomez-Herrero, J.; Baro, A. M. WSXM: A software for scanning probe microscopy and a tool for nanotechnology *Rev. Sci. Instrum.* **2007**, *78*, 013705.
- (39) Yu, W. W.; Qu, L. H.; Guo, W. Z.; Peng, X. G. Experimental determination of the extinction coefficient of CdTe, CdSe, and CdS nanocrystals *Chem. Mater.* **2003**, *15*, 2854.
- (40) Wuister, S. F.; de Mello Donegá, C.; Meijerink, A. Influence of Thiol Capping on the Exciton Luminescence and Decay Kinetics of CdTe and CdSe Quantum Dots *J. Phys. Chem. B.* **2004**, *108*, 17393.
- (41) Aldana, J.; Lavelle, N.; Wang, Y. A.; Peng, X. G. Size-dependent dissociation pH of thiolate ligands from cadmium chalcogenide nanocrystals *J. Am. Chem. Soc.* **2005**, *127*, 2496.
- (42) Dabbousi, B. O.; Rodriguez-Viejo, J.; Mikulec, F. V.; Heine, J. R.; Mattoussi, H.; Ober, R.; Jensen, K. F.; Bawendi, M. G. (CdSe)ZnS Core-Shell Quantum Dots: Synthesis and Optical and Structural Characterization of a Size Series of Highly Luminescent Materials *Journal of Physical Chemistry B* **1997**, *101*, 9463.
- (43) Jin, S.; Lian, T. Electron Transfer Dynamics from Single CdSe/ZnS Quantum Dots to TiO₂ Nanoparticles *Nano Lett.* **2009**, *9*, 2448.
- (44) Makhal, A.; Yan, H.; Lemmens, P.; Pal, S. K. Light Harvesting Semiconductor Core,àShell Nanocrystals: Ultrafast Charge Transport Dynamics of CdSe,àZnS Quantum Dots *J. Phys. Chem. C.* **2009**, *114*, 627.
- (45) Shen, Q.; Kobayashi, J.; Diguna, L. J.; Toyoda, T. Effect of ZnS coating on the photovoltaic properties of CdSe quantum dot-sensitized solar cells *J. Appl. Phys.* **2008**, *103*, 084304/1.
- (46) Torimoto, T.; Kontani, H.; Shibutani, Y.; Kuwabata, S.; Sakata, T.; Mori, H.; Yoneyama, H. Characterization of Ultrasmall CdS Nanoparticles Prepared by the Size-Selective Photoetching Technique *J. Phys. Chem. B.* **2001**, *105*, 6838.

- (47) van Dijken, A.; Janssen, A. H.; Smitsmans, M. H. P.; Vanmaekelbergh, D.; Meijerink, A. Size-Selective Photoetching of Nanocrystalline Semiconductor Particles *Chem. Mater.* **1998**, *10*, 3513.
- (48) Uematsu, T.; et al. Tuning of the fluorescence wavelength of CdTe quantum dots with 2-nm resolution by size-selective photoetching *Nanotechnology* **2009**, *20*, 215302.
- (49) Resch, U.; Weller, H.; Henglein, A. Photochemistry and radiation chemistry of colloidal semiconductors. 33. Chemical changes and fluorescence in CdTe and ZnTe *Langmuir* **1989**, *5*, 1015.
- (50) Matsumoto, H.; Sakata, T.; Mori, H.; Yoneyama, H. Narrowing Size Distribution of CdS Nanocrystals by Size Selective Photocorrosion *Chem. Lett.* **1995**, *24*, 595.
- (51) Meissner, D.; Memming, R.; Kastening, B. Photoelectrochemistry of cadmium sulfide. 1. Reanalysis of photocorrosion and flat-band potential *J. Phys. Chem.* **1988**, *92*, 3476.
- (52) Gerischer, H.; Mindt, W. *Electrochim. Acta.* **1968**, *13*, 1329.
- (53) Bhattacharya, C.; Datta, J. Studies on anodic corrosion of the electroplated CdSe in aqueous and non-aqueous media for photoelectrochemical cells and characterization of the electrode/electrolyte interface *Mater. Chem. Phys.* **2005**, *89*, 170.
- (54) Marcu, V.; Strehlow, H. H. Stability of CdSe and Se Layers in $K_4[Fe(CN)_6]/K_3[Fe(CN)_6]$ Solutions *J. Electrochem. Soc.* **1991**, *138*, 758.
- (55) Frese, J. K. W. Electrochemical Studies of Photocorrosion of n-CdSe *J. Electrochem. Soc.* **1983**, *130*, 28.
- (56) Aldana, J.; Wang, Y. A.; Peng, X. Photochemical Instability of CdSe Nanocrystals Coated by Hydrophilic Thiols *J. Am. Chem. Soc.* **2001**, *123*, 8844.

IV.8 Future Work

In order to optimize visible light absorption in semiconductor sensitized solar cells, it is highly desirable to utilize quantum-confined systems of low band gap bulk materials (e.g. PbS bulk $E_g = 0.4$ eV). However implementation of nanocrystals in QDSSCs is sometimes limited by the stability of the material in a

liquid electrolyte. This study demonstrated that wide band gap ZnS shells could passivate CdSe QDs without inhibiting charge carrier separation within the QD core. However, a systematic study examining the electron injection efficiency of identical QD cores with inorganic shells exhibiting staggered band alignment has not been performed. For example, Scheme 3 illustrates the electronic structure of CdTe/X core/shell nanocrystals (where X = CdSe, ZnTe and ZnSe) approximated from the bulk valence and conduction band (VB and CB) energy levels for each material.[30] Scheme 1a and 1b illustrates type-II band alignment whereby the staggered VB and CB positions of the core and shell imposes a potential energy barrier for one charge carrier (electron or hole). Scheme 1c depicts the type-I case (analogous to CdSe/ZnS nanocrystals) where a large band gap material is grown around the core and thus a potential energy barrier for both charge carriers is imposed.



Scheme 3. Electronic structure of CdTe core nanocrystals with epitaxially grown inorganic shell materials. a) type-II band alignment of CdTe/CdSe shows confinement of the hole. b) type-II band alignment of CdTe/ZnTe shows electron confinement. c) type-I case for CdTe/ZnSe where both the electron and hole are confined to the core.

Once the fundamental mechanisms determining ET and HT from core/shell nanocrystals to TiO_2 are established, it may be possible to stabilize a wide variety of low band gap QDs (InP, InAs, PbS) with stable wide band gap inorganic shells (ZnS , SiO_2) in the so-called type I band alignment configuration. This can be accomplished by bulk solution phase synthesis of core/shell QDs, as well as atomic layer deposition of a stable inorganic tunneling barrier over core QDs deposition on the TiO_2 surface. The panchromatic response of stable QD sensitizers will contribute to the development of highly efficient and stable QDSSCs.

CHAPTER V

MULTIPLE EXCITON COLLECTION IN A SENSITIZED PHOTOVOLTAIC SYSTEM

This dissertation chapter contains the manuscript of a research article published in *Science* **2010**, 330, 63-66. This work demonstrated for the first time absorbed photon-to-current efficiencies greater than 100% due to multiple exciton collection from PbS quantum dots adsorbed on TiO₂ single crystals. Due to the strict document length requirements in *Science*, supporting information figures and tables (designated Figure SX or Table SX) are included in the main text in this dissertation. References that appeared in the supporting information are numbered SX.

The following are contributions to this article from Justin B. Sambur: (i) ligand exchanged PbS nanocrystal samples that were prepared by Thomas Novet at Voxel Inc. (Beaverton, OR), (ii) performed all AFM and photocurrent measurements; (iii) co-wrote the manuscript with Prof. Parkinson and responded to reviewer comments in order to publish the manuscript in the *Science* in its current form.

Multiple Exciton Collection in a Sensitized Photovoltaic System

Justin B. Sambur, Thomas Novet, Bruce A. Parkinson

V.1 Abstract

Multiple exciton generation, the creation of two electron hole pairs from one high-energy photon, is well established in bulk semiconductors, but assessments of the efficiency of this effect remain controversial in quantum confined systems like semiconductor nanocrystals. We use a photoelectrochemical system composed of PbS nanocrystals chemically bound to TiO₂ single crystals to demonstrate the collection of photocurrents with quantum yields greater than one electron per photon. The strong electronic coupling and favorable energy level alignment between PbS nanocrystals and bulk TiO₂ facilitate extraction of multiple excitons more quickly than they recombine as well as collection of hot electrons from higher QD states. Our results have implications for increasing the efficiency of photovoltaic devices by avoiding losses due to the thermalization of photogenerated carriers.

V.2 Introduction

The urgent need for massively scalable carbon-free energy sources has focused attention on both increasing the efficiency and decreasing the cost of photovoltaic cells. When electrons are excited by photons with energy (E_{hv}) in excess of a semiconductor band gap, they tend to rapidly thermally relax to the conduction band edge; in this context, Shockley and Queisser calculated the maximum solar to electrical energy conversion efficiency for an optimal single band gap (E_g) semiconductor absorber to be approximately 31% [1]. Third generation solar cells are based on concepts that can potentially circumvent the so-called Shockley-Queisser limit [2]. One such mechanism, currently under active investigation [3-5], is to convert the excess energy of incident photons with $E_{hv} \geq 2E_g$ into additional free carriers in the material. An ideal material would produce 2 carriers per photon beginning at $E_{hv} = 2E_g$ and additional carriers for photons with energies equal to multiples of E_g (ie. for $E_{hv} = 4E_g$, 4 carriers are generated per photon; however 94% of the maximum gain in power conversion efficiency would be produced with just 2 carriers per photon [6]). This process is known as carrier multiplication via impact ionization in bulk semiconductors, but is quite inefficient because it usually requires E_{hv} to be much greater than $2E_g$ to generate an additional carrier per incident photon. However there have been suggestions[7,8] that the process could be more efficient in semiconductor nanocrystals or quantum dots (QDs) due to the electronic structure associated with carrier confinement in 3 dimensions. In QDs the process is known as multiple exciton generation (MEG) because the carriers are not free but instead

are correlated as a result of confinement. Optical measurements of various nanomaterial systems, including colloidal QD solutions [9-17], QD thin films [18] and single-walled carbon nanotubes (SWCNT) [19] have identified signatures of MEG, but the generation efficiency in nanomaterials relative to bulk materials is still under discussion [20-22].

Despite numerous reports of optical detection of MEG in QDs, multiple exciton collection (MEC) from QDs, converting absorbed photons into photocurrents with quantum yields greater than one, has not yet been observed in a photovoltaic device. Recent reports measured MEG photocurrent in individual SWCNT photodiodes operating at low temperatures [23], separation of multi-excitons generated by multi-photon absorption in colloidal CdSe QDs in solutions of electron acceptors [24] and a photodetector made with PbS QDs that showed enhanced photoconductivity at higher photon energies attributed to MEG [25]. High short circuit photocurrents have been achieved in photovoltaic devices consisting of several hundred nm thick layers of PbSe [26] or PbS [27,28] QDs but quantum yields greater than unity have not been confirmed.

The dye-sensitized solar cell, a subject of intense research since its invention in 1991 [29], is a photoelectrochemical photovoltaic device that has the potential to be cost-effectively mass-produced. The most common manifestation of this device consists of a thin film of inexpensive nanocrystalline titanium dioxide that acts as both a charge transporting substrate and as a high surface area scaffold for attaching visible light-absorbing dye molecules (sensitizers) that inject photo-excited electrons into the TiO₂ conduction band. Recently QDs have

been investigated as sensitizers because of their potential for enhanced stability compared to conventional dyes, as well as high light absorption cross sections that can be tuned to cover a large fraction of the solar spectrum simply by varying the particle size [30,31]. Despite such beneficial attributes, quantum dot sensitized solar cells (QDSSCs) have not achieved efficiencies or stabilities competitive with conventional dye sensitized solar cells. One reason for this is that the surface chemistry for the chemical attachment of the QDs to the TiO₂ surface was not well understood or controlled. In several of our recent studies we used single crystals of both the anatase and rutile forms of TiO₂ as simple model systems to evaluate the influence of different QD attachment procedures on the electronic coupling of CdSe QDs and CdSe/ZnS core/shell QDs to the TiO₂ surface by measuring the photocurrent yields due to electron transfer from photoexcited QDs into TiO₂ [32,33]. We utilized a surface chemistry strategy whereby short-chain, bifunctional passivating ligands such as 3-mercaptopropionic acid (MPA) stabilize the QDs in water while chemically binding the nanocrystals to the TiO₂ surface via thiolate and carboxylic acid moieties, respectively. Atomic force microscopy (AFM) confirmed that our surface chemistry strategy reproducibly resulted in a single layer of QDs covalently bound to the atomically flat single crystal substrates with no three dimensional QD clusters.

The minimum photon energy for observing MEG in CdSe or CdSe/ZnS QDs would be twice the bulk band gap (>3.4 eV). Considering that quantum confinement increases the band gap compared to the bulk, we decided to shift

our focus to PbS, with a considerably lower bulk band gap value of 0.37-0.41 eV at 300 K [35]. PbS QDs are readily synthesized with band gap energies ranging from 0.5 to 2.0 eV, making it possible to measure sensitized photocurrents associated with MEG using photons sufficiently low in energy to preclude direct excitation of the TiO₂ band gap (3.0 eV for rutile and 3.2 eV for anatase).

The kinetically controlled pathways for photogenerated electrons and holes in a QDSSC are depicted in Figure 1. Efficient production of sensitized photocurrents requires the energy of the QD excited state to be higher (more negative on the electrochemical scale) than the conduction band energy of the semiconductor substrate and well electronically coupled to the conduction band states of the semiconductor (Figure 1A). After electron transfer (ET), the photo-oxidized QD is reduced by hole transfer (HT) to a redox species in solution with a reduction potential more positive than the ground state of the QD. In addition to the energetic constraints for efficient ET or HT, various recombination processes such as electron transfer from the TiO₂ conduction band to the QDs (or electrolyte), as well as relaxation of the photo-excited electron to the QD ground state, compete with the forward processes (Figure 1B). Therefore the ratio of rates of the forward (ET or HT) to the reverse (recombination) processes must be high enough to ensure that photocurrent generation is kinetically favored. Aside from the general recombination mechanisms inherent in QDSSCs, MEC requires very fast electron injection in order to outpace exciton-exciton annihilation. The measured fast electron injection times of <1 ns [36] and 50 fs [37] from photoexcited PbS and PbSe QDs respectively into TiO₂, as well as a 4 ps hole

transfer time from PbS QDs to a solid-state organic hole acceptor [38], suggests that MEC can occur on a faster time scale than the 50 ps bi-exciton lifetime (τ_{xx}) measured in isolated PbS QDs [39] (Figure 1B).

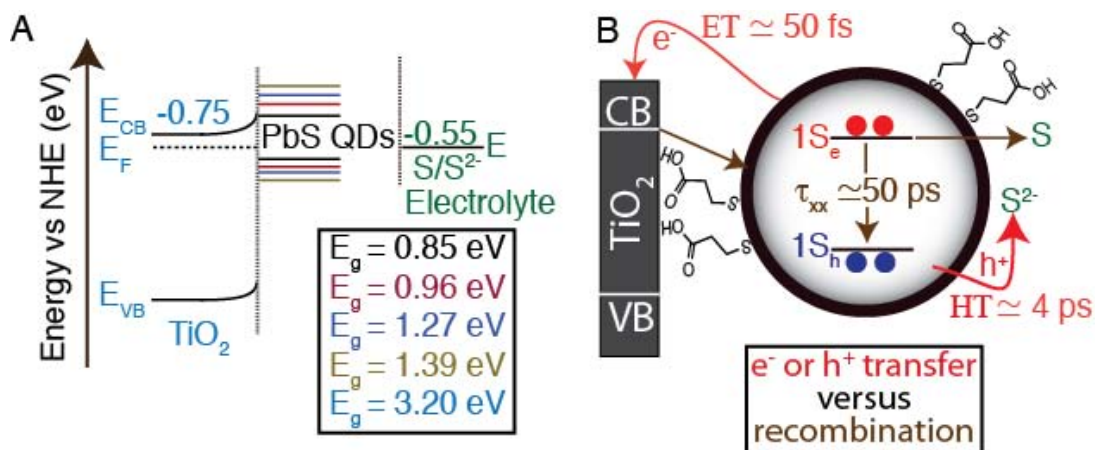


Figure 1. Band energy diagram indicating the relevant energy levels and kinetic processes that describe PbS QD electron and hole transfer (ET and HT) into the TiO₂ conduction band and the sulfide/polysulfide electrolyte, respectively. (A) Energy level alignment of the TiO₂ conduction band (35) with variously sized PbS QDs and the S/S²⁻ redox couple at pH 13. The inset shows the band gap energies of TiO₂ and the QDs used in this study. (B) Representation of a QD adsorbed on a TiO₂ single crystal and the approximate time scales for efficient ET and HT compared to the biexciton lifetime (t_{xx}), as well as other possible recombination pathways. 1S_e and 1S_h refer to the first excited electron and hole state, respectively. Red and brown arrows indicate the favorable processes and possible recombination pathways, respectively.

V.3 Experimental Methods

Materials. Lead oxide, oleic acid, octadecene, sodium sulfide, sulfur tetramethylammonium hydroxide pentahydrate, 3-mercaptopropionic acid and hexamethyldisilathiane were all purchased from Aldrich and used as received.

Synthesis of oleic acid-capped PbS QDs. The synthesis of PbS-oleate nanoparticles followed a procedure similar to the one outlined by Hines and Scholes [S1]. All syntheses were conducted using standard Shlenk line

techniques. In a typical synthesis, 0.3g (1.34 mmol) PbO, 4 ml (12.6 mmol) oleic acid, and 4 ml octadecene were placed in a three neck flask and heated under vacuum to 100°C. Once all the lead oxide had dissolved, usually after 30 minutes, nitrogen was introduced and the temperature was raised to the nucleation temperature (100° to 150°C) necessary for the desired particle size. The lead oleate solution was held at the nucleation temperature for a minimum of 30 minutes. In a separate flask, 0.167 ml (0.834 mmol) hexamethyldisilathiane was dissolved in 8 ml octadecene. Nitrogen was bubbled through the hexamethyldisilathiane solution for 30 minutes to purge the solution of oxygen. The hexamethyldisilathiane solution was then injected into the lead oleate solution and allowed to cool to room temperature. The resulting PbS-oleate nanoparticles were washed by repeated precipitation with acetone and re-dissolution in toluene to remove residual reaction debris.

Ligand exchange of oleic acid-capped PbS QDs. We followed an adapted procedure developed by Peng and co-workers for CdSe QDs [S2]. Briefly, 40 ml of MPA was added to 15 ml of water and adjusted to pH 11 with tetramethylammonium hydroxide pentahydrate. After degassing the solution for 30 min with high purity nitrogen, approximately 10 mg of oleic acid-capped PbS QD powder was added while a steady N₂ stream continuously purged the solution. The ligand exchange procedure occurs very rapidly, and to avoid nanocrystal ripening, the clean anatase (001) electrode was immediately exposed to the QD solution.

Preparation of TiO₂ single crystal surfaces. Two-side mechanically polished, 500 μm thick crystals of rutile (001) were obtained from MTI Corporation. The anatase electrode was constructed from a (001) face of a natural crystal mined in Hargvidda, Tyssedal in Norway. The doping density of the anatase (001) crystal was determined to be $5.7 \times 10^{18} \text{ cm}^{-3}$ by Mott-Schottky analysis. The crystals were polished and annealed according to our previously published procedures [S3]. Prior to dye or QD sensitization, the crystals were gently polished for 30 seconds with a soft polishing cloth using 20 nm colloidal silica (Buehler, Inc.), followed by a 5-10 second immersion in 10% aqueous HF solution and rinsing with copious amounts of 18 MΩ Millipore water. The electrodes were then held at 1.0 V vs. a graphite rod in 1 M HCl in a quartz photoelectrochemical cell during 20 min of illumination using an unfiltered 100 W Oriel Xe arc lamp. The strongly oxidizing valence band holes generated during the UV treatment process greatly enhanced the sensitization yields by removing unwanted contaminants from the TiO₂ surface [S4]. Following UV treatment, the electrodes were quickly rinsed with Millipore water, dried with a nitrogen stream for 5 seconds, and immersed in aqueous ligand exchanged QD dispersions in the dark for 5 min.

Determination of PbS QDs energy levels relative to TiO₂. Photocurrent spectroscopy was used to determine the approximate energy level positions of PbS QDs. A 0.85 eV (9.9 nm) band gap QD did not inject efficiently from the lowest excited state (Figure 3); thus we approximate the band positions of the 0.85 eV QDs as just below the conduction band of TiO₂ at pH 13 in a sulfide electrolyte, consistent with prior literature reports [S5-S7]. Band positions for the

smaller QDs were derived by increasing the gap with equal shifts in the CB and VB due to the approximately equal effective masses of holes and electrons in PbS.

Optical measurements. Prior to data acquisition the bare and QD-modified two-side polished rutile (001) surfaces were characterized by AFM and compared to the anatase (001) surfaces used for photoelectrochemical measurements. Two nearly identical rutile (001) blank and QD-modified crystals were placed in the reference and sample beams of a Perkin Elmer Lambda 950 UV/Vis spectrometer. The spectra were acquired in 0.5 nm wavelength steps with the maximum detector acquisition time (10 seconds). The absorbance spectra were only collected in the visible range due to the extreme sensitivity (noise < 0.0004 A at optical densities of 4 A at 500nm) of the PMT detector. The LHE spectra were corrected for the 2 monolayer QD path lengths of the double-sided crystals. Due to the slight difference in band gap energy between the 0.96 eV and 0.94 eV QD samples, LHE data for the 0.96 eV QDs was used to calculate the APCE values for the 0.94 eV QDs.

Although we are currently limited to performing absorbance and photocurrent measurements on different crystals because doped TiO₂ crystals are opaque, our approach of calculating APCE values is reliable for several reasons. We focus mainly on possible sources of error in the optical data because very low absorbance values are used to calculate APCE values. Determination of APCE values greater than unity due to an artifact or error in the optical absorbance measurements would result from an underestimation of the

'true' absorbance at a given photon energy. Specifically, the single crystal absorbance values need to deviate negatively by more than a factor of 2 compared to the 'true' values beginning at photon energies of 2.8 eV. However, the single crystal absorbance spectra do not show anomalous behavior compared to the bulk solution sample (Figure S4), especially in the high photon energy region where MEC is observed. The illumination intensities ($<10 \mu\text{W}/\text{cm}^2$) employed for optical and photoelectrochemical measurements were far less than the kW/cm^2 , MW/cm^2 or GW/cm^2 intensities needed to cause non-linear absorption effects. Such artifacts are not relevant in our steady-state photocurrent measurements, especially multiple photon absorption since this will not result in APCE values greater than 100%. Furthermore any reflective losses of photons at the QD/TiO₂ interface would result in higher observed absorbance values and therefore lower calculated APCE values.

Photoelectrochemical measurements. Incident photon to current efficiency (IPCE) spectra were measured using a Stanford Research Systems (SRS) model SR570 low noise current preamplifier connected between the working and counter electrodes. The signal from the pre-amplifier was then fed into a SRS model SR830 DSP lock-in amplifier. Illumination from a 100 W Oriel tungsten lamp (using 385 or 650nm cut-off filters for wavelengths shorter than 1000nm and a 1000nm long pass filter for the near-IR region) was passed through a computer controlled grating monochromator (2 nm step interval) and chopped at 13 Hz to provide a modulated photocurrent signal. The raw photocurrent signal was corrected for photon flux using a lamp power spectrum recorded at 2 nm

intervals using a thermopile detector. A ThorLabs C-Series photodiode power meter was used to measure the incident power through the monochromator for the DC photocurrent measurements. Steady-state short circuit photocurrent responses were monitored with an Ivium Compactstat potentiostat. The error in the APCE was propagated from the standard deviation between all the light on (photo) and light off (dark) current signals (Fig S3 A-C).

Atomic force microscopy (AFM) measurements. Tapping mode AFM (Digital Instruments Nanoscope IIIA controller and a multimode SPM) was used to characterize the PbS QDs on rutile (001) and anatase (001) using an Olympus AC160TS probe with a 42 N/m force constant and resonant frequency of ~300 kHz. AFM images were processed using Digital Instruments software.

V.4 Results and Discussion

The structurally well-characterized interface of our electrolyte/PbS QD/single crystal TiO₂ system and the presence of a space charge field at the TiO₂ surface, that can quickly accelerate the injected electrons away from the interface, make this system particularly suitable to observe photocurrent collection from MEG in the adsorbed QDs. We synthesized four QD samples with particle diameters of 9.9 ± 0.8 nm, 4.5 ± 0.3 nm, 3.1 ± 0.3 nm and 2.5 ± 0.3 nm (see Figure S1) with associated band gap energies (determined by the energy position in the absorbance spectra of the first exciton peak maxima) of 0.85 eV, 0.96 eV, 1.27eV and 1.39 eV, respectively. The semiconductor electrode is a nearly atomically flat anatase (001) surface that was imaged with AFM before and after exposure to MPA-capped PbS QDs. Figure 2A shows

>100 nm terraces on the electrode surface before being uniformly coated by treatment with 4.5 nm MPA-capped PbS QDs (Figure 2B; see also Figure S2 for QDs on rutile (001)). The loose packing of the MPA-capped PbS QDs chemically linked to the TiO₂ surface suggests relatively smaller QD-QD interaction (or electronic coupling) when compared to a close-packed monolayer or multilayer films [26,37].

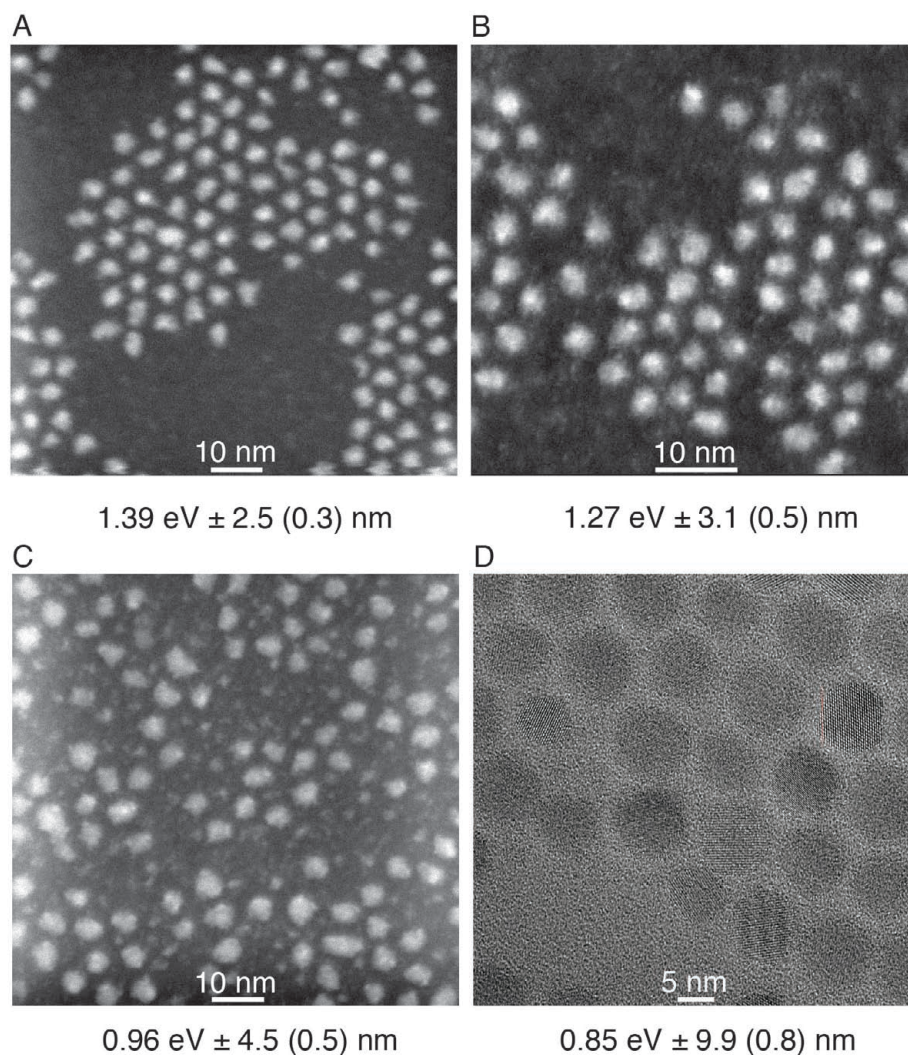


Figure S1. Transmission electron micrographs of the various sizes of oleic acid capped PbS QDs used in this study. The error was determined from the standard deviation in diameters across the ensemble of particles.

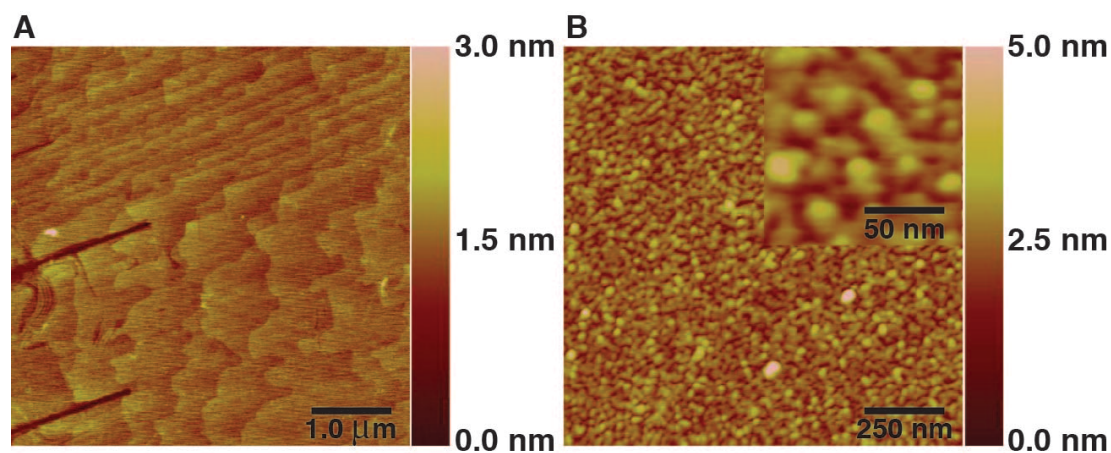


Figure 2. Atomic force microscopy images of the anatase (001) electrode before and after the PbS QD adsorption procedure. (A) Bare electrode surface with an average terrace width of 350 nm with sporadic polishing damage indicated by ~2-5 nm grooves into the surface. (B) ~4.5 nm diameter MPA-capped PbS QDs adsorbed on the same surface. The inset shows the loosely packed QDs at high resolution.

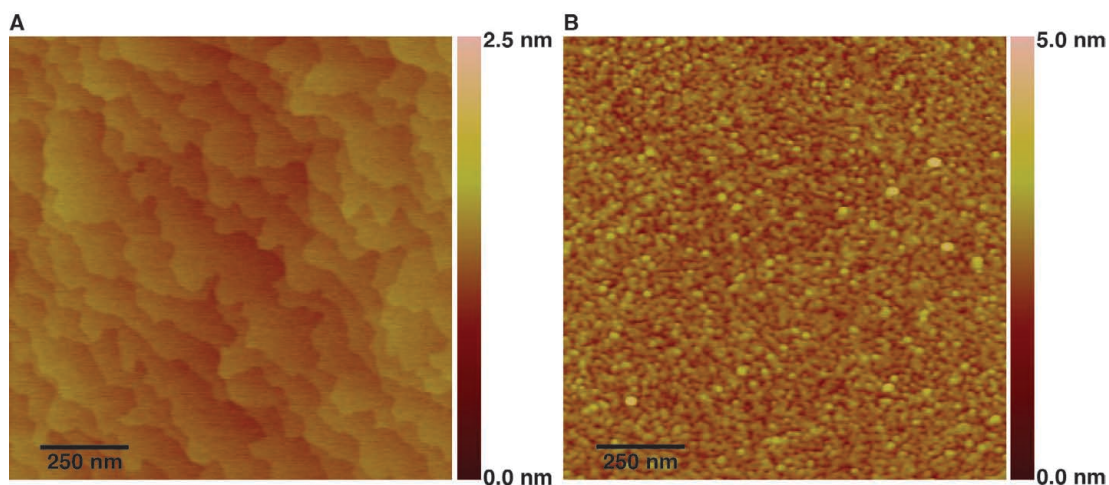


Figure S2. AFM images of the rutile (001) electrode before and after the PbS QD adsorption procedure. (A) bare electrode surface with an average terrace width of 75 nm. (B) ~4.5 nm diameter MPA-capped PbS QDs adsorbed on the same surface.

Since the alignment of the QD excited states relative to the TiO_2 conduction band is size-dependent (Figure 1A), we used photocurrent spectroscopy to resolve the sensitized photocurrents as a function of incident

photon energy for each QD size. We measured the light power at each incident photon energy to calculate the incident photon to current efficiency (IPCE) spectra (Figure 3) from the sensitized photocurrents according to equation 1.

$$IPCE = \frac{hc}{\lambda} \left[\frac{\text{photocurrent density}(\mu\text{A}/\text{cm}^2)}{\text{light power}(\mu\text{W}/\text{cm}^2)} \right] \quad (1)$$

The photocurrent response for QDs with E_g of 0.96 eV and larger (smaller diameter than 4.5 nm) showed distinct excitonic features at nearly the same photon energies observed in the absorbance spectra of the QDs suspended in water. Larger PbS QDs ($E_g = 0.85$ eV) did not sensitize the same anatase electrode at the energy of the first exciton because this excited state energy is more positive on the electrochemical scale than the TiO_2 conduction band energy [28, 40, 41]. However we observe sensitization from these QDs at 700 nm or 1.77 eV (Figure 3A) indicating hot electron injection from higher QD excited states. A very recent study of PbSe QDs adsorbed on a rutile crystal in vacuum measured the time for hot electron injection to be extremely fast (50 fs) [37]. Previous studies with similarly sized PbS QDs prepared by chemical bath deposition directly on mesoporous TiO_2 films showed a photocurrent onset at approximately 800 nm or 1.5 eV [42], despite an onset of light absorption at ~1.2 eV. Thus electron injection from the lowest excitonic states of PbS QDs into nanocrystalline TiO_2 was not observed previously in photocurrent spectra. This comparison suggests strong electronic coupling of PbS QD excited states to the TiO_2 conduction band in our system resulting in facile charge injection and separation of the photoinjected electrons due to the space charge field present at

the semiconductor-electrolyte interface. Therefore multiple excitons produced from higher energy photons in the lowest energy PbS QD excited state should be collected as photocurrents with quantum yields greater than one.

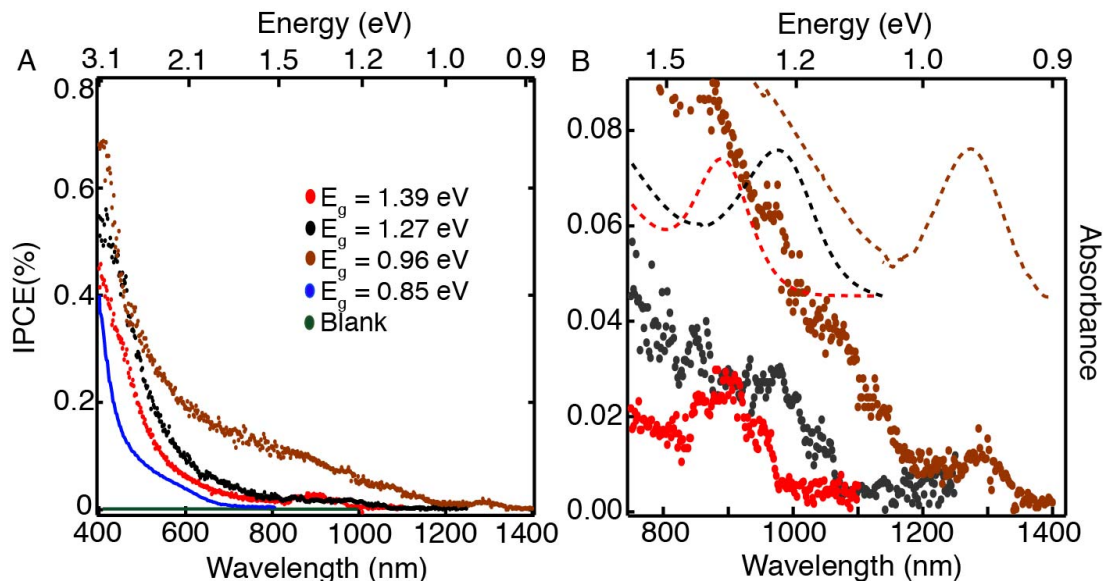


Figure 3. Incident photon to current efficiency (IPCE) spectra of various band gap PbS QDs adsorbed on an anatase (001) electrode. Photocurrents were acquired in an aqueous electrolyte (0.5 M Na_2S , 0.01 M S in 0.1 M NaOH) at short circuit in a two-electrode configuration versus a platinum wire. (A) IPCE spectra versus wavelength for each QD size. The green trace represents the bare anatase (001) photocurrent response. (B) IPCE spectra displaying the near-IR region that compares the photocurrent (solid dots) and QD absorbance in water (dashed lines).

For our planar electrodes covered with a single layer of QD sensitizers the IPCE values are several orders of magnitude lower than those observed in typical sensitized mesoporous TiO_2 solar cells due to the low light absorption from the single layer of QDs. For this reason, the small photocurrent response in the near-IR spectral region was acquired using lock-in detection and a chopped monochromatic light source. Although this technique is very sensitive for measuring small photocurrent signals, the quantification of MEG effects requires

accurate measurement of the absorbed photon to current efficiency (APCE, eq. 2). APCE values take into account the light harvesting efficiency (LHE; eq. 3), or light actually absorbed by the monolayer of QDs.

$$\text{APCE (\%)} = \text{IPCE (\%)} / \text{LHE (\%)} \quad (2)$$

$$\text{LHE (\%)} = 1 - 10^{-\text{Absorbance}} \quad (3)$$

Accurate determination of APCE values required accurate measurements of both the optical absorbance of the QDs adsorbed on the TiO₂ surface and steady-state short circuit photocurrents at various incident photon energies (Figure S3A-C). The absorbance measurements were performed on undoped semi-transparent rutile (001) TiO₂ single crystals with both sides polished (doped anatase and rutile crystals required for photocurrent measurements are not transparent) using a dual-beam configuration in the UV-Vis spectrometer (Figure S3D). Multiple regions of the rutile and anatase crystal surfaces, that were exposed to the same QD solutions at the same time, were imaged with AFM in order to assure that the densities of QDs on all the surfaces were nearly identical to those shown in Figure 2B (also see Figure S2). The absorbance spectra of the PbS QDs adsorbed on the rutile single crystal were similar to the solution absorbance spectra (Figure S4). Due to the larger band gap for the anatase polymorph compared to rutile (3.2 eV vs 3.0 eV), anatase was utilized for the MEC measurements to eliminate any contribution from direct excitation of TiO₂ to the sensitized photocurrent signal at the wavelengths where MEG would be expected.

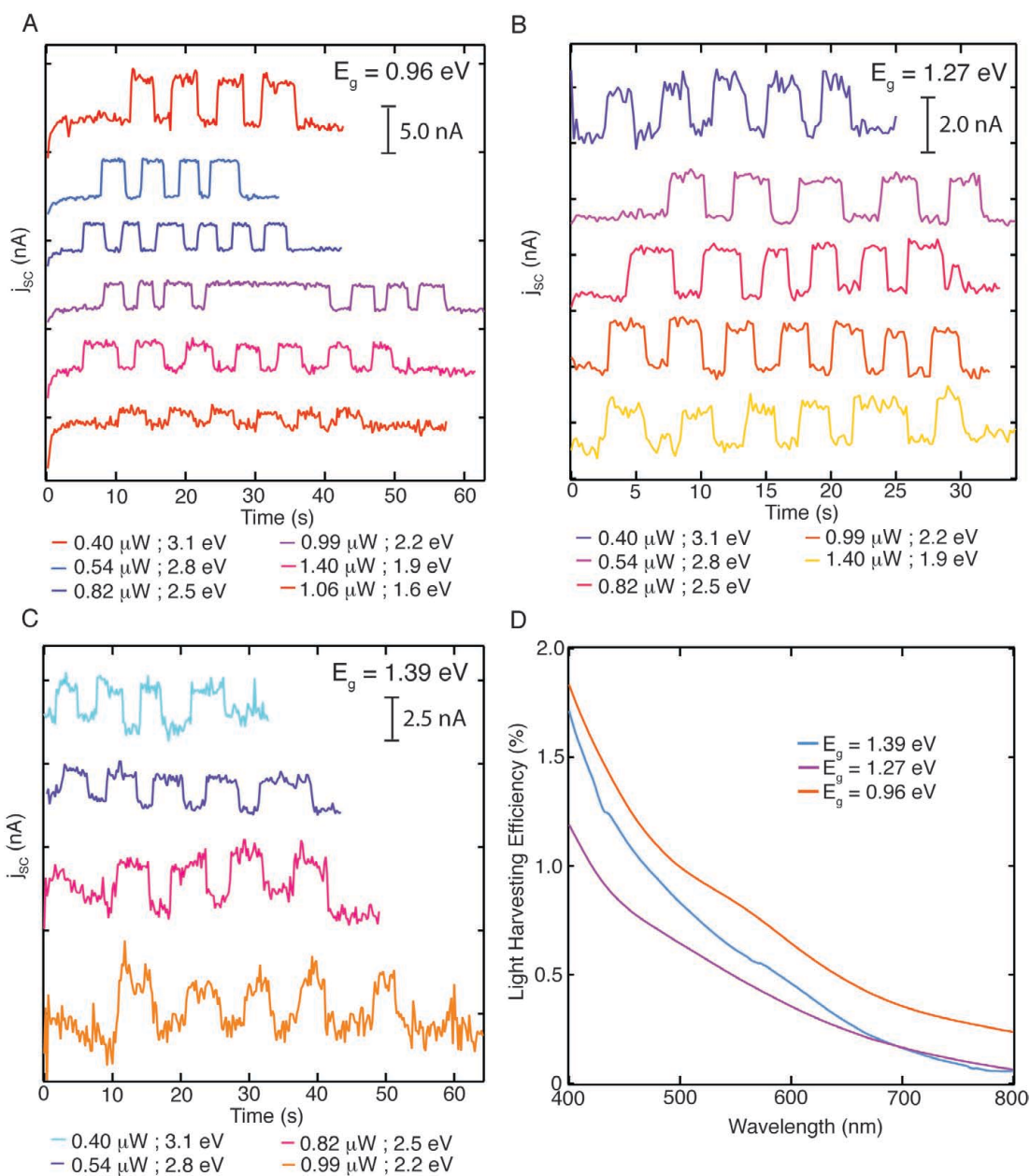


Figure S3. (A-C) Steady-state dark and photocurrent measurements for the different diameter PbS QDs studied on the same 9.3 mm² anatase (001) single crystal. The photocurrents were acquired in an aqueous electrolyte (0.5 M Na₂S, 0.01 M S in 0.1 M NaOH) at short circuit in a two electrode configuration versus a platinum wire. The incident light beam was adjusted such that illumination occurred entirely within the electrode surface. (D) Light harvesting efficiency spectra of each QD sample on two-side polished, 500 μ m rutile (001) single crystals.

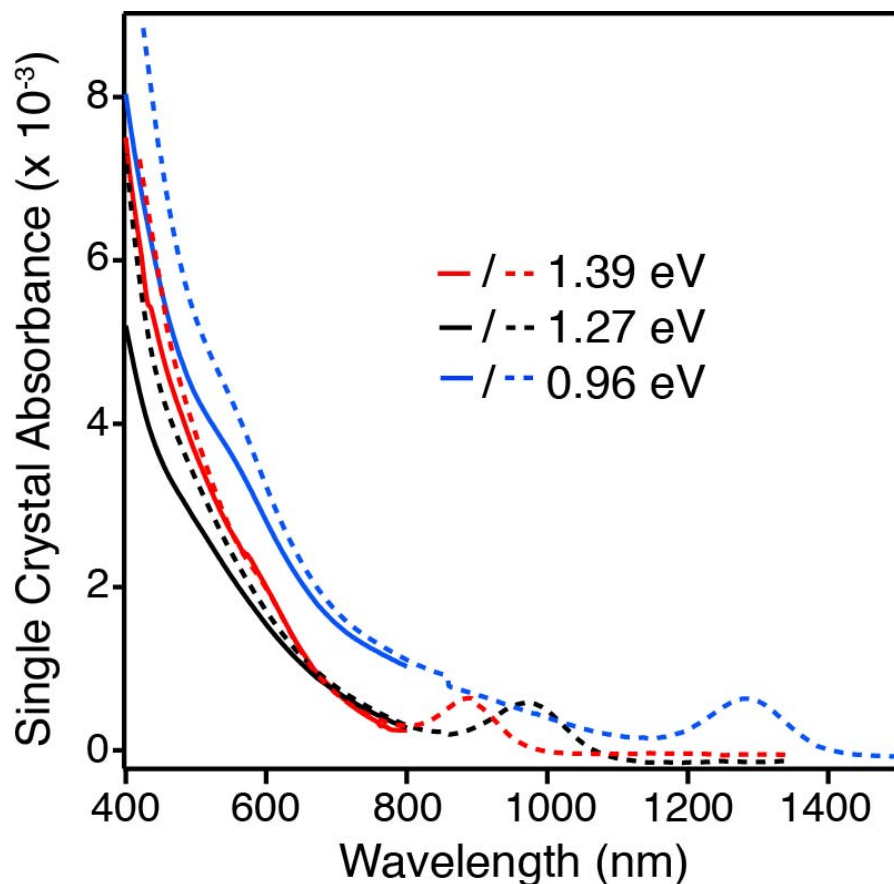


Figure S4. Qualitative comparison of the absorbance spectra for PbS QDs adsorbed on single crystal TiO_2 (solid lines) with the colloidal aqueous solution absorbance spectra (dashed lines) for each QD sample.

Figures 4 A and B show the calculated APCE values both as a function of excitation energy and the ratio of the excitation energy to the nanocrystal band gap ($E_{\text{hv}}/E_{\text{g}}$) for the three sizes of PbS QDs (tabulated data is shown in Tables S1-S4). The APCE values, not adjusted for solution absorbance or reflections from the cell window and crystal surface, remained nearly constant for each QD sample at $70 \pm 13\%$ (standard deviation of photocurrent data) from 1.6 eV up to an absolute photon energy of 2.5 eV (Figure 4A). No increase in the quantum yields indicative of MEC was observed despite crossing the threshold of

illumination with photon energies of twice the band gap for the 4.5 nm PbS QDs ($0.96 \times 2 = 1.92$ eV). However at 2.8 and 3.1 eV illumination, the QDs with $E_g = 0.96$ eV (corresponding to photon energies of 2.9 and 3.2 times the band gap) exhibited APCE values that exceeded unity. There are also indications that APCE values, uncorrected for reflection and absorption losses, approach or exceed 100% at the highest photon energies for QDs with $E_g = 1.27$ and 1.39 eV, however these values remain within the experimental error of the lower energy photocurrent measurements.

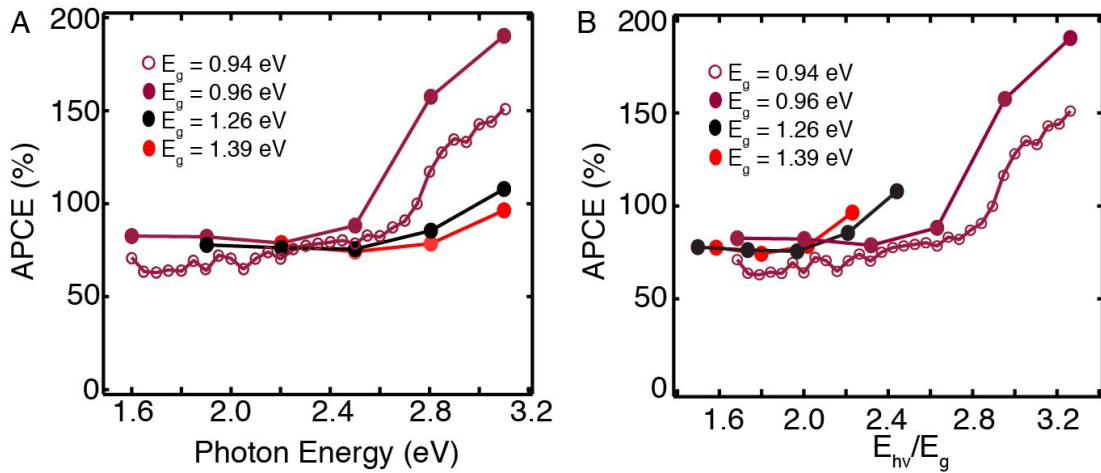


Figure 4. Absorbed photon to current efficiency (APCE) values as a function of the illumination energy. (A) APCE vs. the absolute incident photon energy. (B) APCE vs. the incident photon energy divided by the QD band gap energy (indicating the multiples of the band gap). Adjustments to increase the APCE due to solution absorption and reflection from the cell window and TiO_2 crystal were not performed.

Table S1. Tabulated data obtained from the steady state photocurrent and optical absorption measurements for PbS QDs with $E_g = 0.96$ eV.

Energy (eV)	Power (mW)	Photocurrent (mA)	IPCE (%)	LHE (%)	APCE (%)
3.10	0.40	4.50×10^{-3}	3.49	1.83	190.2
2.81	0.54	4.15×10^{-3}	2.16	1.37	157.5
2.50	0.82	2.93×10^{-3}	0.89	1.01	88.2
2.20	0.99	2.79×10^{-3}	0.62	0.78	78.8
1.90	1.40	2.82×10^{-3}	0.38	0.46	82.2
1.60	1.06	1.44×10^{-3}	0.21	0.26	82.6

Table S2. Tabulated data obtained from the steady state photocurrent and optical absorption measurements for PbS QDs with $E_g = 1.27$ eV.

Energy (eV)	Power (mW)	Photocurrent (mA)	IPCE (%)	LHE (%)	APCE (%)
3.10	0.40	1.66×10^{-3}	1.28	1.19	107.8
2.81	0.54	1.41×10^{-3}	0.73	0.85	85.4
2.50	0.82	1.63×10^{-3}	0.49	0.65	75.5
2.20	0.99	1.57×10^{-3}	0.34	0.45	76.2
1.90	1.40	1.38×10^{-3}	0.18	0.24	77.8

Table S3. Tabulated data obtained from the steady state photocurrent and optical absorption measurements for PbS QDs with $E_g = 1.39$ eV.

Energy (eV)	Power (mW)	Photocurrent (mA)	IPCE (%)	LHE (%)	APCE (%)
3.10	0.40	2.13×10^{-3}	1.65	1.71	96.4
2.81	0.54	1.68×10^{-3}	0.87	1.11	78.5
2.50	0.82	2.07×10^{-3}	0.63	0.85	74.2
2.20	0.99	2.00×10^{-3}	0.44	0.87	77.5

Table S4. Tabulated data obtained from the steady state photocurrent and optical absorption measurements for the second sample of PbS QDs with $E_g = 0.94$ eV.

Energy (eV)	Power (mW)	Photocurrent (mA)	IPCE (%)	LHE (%)	APCE (%)
1.60	4.43	5.17×10^{-3}	0.19	0.26	0.71
1.65	4.91	5.41×10^{-3}	0.18	0.29	0.64
1.70	5.41	6.30×10^{-3}	0.20	0.32	0.63
1.75	5.77	7.25×10^{-3}	0.22	0.34	0.64
1.80	6.12	8.19×10^{-3}	0.24	0.38	0.64
1.85	6.44	1.02×10^{-2}	0.29	0.42	0.69
1.90	6.65	1.04×10^{-2}	0.30	0.47	0.64
1.95	6.84	1.32×10^{-2}	0.38	0.52	0.72
2.00	6.95	1.40×10^{-2}	0.40	0.57	0.71

2.05	6.95	1.38×10^{-2}	0.41	0.63	0.65
2.10	6.89	1.58×10^{-2}	0.48	0.68	0.70
2.15	6.69	1.70×10^{-2}	0.55	0.74	0.74
2.20	6.41	1.62×10^{-2}	0.56	0.79	0.70
2.25	6.08	1.69×10^{-2}	0.62	0.83	0.75
2.30	5.61	1.64×10^{-2}	0.68	0.87	0.78
2.35	5.07	1.53×10^{-2}	0.71	0.91	0.79
2.40	4.66	1.44×10^{-2}	0.74	0.94	0.79
2.45	4.62	1.47×10^{-2}	0.78	0.97	0.80
2.50	4.91	1.56×10^{-2}	0.79	1.01	0.78
2.55	4.42	1.52×10^{-2}	0.88	1.06	0.83
2.60	3.86	1.35×10^{-2}	0.91	1.11	0.82
2.65	3.30	1.26×10^{-2}	1.01	1.16	0.87
2.70	3.39	1.40×10^{-2}	1.12	1.23	0.91
2.75	3.11	1.46×10^{-2}	1.29	1.30	1.00
2.80	2.75	1.57×10^{-2}	1.60	1.37	1.17
2.85	2.41	1.56×10^{-2}	1.85	1.44	1.28
2.90	2.18	1.53×10^{-2}	2.03	1.50	1.35
2.95	1.88	1.34×10^{-2}	2.11	1.59	1.33
3.00	1.57	1.25×10^{-2}	2.40	1.68	1.43
3.05	1.39	1.15×10^{-2}	2.53	1.75	1.44
3.10	1.20	1.07×10^{-2}	2.76	1.83	1.51

An additional sample of PbS nanocrystals with $E_g = 0.94$ eV was synthesized in order to ascertain any sample dependence [43] on the APCE yields (plotted in Figure 4A and B) and to more precisely map out the photon energy dependence of the MEC yields. The absolute magnitudes of the APCEs are smaller by 5-10% and 20-40% at photon energies in the non-MEC and MEC collection regions respectively, but still nearly doubles at the higher photon energies. We emphasize that in order to observe APCE values of over 100% the anatase electrode surface must not be contaminated and should exhibit large (>50 nm) nearly atomically flat terraces in AFM images. Therefore in addition to any possible QD sample-to-sample variation in the MEC yields, we consider the condition of the electrode surface to be paramount in obtaining high and reproducible sensitized photocurrents.

There are conflicting reports regarding the energy threshold for MEG and by how much the quantum yields exceed unity in quantum-confined systems in solution measured with optical methods [43]. However, there are significant differences between optically and photoelectrochemically measured MEG. MEC in our photoelectrochemical photovoltaic system is calculated from very straightforward measurements of steady state currents, photon fluxes and optical absorption. Detection of MEG in isolated colloidal QDs using ultrafast optical techniques requires complex data analysis, and may be complicated by artifacts associated with trap states, charging of the QDs, and multiple photon absorption in a single QD that could result in higher apparent MEG yields [43]. The photocurrents we measure exhibit no short time scale transients associated with

charge trapping and de-trapping of carriers (Figure S3A-C). Furthermore, steady state MEC photocurrents (APCE = 170%) were sustained for 8 hrs of continuous illumination with $4.3 \mu\text{W}/\text{cm}^2$ of 3.1 eV incident photons where each QD undergoes nearly 1000 turnovers or on average about one multiple electron injection and collection every minute.

Although our APCE values greater than 100% onset at slightly lower energy and are higher than the optically determined MEG yields for isolated colloidal PbS QDs [10], it was recently shown that the internal gain in PbS QD photoconductive photodetectors increased at $E_{\text{h}\nu}/E_{\text{g}} = 2.7$ and nearly doubled at $E_{\text{h}\nu}/E_{\text{g}} = 3.2$ [25]. Despite the different mechanisms governing current flow in the two systems, the manifestation of MEG at similar values of $E_{\text{h}\nu}/E_{\text{g}}$ and the magnitude of the yields are strikingly similar. The lower bound of the APCE values for our PbS QDs, demonstrating MEC at an absolute incident photon energy of 3.1 eV, is approximately 15-30% greater than MEG yields for oleic acid capped PbS QDs ($E_{\text{g}} = 0.85$ eV) in tetrachloroethylene studied optically by Nozik and co-workers [10]. The different dielectric environment of MPA-capped PbS QDs adsorbed on TiO_2 is one possible cause for the difference in absolute magnitude between our APCE values and MEG yields reported in typical solution spectroscopic measurements (ie. water and a TiO_2 surface vs. QDs capped with long-chain hydrocarbon surfactants in non-aqueous solutions). However it appears that onset of MEC occurs at approximately $2.5 \pm 0.25 E_{\text{g}}$ for the QD sizes studied herein, in agreement with the onset of MEG determined optically with InP quantum dots with various band gaps [14]. At present, optical

measurements of MEG from PbS QDs capped with short-chain thiols in an aqueous medium are not available for direct comparison to our results.

The results presented herein are encouraging for the future design and development of photovoltaic devices to exploit MEG and MEC and surpass the Shockley-Queisser efficiency limit and approach the ideal single MEG absorber efficiency of 45% [7]. However it remains unclear to what extent MEC can improve the power conversion efficiency in a thin film or QD sensitized device especially if the onset of MEC is at nearly three times the QD band gap.

V.5 Acknowledgements

We thank M.G. Bawendi, A.J. Nozik and D.P. Shepherd for helpful discussions. J.B.S and B.A.P. acknowledge U.S. Department of Energy – Basic Energy Sciences Grant No. DE-FG03-96ER14625 for funding. T.N. acknowledges Department of Energy grant DE-FG36-08GO18025 for financial support.

V.6 References

- (1) Shockley, W.; Queisser, H. J. Detailed Balance Limit of Efficiency of p-n Junction Solar Cells *J. Appl. Phys.* **1961**, *32*, 510.
- (2) Green, M. A. *Third Generation Photovoltaics*; Bridge Printery: Sydney, 2001.
- (3) Shabaev, A.; Efros, A. L.; Nozik, A. J. Multiexciton Generation by a Single Photon in Nanocrystals *Nano Lett.* **2006**, *6*, 2856.
- (4) Rupasov, V. I.; Klimov, V. I. Carrier multiplication in semiconductor nanocrystals via intraband optical transitions involving virtual biexciton states *Phys. Rev. B* **2007**, *76*, 125321.
- (5) Franceschetti, A.; An, J. M.; Zunger, A. Impact Ionization Can Explain Carrier Multiplication in PbSe Quantum Dots *Nano Lett.* **2006**, *6*, 2191.

- (6) Hanna, M. C.; Nozik, A. J. Solar conversion efficiency of photovoltaic and photoelectrolysis cells with carrier multiplication absorbers *J. Appl. Phys.* **2006**, *100*, 074510.
- (7) Nozik, A. J. Multiple exciton generation in semiconductor quantum dots *Chem. Phys. Lett.* **2008**, *457*, 3.
- (8) Benisty, H. Reduced electron-phonon relaxation rates in quantum-box systems- theoretical analysis *Phys. Rev. B* **1995**, *51*, 13281.
- (9) Gachet, D.; Avidan, A.; Pinkas, I.; Oron, D. An Upper Bound to Carrier Multiplication Efficiency in Type II Colloidal Quantum Dots *Nano Lett.* **2009**, *10*, 164.
- (10) Ellingson, R. J.; Beard, M. C.; Johnson, J. C.; Yu, P. R.; Micic, O. I.; Nozik, A. J.; Shabaev, A.; Efros, A. L. Highly efficient multiple exciton generation in colloidal PbSe and PbS quantum dots *Nano Lett.* **2005**, *5*, 865.
- (11) Murphy, J. E.; Beard, M. C.; Norman, A. G.; Ahrenkiel, S. P.; Johnson, J. C.; Yu, P. R.; Micic, O. I.; Ellingson, R. J.; Nozik, A. J. PbTe colloidal nanocrystals: Synthesis, characterization, and multiple exciton generation *J. Am. Chem. Soc.* **2006**, *128*, 3241.
- (12) Pijpers, J. J. H.; Hendry, E.; Milder, M. T. W.; Fanciulli, R.; Savolainen, J.; Herek, J. L.; Vanmaekelbergh, D.; Ruhman, S.; Mocatta, D.; Oron, D.; Aharoni, A.; Banin, U.; Bonn, M. Carrier multiplication and its reduction by photodoping in colloidal InAs quantum dots. *J. Phys. Chem. C* **2008**, *111*, 4783.
- (13) Schaller, R. D.; Pietryga, J. M.; Klimov, V. I. Carrier multiplication in InAs nanocrystal quantum dots with an onset defined by the energy conservation limit *Nano Lett.* **2007**, *7*, 3469.
- (14) Trinh, M. T.; Houtepen, A. J.; Schins, J. M.; Hanrath, T.; Piris, J.; Knulst, W.; Goossens, A.; Siebbeles, L. D. A. In spite of recent doubts carrier multiplication does occur in PbSe nanocrystals *Nano Lett.* **2008**, *8*, 1713.
- (15) Stubbs, S. K.; Hardman, S. J. O.; Graham, D. M.; Spencer, B. F.; Flavell, W. R.; Glarvey, P.; Masala, O.; Pickett, N. L.; Binks, D. J. Efficient carrier multiplication in InP nanoparticles *Phys. Rev. B* **2010**, *81*, 081303.
- (16) Ji, M.; Park, S.; Connor, S. T.; Mokari, T.; Cui, Y.; Gaffney, K. J. Efficient Multiple Exciton Generation Observed in Colloidal PbSe Quantum Dots with Temporally and Spectrally Resolved Intraband Excitation *Nano Lett.* **2009**, *9*, 1217.

- (17) Kobayashi, Y.; Udagawa, T.; Tamai, N. Carrier Multiplication in CdTe Quantum Dots by Single-photon Timing Spectroscopy *Chem. Lett.* **2009**, *38*, 830.
- (18) Beard, M.; Midgett, A. G.; Law, M.; Semonin, O. E.; Ellingson, R. J.; Nozik, A. Variations in the Quantum Efficiency of Multiple Exciton Generation for a Series of Chemically Treated PbSe Nanocrystal Films *Nano Lett.* **2009**, *9*, 836.
- (19) Wang, S.; Khafizov, M.; Tu, X.; Zheng, M.; Krauss, T. D. Multiple Exciton Generation in Single-Walled Carbon Nanotubes *Nano Lett.* **2010**, *10*, 2381.
- (20) Nair, G.; Geyer, S.; Chang, L.; Bawendi, M. Carrier multiplication yields in PbS and PbSe nanocrystals measured by transient photoluminescence *Phys. Rev. B* **2008**, *78*, 125325.
- (21) Delerue, C.; Allan, G.; Pijpers, J. J. H.; Bonn, M. Carrier multiplication in bulk and nanocrystalline semiconductors: Mechanism, efficiency, and interest for solar cells *Phys. Rev. B* **2010**, *81*, 125306.
- (22) Ben-Lulu, M.; Mocatta, D.; Bonn, M.; Banin, U.; Ruhman, S. On the absence of detectable carrier multiplication in a transient absorption study of InAs/CdSe/ZnSe core/shell1/shell2 quantum dots *Nano Lett.* **2008**, *8*, 1207.
- (23) Gabor, N. M.; Zhong, Z.; Bosnick, K.; Park, J.; McEuen, P. L. Extremely Efficient Multiple Electron-Hole Pair Generation in Carbon Nanotube Photodiodes *Science* **2009**, *325*, 1367.
- (24) Huang, J.; Huang, Z.; Yang, Y.; Zhu, H.; Lian, T. Multiple Exciton Dissociation in CdSe Quantum Dots by Ultrafast Electron Transfer to Adsorbed Methylene Blue *J. Am. Chem. Soc.* **2010**, *132*, 4858.
- (25) Sukhovatkin, V.; Hinds, S.; Brzozowski, L.; Sargent, E. H. Colloidal Quantum-Dot Photodetectors Exploiting Multiexciton Generation *Science* **2009**, *324*, 1542.
- (26) Luther, J.; Law, M.; Beard, M.; Song, Q.; Reese, M.; Ellingson, R.; Nozik, A. Schottky Solar Cells Based on Colloidal Nanocrystal Films *Nano Lett.* **2008**, *8*, 3488.
- (27) Tang, J.; Brzozowski, L.; Barkhouse, D. A. R.; Wang, X.; Debnath, R.; Wolowiec, R.; Palmiano, E.; Levina, L.; Pattantyus-Abraham, A. G.; Jamakosmanovic, D.; Sargent, E. H. Quantum Dot Photovoltaics in the Extreme Quantum Confinement Regime: The Surface-Chemical Origins of Exceptional Air- and Light-Stability *ACS Nano* **2010**, *4*, 869.

- (28) Pattantyus-Abraham, A. G.; Kramer, I. J.; Barkhouse, A. R.; Wang, X.; Konstantatos, G.; Debnath, R.; Levina, L.; Raabe, I.; Nazeeruddin, M. K.; Gratzel, M.; Sargent, E. H. Depleted-Heterojunction Colloidal Quantum Dot Solar Cells *ACS Nano* **2010**, *4*, 3374.
- (29) O'Regan, B.; Grätzel, M. A low-cost, high-efficiency solar cell based on dye-sensitized colloidal TiO₂ films *Nature* **1991**, *353*, 737.
- (30) Hodes, G. Comparison of Dye-and Semiconductor-Sensitized Porous Nanocrystalline Liquid Junction Solar Cells *J. Phys. Chem. C* **2008**, *112*, 17778.
- (31) Kamat, P. V. Quantum Dot Solar Cells. Semiconductor Nanocrystals as Light Harvesters *J. Phys. Chem. C* **2008**, *112*, 18737.
- (32) Sambur, J. B.; Riha, S. C.; Choi, D.; Parkinson, B. A. Influence of Surface Chemistry on the Binding and Electronic Coupling of CdSe Quantum Dots to Single Crystal TiO₂ Surfaces *Langmuir* **2010**, *26*, 4839.
- (33) Sambur, J. B.; Parkinson, B. A. CdSe/ZnS Core/Shell Quantum Dot Sensitization of Low Index TiO₂ Single Crystal Surfaces *J. Am. Chem. Soc.* **2010**, *132*, 2130.
- (34) Materials and Methods are detailed in supporting material at *Science Online* (included directly in this dissertation).
- (35) Strehlow, W. H.; Cook, E. L. Compilation of Energy Band Gaps in Elemental and Binary Compound Semiconductors and Insulators *J. Phys. Chem. Ref. Data* **1973**, *2*, 163.
- (36) Leventis, H. C.; O'Mahony, F.; Akhtar, J.; Afzaal, M.; O'Brien, P.; Haque, S. A. Transient Optical Studies of Interfacial Charge Transfer at Nanostructured Metal Oxide/PbS Quantum Dot/Organic Hole Conductor Heterojunctions *J. Am. Chem. Soc.* **2010**, *132*, 2743.
- (37) Tisdale, W. A.; Williams, K. J.; Timp, B. A.; Norris, D. J.; Aydil, E. S.; Zhu, X.-Y. Hot-Electron Transfer from Semiconductor Nanocrystals *Science* **2010**, *328*, 1543.
- (38) Plass, R.; Pelet, S.; Krueger, J.; Grätzel, M.; Bach, U. Quantum Dot Sensitization of Organic/Inorganic Hybrid Solar Cells *J. Phys. Chem. B* **2002**, *106*, 7578.
- (39) Istrate, E.; Hoogland, S.; Sukhovatkin, V.; Levina, L.; Myrskog, S.; Smith, P. W. E.; Sargent, E. H. Carrier relaxation dynamics in lead sulfide colloidal quantum dots *J. Phys. Chem. B* **2008**, *112*, 2757.

- (40) Hyun, B.-R.; Zhong, Y.-W.; Bartnik, A. C.; Sun, L.; Abruña, H. D.; Wise, F. W.; Goodreau, J. D.; Matthews, J. R.; Leslie, T. M.; Borrelli, N. F. Electron Injection from Colloidal PbS Quantum Dots into Titanium Dioxide Nanoparticles *ACS Nano* **2008**, *2*, 2206.
- (41) Dissanayake, D.; Lutz, T.; Curry, R. J.; Silva, S. R. P. Measurement and validation of PbS nanocrystal energy levels *Appl. Phys. Lett.* **2008**, *93*, 3.
- (42) Lee, H.; Leventis, H. C.; Moon, S.-J.; Chen, P.; Ito, S.; Haque, S. A.; Torres, T.; Nüesch, F.; Geiger, T.; Zakeeruddin, S. M.; Grätzel, M.; Nazeeruddin, M. K. PbS and CdS Quantum Dot-Sensitized Solid-State Solar Cells: Old Concepts, New Results *Adv. Funct. Mater.* **2009**, *19*, 2735.
- (43) McGuire, J. A.; Joo, J.; Pietryga, J. M.; Schaller, R. D.; Klimov, V. I. New Aspects of Carrier Multiplication in Semiconductor Nanocrystals *Acc. Chem. Res.* **2008**, *41*, 1810.
- (S1) Hines, M. A.; Scholes, G. D. Colloidal PbS nanocrystals with size-tunable near-infrared emission: Observation of post-synthesis self-narrowing of the particle size distribution *Adv. Mater.* **2003**, *15*, 1844.
- (S2) Aldana, J.; Lavelle, N.; Wang, Y. A.; Peng, X. G. Size-dependent dissociation pH of thiolate ligands from cadmium chalcogenide nanocrystals *J. Am. Chem. Soc.* **2005**, *127*, 2496.
- (S3) Lu, Y.; Jaeckel, B.; Parkinson, B. A. Preparation and characterization of terraced surfaces of low-index faces of anatase, rutile, and brookite *Langmuir* **2006**, *22*, 4472.
- (S4) Ushiroda, S.; Ruzycski, N.; Lu, Y.; Spitler, M. T.; Parkinson, B. A. Dye sensitization of the anatase (101) crystal surface by a series of dicarboxylated thiocyanine dyes *J. Am. Chem. Soc.* **2005**, *127*, 5158.
- (S5) Wang, D.; Zhao, H.; Wu, N.; El Khakani, M. A.; Ma, D. Tuning the Charge-Transfer Property of PbS-Quantum Dot/TiO₂-Nanobelt Nanohybrids via Quantum Confinement *J. Phys. Chem. Lett.* **2010**, *1*, 1030.
- (S6) Pattantyus-Abraham, A. G.; Kramer, I. J.; Barkhouse, A. R.; Wang, X.; Konstantatos, G.; Debnath, R.; Levina, L.; Raabe, I.; Nazeeruddin, M. K.; Gratzel, M.; Sargent, E. H. Depleted-Heterojunction Colloidal Quantum Dot Solar Cells *ACS Nano* **2010**, *4*, 3374.
- (S7) Dissanayake, D.; Lutz, T.; Curry, R. J.; Silva, S. R. P. Measurement and validation of PbS nanocrystal energy levels *Appl. Phys. Lett.* **2008**, *93*, 3.

V.7 Future Work

This study demonstrated multiple exciton collection for the first time using a single layer of QD light absorbers on planar TiO_2 substrates. Although this approach afforded high-resolution structural characterization of the TiO_2/QD interface, power conversion efficiency is ultimately limited by light absorption from the single layer of QDs. In order to scale up the QD coverage it is possible to 1) increase the surface area of the oxide using nanoparticles or 2) grow QD thin films directly on the planar oxide [26-28] (compact ZnO or TiO_2 thin film). However, high surface area metal oxide supports may exhibit enhanced QD agglomeration within nanopores that are not amenable to high-resolution structural characterization. However, our single crystal substrates are excellent model systems to study electron injection efficiency as a function of QD film thickness.

QD thin films may be prepared by drop casting, spin coating or the so-called layer by layer (LbL) growth procedure. The LbL growth procedure involved low velocity immersion (and removal) of a metal oxide substrate into a concentrated solution of QDs (typically 30-100 mg QDs capped with long chain ligands/ml of organic solvent). Following removal of the substrate from the organic QD solution, it is often immersed in a solution of short chain ligand (hydrazine, 1,2-ethanedithiol, MPA, etc.) to enhance the electronic coupling of the QD to the oxide. Figure 5 compares the morphology of oleic acid capped PbSe QDs adsorbed on TiO_2 from Tisdale *et al.* [37] (study on hot electron injection) and oleic acid capped PbS QDs adsorbed on single crystal TiO_2 after 2

cycles of the LbL procedure. Analysis of the image height profiles (bottom of Figure 5) shows distinct steps from the substrate to each QD layer. The AFM tip does not penetrate either the QD monolayer or bilayer to the substrate. Although there are pinholes in the QD layers, it is clear that the packing density of the QDs is significantly increased compared to our surface chemistry strategy using low concentration (0.1-1.0 mg/ml) QD solutions (Figures 2 and S2).

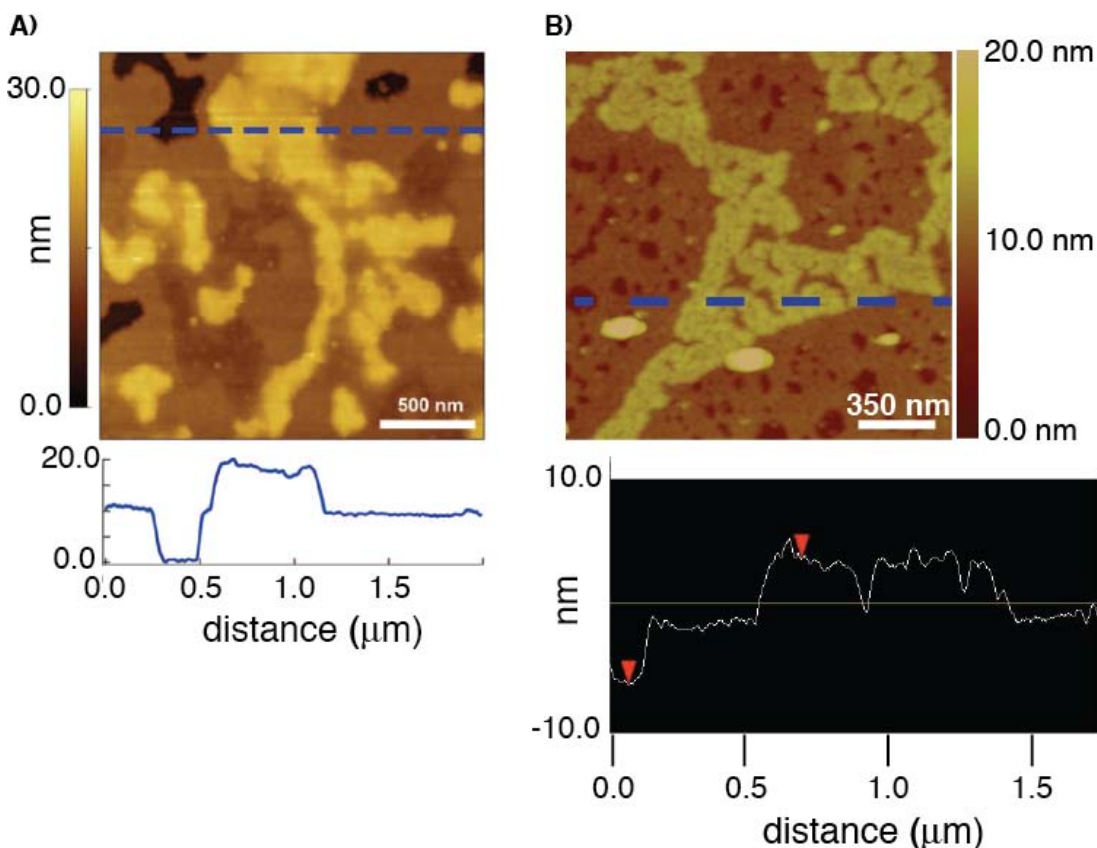


Figure 5. AFM images of ~1.5-monolayer films of (A) 6.7 nm oleic acid-capped PbSe nanocrystals [37] and (B) 4.5 nm oleic acid-capped PbS nanocrystals (deposited from 30 mg/ml hexanes) supported on atomically flat rutile (110).

The significant advantage of this approach is that single QD layers can be sequentially grown on planar TiO₂ electrodes. However preliminary photocurrent

measurements employing a mounted TiO_2 electrode following 2 LbL cycles of oleic acid-capped QDs and immersion in 0.5 M MPA in methanol were unsuccessful. It is likely that the removal of the native oleic acid ligand was incomplete and thus electron injection was inhibited by the bulky capping ligands. Since the LbL procedure can be performed on any planar substrate and does not invoke surface chemistry to covalently bond the QD to the oxide, it is possible that removal of excess organic surfactant is affected by solvent conditions or substrate-specific interactions with the native ligand (e.g. SnO_2 , ZnO , TiO_2 interactions with bulky TOPO, oleic acid or octadecylamine ligands). Future work should focus on acquiring photocurrent measurements in QD thin films as a function of LbL cycles.

CHAPTER VI

INTERFACIAL MORPHOLOGY AND PHOTOELECTROCHEMISTRY OF CONJUGATED POLYELECTROLYTES ADSORBED ON SINGLE CRYSTAL TITANIUM DIOXIDE

This dissertation chapter contains a manuscript that was submitted to *Langmuir*. The work correlated morphology and thickness of polymer sensitizers with the photo-induced electron transfer yields to single crystal TiO₂ electrodes. The study was a collaborative effort between the Parkinson group and researchers at the University of Florida. Seoung Ho Lee, a graduate student in Dr. Kirk Schanze's group, prepared the samples. Dr. John Reynolds and Dr. Kirk Schanze advised on experiments and edited the manuscript.

The following are contributions to this article from Justin B. Sambur: (i) performed all AFM and photocurrent measurements for samples used in this manuscript; (ii) wrote the manuscript with the helpful insight of Dr. Bruce Parkinson, Dr. Kirk Schanze and Dr. John Reynolds.

Interfacial Morphology and Photoelectrochemistry of Conjugated Polyelectrolytes Adsorbed on Single Crystal TiO₂

Justin B. Sambur, Christopher M. Averill, Colin Bradley, Jennifer Schuttlefield,
Seoung Ho Lee, John R. Reynolds, Kirk S. Schanze, Bruce A. Parkinson

VI.1 Abstract

The nanoscale morphology and photoactivity of conjugated polyelectrolytes (CPEs) deposited from different solvents onto single crystal TiO₂ was investigated with atomic force microscopy (AFM) and photocurrent spectroscopy. CPE surface coverages on TiO₂ could be incrementally increased by adsorbing the CPEs from static solutions. The solvents used for polymer adsorption influenced the surface morphology of the CPEs on the TiO₂ surface. Photocurrent spectroscopy measurements in aqueous electrolyte, using iodide as a hole scavenger, revealed that the magnitude of the sensitized photocurrents was related to the surface coverages and degree of aggregation of the CPEs as determined by AFM imaging. Absorbed photon-to-current efficiencies approaching 50% were measured for CPE layers as thick as 4 nm on TiO₂. These results suggest that precise control of CPE morphology at the TiO₂ interface can be achieved through optimization of the deposition conditions to improve the power conversion efficiencies of polymer sensitized solar cells.

VI.2 Introduction

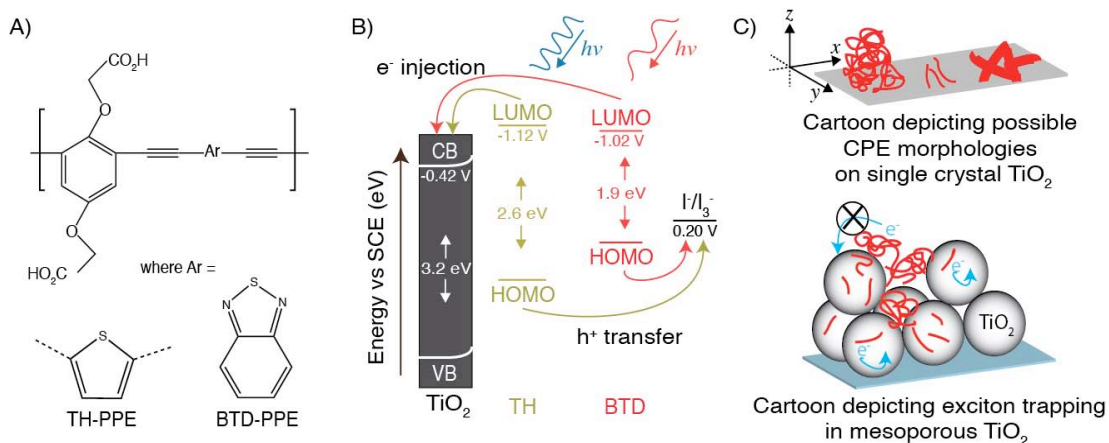
The dye-sensitized solar cell (DSSC) is a photoelectrochemical photovoltaic device that has the potential to be cost-effectively mass-produced.[1] The device consists of a thin film of inexpensive nanocrystalline titanium dioxide that acts as both a charge transporting substrate and as a high surface area scaffold for attaching visible light-absorbing dye molecules (sensitizers) that inject photo-excited electrons into the TiO₂ conduction band.[2] Although the physical principles governing device operation and many variations of the components have been investigated in great detail over the last two decades, no technological breakthroughs that substantially improved the power conversion efficiency (η) have occurred. Current research efforts toward improving η include alternative sensitizers, architecture or composition of the oxide support and new liquid redox electrolytes or solid-state hole conductors.[3]

Optoelectronic devices based on semiconducting conjugated polymers have the advantages of low-cost processing and environmentally friendly scalability of lightweight, flexible devices.[4-6] Depending on the role of the polymeric material in a device, chemical modification of the polymer backbone structure allows for tunable optical, electronic and physical properties. Precise synthetic control of the material properties has already led to polymer-based photovoltaic devices with moderate efficiencies when employed in bulk heterojunction (BH) solar cells (efficiencies of 6-8%) or as sensitizers in DSSCs (efficiencies of 1-3%).[7-16] Conjugated polyelectrolytes (CPE) are actively being explored, as alternative sensitizers to molecular dyes, in DSSCs due to their high

light absorption, synthetic control of redox properties of the HOMO and LUMO (highest occupied molecular orbital and lowest unoccupied molecular orbital) energy levels and the ability to manipulate the charge state of the solubilized polyelectrolyte.[4,5,17-19]

BH solar cells and DSSCs can be considered as fundamentally similar devices because both light absorption and charge separation occurs at interfaces that must be designed for efficient charge collection (BH = polymer donor/polymer acceptor interface, DSSC = TiO₂/CPE/electrolyte interface). A crucial factor dictating solar-to-electrical power conversion in either device is the morphology of the conjugated polymer at the interface where charge separation occurs. However elucidating local structure in these devices is often difficult due to the buried interfaces in the complex, high surface area architectures that are mostly inaccessible to scanning probes or electron beams. Ginger and co-workers pioneering work, using advanced scanning probe microscopy techniques, demonstrated how nanoscale morphological variation in a BH solar cell could be directly correlated to local variations in electron hole pair generation and current collection.[20-23] Despite the critical role that polymer morphology at the TiO₂ interface is expected to play in overall DSSC device performance, the nanoscale morphology of CPE sensitizers on TiO₂ has not been studied in detail. This study uses nearly atomically flat, single crystal TiO₂ (both anatase and rutile) electrodes as model systems to correlate conjugated polyelectrolyte surface morphology with sensitized photocurrent yields. The CPEs synthesized for this study (Scheme 1A) share a common carboxylated dialkoxyphenylene-1,4-

ethynylene backbone to facilitate COO-TiO₂ binding[9,10,12] but differ in the alternating arylene ethynylene moiety [2,5-thienyl (TH) or 1,4-benzo[2,1,3]thiadiazole (BTD)] that determines the HOMO-LUMO gap of the material.[18] From the ground state reduction potentials of each CPE,[18] we estimate >0.5 V driving force for photo-excited electron injection from either CPE into bulk TiO₂ (Scheme 1B). Despite sufficient thermodynamic driving force for electron injection, the two CPE sensitizers had very different conversion efficiencies when employed as sensitizers in mesoporous DSSC devices.[18] Since electron injection is thermodynamically favorable at CPE/TiO₂ interfaces, the disparity in the device efficiencies may originate from exciton trapping and recombination due to either poor transport in single polymer chains or between chains or poor electronic coupling between the polymer and the TiO₂ conduction band.



Scheme 1. (A) Chemical structures for the conjugated polyelectrolyte sensitizers studied herein. (B) Band energy diagram showing the HOMO-LUMO energy level alignment of each CPE with the anatase TiO₂ conduction and valence bands (CB and VB) at pH 5.5.[24] (C) Representation of various CPE morphologies (depicted as red lines) on a single crystal TiO₂ substrate (top) and how these variable CPE morphologies can lead to exciton trapping or recombination in mesoporous TiO₂ films (bottom).

Atomic force microscopy (AFM) is an ideal tool to observe CPE adsorption morphologies on flat, single crystal TiO_2 substrates. A variety of surface-bound polymer species (Scheme 1C, top) could be present due to inhomogeneity of polymer samples that may exhibit broad size distributions or a variety of conformations in the solvated state. Nonetheless we anticipate that the carboxylated polymer backbone facilitates polymer- TiO_2 covalent binding analogous to the binding mechanism for transition metal complex sensitizers.[2] Scheme 1C (bottom) shows a cartoon illustration of a mesoporous TiO_2 device depicting how polymer morphology may effect the photo-excited electron injection efficiency. For instance, inefficient exciton transport may occur for aggregated polymer chains whose photogenerated excitons must hop between several polymer chains to reach the TiO_2 interface. Alternatively, individually adsorbed CPE chains are expected to inject electrons more efficiently especially if they have multiple carboxylate attachments. Deconvoluting the origin of the sensitized photocurrents from CPE conformations (ie. aggregated chains versus isolated chains or many TiO_2 attachments versus few attachments) amongst the multitude of CPE sensitizers is difficult at the buried interfaces in mesoporous TiO_2 . Therefore previous studies were limited to indirectly correlating CPE morphology with current-voltage behavior by manipulating device processing conditions such as temperature dependent CPE adsorption,[10] blending versus spin coating,[9,11,12] or device annealing.[12] Although this approach may lead to future device improvements, cell efficiencies can be affected by multiple

factors and does not provide information regarding how the CPE morphology directly effects the electron injection yields.

Herein we demonstrate distinct adsorption behaviors for TH and BTB on TiO₂ crystals that were a result of the processing conditions during CPE adsorption (ie. solvent, exposure time, concentration). The particular adsorption behavior of each CPE was directly correlated to the spectral properties and sensitized photocurrent yields. These results corroborate previous hypotheses that DSSC device performances are affected by CPE morphology at the TiO₂ interface and may aid the development of more efficient CPE-sensitized devices.

VI.3 Experimental Methods

Materials. The polymer samples, TH and BTB-PPE were synthesized as previously described.[18] After purification by dialysis the polymers were dissolved in aqueous solution as Na⁺ salts. The salts were neutralized by the addition of aqueous HCl, which resulted in polymer precipitation. The solid polymers were redissolved in either DMF or MeOH and the resulting solutions were used for deposition onto the TiO₂ substrates.

Preparation of TiO₂ single crystal surfaces. Planar rutile (MTI Corporation, Richmond, CA, USA) or Norwegian anatase single crystal substrates were used as model systems to correlate the morphology and photocurrent yields of CPE sensitizers adsorbed on TiO₂. Clean, atomically flat TiO₂ surfaces were prepared using a slightly modified approach of our previous published procedures.[25,26] See supporting information for full experimental procedures.

Adsorption of CPEs on TiO₂. Several polymer deposition procedures were evaluated in order to determine the most effective procedure to systematically control the polymer surface coverage. Our initial efforts focused on drop casting polymer solutions onto TiO₂ single crystals. Sensitization solutions for drop-casting were prepared from serial dilution of stock TH and BTD/DMF solutions. The polymer was confined to a small region of the electrode surface by allowing 1 μ l of each concentration (from low to high concentration) to completely evaporate. Following photoelectrochemical measurements the electrode was dried with a 15 psi stream of N₂ prior to an additional sensitization step. Although drop casting allowed for controlled amounts of the polymer to be deposited, as will be discussed later, the drop-casting method was not reliable for systematically obtaining reproducible and uniform polymer surface coverages.

Adsorption of carboxylated CPEs from static solutions of methanol or DMF on single crystal TiO₂ surfaces was the preferred deposition method. The solvents for the sensitizer were filtered (200 μ m syringe filter, Nalgene) to remove macroscopic undissolved polymer particles and degassed with N₂ for 30 minutes prior to adding the solid CPE sample. Saturated CPE solutions were prepared by sonicating the mixture for 3 hours to saturate the CPE solution. The final stock solutions were filtered to remove undissolved, bulk particles and the resulting polymer concentrations were determined to be 54.0 μ g TH /ml DMF, 36.9 μ g BTD/ml DMF, and 8.3 μ g TH/ml methanol. It was not possible to dissolve an appreciable amount of BTD in methanol. Lower concentration

TH/DMF or BTM/DMF sensitization solutions were prepared by serial dilution of these stock solutions.

Rutile or anatase crystals, not mounted as electrodes, were used for AFM characterization and exposed to the same solution at the same time as mounted electrodes. To avoid contamination of the mounted electrode surfaces due to degradation of the encapsulating epoxy, 10 μL of sensitization solution was pipetted onto the entire electrode surface rather than immersing the entire mounted electrode. The solution layer was completely removed from the crystal surface by rinsing with the same filtered solvent as the sensitization solution and drying with a high pressure N_2 stream (15 psi). Following photoelectrochemical measurements the electrode was dried with a 15 psi stream of N_2 and additional CPE solution was pipetted on to the dry surface.

TH and BTM adsorption from DMF solutions required short deposition steps (<10 minute intervals) compared to methanol solutions of TH (>10 hour intervals are possible) in order to limit the epoxy exposure to the DMF in which it is partially soluble. Whereas short time deposition steps were sufficient to study BTM adsorption from DMF, it was necessary to prepare a series of TH/DMF solutions of increasing concentration that were used to systematically increase the surface coverage with short time deposition steps.

Photoelectrochemical measurements. Incident photon to current efficiency (IPCE) spectra were measured using a Stanford Research Systems (SRS) model SR570 low noise current preamplifier connected between the working and Pt counter electrodes. The signal from the pre-amplifier was then fed into a SRS

model SR830 DSP lock-in amplifier. Illumination from a 100 W Oriel tungsten lamp (using a 385 cut-off filter) was passed through a computer controlled grating monochromator (2 nm step interval) and chopped at 13 Hz to provide a modulated photocurrent signal. The raw photocurrent signal was corrected for photon flux using a lamp power spectrum recorded at 2 nm intervals using a thermopile detector. A ThorLabs C-Series photodiode power meter was used to measure the incident power through the monochromator. Current-voltage (I-V) curves and Mott-Schottky plots were recorded with an Ivium Compactstat potentiostat in a 3-electrode configuration. The electrolyte composition in all experiments was 0.25 M KCl and 0.01 M KI (KI was not used in Mott-Schottky analysis) in 18 M Ω Millipore water.

Atomic force microscopy (AFM) measurements. Tapping mode AFM (Digital Instruments Nanoscope IIIA controller and a multimode SPM) was used to characterize the crystal surfaces using an Olympus AC160TS probe with a 42 N/m force constant and resonant frequency of ~300 kHz. The un-mounted crystals used for AFM were exposed to the same polymer solution at the same and treated identically as the mounted electrodes used for photocurrent measurements. AFM images were processed using Digital Instruments software. A minimum of 50 μm^2 was imaged directly with AFM in different macroscopic regions of the TiO₂ crystal surfaces.

VI.4 Results and Discussion

The goal of this study was to incrementally increase CPE surface coverage on TiO₂ single crystals in order to correlate the polymer surface coverage and interfacial morphology with the photo-excited electron injection efficiency. CPE adsorption from static solution onto TiO₂ single crystals was chosen to mimic the general procedure used to adsorb molecular sensitizers to mesoporous TiO₂ films.² We extend previous work with CPE sensitized TiO₂ devices and focus entirely on the relationship between morphology and sensitized photocurrent yields at the CPE/TiO₂ interface.

Morphology of CPEs on TiO₂

Our initial efforts to correlate the photo-excited electron injection efficiency with polymer film thickness utilized a drop-casting procedure. Although the drop-casting procedure ensured deposition of a known amount of polymer from a stock solution, we were unable to reproducibly control the spatial distribution and thickness of the polymer deposit on the TiO₂ single crystal (see optical micrographs in Figure S1A). Photoelectrochemical, morphology and optical absorption data from a typical drop-casting experiment of TH/DMF solutions are shown in the supporting information (Figure S1). The data (see thorough discussion in the supporting information) clearly demonstrates that the electron injection efficiency decreased with increasing film thickness. However we were unable to quantitatively determine a maximum length scale for efficient electron injection into TiO₂ because it was not possible to incrementally and uniformly control the nanoscale polymer surface coverage or thickness via the drop-casting

procedure. Therefore the widely used procedure to adsorb inorganic complex dyes to mesoporous TiO₂ films was used where single crystal TiO₂ surfaces are exposed to static polymer solutions.

Figure 1 shows typical AFM images observed in many regions of the rutile (001) surface before (Figure 1A) and after a series of 10 minute deposition steps using increasingly concentrated TH/DMF solutions (Figures 1B and D). Figure 1A shows the clean rutile (001) surface with an average terrace width of ~130 nm. Polymer adsorption from low concentration DMF solutions ($\leq 3.4 \mu\text{g/ml}$; Figures 1B and C) produced some polymer bundles, presumably consisting of aggregated chains, protruding $<8 \text{ \AA}$ perpendicular to the plane of the surface (z height, see Scheme 1C bottom for axis definition) as well as small spherical aggregates ranging from 10-30 \AA in height that were randomly dispersed on the TiO₂ surface. After exposure to 3.4 $\mu\text{g/ml}$ TH in DMF for 10 minutes, only 4.2% of the surface structures exceeded a height of 8 \AA . The underlying TiO₂ substrate terraces remained largely exposed indicating a sub-monolayer surface coverage. The surface coverage of TH increased after each exposure to increasingly more concentrated polymer solutions. Most of the surface ($>85\%$) was covered by spherical polymer aggregates after exposure to a 54.0 $\mu\text{g/ml}$ polymer solution (Figure 1D). A more ordered structure that may be aligned polymer bundles was observed along with larger agglomerates in some regions of the sample (Figure 1E). These linear aggregates appear to align in a particular direction that may be associated with a crystallographic direction of the TiO₂ surface. Additional polymer adsorption was not observed despite prolonged exposure to the most

concentrated polymer solution. Thus the growth of TH layers from static DMF solutions can be characterized as uniform surface limited adsorption of polymer bundles over the TiO_2 surface with perhaps some orientational preference.

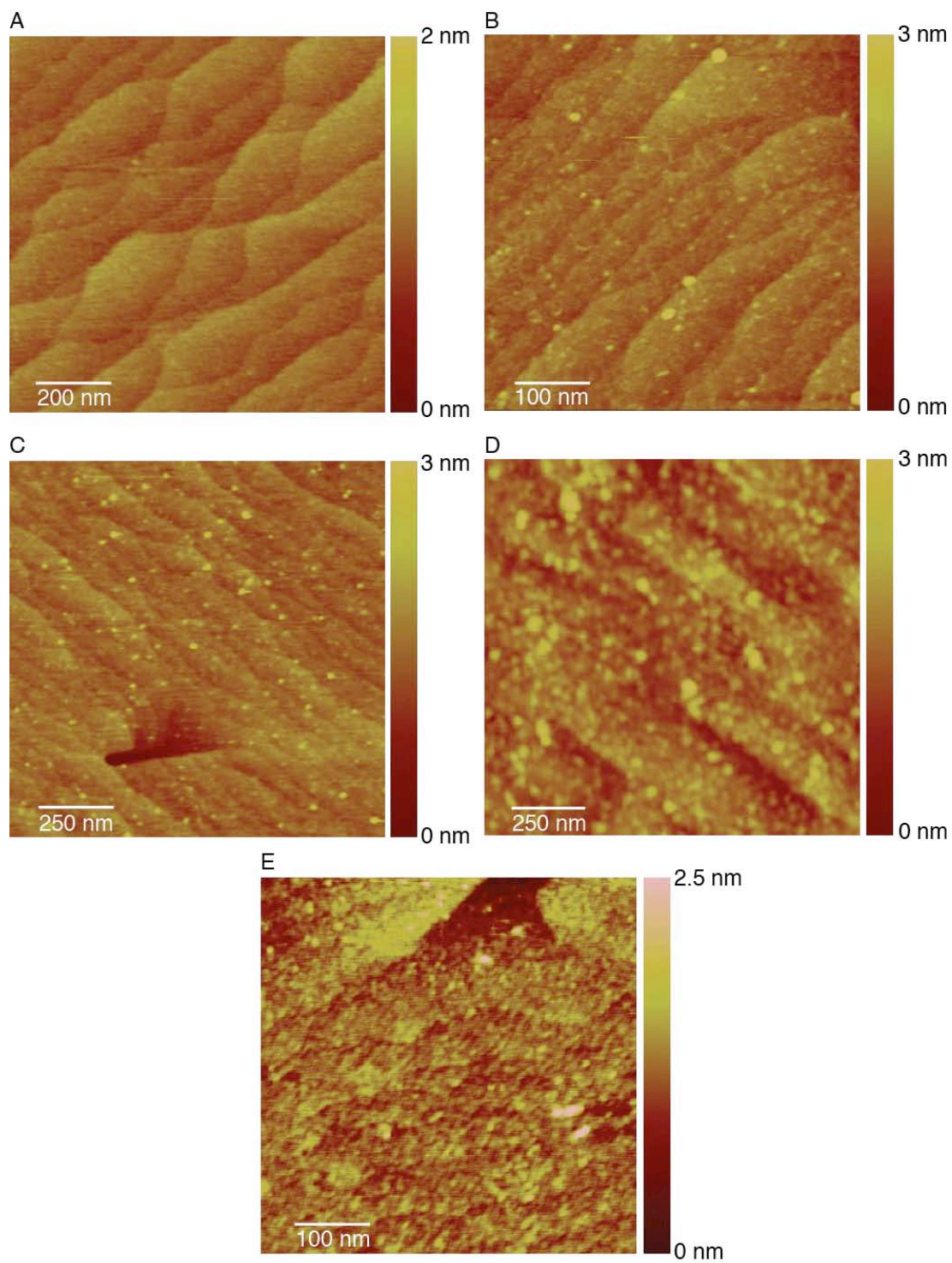


Figure 1. AFM images of A) bare rutile (001) and after 10 minute exposure to B) 1.6 $\mu\text{g/ml}$, C) 3.4 $\mu\text{g/ml}$ and D and E) 54.0 $\mu\text{g/ml}$ solutions of TH in DMF.

A clear example of the effects of the adsorption procedure on the CPE surface morphology is demonstrated in Figure 2. This series of AFM images was acquired before (Figure 2A) and after immersion of a rutile (110) crystal in an 8.3 $\mu\text{g}/\text{ml}$ TH methanol solution as a function of time (Figures 2B-E). Deposition of TH from methanol exhibited strikingly different adsorption morphologies despite the similar polymer concentration of TH in DMF. Similar surface structures were also observed on rutile (001) (same orientation as Figure 1), which supports the hypothesis that the deposition procedure dictates CPE adsorption and not the substrate surface orientation. After 15 seconds of deposition time (Figure 2B) approximately 30% of the TiO_2 surface exceeded 8 \AA in height. Higher resolution imaging revealed that polymer agglomerates approximately 3 nm in height were also present on the surface. After 3 minutes of exposure to the TH/methanol solution (Figure 2C), the TiO_2 surface consisted of an interconnected network structure approximately 3 nm in height. Our adsorption procedure cannot result in cross-linking of polymer chains, and thus the term network refers to the appearance of a CPE surface morphology. Prolonged exposure to the polymer solution (Figure 2D; 57 minutes) did not result in an increase in the network height, however high resolution imaging (insets of Figures 2C and 2D) revealed that the average the width of the network structures increased from approximately 70 nm to 100 nm. After 17.5 hours of immersion time (Figure 2E), 92% of the surface was composed of polymer features < 3.5 nm in height. Due to the small height of the network (~3 nm), compared to the very large polymer aggregates observed in Figure 2E (many exceeding 10 nm and some as large as

50 nm; note the 23 nm increase in the height scale from the bare surface, Figure 2A), the polymer network is not easily discernable in the large area AFM image. The inset of Figure 2E indicates that the surface network is still intact but may have decreased slightly in width, although it was difficult to simultaneously resolve the heights of the taller aggregates (exceeding 30 nm) and flatter features. In summary, aggregate growth persisted with deposition time from TH/methanol solutions; unlike the surface-limiting behavior observed for TH adsorption from DMF solutions. Control AFM experiments with un-mounted TiO₂ crystals (that could be exposed to DMF for >10 hr) concluded that the surface morphology of TH deposited from DMF solutions as a function of concentration was in agreement with the morphological trends shown in Figure 1. Therefore it is evident that the solvent used for polymer deposition influences the surface morphology of TH adsorbed on TiO₂.

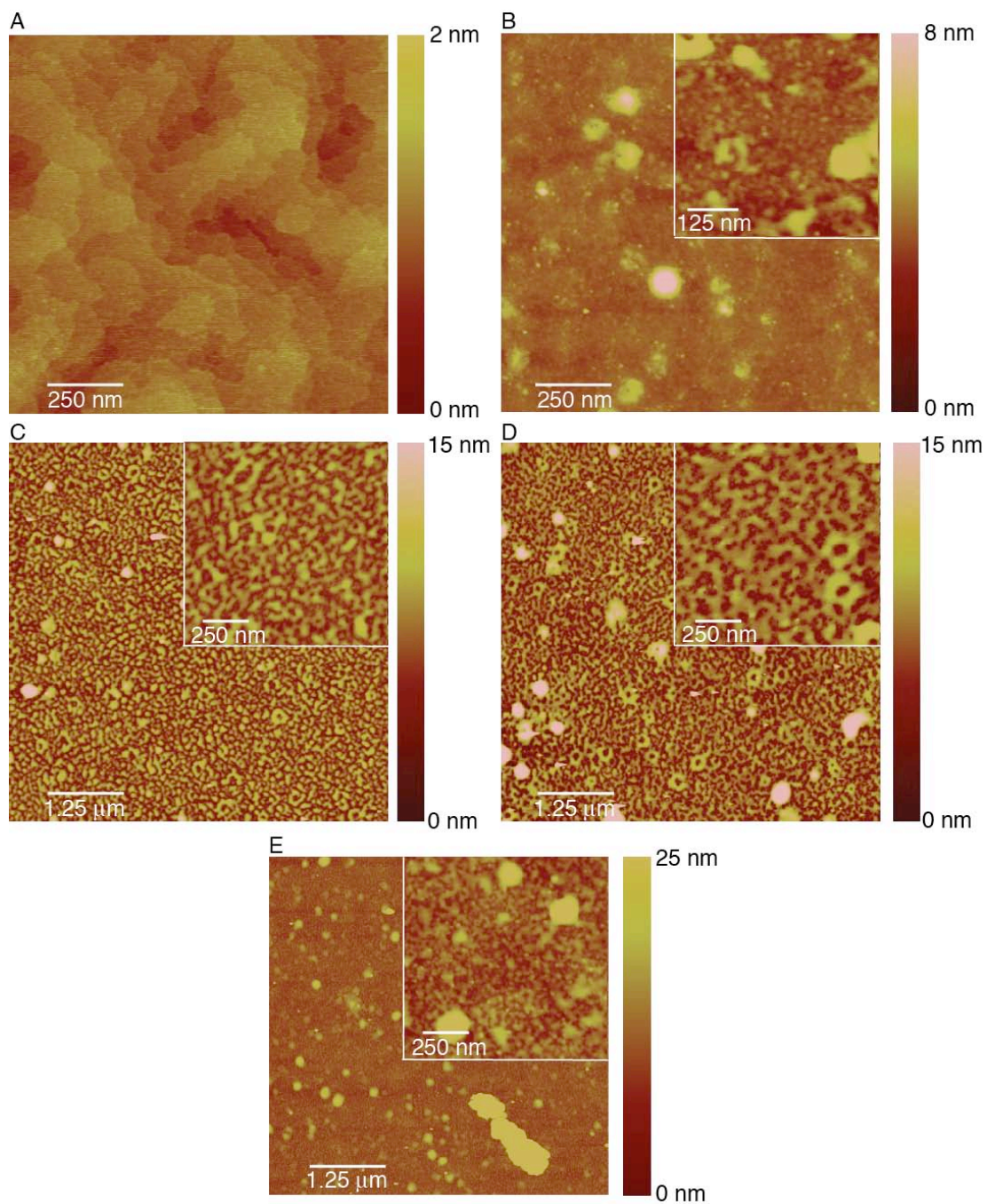


Figure 2. AFM images of A) bare rutile (110) and after exposure to a stock solution of 8.3 $\mu\text{g/ml}$ TH in methanol for B) 15 sec, C) 3 min, D) 57 min and E) 17.5 hr.

Finally, we focus on the morphology of BTD deposited from DMF. Figure 3 shows AFM images of a rutile (110) surface before (Figure 3A) and after sequential deposition steps from a 7.4 $\mu\text{g/ml}$ solutions BDT/DMF solution. The clean rutile (110) surface exhibited terraces with an average width of 100 nm. After a 15 second deposition step a majority of sampled areas consisted of <5% coverage of <1.5 nm high polymer aggregates randomly distributed across many terraces. Despite the relatively constant height of the polymer aggregates, the lateral dimensions of the aggregates varied from <3 nm to as large as 175 nm. Surface aggregate growth proceeded with increasing deposition time in the lateral dimensions with little change in height (Figure 3B, 1 minute). We identified two populations of large and small aggregates whose average lateral dimensions were 340 nm^2 and 75 nm^2 respectively. However the surface coverage of BTD differed in macroscopic regions of the sample. By contrast, such differences in macroscopic morphology were not observed for TH deposition from DMF or methanol. For example, after 2 minutes total deposition time (Figure 3D), barren regions with <1% local surface coverage of features exceeding 1 nm in height were observed in many large area 5 x 5 μm scans. In other regions (Figure 3E, 5 minutes deposition time), aggregates with lateral dimensions ranging from 9 nm^2 to 350 nm^2 comprised about 10% of the image. Figure 3F shows an interesting boundary between high and low aggregate density regions, corresponding to local surface coverages exceeding a 1 nm threshold in height of 55% and 4% respectively. The AFM data showed microscopic regions consisting of both short and tall aggregates with small lateral

dimensions (Figure 3F) as well as aggregates with 1 nm height but covering large areas (Figure 3C). To summarize the AFM results, after randomly imaging more than 750 μm^2 of the TiO_2 crystal following 20 minutes of total deposition time, <50% of the surface consisted of aggregates (like those in Figures 3E and F) dispersed randomly on the TiO_2 surface. Although it remains unclear why the morphology of BTM deposited from static DMF solution on TiO_2 was so irregular, we discuss several possibilities that could account for the behavior. First, an adsorption/desorption equilibrium process could account for the barren regions observed in some regions of the sample (Figure 3D). The generally low surface coverage suggests a weak BTM/ TiO_2 interaction and higher propensity for BTM to remain in the DMF solvated state. Second, polymer aggregates with different shapes and sizes may exist in the polymer solution which gives rise to a variety of surface-bound aggregates.

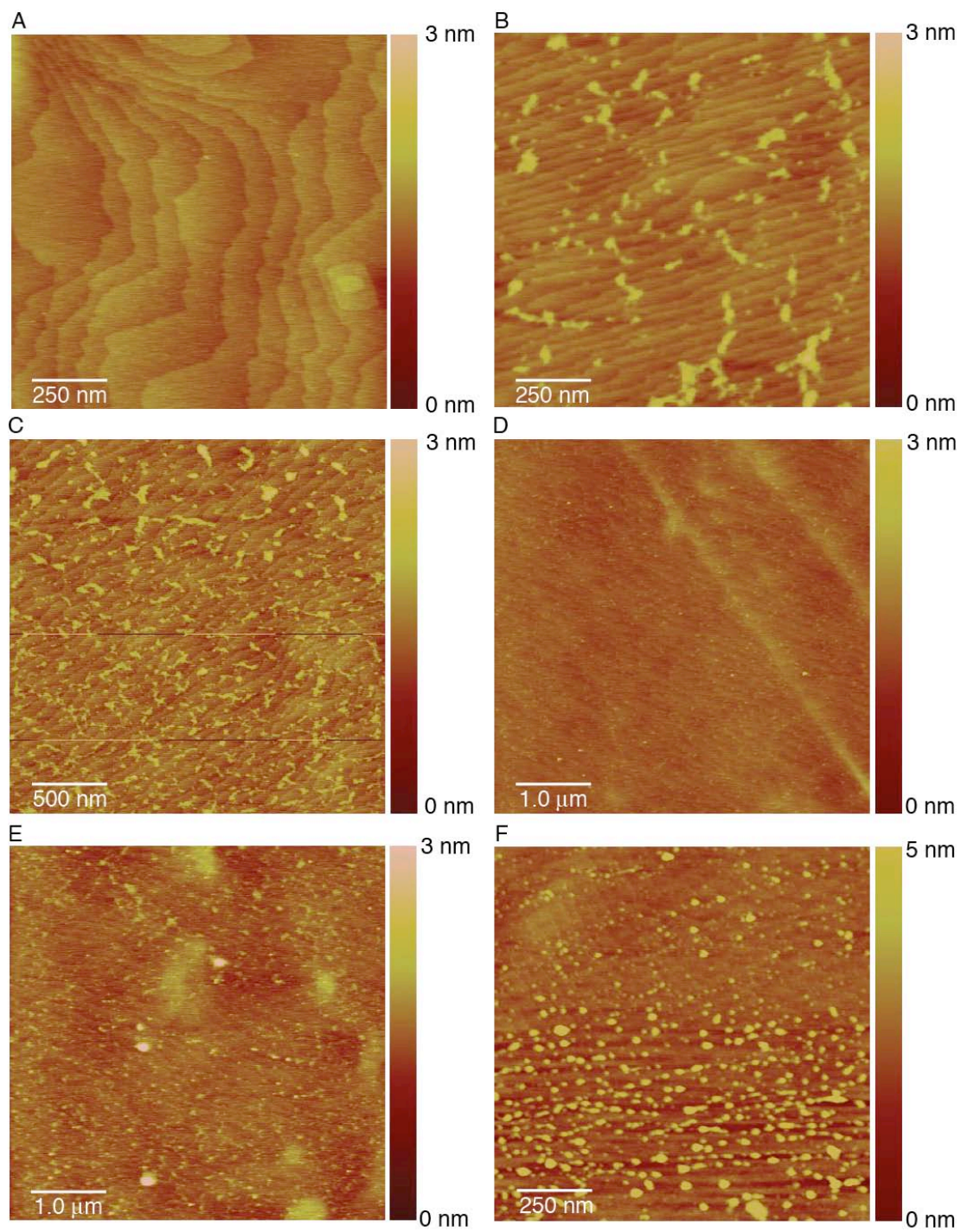


Figure 3. AFM images of A) bare rutile (110) and after B) 15 second, C) 1 minute, D) 2 minute, E) 5 minute and F) 10 minute exposure to 7.4 μg/ml solutions of BTD in DMF.

We studied CPE adsorption by AFM under ambient conditions on a variety of rutile (110), (001) and (101) and anatase (101) and (001) TiO₂ single crystals but rarely observed an orientational preference of the CPE sensitizer with respect to the crystallographic orientation of the substrate. In addition, the morphology and surface coverage trends of both CPEs were not specific to a particular TiO₂ surface orientation. Ultra high vacuum scanning tunneling microscopy experiments previously identified specific binding mechanisms of small molecule sensitizers that organize into overlayer surface structures with lattice parameters commensurate with the TiO₂ substrate lattice.[27-30] The inability of CPE adsorbates to form well-ordered overlayers on single crystal TiO₂ is most likely due to the large dimensions of polymers that presumably chemisorb through multiple binding sites over many TiO₂ unit cell dimensions. This observation is also consistent with our previous work with 3-5 nm CdSe nanocrystals on single crystal TiO₂ substrates.[31] In addition, the size dispersity inherent in polymer (or nanocrystal) samples may prevent well-ordered packing of the bulky adsorbates. The results presented herein demonstrate that the adsorption method (ie. solvent, time, concentration) dictates the adsorption behavior of CPEs on planar TiO₂ substrates rather than the substrate surface orientation.

Scanning probe microscopy revealed very different adsorption behavior for TH from two different solvents as well as microscopic variability of BTM morphologies when deposited from DMF. Unlike adatom growth on single crystal substrates, where the adsorbate is smaller than a unit cell dimension and well-defined growth modes can be identified[32], the large size and polydispersity of

polymer chains makes a precise designation of a particular growth mode between TH or BTM and TiO₂ difficult. Deposition of TH from DMF was characterized as surface limited without significant island growth or the development of additional polymer layers. In the case of methanol deposition, the development of a 3.5 nm polymer layer thickness preceded island growth. Therefore the deposition of TH from DMF and methanol solutions on single crystal TiO₂ may be approximated by Frank-van der Merwe and Stranski-Krastanov growth modes, respectively.[32] A distinct growth mode for BTM deposition from DMF on TiO₂ could not be identified because a uniform, consistent structure was not observed on all regions of the surface.

Previous optical absorption and fluorescence quenching studies of a series of poly(arylene ethynylene) conjugated polyelectrolytes, sharing the same backbone structure as TH but containing sulfonate side groups, demonstrated that the polymer chains were well-solvated in methanol and tended to aggregate in methanol/water mixtures.[5] Whereas methanol is considered a good solvent for TH-SO₃⁻ because the polymer is dissolved in a dispersed molecular-like state, we found that the room temperature solubility of TH in DMF and methanol was ~54 µg/ml and 8.3 µg/ml, respectively. The difference in solubility between TH with different side groups suggests that methanol is not a good solvent for TH. It is therefore likely that the degree of aggregation or conformation of the polymer chains differs between the two solvents and thus dictates the polymer adsorption process on the surface. In DMF TH is well-solvated limiting growth to the TiO₂ surface and further adsorption involving lateral chain-chain interactions is not

avored. The tendency to form a conformal layer on the TiO₂ surface with increasing deposition time from methanol suggests that as polymer chains diffuse to polymer/TiO₂ interface, chain-chain interactions are energetically favorable and facilitates the aggregated growth of a polymer network.

Regardless of the exact growth mode mechanisms, AFM imaging demonstrated that CPE surface morphology is influenced by the adsorption conditions. Most importantly, each procedure yielded distinct surface morphologies that could provide useful information to relate to the efficiency of photo-excited electron collection.

Photocurrent spectroscopy of CPEs adsorbed on TiO₂

We exposed mounted single crystal TiO₂ electrodes (see Experimental Section) to the same polymer solutions at the same time as the unmounted crystals used for AFM and measured the sensitized photocurrent yields after each deposition step. It was necessary to study TH and BTB adsorption from DMF on mounted electrodes (same as unmounted crystals for AFM analysis) in short time intervals (~10 min) in order to limit the exposure time of the electrode mounting epoxy, which is somewhat soluble in DMF.

Figure 4 compares the incident photon to current efficiency (IPCE) spectra of TH and BTB deposited from DMF or methanol. The dashed red line in each figure represents the solution absorbance spectrum of each CPE sensitization solution. Figure 4A shows the IPCE spectra of TH deposited on an anatase (101) electrode as a function of TH concentration in DMF solvent (same procedure as the rutile (001) crystal used for AFM images in Figure 1). Similar

trends in IPCE magnitudes were observed for rutile (110) and (001) electrodes. Efficient electron injection from CPEs to both commercially available rutile and naturally occurring anatase crystals is significant because anatase is the dominant polymorph in mesoporous DSSCs.[2] In addition, there is no photocurrent contribution from direct excitation of the anatase band gap (3.2 eV), allowing for direct comparison over the entire spectral range of the solution absorbance and IPCE spectra (Figures 4B and 4C show the rutile photocurrent onset at 425 nm). The sensitized photocurrent from TH adsorbed from DMF (Figure 4A) onsets at 530 nm and reaches a maximum value at 434 nm, indicating no shift between the photocurrent and absorbance peak maxima ($Abs_{max} = 436$ nm; monochromator resolution is 2 nm). The inset in Figure 4A shows the increase in magnitude of the peak photocurrent values with each deposition step until a maximum was reached. The trend in sensitized photocurrent yields qualitatively reflects the saturated surface limited coverage observed with AFM imaging.

Figure 4B shows the photocurrent spectra for BDT deposited from DMF on a rutile (110) crystal compared to the solution absorbance spectrum. The IPCE spectra exhibit a broad spectral response that onsets at 650 nm as a result of the lower band gap of BDT when compared to TH.[18] However, the maximum IPCE value (3 minute deposition) for BDT deposited from DMF was 65% less than the maximum IPCE value observed for TH for the same solvent. The inset of Figure 4B shows that the maximum IPCE value after the initial 15 second deposition step is >50% of the highest IPCE value. The IPCE values do not

monotonically increase as in the TH sensitized system. Additionally, there are distinct features in the IPCE spectra that are not easily discernable in the absorbance spectrum of the sensitization solution. The largest magnitude feature centered at 456 nm may be described as a doublet with corresponding peak wavelength maxima of 448 nm and 466 nm, respectively. There is also a shoulder at approximately 540 nm in the IPCE spectra that matches a similar feature in the absorbance spectrum of the BTD deposition solution. The low sensitization yields, discrete spectral features and irregular adsorption behavior of BDT compared to TH can be interpreted in several ways and will be discussed further below.

The IPCE spectra measured after TH deposition from methanol as a function of time on a rutile (110) crystal (same mounted electrode as in Figure 4B) is shown in Figure 4C. The deposition solution absorbance spectrum exhibits a broad spectral feature with a peak wavelength of 408 nm, that is blue shifted by 24 nm from the solution absorbance in DMF and 38 nm from the IPCE spectra. Previous photophysical studies with a similar CPE described a red shift in solution absorbance spectra in H₂O/methanol mixtures indicating an aggregated polymer.[33] The red shifted photocurrent spectra relative to the methanol absorbance can be attributed to CPE aggregation because AFM imaging revealed a 4 nm polymer layer on the TiO₂ surface (Figure 2). The sensitized photocurrent onset is apparently red-shifted to 580 nm compared to TH IPCE spectra acquired after DMF deposition (530 nm). In addition, the maximum IPCE value for TH deposited from methanol was 21 times greater than

the maximum photocurrent response from TH deposited from DMF. The difference in IPCE magnitude, as well as the sensitized photocurrent onset, may originate from differences in the light harvesting efficiency due to the amount of polymer deposited on the surface from each solvent.

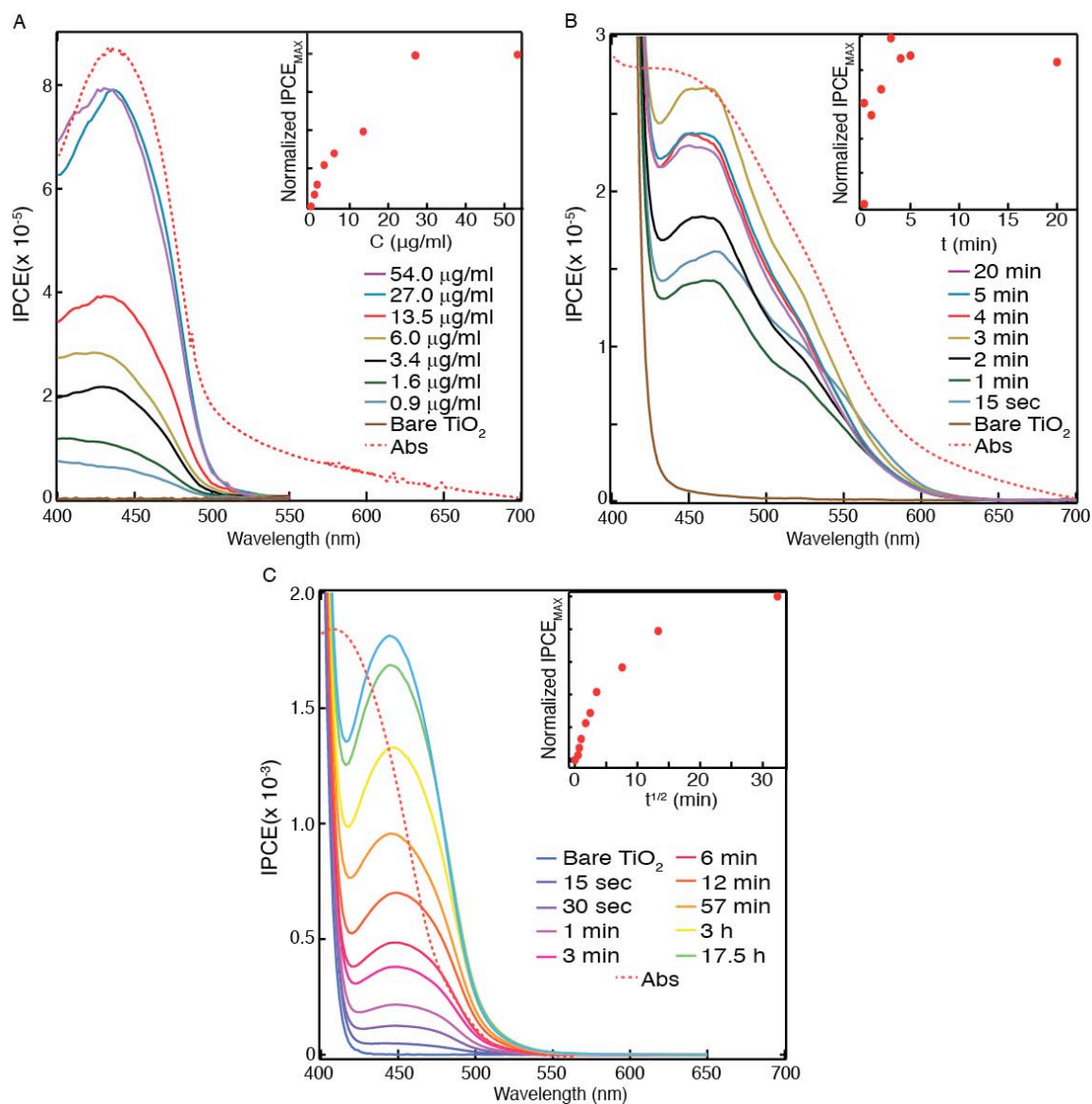


Figure 4. IPCE spectra of (A) TH deposited from DMF solution on an anatase (101) electrode as a function of concentration, (B) BTD deposited from a 7.4 μg/ml DMF solution on a rutile (110) electrode as a function of time and (C) TH deposited from an 8.3 μg/ml methanol solution on the same rutile (110) electrode as in (B) a function of time. The dashed red line in each figure represents the shape of the solution absorbance spectrum. The inset in each figure demonstrates the trend in the photocurrent spectra by plotting the normalized IPCE values at the wavelength maximum versus the deposition step. All photocurrent spectra were measured at short circuit versus a Pt wire in an aqueous solution with 0.2 M KCl supporting electrolyte and 0.01 M KI as a redox mediator.

It is interesting to note the contrasting trends in the photocurrent and AFM/optical microscopy data from two deposition procedures (ie. adsorption from static solutions and drop-casting) in regards to the carboxylated polymer/TiO₂ covalent binding mechanism. The maximum IPCE values for all carboxylated CPEs adsorbed on TiO₂ single crystals prepared from static solutions did not decrease substantially (insets of Figure 4A-C), whereas the maximum values in the IPCE spectra of drop cast films increased to a maximum and then subsequently decreased by an order of magnitude (plotted in Figure S1F). In addition, the scale bars in the AFM images (Figures 1-3) are 10²-10⁴ times less than the approximate film thicknesses determined on drop-cast films. Thus the thickness of carboxylated polymer layers deposited from static solutions was not comparable to films made using the drop-casting procedure on single crystal TiO₂ surfaces. We attribute the reproducible surface limited growth from static solutions to the covalent binding of carboxylated CPEs to TiO₂ through the multitude of carboxylate moieties on the polymer backbone. The ability to incrementally increase the polymer surface coverage while avoiding thick film growth may also be deterred by a relatively weak van der Waals force between adjacent polymer chains compared to the strong carboxylate-TiO₂ covalent bond. Deposition of TH from methanol and DMF provided a platform to study the effects of TH thickness on electron injection efficiency. To gain insight into the absorbed photon-to-current efficiency (APCE) we attempted to determine the light harvesting efficiency of TH films deposited on TiO₂ from each solvent using optical absorbance measurements. Unfortunately the low optical density of TH

deposited on TiO₂ from DMF (approximately 4X less material compared to methanol deposition according to AFM surface threshold analysis) prevented direct determination of absorbance values in a single optical pass configuration. Nonetheless the absorbance spectrum was measured after 12 min of TH deposition from methanol (maximum surface coverage prior to large island growth) on rutile (001) in air (see supporting information Figure S2). The small absorbance maximum of 2.86×10^{-4} at 460 nm was used to calculate the light harvesting efficiency (LHE) at this wavelength according to Equation 1 and subsequently used to calculate the APCE value using Equation 2.

$$\text{LHE (\%)} = 1 - 10^{-\text{Absorbance}} \quad (1)$$

$$\text{APCE (\%)} = \text{IPCE (\%)} / \text{LHE (\%)} \quad (2)$$

In order to approximate the APCE value for TH deposited from DMF, we assume a linear relationship of the maximum absorbance to the polymer concentration on the surface, and considering the thickness of TH deposited from DMF (single polymer layer) and methanol were approximately 1 nm and 4 nm respectively, we approximate the LHE value for TH deposited from DMF as 25% of the methanol value. The APCE values for TH deposited on TiO₂ from methanol and DMF are listed in Table 1. Although the APCE value is 45% larger for polymer deposition from methanol compared to DMF, we note that the maximum APCE for DMF deposition is determined from an assumed LHE value. The 50% APCE value determined herein is in agreement with the IPCE maxima

for high optical density (where IPCE \equiv APCE) TH sensitized mesoporous TiO₂ cells.[18] We also note that high APCE values were not solely limited to TH deposition from a ‘good’ solvent. This work suggests new procedures for CPE sensitization of mesoporous TiO₂ devices.

Table 1. Quantum efficiencies for TH sensitized TiO₂ single crystal electrodes from DMF and methanol.

Solvent	IPCE (%)	LHE (%)	APCE (%)
DMF	$8.0 \times 10^{-3} \pm 1.2 \times 10^{-3}$	$2.2 \times 10^{-2} \pm 1.0 \times 10^{-2*}$	$36 \pm 17\%^*$
Methanol	$6.3 \times 10^{-2} \pm 1.0 \times 10^{-2}$	$1.2 \times 10^{-1} \pm 2.0 \times 10^{-2}$	$52 \pm 12\%$

*LHE value is assumed (see main text).

Comparison of the polymer morphology and APCE values from the two solvents sheds light on charge transport characteristics at the polymer/TiO₂ interface. If the maximum APCE value for the thin film (thickness is <4 nm for methanol deposition) is relatively larger or at least equivalent to the single layer value (thickness <1 nm for DMF deposition), then photo-excited excitons generated distal to the polymer/TiO₂ interface can be efficiently transported through the conjugated polymer to the interface where charge injection occurs. For thicknesses larger than 4 nm however, transport of excitons is not efficient because AFM imaging of polymer deposition from methanol showed a substantial increase in polymer thickness while the IPCE values saturate (thereby decreasing APCE). The finding that excitons can transport several nm through the polymer films to the TiO₂ interface is consistent with recent studies of exciton transport in CPE films grown by a layer by layer method which showed an exciton diffusion length of 2 nm.[34] In addition, donor/acceptor materials in

BH solar cells are typically mixed such that photo-generated excitons diffuse efficiently to the interface (a length scale of approximately 10 nm).[35,36] Thus relatively high APCE values for a thin layer of TH on TiO₂ is consistent with the length scale of exciton diffusion in BH solar cells.

Unfortunately we were unable to directly determine the light harvesting efficiency due to the low coverage of BDT on the planar TiO₂ crystal. Therefore the absorbed photon-to-current efficiency (APCE), which may still be high for the BTD sensitizer, remains unknown. The low sensitization yields of BTD compared to TH observed herein agree with the poor performance of BTD sensitized mesoporous TiO₂ devices[18] and several hypothesis regarding the APCE values can be explained by considering the AFM imaging results (Figure 3). The maximum IPCE value after the first deposition step was >50% of the maximum observed value despite a BTD surface coverage of <5%. We approximate a 20-40% macroscopic surface coverage of BTD after the final deposition step, and therefore the IPCE values do not increase with increasing the amount of BTD adsorbed on TiO₂. A thick film was not observed during BTD adsorption from DMF and therefore these results suggest that electron injection efficiency of BTD is low, even for thin structures. IPCE values measured with optically dense (absorbing >90% incident light) BTD sensitized mesoporous TiO₂ solar cells also suggest that the APCE values for BDT are lower than for TH.[18]

It is also interesting to note the doublet feature centered at 456 nm in the IPCE spectrum, which is not well resolved in the solution absorbance spectrum. Assuming the hypothesis that a variety of aggregate shapes and sizes exist in

the sensitization solution, and therefore the broad solution absorbance spectrum represents an ensemble averaging of all conformations, then the discrete features in the IPCE spectrum may indicate electron injection from particular BDT conformations. A particular conformation or aggregate of surface bound BDT may exhibit characteristic optical transitions that could account for the IPCE spectrum in Figure 4B. For samples with macroscopically varying surface structures, sophisticated AFM/confocal microscopy techniques would be necessary to locate particular CPE morphologies and then evaluate the electron injection efficiency.[20]

Finally the dark and illuminated sensitized current-voltage characteristics of the single crystal rutile (110) electrode after 17.5 hr immersion in 8.3 $\mu\text{g/ml}$ TH/methanol solution are shown in Figure 5. The current-voltage curves were measured at a scan rate of 5 mV/sec in an aqueous solution with 0.2 M KCl supporting electrolyte, 0.01 M KI and 1×10^{-4} M I_2 in a 3 electrode configuration versus a Ag/AgCl, 3M NaCl reference electrode and Pt counter electrode. The voltage axis was subsequently adjusted to the I^-/I_2 redox potential using the 100:1 I^- to I_2 ratio to indicate the 0 V reference potential (short circuit) versus the redox mediator. The open circuit voltage (V_{OC}) and short circuit current (I_{SC}) were 0.75 V and 20.0 nA, respectively. The voltage and current at the maximum power (MP) point (dashed red lines, Figure 5) was 0.62 V and 18.3 nA, respectively, which yielded a fill factor of 75.1%. The high fill factor is partly due to the negligible resistive losses in a single crystal photoelectrochemical cell passing nA currents, but also demonstrates efficient carrier collection from the

thin TH polymer layer. The power conversion efficiency was not determined due to the low light absorption of the thin polymer layer.

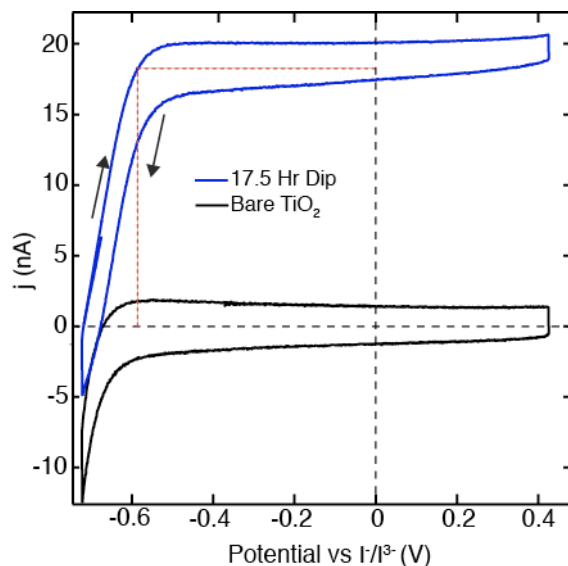


Figure 5. Cyclic voltammograms under illumination ($15.4 \mu\text{W}$ of 460 nm or 2.7 eV) entirely within the 21 mm^2 area of a bare (black trace) and TH-modified (blue trace; 17.5 hr in methanol solution) rutile (110) crystal. The measurements were performed at a 5 mV/sec scan rate in an aqueous solution with 0.2 M KCl supporting electrolyte, 0.01 M KI and $1 \times 10^{-4} \text{ I}_2$ in a 3 electrode configuration versus a Ag/AgCl , 3M NaCl reference electrode and Pt counter electrode. The voltage axis was subsequently adjusted to the I^-/I_2 redox potential using the $100:1 \text{ I}^-$ to I_2 ratio. The dashed red lines mark the maximum power point.

VI.5 Conclusions

We utilized scanning probe microscopy to study CPE adsorption morphologies on single crystal TiO_2 from two solvents. Deposition of TH from DMF and methanol solutions on single crystal TiO_2 may be approximated by Frank-van der Merwe and Stranski-Krastanov growth, respectively. BTD is adsorbed randomly on the surface and in low coverage. Correlation of AFM and sensitized photocurrent data revealed efficient exciton collection for 4 nm thick polymer layers on single crystal TiO_2 . The moderate 50% APCE value measured

in this study for a 4 nm thick TH polymer layer on TiO₂ compares favorably for highly optimized inorganic complex and molecular organic sensitizers that approach 80-100% APCE in mesoporous and single crystal TiO₂ substrates.^{26,37} The results herein suggest that polymer sensitized solar cell devices utilizing mesoporous TiO₂ scaffolds can optimize adsorption parameters such as solvent properties, temperature etc. in order to increase overall power conversion efficiency. However, thick sensitizer layers on a mesoporous oxide may inhibit polymer chains from diffusing into the mesopores, resulting in non-uniform polymer coverage throughout the entire scaffold.

VI.6 Supporting Information.

Experimental procedure for TiO₂ crystal preparation, electrode mounting, procedure for optical measurements, drop-casting results and single crystal absorbance spectrum of TH adsorbed from methanol on TiO₂.

Experimental Methods

Preparation of TiO₂ crystals. One side mechanically polished 10 mm x 10 mm x 1 mm thick crystals of rutile (110), (001) and (101) were obtained from Commercial Crystal Laboratories. The anatase samples were naturally occurring mineral crystals that were mined in Hargvidda, Tyssedal in Norway. These bipyramidal anatase crystals exhibited low-energy growth surfaces with large wedge-shaped (101) faces and (001) end caps. Rutile and anatase crystals were gently polished by hand in a figure eight motion for 3 minutes on a soft polishing cloth using 20 nm colloidal silica solution (Buehler, Inc.), followed by a 5 minute immersion in 10% aqueous HF solution to remove residual silica polish and

rinsing with copious amounts of 18 M Ω Millipore water. The anatase crystals were annealed at 650°C in N₂ for 6 hours to generate >50 nm terraces as observed by atomic force microscopy (AFM). The rutile crystals were first annealed at 650°C in air for 6 hours to generate >100 nm terraces as observed by atomic force microscopy (AFM). In order to induce n-type conductivity, the insulating rutile crystals were annealed in a continuous stream of N₂:H₂ (30 sccm:10 sccm) for 3 hours. The surface stress incurred during the reductive doping procedure induces <5 Å surface roughness. Therefore the rutile crystals were polished in colloidal silica, immersed in 10% HF for 5 min, then annealed for 3 hours under N₂ to regenerate the atomically flat terraced surfaces. The doping density of the rutile and anatase crystals were determined by Mott-Schottky analysis as $1 \pm 0.5 \times 10^{18} \text{ cm}^{-3}$.

Electrodes were prepared by threading a copper wire through a glass tube and soldering the wire to a copper disk. Ohmic contact between the crystals and copper disk was accomplished by scratching the un-polished crystal side with a razor blade, applying Ga:In eutectic (75:25 by weight) to the grooves and then physically pressing the crystal onto a copper disk. The crystals were physically bonded to the disk using epoxy (Loctite, 1C, Hysol) and the exposed metallic portions were electrically insulated using epoxy and an outer layer of silicone rubber (Dow Corning 732 multi-purpose sealant).

Prior to polymer adsorption, a cleaning procedure was performed whereby the electrodes were illuminated for 20 minutes using an unfiltered 100 W Oriel Xe arc lamp with an applied bias of 1.0 V vs. a graphite rod in a quartz

photoelectrochemical cell containing 0.5 M HClO₄ in Millipore water. The strongly oxidizing valence band holes generated during the UV treatment process greatly enhanced the sensitization yields by removing unwanted contaminants from the TiO₂ surface.[S1]

Optical measurements. Two nearly identical two-side polished 10.0 mm x 10.0 mm x 500 μm thick rutile (001) surfaces were used as substrates for absorbance measurements. One crystal was immersed in the TH/methanol solution for 12 min, characterized by AFM, and placed in the sample beam of a Perkin Elmer Lambda 950 UV/Vis spectrometer. The unmodified crystal was placed in the reference beam. The spectra were acquired in 0.5 nm wavelength steps with the maximum detector acquisition time (10 seconds).

Results and Discussion

Drop-casting of TH on Single Crystal TiO₂

To understand charge transport in thin polymer layers on single crystal TiO₂ as a function of film thickness, we prepared thin layers by drop casting 1.0 μl of PPE-TH-COOH/DMF solutions on a rutile (110) electrode. Direct measurement of film thicknesses by AFM imaging was not possible in either contact or tapping mode, often resulting in physical damage or complete removal of the film from the surface. Optical microscopy (Figure S1A) and false color photocurrent mapping (Figure S1B; obtained by rastering a 532 nm laser over the electrode surface) confirmed the presence of a polymer film whose dimensions far exceeded the specifications of the high resolution AFM scanner. It is evident that the film has a 'coffee-ring' morphology induced by different rates

of solvent evaporation of the 1 μl drop and the polymer thickness is not uniform across the crystal surface. In order to approximate the film thickness, we prepared films on quartz plates and assumed a linear relationship between absorbance and optical path length using previously determined values (in solution) for the absorptivity per polymer repeat unit.[S2] The absorbance spectra were converted to LHE via equation 1 in main text and shown in Figure S1C.

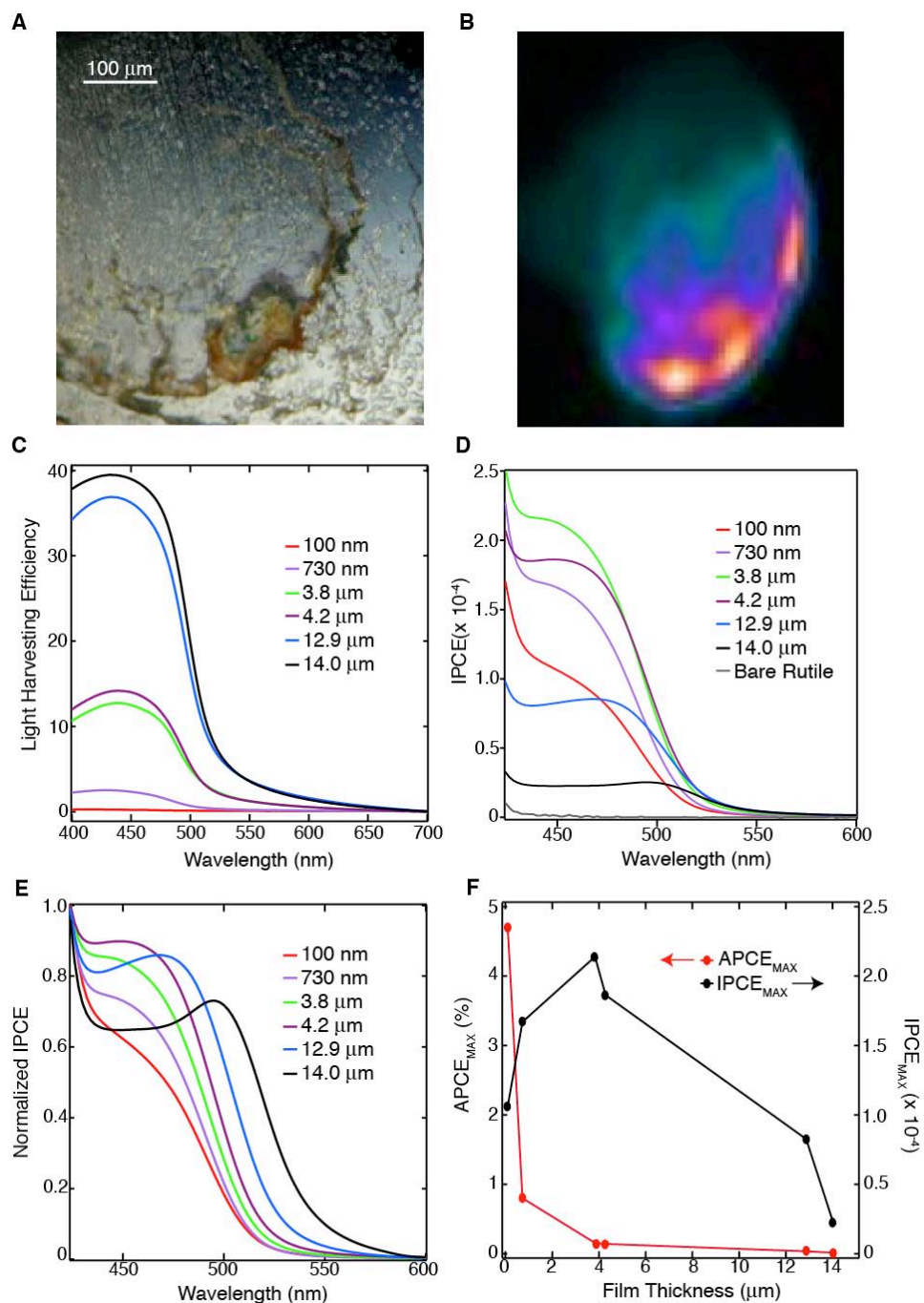


Figure S1. A) Representative optical microscope image of the 4.2 μm film drop cast PPE-TH-COOH film. B) False color photocurrent map of the same 4.2 μm film. C) Light harvesting efficiency of the polymer films measured on quartz substrates. D) IPCE spectra of the drop cast films measured at short circuit versus a Pt wire in an aqueous solution with 0.2 M KCl supporting electrolyte and 0.01 M KI as a redox mediator. E) Normalized IPCE spectra from panel D. F) Relationship between APCE and IPCE values as a function of polymer film thickness.

Whereas adsorption of PPE-TH-COOH from static DMF solutions exhibited surface limited growth (Figure 1) and maximum IPCE values that saturated (Figure 4A), the maximum values in the IPCE spectra of drop cast films (Figure S1D) increased to a maximum and then subsequently decreased (plotted in Figure S1F). The IPCE values at 460 nm more than double from approximate film thickness of 100 nm to 3.8 μm (Figure S1F) but then substantially decline by an order of magnitude with increasing film thickness. However the APCE values calculated according to equation 2 in the main text (Figure S1F) continually decrease with increasing film thickness.

One possible mechanism for poor charge collection of thicker polymer films is evident in the normalized IPCE spectra (Figure S1E). A red shifted peak at 496 nm for the thickest 14 μm film can be qualitatively related to the spatial position of collected excitons in the thick polymer film. Whereas long wavelength photons can penetrate deep into the polymer film and generate excitons near the PPE-TH-COOH/TiO₂ interface, short wavelength photons are absorbed many microns from the interface and are not collected. Therefore the IPCE values decrease in the high energy region of the visible spectrum compared to the longer wavelengths.

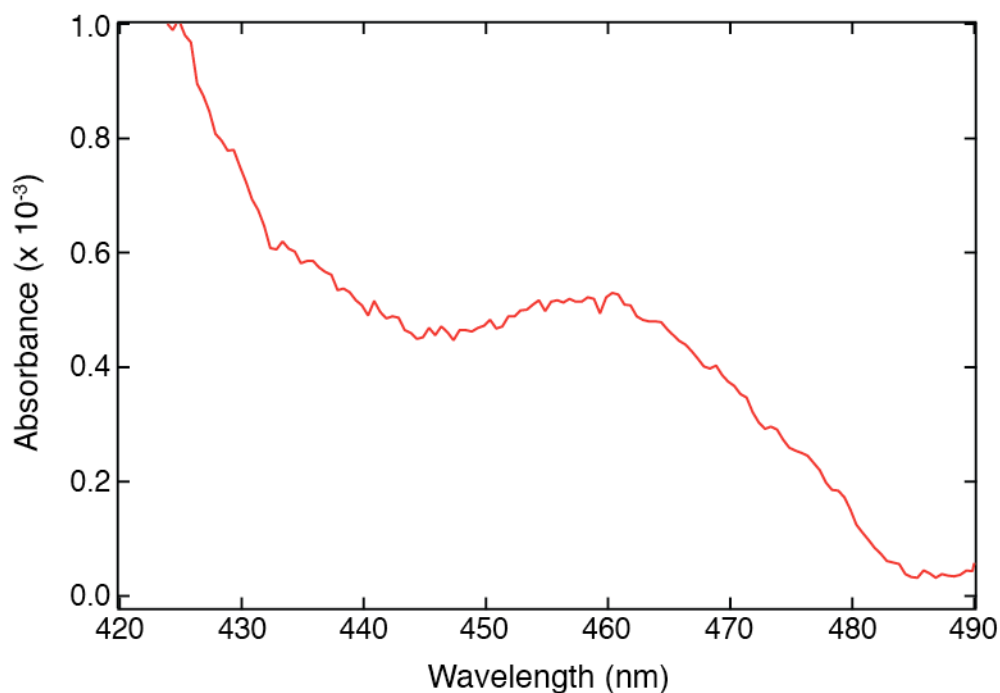


Figure S2. Absorbance spectrum of TH on a two-side polished 500 μm rutile (110) crystal after 12 min of deposition from methanol.

VI.7 Acknowledgments. The work at the University of Wyoming is supported by the U.S. Department of Energy – Basic Energy Sciences Grant No. DE-FG03-96ER14625. Work at the University of Florida is supported by the US Department of Energy (Grant No. DE-FG02-03ER15484).

VI.8 References

- (1) O'Regan, B.; Grätzel, M. A low-cost, high-efficiency solar cell based on dye-sensitized colloidal TiO_2 films *Nature* **1991**, *353*, 737.
- (2) Hagfeldt, A.; Grätzel, M. Molecular photovoltaics *Acc. Chem. Res* **2000**, *33*, 269.
- (3) Grätzel, M. Recent Advances in Sensitized Mesoscopic Solar Cells *Acc. Chem. Res.* **2009**, *42*, 1788.
- (4) Schanze, K. S.; Shelton, A. H. Functional Polyelectrolytes *Langmuir* **2009**, *25*, 13698.

- (5) Jiang, H.; Taranekar, P.; Reynolds, J.; Schanze, K. Conjugated Polyelectrolytes: Synthesis, Photophysics, and Applications *Angew. Chem. Int. Ed.* **2009**, *48*, 4300.
- (6) Adams, D. M.; Brus, L.; Chidsey, C. E. D.; Creager, S.; Creutz, C.; Kagan, C. R.; Kamat, P. V.; Lieberman, M.; Lindsay, S.; Marcus, R. A.; Metzger, R. M.; Michel-Beyerle, M. E.; Miller, J. R.; Newton, M. D.; Rolison, D. R.; Sankey, O.; Schanze, K. S.; Yardley, J.; Zhu, X. Charge Transfer on the Nanoscale: Current Status *J. Phys. Chem. B.* **2003**, *107*, 6668.
- (7) Brabec, C. J. Organic photovoltaics: technology and market *Sol. Energ. Mat. Sol. C.* **2004**, *83*, 273.
- (8) Kim, J. Y.; Lee, K.; Coates, N. E.; Moses, D.; Nguyen, T.; Dante, M.; Heeger, A. J. Efficient Tandem Polymer Solar Cells Fabricated by All-Solution Processing *Science* **2007**, *317*, 222.
- (9) Kim, Y.-G.; Walker, J.; Samuelson, L. A.; Kumar, J. Efficient Light Harvesting Polymers for Nanocrystalline TiO₂ Photovoltaic Cells *Nano Lett.* **2003**, *3*, 523.
- (10) Saji, V. S.; Zong, K.; Pyo, M. NIR-absorbing poly(thieno[3,4-b]thiophene-2-carboxylic acid) as a polymer dye for dye-sensitized solar cells *J. Photoch. Photobio. A.* **2010**, *212*, 81.
- (11) Arango, A. C.; Carter, S. A.; Brock, P. J. Charge transfer in photovoltaics consisting of interpenetrating networks of conjugated polymer and TiO₂ nanoparticles *Appl. Phys. Lett.* **1999**, *74*, 1698.
- (12) Bhongale, C. J.; Thelakkat, M. Efficient hybrid polymer/titania solar cells sensitized with carboxylated polymer dye *Sol. Energ. Mat. Sol. C.* **2010**, *94*, 817.
- (13) van Hal, P. A.; Christiaans, M. P. T.; Wienk, M. M.; Kroon, J. M.; Janssen, R. A. J. Photoinduced Electron Transfer from Conjugated Polymers to TiO₂ *J. Phys. Chem. B.* **1999**, *103*, 4352.
- (14) Li, G.; Shrotriya, V.; Yao, Y.; Huang, J.; Yang, Y. Manipulating regioregular poly(3-hexylthiophene) : [6,6]-phenyl-C61-butyric acid methyl ester blends-route towards high efficiency polymer solar cells *J. Mater. Chem.* **2007**, *17*, 3126.
- (15) Chen, L.-M.; Xu, Z.; Hong, Z.; Yang, Y. Interface investigation and engineering - achieving high performance polymer photovoltaic devices *J. Mater. Chem.* **2010**, *20*, 2575.

- (16) Liu, X.; Zhu, R.; Zhang, Y.; Liu, B.; Ramakrishna, S. Anionic benzothiadiazole containing polyfluorene and oligofluorene as organic sensitizers for dye-sensitized solar cells *Chem. Commun.* **2008**, 3789.
- (17) Mwaura, J. K.; Zhao, X.; Jiang, H.; Schanze, K. S.; Reynolds, J. R. Spectral Broadening in Nanocrystalline TiO₂ Solar Cells Based on Poly(p-phenylene ethynylene) and Polythiophene Sensitizers *Chem. Mater.* **2006**, *18*, 6109.
- (18) Jiang, H.; Zhao, X.; Shelton, A. H.; Lee, S. H.; Reynolds, J. R.; Schanze, K. S. Variable-Band-Gap Poly(arylene ethynylene) Conjugated Polyelectrolytes Adsorbed on Nanocrystalline TiO₂: Photocurrent Efficiency as a Function of the Band Gap *ACS Appl. Mater. Interfaces* **2009**, *1*, 381.
- (19) Fang, Z.; Eshbaugh, A. A.; Schanze, K. S. Low-Bandgap Donor-Acceptor Conjugated Polymer Sensitizers for Dye-Sensitized Solar Cells *submitted* **2010**.
- (20) Groves, C.; Reid, O. G.; Ginger, D. S. Heterogeneity in Polymer Solar Cells: Local Morphology and Performance in Organic Photovoltaics Studied with Scanning Probe Microscopy *Acc. Chem. Res.* **2010**, *43*, 612.
- (21) Giridharagopal, R.; Shao, G.; Groves, C.; Ginger, D. S. New SPM techniques for analyzing OPV materials *Mater. Today* **2010**, *13*, 50.
- (22) Giridharagopal, R.; Ginger, D. S. Characterizing Morphology in Bulk Heterojunction Organic Photovoltaic Systems *J. Phys. Chem. Lett.* **2010**, *1*, 1160.
- (23) Takeda, N.; Parkinson, B. A. The relationship between squaraine dye surface morphology and sensitization behavior on SnS₂ electrodes *Electrochimica Acta* **2000**, *45*, 4559.
- (24) Palomares, E.; Clifford, J. N.; Haque, S. A.; Lutz, T.; Durrant, J. R. Control of Charge Recombination Dynamics in Dye Sensitized Solar Cells by the Use of Conformally Deposited Metal Oxide Blocking Layers *J. Amer. Chem. Soc.* **2002**, *125*, 475.
- (25) Lu, Y.; Jaekel, B.; Parkinson, B. A. Preparation and characterization of terraced surfaces of low-index faces of anatase, rutile, and brookite *Langmuir* **2006**, *22*, 4472.
- (26) Ushiroda, S.; Ruzycki, N.; Lu, Y.; Spitler, M. T.; Parkinson, B. A. Dye sensitization of the anatase (101) crystal surface by a series of dicarboxylated thiocyanine dyes *J. Am. Chem. Soc.* **2005**, *127*, 5158.

- (27) Matsuura, A. Y.; Obayashi, T.; Kondoh, H.; Ohta, T.; Oji, H.; Kosugi, N.; Sayama, K.; Arakawa, H. Adsorption of merocyanine dye on rutile TiO₂(110) *Chem. Phys. Lett.* **2002**, *360*, 133.
- (28) Sasahara, A.; Pang, C. L.; Onishi, H. STM Observation of a Ruthenium Dye Adsorbed on a TiO₂(110) Surface *J. Phys. Chem. B.* **2006**, *110*, 4751.
- (29) Zuleta, M.; Yu, S.; Ahmadi, S.; Boschloo, G.; Gothelid, M.; Hagfeldt, A. Monitoring N719 Dye Configurations on (1x_n)-Reconstructed Anatase (100) by Means of STM: Reversible Configurational Changes upon Illumination *Langmuir* **2010**, *26*, 13236.
- (30) Li, S. C.; Wang, J. G.; Jacobson, P.; Gong, X. Q.; Selloni, A.; Diebold, U. Correlation between Bonding Geometry and Band Gap States at Organic/Inorganic Interfaces: Catechol on Rutile TiO₂(110) *J. Amer. Chem. Soc.* **2009**, *131*, 980.
- (31) Sambur, J. B.; Riha, S. C.; Choi, D.; Parkinson, B. A. Influence of Surface Chemistry on the Binding and Electronic Coupling of CdSe Quantum Dots to Single Crystal TiO₂ Surfaces *Langmuir* **2010**, *26*, 4839.
- (32) Oura, K.; Lifshits, V. G.; Saranin, A. A.; Zotov, A. V.; Katayama, M. *Surface Science: An Introduction*; Springer: Berlin, 2003.
- (33) Tan, C.; Pinto, M. R.; Schanze, K. S. Photophysics, aggregation and amplified quenching of a water-soluble poly(phenylene ethynylene) *Chem. Commun.* **2002**, 446.
- (34) Vella, J. *Ph.D. Dissertation 2009*, University of Florida, Gainesville.
- (35) Scully, S. R.; McGehee, M. D. Effects of optical interference and energy transfer on exciton diffusion length measurements in organic semiconductors *J. Appl. Phys.* **2006**, *100*, 034907.
- (36) Shaw, P. E.; Ruseckas, A.; Samuel, I. D. W. Exciton Diffusion Measurements in Poly(3-hexylthiophene) *Adv. Mater.* **2008**, *20*, 3516.
- (37) Enea, O.; Moser, J.; Grätzel, M. Achievement of incident photon to electric-current conversion yields exceeding 80% in the spectral sensitization of titanium-dioxide by coumarin *J. Electroanal. Chem.* **1989**, *259*, 59.
- (38) Matthews, O. A.; Shipway, A. N.; Stoddart, J. F. Dendrimers - Branching out from curiosities into new technologies *Progress in Polymer Science* **1998**, *23*, 1.

- (S1) Ushiroda, S.; Ruzycki, N.; Lu, Y.; Spitler, M. T.; Parkinson, B. A. Dye sensitization of the anatase (101) crystal surface by a series of dicarboxylated thiocyanine dyes *J. Am. Chem. Soc.* **2005**, *127*, 5158.
- (S2) M. R. Pinto, B. M. Kristal, K. S. Schanze, A Water-Soluble Poly(phenylene ethynylene) with Pendant Phosphonate Groups. Synthesis, Photophysics, and Layer-by-Layer Self-Assembled Films *Langmuir* **19**, 6523 (2003).

VI.9 Future Work

The solvated state of CPE chains may significantly affect the morphology at the oxide interface. In order to investigate these effects quantitatively, dynamic light scattering experiments should be used to determine the size distribution of CPEs in various solvents. In this way average sizes of CPE aggregates in solution can be correlated with aggregates on the TiO₂ surface. Adjusting the CPE concentration, solvent, temperature or addition of other solutes may allow for precise control of the CPE solvated state and thus interfacial morphology.

In addition to linear polymer conformations, the Schanze and Reynolds groups at the University of Florida synthesized dendrimer samples whose HOMO-LUMO energy level positions satisfy the thermodynamic requirements for electron injection into the TiO₂ conduction band. Dendrimers are large, monodisperse branched molecules (shown in Figure 6) whose optical, electronic, chemical and solubility properties can be tailored via precise synthetic control.[38] For example, a series of zero, first, second etc. generation dendrimers with the same branching (π -conjugated backbone) and surface units (carboxylate) can be synthesized and adsorbed on the TiO₂ surface. Analogous to the experiments performed herein, the morphology of the adsorbed dendrimer

and the IPCE values can be studied as a function of generation number. It may also be possible to attach catalytic species to the surface of the dendrimer so that photogenerated holes can perform desired oxidative reactions.

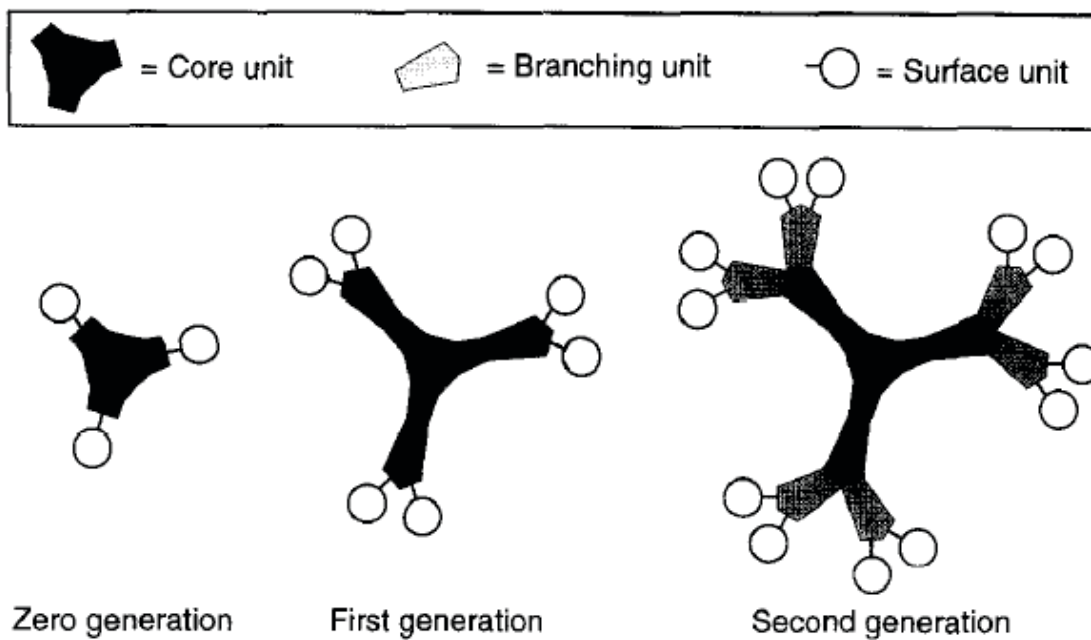


Figure 6. Cartoon illustration of the terms core unit, branching unit, surface unit and generation used to describe dendrimer samples.[38]

APPENDIX

A.1. Recent progress in preparation of single crystal TiO₂ substrates

Parkinson and co-workers previously described procedures to obtain terraced surface structures on various crystallographic faces of commercially grown rutile and naturally occurring anatase TiO₂ crystals.[1] The procedure consisted of figure-eight hand polishing with 0.5 μm and 0.03 μm alumina particles (in order of large to small alumina particles) and 20 nm colloidal silica followed by air annealing at 650 °C. This initial work did not discuss the effects of long-term crystal use and surface quality of crystals annealed in a hydrogen atmosphere (to reductively dope the samples). Instead, the UV cleaning procedure was shown to generate a clean electrode surface following consecutive dye sensitization procedures using electron injection yields as an indirect method to judge surface quality. Since QD or polymer sensitized TiO₂ crystals exhibit features that are easily observable by scanning probe microscopy, analysis of TiO₂ crystals before and after sensitizer adsorption was routinely performed for the research described in this dissertation and lead to further understanding of the surface chemistry of TiO₂ under ambient conditions.

A.2. Preparation of terraced, reduced rutile (110) TiO₂ single crystals

Figure 1A shows an AFM image of as-received rutile (110) from MTI Crystal Inc. Although some macroscopic surface damage could be observed (like the groove in Figure 1A), the majority of the crystal exhibited less than 1 Å surface roughness. In a manner consistent with previously published procedures,[1] the rutile crystal was gently polished by hand in a figure eight motion for 5-10 minutes on a soft polishing cloth using *only* 20 nm colloidal silica solution (Buehler, Inc.), rinsed with copious amounts of 18 MΩ Millipore water and annealed at 650 °C in air for 6 hours to generate ~80 nm terraces (Figure 1B). The particles observed in Figure 2B were approximately 10 nm in height and 40 nm wide and were suspected to be residual colloidal silica polish. Immersion of this substrate in 10% HF for 10 min followed by sonication in 18 MΩ Millipore water for 1 hr removed most of the residual polish (Figure 1C).

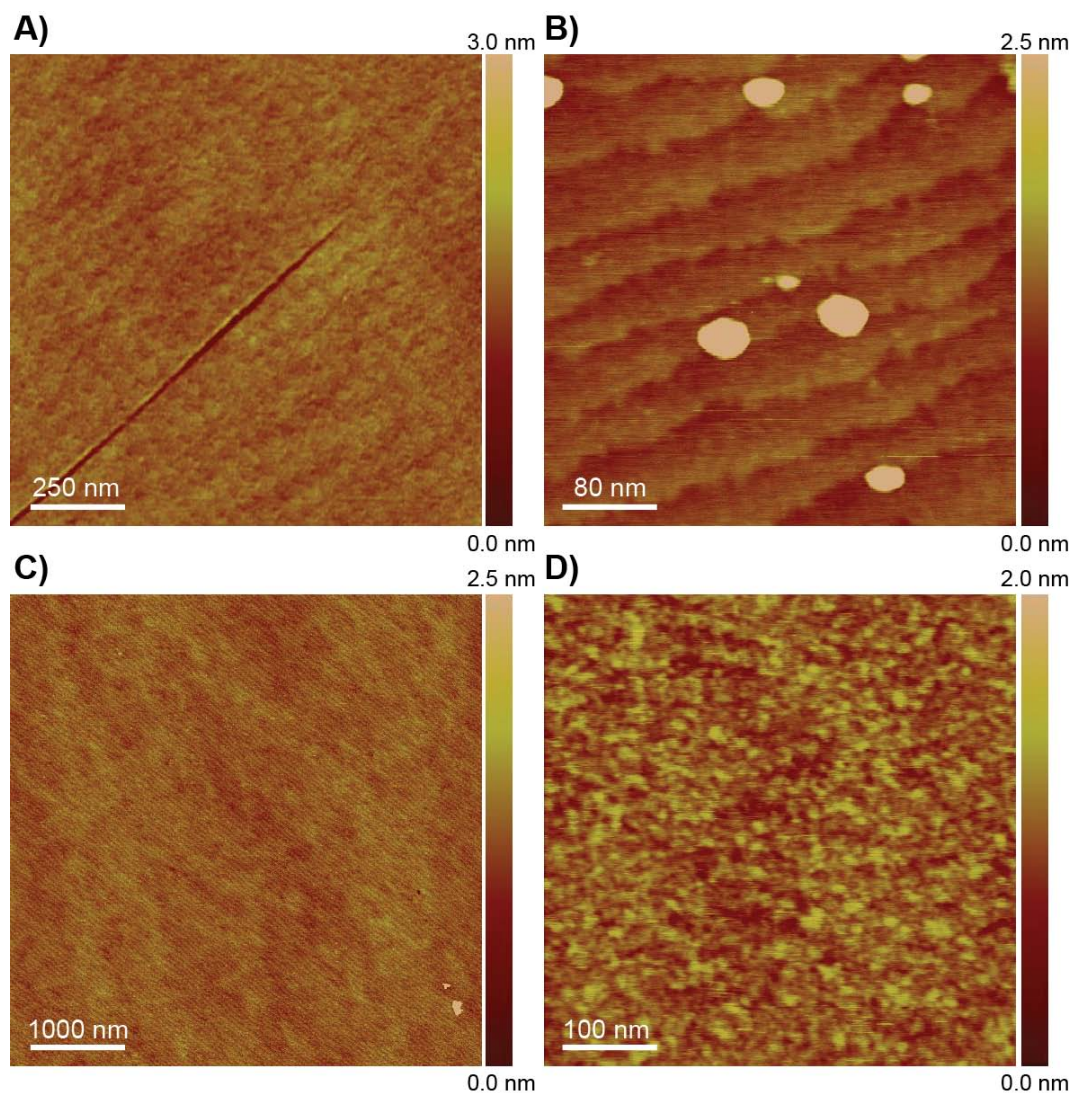


Figure 1. A) AFM image of an as-received rutile (110). B) AFM image following polishing of the same crystal with 20 nm colloidal silica and 6 hr air annealing at 650 °C. C) Large area scan following immersion in HF to remove residual silica polish and air annealing at 650 °C. D) AFM image showing the surface roughness incurred after the hydrogen annealing procedure.

In order to induce n-type conductivity in the commercial samples, the colorless insulating rutile crystals were annealed in a continuous stream of $N_2:H_2$ (30 sccm:10 sccm) for 3 hours. Following this hydrogen annealing procedure, the appearance of the insulating crystals changed to dark purple or black (arising

from Ti^{3+} sites).[2] Qualitatively, the darker appearance of crystals indicates a higher doping density (e.g. light blue crystals have lower doping densities than black crystals). However, the surface stress incurred during the reductive doping procedure induces approximately 2 Å of surface roughness (Figure 1D). Regeneration of the terraced rutile surface was accomplished by polishing with colloidal silica, immersion in 10% HF for 5 min, followed by annealing for 3 hours under N_2 flow only. Although this procedure resulted in a terraced TiO_2 surface (like that shown in Figure 1C), the crystals qualitatively exhibited lower doping density (appeared lighter) than the original H_2 annealed samples. Adjusting the temperature and flow conditions during H_2 annealing may allow for highly doped, atomically flat rutile substrates.

A.3. Recycling crystals for multiple sensitization experiments

Unlike inexpensive mesoporous TiO_2 substrates that may be freshly prepared for device fabrication, commercial single crystal rutile TiO_2 substrates are >\$140/crystal and therefore must be re-used for sensitization experiments. Perhaps due to the inorganic nature of QD sensitizers or multiple QD ligand- TiO_2 chemical bonds, it was difficult to solely rely on the UV cleaning procedure (using the same electrolytes as previously described) to achieve reproducibly high IPCE values for multiple QD sensitization experiments. For example, Figure 2A shows a QD-sensitized rutile (110) TiO_2 crystal after 1 cycle of UV treatment, colloidal silica polishing, HF treatment and air annealing.

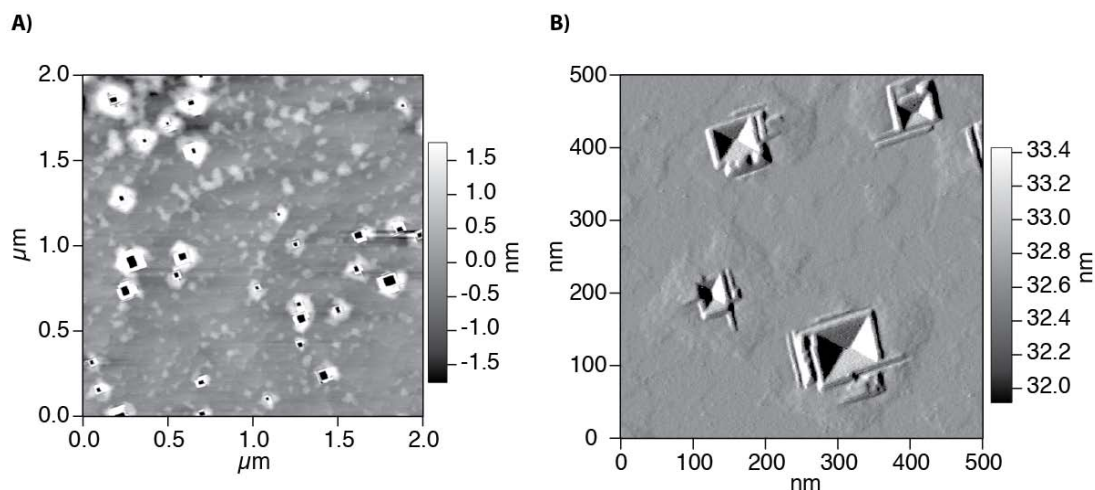


Figure 2. A) AFM height image of a rutile (110) crystal after cleaning treatments following a PbS QD sensitization experiment. B) Amplitude image of the pits observed in the height images reveals internal faceting within the inverted pyramid pits.

Although terraces were slightly visible in the AFM height image (Figure 2A), the surface structure was dominated by residual contamination and pits in the surface. Interestingly however, the higher magnification amplitude image (Figure 2B) of the pitted regions of the crystal reveal inverted pyramid pit defects at the surface that were present over large areas of the sample.

In order to completely remove surface contaminants, it was necessary to perform several (3-10) cycles of 0.05 micron alumina and 20 nm colloidal silica polishing followed by annealing at 650 °C in air. Figures 3A and 3B show representative large area AFM images of two separate crystals following alumina polishing. The dark stripes across the surface represent 4-10 nm grooves caused by the aggressive alumina polish. Despite this physical damage to the surface, smaller scan sizes (Figure 3C) revealed ‘wedding-cake’ terraces between the deep grooves. Figure 3D represents an interesting region of one rutile (110)

sample at the interface of two different surface structures. Figures 3E and 3F represent higher resolution imaging of the left and right portions of Figure 3D respectively showing regions of rectangular and wedding-cake terraces. Although it is not clear what specific surface treatments cause these surface structures (e.g. cycling between hydrogen and air annealing, polishing, temperature, annealing time), Diebold notes in a comprehensive review of the surface chemistry of TiO_2 that “The rich array of surface structures achievable on TiO_2 (110) may provide a playground for surface science experiments where the influence of different adsorption sites can be tested.”[2] It may be important to compare QD adsorption on each type of isolated terraced structure to determine the reactivity of surface sites (via QD surface coverage) and subsequent effects on sensitized photocurrent yields.

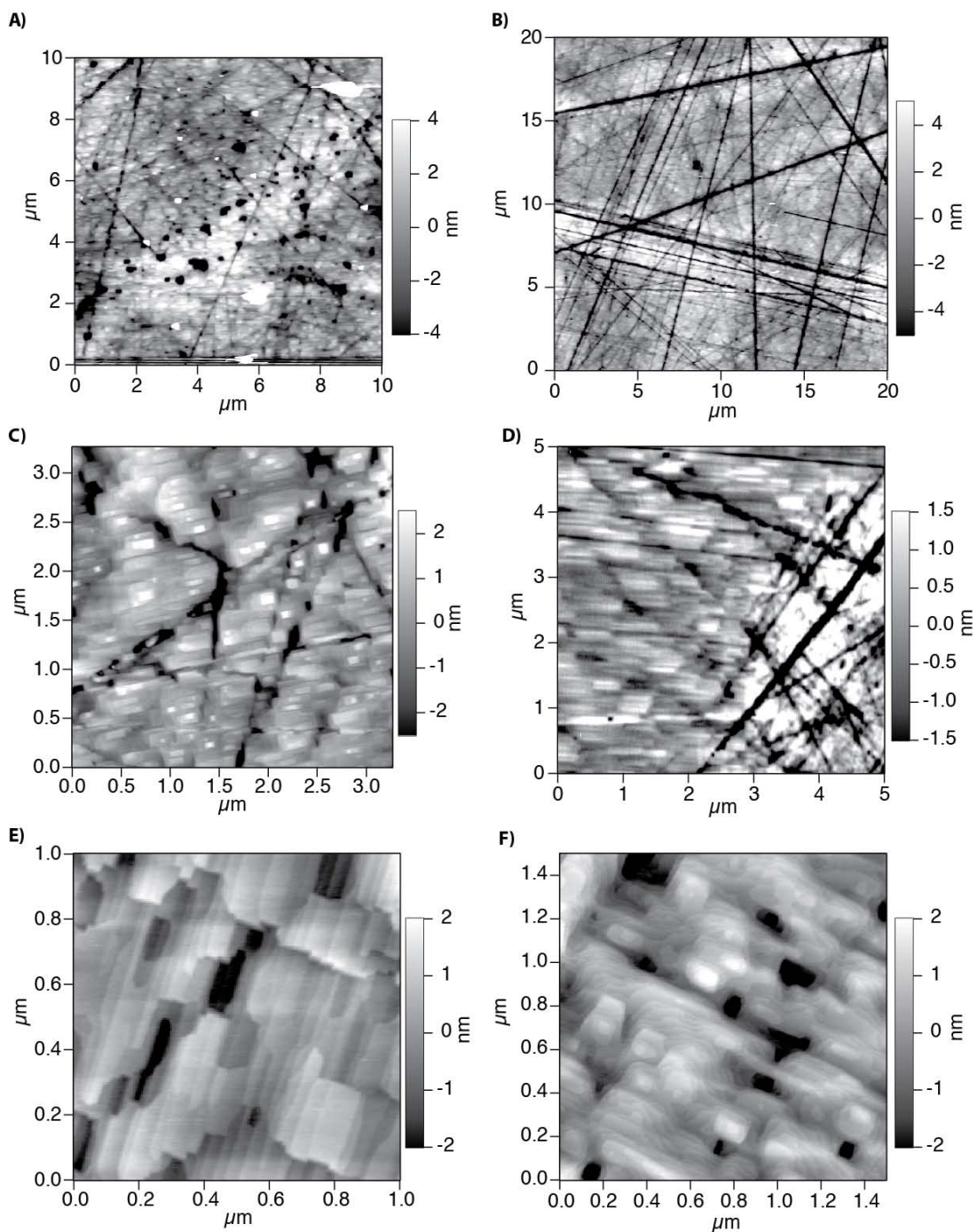


Figure 3. A) and B) AFM images showing macroscopic alumina polishing damage on two separate rutile (110) crystals following air annealing at 650 °C. C) small area scan of the same crystal as (B) reveals the ‘wedding-cake’ terraced structure. D) AFM image showing a boundary between two different surface structures on the same crystal. E) and F) are small area scans corresponding to the left and right of (D), respectively.

Going forward it will be highly desirable to control the detailed surface structure of rutile crystals following multiple QD or dye sensitization experiments. It is clear that the macroscopic damage to the surface caused by alumina polishing must be remedied. Figure 4A shows a large area AFM scan of the same crystal shown in Figure 3B that was subjected to high temperature annealing at 1000 °C for 8 hr. High resolution imaging (Figure 4B) indicated about a two-fold increase in the average terrace width (from approximately 80 nm to 180-200 nm) from the as-received rutile annealed at 650 °C (Figure 1B). Although this procedure remediates surface damage, it has not been explored whether the large terraces can be preserved following hydrogen annealing to produce a desired doping level. One attractive approach is to exploit the high temperature air annealing procedure to remedy alumina polishing damage of conducting crystals such as naturally occurring anatase or Nb-doped rutile (shown in Figure 4C and 4D). Unlike commercially grown rutile, these crystals may be annealed in air without changing the doping density. High temperature air annealing potentially offers a route to macroscopically clean, terraced surfaces without multiple polishing and annealing cycles.

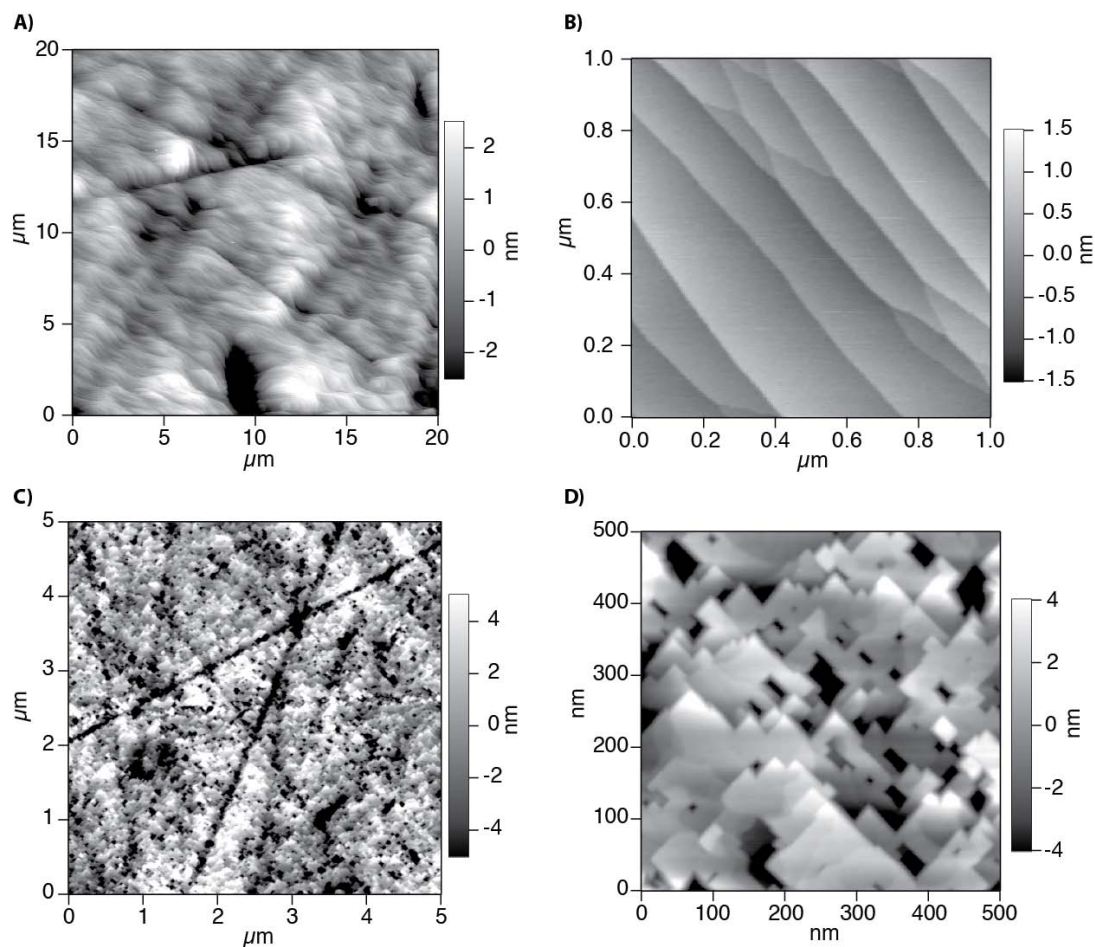


Figure 4. A) Large and B) small area AFM images of the same rutile (110) crystal shown in Figure 3B following 1000 °C annealing in air for 8 hr. C) Large and D) small area AFM images of a Nb-doped rutile (110) crystal exhibiting some macroscopic polishing damage.

A.4. Repetitive use of various orientations of rutile

Rutile (110) is the most widely studied orientation of TiO_2 in surface science experiments because it is the most thermodynamically stable face.[2] QD sensitization experiments on various rutile orientations such as (001), (011), (100) and (101) did not reveal noticeable, reproducible trends in surface reactivity or electron injection yields. This is in contrast to previous studies of dye sensitization on single crystal electrodes[3] and is surprising given that each

surface should exhibit some difference in reactivity, dielectric properties and conductivity along certain crystallographic axes.[2] One possible explanation is that the surface quality of these crystals were prone to surface reconstruction after several surface cleaning procedures. For example, Figure 5 shows a rutile (001) following 3 cycles of colloidal silica polishing and air annealing at 650 °C. Fukui *et al.* previously observed this 'maze' surface and qualitatively described it as 'bleacher-like' reconstruction that formed following high temperature annealing in vacuum and was attributed to crossed rows along the $[1\bar{1}0]$ and $[\bar{1}10]$ directions.[4] Developing reliable procedures to control the surface chemistry of various commercially available crystallographic orientations of rutile for repetitive use may allow for more detailed and reproducible investigations of QD or polymer adsorption on a variety of TiO_2 crystal orientations and surface structures.

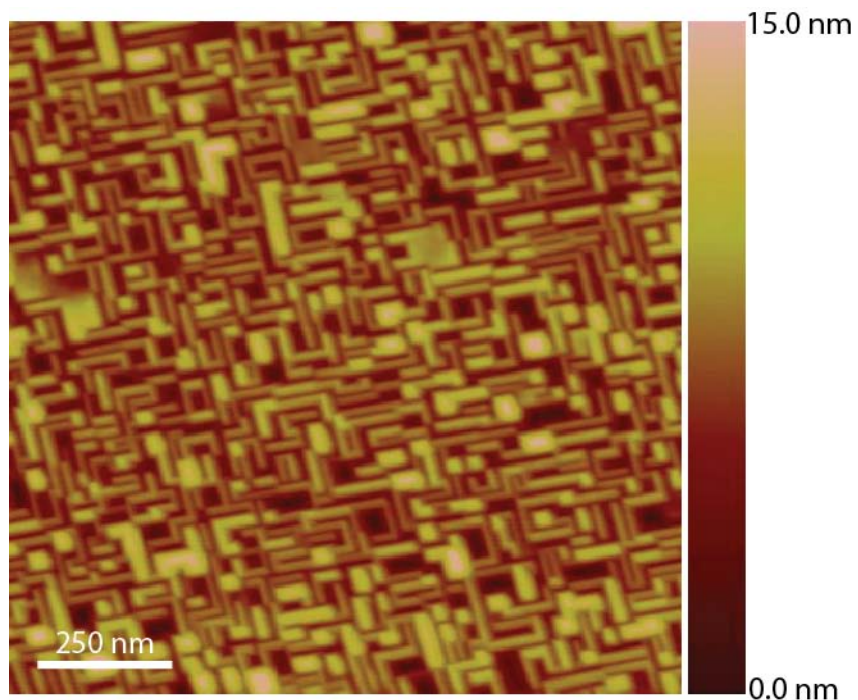


Figure 5. AFM image of the ‘bleacher-like’ surface structure obtained on a rutile (001) crystal after 3 cycles of silica polishing and 650 °C annealing in air.

The trend in crystal surface quality following multiple QD or dye sensitization experiments was also observed for naturally occurring anatase crystals. Multiple alumina and colloidal silica polishing and low temperature (500 °C) air annealing cycles were necessary to regenerate terraces on anatase (001) and (101) crystal faces. Due to the odd shape of some natural crystals, great care was taken to apply gentle pressure during polishing to avoid surface damage. A systematic study of the effects of high temperature air annealing on the doping density of natural anatase crystals may allow for large terrace formation without changing the doping density significantly.

A.5 References

- (1) Lu, Y.; Jaeckel, B.; Parkinson, B. A. Preparation and Characterization of Terraced Surfaces of Low-Index Faces of Anatase, Rutile, and Brookite *Langmuir* **2006**, *22*, 4472.
- (2) Diebold, U. The surface science of titanium dioxide *Surf. Sci. Rep.* **2003**, *48*, 53.
- (3) Lu, Y.; Choi, D.-j.; Nelson, J.; Yang, O. B.; Parkinson, B. A. Adsorption, Desorption, and Sensitization of Low-Index Anatase and Rutile Surfaces by the Ruthenium Complex Dye N3 *J. Electrochem. Soc.* **2006**, *153*, E131.
- (4) Fukui, K.-i.; Tero, R.; Iwasawa, Y. Atom-Resolved Structures of TiO₂(001) Surface by Scanning Tunneling Microscopy *Jpn. J. Appl. Phys.* **2001**, *40*, 4331.